

Deformation Microstructures  
—  
Antarctic Ice from EPICA Dronning  
Maud Land and Artificial Creep Test  
Ice

Ilka Hamann

Alfred Wegener Institute for Polar and Marine Research  
Columbusstrasse  
27568 Bremerhaven  
Germany

Fachbereich Geowissenschaften (FB5)  
Universität Bremen  
Bibliothekstrasse 1  
28359 Bremen  
Germany

October 31, 2007

## **Gutachter**

Prof. Dr. H. Miller

Prof. Dr. C. Spiegel

## **Prüfer**

Prof. Dr. R. X. Fischer

Dr. J. Freitag

## **Promotionskolloquium**

am 20. Dezember 2007

# Erklärung

Ich habe

- die Arbeit ohne unerlaubte fremde Hilfe angefertigt,
- keine anderen als die angegebenen Quellen und Hilfsmittel benutzt und
- die, den benutzten Werken wörtlich oder inhaltlich entnommenen Stellen als solche kenntlich gemacht.

# Contents

<b>Summary</b>	<b>4</b>
<b>Zusammenfassung</b>	<b>6</b>
<b>Acknowledgement</b>	<b>8</b>
<b>1 Introduction and Objectives</b>	<b>10</b>
1.1 Objectives . . . . .	12
1.2 Scope of the Thesis . . . . .	12
<b>2 List of Publications Submitted for the Thesis</b>	<b>13</b>
<b>3 Methods</b>	<b>16</b>
3.1 Ice-core processing . . . . .	16
3.2 Creep-experiment and ice-sample production . . . . .	16
3.3 Sample preparation . . . . .	18
3.4 Microscopic observations . . . . .	19
3.5 Microstructure measurements . . . . .	19
3.6 Crystal-orientation measurements . . . . .	22
<b>4 The EPICA Dronning Maud Land Ice Core and Comparison with Creep Experiments</b>	<b>24</b>
4.1 Ice mechanical behaviour . . . . .	25
4.1.1 Creep deformation of ice . . . . .	26
4.2 Study of deformation-related recrystallization by analysis of microstructures . . . . .	27
4.2.1 Subgrain boundaries, Grain boundaries and their interaction/controlled by deformation . . . . .	28
4.2.2 Subgrain-boundary types . . . . .	34
<b>5 Conclusions</b>	<b>39</b>

<b>6 Outlook</b>	<b>41</b>
<b>References</b>	<b>41</b>
<b>Appendix - Publications</b>	<b>52</b>
<b>A Publication I - Evolution of ice crystal microstructure during creep experiments</b>	<b>52</b>
<b>B Publication II - Subgrain boundaries in EPICA-Dronning Maudland (EDML) deep ice core</b>	<b>64</b>
<b>C Publication III - Deformation microstructures in an Antarctic ice core (EDML) and in experimentally deformed artificial ice</b>	<b>78</b>
<b>D Publication IV - Microstructure mapping: a new method for imaging deformation-induced microstructural features of ice on the grain scale</b>	<b>88</b>
<b>E Publication V - Is Antarctica like a birthday cake?</b>	<b>98</b>
<b>F Publication VI - Implications for and findings from deep ice core drillings - An example: the ultimate tensile strength of ice at high strain rates</b>	<b>108</b>
<b>G Publication VII - Direct Evidence for Radar Reflector originating from Changes in Crystal-Orientation Fabric</b>	<b>114</b>
<b>H Publication VIII - One-to-one coupling of glacial climate variability in Greenland and Antarctica</b>	<b>125</b>

# Summary

The primary objective of this thesis is the investigation of microstructures obtained from samples from the EPICA Dronning Maud Land ice core from Antarctica. The goal is to gain understanding of deformation processes and deformation-related recrystallization mechanisms using these structures. The structures are visualized with the new microstructure mapping method using the preferred sublimation along defect regions in the crystal. This method enables observation in high resolution as well as overview over a significant sample volume. In order to provide unambiguous proof of their deformational origin and to offer interpretation and characterization, experimental reproduction of the microstructural features are performed using creep tests. Subgrain boundaries and grain-boundary morphology are identified as the most direct effects of deformation and recrystallization processes, which are still easily observable. They can be used additionally to the conventional parameters (grain size, crystal-orientation distribution) to determine these mechanisms. Different subgrain-boundary types observed in experimentally deformed samples as well as in natural ice indicate several formation processes.

Results obtained from this new and novel data suggest a profound reconsideration of the classical tripartition of recrystallization regimes described in the literature in ice sheets. Instead, dynamic recrystallization in two of its forms (rotation recrystallization and strain-induced migration recrystallization) dominates the microstructure evolution in all depth regions of the EDML ice core.

Results of systematic microstructure analysis of creep-test samples demonstrate the correlation of grain-substructure evolution and strain hardening during primary creep. Subgrain boundaries and dislocation walls acting as obstacles for dislocation motion was identified thereby as a main process of strain hardening in ice.

The comparison of results from experimentally and naturally deformed ice enables a specification of the well-known difference in flow behaviour for low- and high-stress regimes: in low-stress regimes dislocation-density

decreasing processes (recovery and dynamic recrystallization), which restore the properties of the material, play a significantly more important role than in high-stress regimes.

# Zusammenfassung

Hauptanliegen dieser Arbeit ist die Untersuchung der Mikrostrukturen, die an Proben des antarktischen EPICA Dronning Maud Land Eiskerns gewonnen wurden. Ziel ist ein Erkenntnisgewinn hinsichtlich der Deformationsprozesse und der damit verbundenen Rekristallisationsmechanismen anhand dieser Strukturen. Die Strukturen werden mit der neuen *Microstructure Mapping* Methode sichtbar gemacht, wobei die bevorzugte Sublimation entlang von Kristalldefektregionen genutzt wird. Die Methode ermöglicht Beobachtungen in hoher Auflösung aber auch im Überblick über aussagekräftige Probenvolumina. Um die Deformationsherkunft der Strukturen unzweideutig beweisen zu können und um Interpretations- und Charakterisierungsmöglichkeiten zu bieten, wurden sie experimentell in Kriechdeformationstests reproduziert. Subkorn Grenzen und Korngrenzmorphologie sind dabei als direkteste aber doch einfach beobachtbare Effekte von Deformations- und Rekristallisationsprozessen identifiziert worden. Sie können zusätzlich zu den konventionellen Parametern (Korngröße, Kristallorientierungsverteilungen) verwendet werden, um diese Mechanismen zu bestimmen. Verschiedene Subkorn Grenztypen, die sowohl in experimentell deformiertem als auch in natürlichem Eis beobachtet wurden, deuten auf unterschiedliche Entstehungsprozesse hin.

Ergebnisse, die mit diesen neuen und neuartigen Daten gewonnen wurden, regen eine tief greifende Prüfung der klassischen, in der Literatur beschriebenen, Dreiteilung von Rekristallisationsregimen mit der Tiefe im Eisschild an. Die dynamische Rekristallisation in zwei ihrer Ausprägungen (Rotation-srekristallisation und straininduzierte Migrations- rekristallisation) dominiert die Mikrostrukturentwicklung in allen Tiefen des EDML Eiskerns.

Ergebnisse der systematischen Mikrostrukturanalyse an Proben von Kriechdeformationstests weisen den Zusammenhang von Kornsubstrukturentwicklung und Deformationshärtung während des Primärkriechstadiums nach. Der Hauptprozess ist dabei die bewegungshemmende Wirkung der Subkorn Grenzen und Versetzungswände für Dislokationen.

Vergleiche der Resultate von experimentell und natürlich deformiertem

Eis erlaubt eine Spezifizierung des bekannten Unterschieds im Fließverhalten von Niedrig- und Hochstressregimen: im Niedrigstressregime spielen dislokationsabbauende Prozesse (Erholung und dynamische Rekristallisation), die die Materialeigenschaften wiederherstellen, eine deutlich wichtigere Rolle als in Hochstressregimen.

# Acknowledgement

This thesis exists thanks to Sepp Kipfstuhl's talents to observe the nature open-minded, his visions to come as close to nature as possible in our understanding and his willingness to see the world in a little bit different way than the rest of us. Sepp, I thank you for teaching me many of your technical skills, but also so many things one can never find in a book. I am greatly indebted to Prof. Nobuhiko Azuma for teaching me so many essential aspects of the ice-deformation study, for inspiring discussions and for his patient help, without which I could have never completed this study. It was an invaluable opportunity to study with him in Nagaoka, not only because of the many things I learned for my study, but also because of those I learned for my life. Nobby, for me, you are the embodiment of a honorable *Sensei*. *Doumo arigatou gozaimashita*. Next I want to mention Sérgio H. Faria, from whose creativity and highly gifted research and teaching skills I benefited so much. Sérgio, thank you for wonderful discussions and your patience and empathy to express the sometimes complicated things in such a way that we can all understand them. I thank Prof. Heinz Miller for giving me the possibility to do this research and for his support in many important situations as well as for his confidence. I am grateful for manifold help and suggestions which were provided by Frank Wilhelms, Olaf Eisen, Anja Lambrecht, Johannes Freitag and many other colleagues. I deeply acknowledge the cooperation and help I received from Atsushi Miyamoto. We had fruitful and joyful measurement campaigns which I hope will be continued. Atsushi, *arigatou, ne*.

I thank all my colleagues and friends from AWI, for their motivating words in difficult times and for the fun we had in so many other situations.

I thank all my Japanese friends and colleagues for the hospitality and help and for so many, but still not enough, insights into their fascinating culture.

I thank the European Project of Ice Coring in Antarctica (EPICA), the Ministry of Education, Culture, Sports, Science and Technology, Japan and the Deutscher Akademischer Austausch Dienst (DAAD) for financial support.

Last but not least my family remains to be mentioned, for their tolerance,

motivation, support, proofreading and more innumerable reasons. Danke, Ihr Lieben! Especially Christian, thank you for your love.

# 1

## Introduction and Objectives

Ice as the most abundant mineral on the Earth's surface plays an important role in our climate system. The cryosphere does not only reflect and record passively climate variations by offering visible expression of climate change, but even influences actively the atmosphere and hydrosphere. The activity of ice sheets as a component of the global water cycle and their passive role as a palaeo-climate archive are two important contributions, whose interpretation in geoscience studies requires the understanding of the mechanical behaviour of ice.

As a component of the global water cycle, the huge ice masses in the polar ice sheets are the main freshwater reservoirs, which could strongly affect the sea level evolution and freshwater flux influencing ocean circulation by even moderate changes in their balances (IPCC, 2007; Lemke et al., 2007; Bindoff et al., 2007). The balance of the ice-sheet system is regulated by ice input, primarily from precipitation, and by ice output fluxes, namely melting and iceberg calving. The impact on sea level evolution is partly due to excess of melting over snow accumulation, but also due to the flow of the glaciers, which controls the spreading of the ice towards the coast and thus the drainage into the oceans by calving of icebergs. Changes in ice flow can explain much of the Antarctic mass changes observed recently (Lemke et al., 2007). Besides basal sliding over the bedrock, whose complexity we are just recently becoming aware of (Vaughan and Arthern, 2007), the important component of the ice sheet flow is the internal deformation. Deformation within the ice sheet is modeled using coarse grid spacings, but models do not include the full suite of physical processes implicated in the ongoing changes (Alley et al., 2005). The flow law usually used in these models and originally formulated by Glen (1955) contains parameters involving mostly unknown effects of impurities and microstructures (Paterson, 1994; Petrenko and Whitworth, 1999, see also Chap. 4.1). Although it has been known for

decades that a number of physical properties of a single crystal are strongly anisotropic and preferred crystal-orientation distributions in polycrystals develop under deformation (e.g. Steinemann, 1958; Gow and Williamson, 1976; Jacka, 1984; Azuma and Higashi, 1985), only recently anisotropic flow laws have been developed to include the strong mechanical anisotropy of the material as a fundamental component of ice structures (e.g. Azuma, 1994; Placidi et al., 2004; Gillet-Chaulet et al., 2005; Faria, 2006; Thorsteinsson, 2006; Petit et al., 2007). Still, the deformation of polar ice sheets is brought about by several processes on the atomic scale, like dislocation motion and diffusion, which cannot be treated in the models yet. As these processes act on the atomic scale, they are difficult to observe directly in deforming polycrystalline ice. Nonetheless, they leave behind certain structures at the grain and subgrain scale indicating deformation mechanisms and, thus, microstructures can be used to study these processes. Comprehension of microstructural features can add to our understanding of flow laws in ice sheets.

The other important motivation to study deformation structures in ice sheets is the role the polar ice sheets play as monitors of our Earth's past climate. Deep ice cores drilled through the ice sheets provide a unique archive of palaeo-climate parameters, which have been accumulated with snowfall layer by layer over hundreds of thousands of years (e.g. Lorius et al., 1979; Petit et al., 1997, 1999; North Greenland Ice Core Project members, 2004; EPICA community members, 2004, 2006). The correct interpretation of these records, especially in terms of dating, requires consideration and knowledge of processes following the deposition. This necessity became especially clear during the interpretation of GRIP and GISP2 ice cores drilled only 28 km apart in Greenland in the 1990's. GRIP drilling was finished shortly before the parallel core and a first interpretation of the records concluded a spectacular climate instability especially during the last interglacial period (GRIP Project Members, 1993; Dansgaard et al., 1993). However, later study of the GISP2 data also revealed a certain trend of irregularity, but a correlation with GRIP, well developed in the top 90% of the cores, was missing below this depth (Grootes et al., 1993; Taylor et al., 1993) and therefore the interpretation could not be supported. The reason for the disagreement in data of the bottom 10% of the two cores was found in the disturbance of the sequence by ice-flow processes. Structural data, such as stratigraphic layers in cloudy and clear ice, helped to argue for overturned folding or boudinage as macro-scale deformation effects (Taylor et al., 1993; Thorsteinsson et al., 1995). Increased attention was paid to deformation in ice sheets by climatologists thereafter.

The two examples mentioned above indicate that structures containing flow information can occur in a multiscale setting in natural ice. Further-

more, structures are not only modified by the flow and interactions of the ice sheet with the environment, they provide also a feedback that affects the ice-sheet flow and its environmental interactions leading to an intricate flow-structure-environment interplay (FSEI) (Faria et al., 2007). A comprehensive understanding of the interplay of flow, structures and their settings and environments is still a topic of recent investigations, and this work can only offer a small contribution.

## **1.1 Objectives**

The objective of the at-hand thesis is to investigate and characterize data obtained by microstructure mapping regarding their potential information about deformation processes. New and novel data on grain substructures provide direct evidences of deformation related micromechanisms, such as dislocation activity and recrystallization, and will contribute to a better understanding of the deformation and recrystallization processes in flowing ice on the grain scale.

## **1.2 Scope of the Thesis**

This work focuses on microstructures on the subgrain scale, where the main portion of deformation of polycrystalline ice under conditions found in ice sheets is taking place as dislocation creep (e.g. Duval et al., 1983; Alley, 1992; Montagnat and Duval, 2000). Comparison with microstructures observed in experimentally deformed artificial ice allow conclusions about the mechanical behaviour of the material under a significant range of variables and controlled conditions.

## 2

# List of Publications Submitted for the Thesis

- PUBLICATION I  
**Evolution of ice crystal microstructure during creep experiments**  
Hamann, I., Weikusat, Ch., Azuma, N., Kipfstuhl, S. (2007)  
Journal of Glaciology, Vol. 53, No. 182, pp. 479-489. See App. A
- PUBLICATION II  
**Subgrain boundaries in EPICA-Dronning Maudland (EDML) deep ice core**  
Hamann, I., Kipfstuhl, S., Faria, S. H., Azuma, N., Miyamoto, A.  
(subm. October 2007)  
Submitted to Journal of Glaciology on October 12<sup>th</sup> 2007. See App. B
- PUBLICATION III  
**Deformation microstructures in an Antarctic ice core (EDML) and in experimentally deformed artificial ice**  
Hamann, I., Kipfstuhl, S., Azuma, N., Faria, S. H., Miyamoto, A.  
(subm. August 2007)  
Submitted to Physics of Ice Core Records, 2<sup>nd</sup> volume (T. Hondoh, ed.)  
on August 31<sup>st</sup> 2007. See App. C
- PUBLICATION IV  
**Microstructure mapping: a new method for imaging deformation-induced microstructural features of ice on the grain scale**

Kipfstuhl, S., Hamann, I., Lambrecht, A., Freitag, J., Faria, S. H., Grigoriev, D., Azuma, N. (2006)

Journal of Glaciology, Vol. 52, No. 178, pp. 398-406. See App. D

Own contributions:

- participation in microstructure mapping project in Antarctica within the EPICA-DML season 2003/04 and in Bremerhaven 2003 to 2007
- image analysis and first interpretations of EDML microphotographs in low-resolution (mesoscopic) view (Paragraph 3.1 in Publication IV - App. D) to measure e. g. grain size
- image analysis, observations and first interpretations of EDML microphotographs in high-resolution (microscopic) view (Paragraph 3.2, 4.2 and 4.3 in Publication IV - App. D) to characterize sublimation features and to determine their relevance
- clarification of the merit the method provides for studies on deformation microstructures (Paragraph 5 and 6 in Publication IV - App. D)

- PUBLICATION V

**Is Antarctica like a birthday cake?**

Faria, S. H., Hamann, I., Kipfstuhl, S., Miller, H. (2006)

Preprint No. 33/06 of the MPI für Mathematik in den Naturwissenschaften, Leipzig. [www.mis.mpg.de/preprints/2006/prepr2006\\_33.html](http://www.mis.mpg.de/preprints/2006/prepr2006_33.html). See App. E

Own contributions:

- participation in microstructure mapping project in Antarctica within the EPICA-DML season 2003/04 and in Bremerhaven 2003 to 2007 (Fig. 1 und 2 in Publication V - App. E) and discussion and research of innovative explanation of new subgrain boundary type
- measurement, processing and discussion of crystal-orientation fabric data (Fig. 1 in Publication V - App. E)

- PUBLICATION VI

**Implications for and findings from deep ice core drillings - An example: the ultimate tensile strength of ice at high strain rates**

Wilhelms, F., Sheldon, S. G., Hamann, I., Kipfstuhl, S. (2007)

Physics and Chemistry of Ice (The proceedings of the International Conference on the Physics and Chemistry of Ice held at Bremerhaven, Germany on July 23<sup>rd</sup>-28<sup>th</sup> 2006) The Royal Society of Chemistry Special Publication No. 311, pp. 635-639. See App. F

Own contributions:

- measurements of grain size versus depth and crystal-orientation fabric data (Paragraph 3.2 and 4 in Publication VI - App. F) and discussion for relevance on fracture behaviour in EDML

- PUBLICATION VII

**Direct Evidence for Radar Reflector originating from Changes in Crystal-Orientation Fabric**

Eisen, O., Hamann, I., Kipfstuhl, S., Steinhage, D., Wilhelms, F. (2007)  
The Cryosphere, 1, pp. 1-10. See App. G

Own contributions:

- measurement, processing and discussion of crystal-orientation fabric data (Paragraph 2.4, 3 and 4 and Fig. 3 and 4 in Publication VII - App. G)

- PUBLICATION VIII

**One-to-one coupling of glacial climate variability in Greenland and Antarctica**

EPICA Community Members\* (2006)

(\* A full list of authors appears at the end of App. H.)

Nature, 444, pp. 195-198, doi:10.1038/nature05301. See App. H

Own contributions:

- participation in the EPICA drilling project in Dronning Maud Land, processing of ice cores and treatment of samples

# 3

## Methods

### 3.1 Ice-core processing

The  $\sim 2774$  m long ice core used for this study was drilled at the Antarctic Kohnen station ( $75^{\circ}00.104'S$ ,  $0^{\circ}04.07'E$ ) in Dronning Maud Land with the framework of the European Project for Ice Coring in Antarctica (EPICA-DML) between 2001 and 2006. The ice core cutting-plan dedicates a 10 mm slat to physical-properties studies cut from the side of the  $\sim 100$  mm diameter core (Fig. 1 in Publication IV - App. D). This cut was done along 1 m pieces every 10 m on-site contemporarily after retrieval of the core. The main part of the core was transported to Bremerhaven uncut and split for further measurements (e.g. Publication VIII - App. H; Fischer et al., 2007; Ruth et al., 2007). From the on-site cut slats  $\sim 9$  cm long vertical thick sections (4 to 5 mm thick), with the long axis parallel to the vertical core axis, were prepared following description in Chap. 3.3 and used for microstructure mapping (Publication IV - App. D).

### 3.2 Creep-experiment and ice-sample production

In order to obtain bubble-free samples with a small grain size and without initial deformation features, samples were produced using large-grained bubble-free ice obtained by slow freezing of pure water under vibration. They were afterwards exposed to a phase transition at  $\sim 300$  MPa,  $\sim 233$  K (Fig. 3.1). This procedure enables us to produce small-volume samples (cylindrical:  $\sim 15$  to 20 mm diameter,  $\sim 50$  mm length) with small grain sizes (mean diameter  $\sim 0.6$  mm) due to nucleation/recrystallization processes during the phase

change from ice II/III to ice Ih. Apart from this procedure, only the hexagonal phase ice Ih is dealt with in the at-hand thesis. In contrast to standard sample production procedures, which usually include pressure sintering, our samples are bubble free, and do not exhibit deformational microstructures (Publication I - App. A).

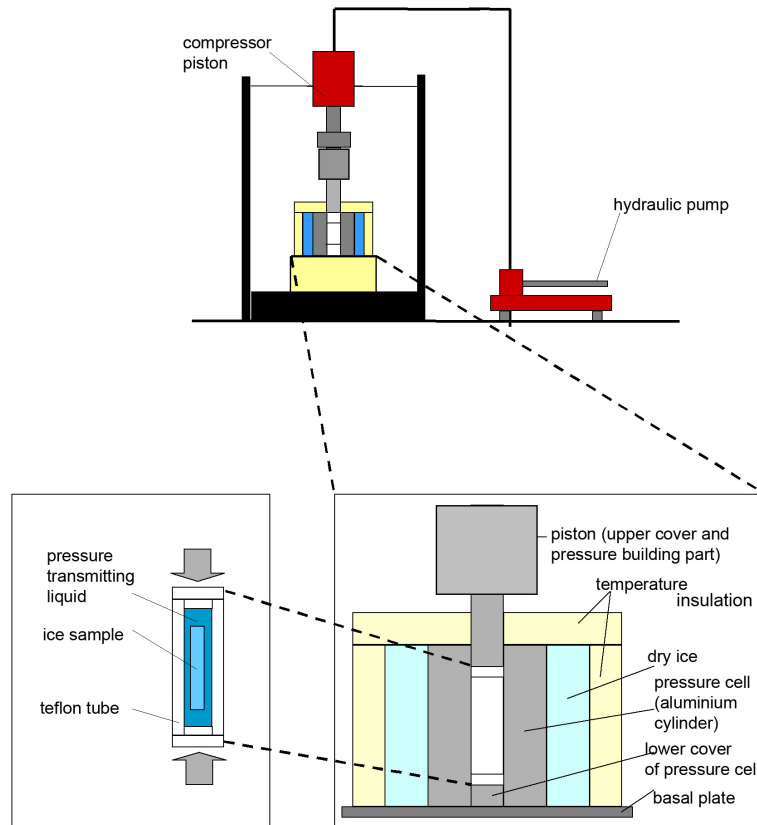


Figure 3.1: *Phase-transition device used for grain refinement of large-grained bubble-free ice to produce creep-test samples. The sample is floating in the teflon tube (see enlargement bottom left) and undergoes  $\sim 300$  MPa hydrostatic pressure. The phase change from ice Ih to ice II is performed fast (within  $\sim 5$  min) and slow (within  $\sim 5$  h) from ice II/III to ice Ih.*

The pristine samples were lathed and top and bottom surfaces were cut parallel with a microtome (cylindrical: 13 to 19 mm diameter, and 14 to 38 mm length). The creep machines we used consist of a basal plate, which is situated in a silicon oil bath, and a loading stage aligned between vertical rails (Fig. 3.2). The silicon oil bath is used to prevent the deforming sample from sublimation and to keep the temperature constant during the test. A displacement sensor is attached to the loading-stage, which moves down as

the sample is compressed, and measures the shortening of the sample. Table 1 in Publication I (App. A) gives a survey of all experiments conducted during the study.

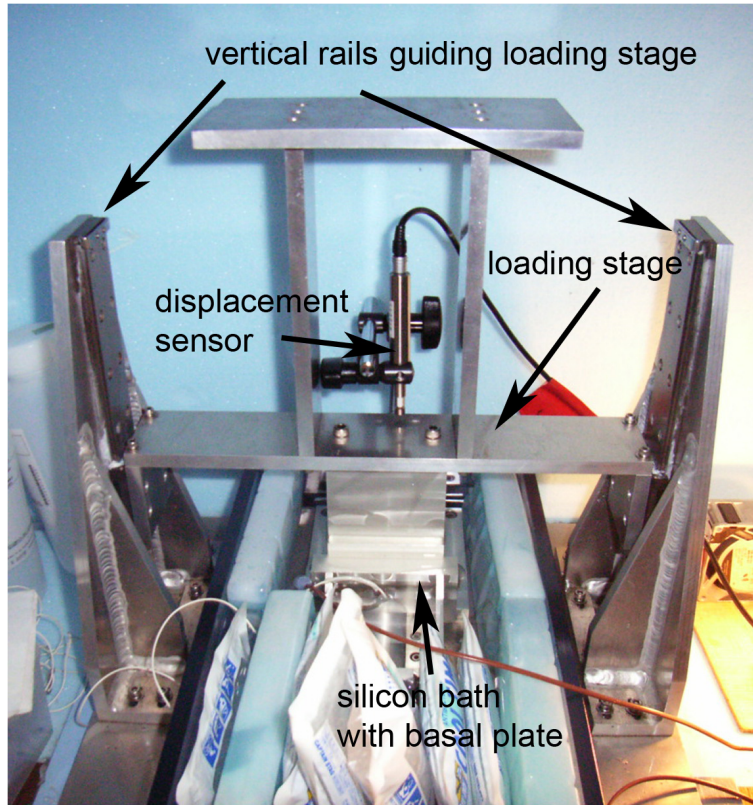


Figure 3.2: *Creep-test device used for deformation in uniaxial compression under constant load. The sample is located in the silicon bath.*

For each creep-test sample at least two thick sections ( $\sim 4$  to 6 mm thick), one cut horizontally and the other vertically, were prepared according to Chap. 3.3.

### 3.3 Sample preparation

With microtomes sections are cut carefully according to standard procedures. Polishing is achieved due to removal of microtome scratches by allowing the surfaces to sublimate (Publication IV - App. D). This works similar to chemical or thermal etching, a method widely employed in materials science to produce etch pits and grooves on the surfaces of metal, mineral and ceramic samples (e.g. Mullins, 1957; Nishida and Narita, 1996; Obbard et al., 2006a).

Sublimation enables a mirror-finishing of the surface and reveals sublimation grooves along grain/subgrain boundaries. Half an hour to half a day are needed to obtain a clear surface, with well-developed grain-boundary grooves. The sublimation time depends very much on ambient conditions (temperature, temperature gradient, humidity and air movement or wind) above the sample.

After the first surface of the sample is sufficiently clear, it is covered with a thin film of silicon oil to prevent over-sublimation. The section is frozen onto a glass plate and the second surface is prepared as described above.

### 3.4 Microscopic observations

The sections are mapped in microscopic resolution (1 pix=3.5  $\mu\text{m}$ ) in transmitted light using a system consisting of an optical microscope, a CCD camera and a xy-stage. In the case of large ice-core thick sections the system was computer-controlled and performed the acquisition automatically. The surface of the whole sample is represented by up to 1800 photomicrographs assembled to a mosaic image (Publication IV - App. D). For the creep-test samples we acquired images manually (Publication I - App. A), covering some typical detail of the section usually chosen close to the centre of the sample to get a representative overview. Some examples of microstructure mapping images are shown in (Fig. 3.3)

Overview pictures of the whole sample between crossed polarizers were used for grain-size and-shape measurements on creep-test samples.

### 3.5 Microstructure measurements

Microstructure mosaic images were assembled and digital image analysis was used to measure statistical data on grain morphology (grain size and shape) and on the occurrence of subgrain boundaries (their frequencies, shapes and location). Softwares used for this purpose are Image-Pro Plus (Media Cybernetics) and the public domain ImageSXM ([www.liv.ac.uk/~sdb/ImageSXM](http://www.liv.ac.uk/~sdb/ImageSXM), extended by S. D. Barrett from NIH Image, <http://rsb.info.nih.gov/nih-image>).

As grain boundaries appear as strong black lines in the photomicrographs (Fig. 3.3) they can be extracted by automatic image analysis using segmentation of the image by thresholding the grey-value image into a binary image (e.g. Russ, 2002, p. 333). In the case of creep-test samples, colored pictures taken between crossed-polarizers were segmented applying an edge-

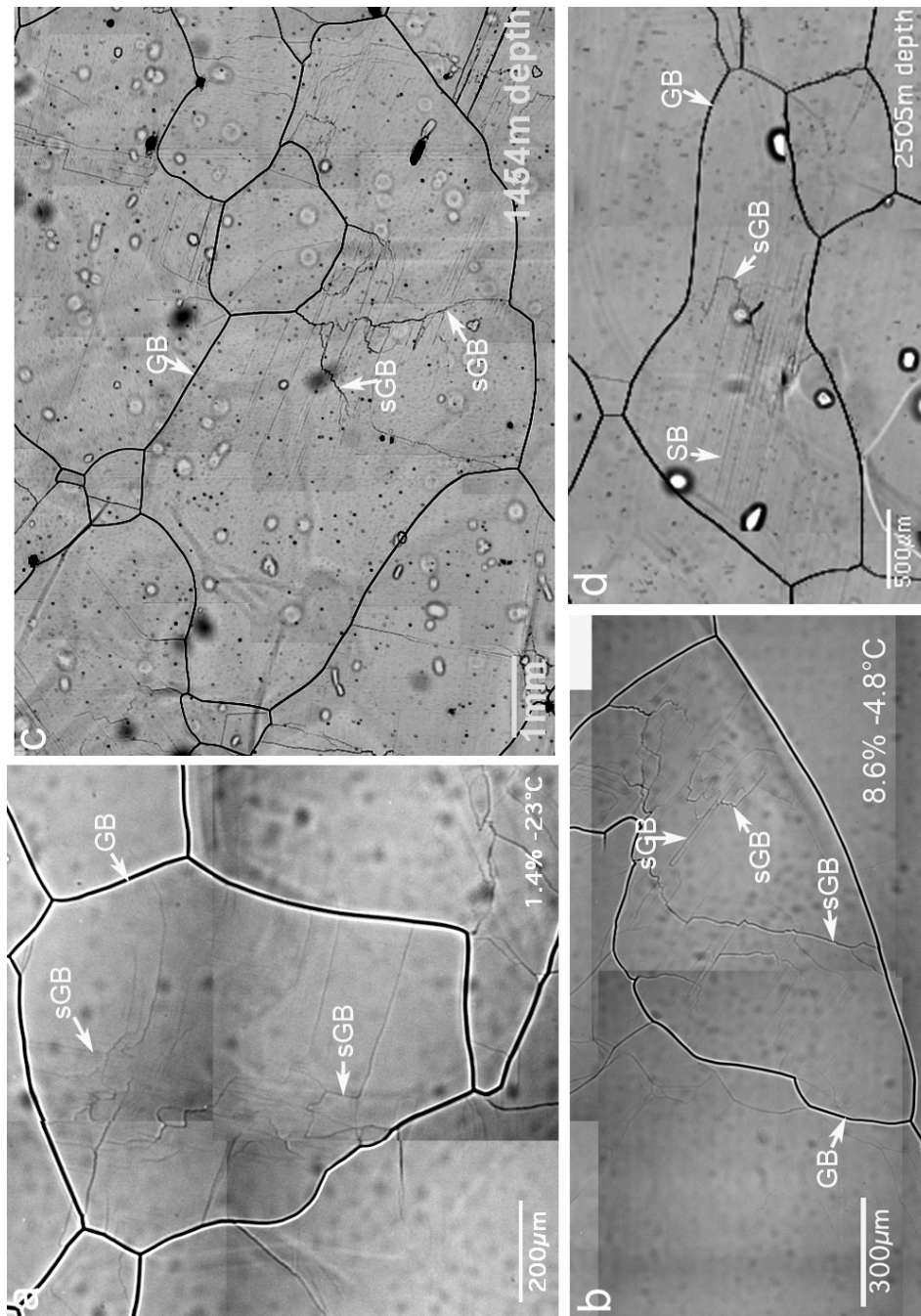


Figure 3.3: *Microstructure mapping examples from vertically cut thick sections. a and b: creep experiment samples. a: deformed at  $-23^{\circ}\text{C}$  with 0.35 MPa until 1.4% strain. b: deformed at  $-4.8^{\circ}\text{C}$  with 0.52 MPa until 8.6% strain. c and d: EDML ice core samples. Depths are given. Some microstructures are indicated by arrows: GB=grain boundary, sGB=subgrain boundary, SB=slip bands). Further examples can be seen in Publications I to V - App. A to E.*

detection sobel filter (e.g. Russ, 2002, p. 357). Both image-segmentation procedures produce a grain-boundary network, which needs some manual corrections. Such grain-boundary networks are used for automatic grain-size measurements and grain-shape characterization (e.g. Fig. 1 in Publication I - App. A).

In contrast to the deep grooves associated with grain boundaries, subgrain-boundary grooves are shallow (Saylor and Rohrer, 1999), have variable depths and appear as light to middle dark grey lines in the photographs. They are difficult to extract automatically as varying depths of grooves and varying background grey values do not allow global thresholds to detect these features in the images automatically. Subgrain-boundary density is calculated using either directly measured subgrain-boundary lengths or subgrain-boundary lengths, which were estimated from subgrain-boundary number and maximum length derived by grain radius (for details see Publication I - App. A and Publication II - App. B). The subgrain-boundary density is defined as the sum of all subgrain-boundary lengths per unit area.

Comparing the sublimation grooves along subgrain boundaries with respect to the crystal orientations, the state of grooving (intensity or depth) turned out to depend on crystal orientation. The typical shapes are easy to observe, if the sublimation surface is within  $\sim 30^\circ$  to the c-axis. Higher angles between c-axis and sublimation surface lead to fainter, less well defined lines in the microstructure map, which can lead to errors in recognition of the features. The reason for this dependence of sublimation on cutting-orientation is probably due to the fact that the best thermal grooving can be obtained if the boundary is perpendicular to the surface, whereas an oblique intersection of boundary and surface produces oblique and shallow grooves. Therefore a considerable amount of subgrain boundaries, which are difficult to characterize, can occur in grains "badly" oriented for sublimation grooving. For ice core samples the situation improves with depth, as preferred crystal-orientation fabric evolution enables sample cutting with many grains "nicely" oriented for sublimation. This leads to an underestimation of subgrain-boundary frequencies in samples with random crystal-orientation fabrics (e.g. shallower depth of the ice core and creep test samples). The data used for this thesis have been obtained from section images without any correction of dependence on crystal orientation, because the described effect was discovered only recently. Besides 3D-effects, such as sectioning effects of complicated grain shapes (e.g. Nishida and Narita, 1996), were not corrected.

## 3.6 Crystal-orientation measurements

For *c*-axes orientation measurements thin sections ( $\sim 0.5$ mm thick) were prepared following Chap. 3.3. They were derived using an automatic fabric analyzer system (Wilson et al., 2003) which enables complete measurement of the whole sample area in 15 to 30 min. Investigator v1.12 (Russell-Head, 2004) was used to determine *c*-axis orientation and misorientation angles. The estimated error of this method is  $\sim 1$  to  $3^\circ$  for the *c*-axis determination. Data are still preliminary because of local effects due to immaturity of the system. However, the impact on the statistics of local unknown effects was checked by repeated measurements with changing sample orientations and could be proved to be negligible. Among 60 to 600 grains per thin section,  $\sim 5$  to 10 grains show these effects.

The etch-pit method was used for several case studies on subgrain-boundary types using samples prepared after Chap. 3.3. Following Matsuda (1979) and Higuchi (1958) the polished sample surface (see Chap. 3.3) was coated with a solution of polyvinyl formal dissolved in ethylene dichloride, also called formvar solution. During evaporation of the solvent a plastic film adhered loosely to the sample surface. Small holes in the replica film enable preferred evaporation at these spots (e.g. Hobbs, 1974). Etch-pits developed by this method appear in variable but characteristic shapes, which can be imagined as negative figures of a part cut from a hexagonal column (Fig. 3.4). The orientation of all crystallographic axes can be obtained from angles or lengths of the geometric figures (Matsuda, 1979). Depending on the quality of the sample surface, which determines the sharpness of the etch-pit images, and handy skills during application of the formvar solution the error is  $\sim 5^\circ$  or higher.

First X-ray Laue diffractometry measurements of full crystallographic orientation were used to confirm that the sublimation grooves indeed represent all (sub)grain boundaries (Miyamoto and Hamann, unpublished data, June 2007). Accuracy of this method and therefore detection limit of misorientations is  $\sim 0.5^\circ$ . Details of this method can be found in Miyamoto et al. (2005).

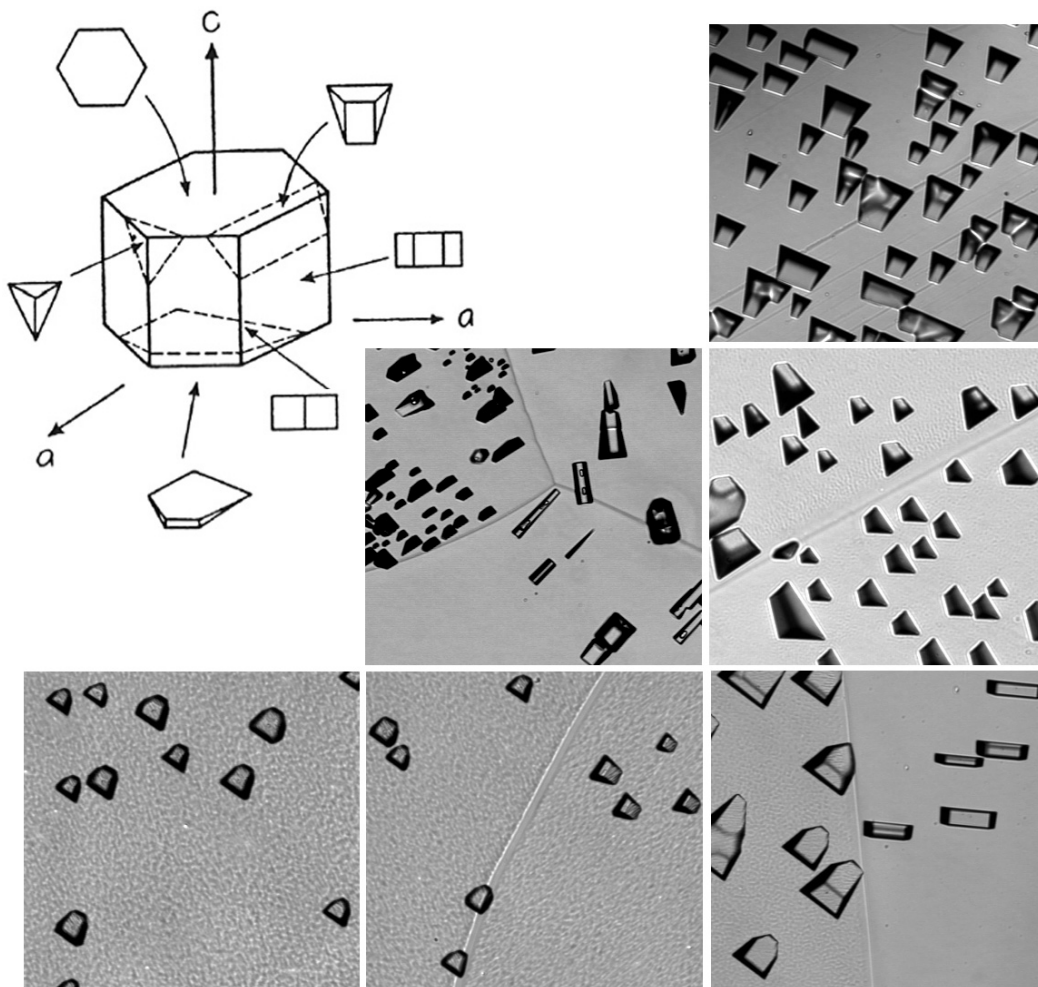


Figure 3.4: *Etch-pit method. Top left: Schematic diagram of various shapes of etch pits (from Higuchi, 1958). Examples in photomicrographs of EDML sample surfaces (1489.9 and 1558.9 m depth) after application of the method. Width of images is 300  $\mu\text{m}$ .*

## 4

# The EPICA Dronning Maud Land Ice Core and Comparison with Creep Experiments

In the following, only the most important findings of this study essential for the discussion of the new understandings are summarized. The original results can be found in the attached publications (App. A to H).

The main objective of the European Project for Ice Coring in Antarctica (EPICA) is to obtain a full documentation of the climatic and atmospheric record archived in Antarctic ice and then to compare this with the Greenland record to get new insights into the natural climate variability and mechanisms of fast climatic changes during the last glacial epoch (European Science Foundation, 1998). In this respect, the special features of the EDML core are the location in the Atlantic sector and the high-resolution climatic record due to a relatively high accumulation ( $64 \text{ kg m}^{-2} \text{ a}^{-1}$ , Oerter et al. (2000)), in comparison to other deep cores of only  $\sim 30 \text{ kg m}^{-2} \text{ a}^{-1}$  in East Antarctica. These characteristics enable the precise correlation of rapid warmer interstadials during the last glaciation period in the southern hemisphere (Antarctic Isotope Maxima) with those previously found in the northern hemisphere (Dansgaard-Oeschger events) (Publication VIII - App. H). Warming in Antarctica typically started significantly earlier than the respective event in Greenland (Publication VIII - App. H) and is linked in its intensity to the duration of cold events in Greenland, which supports a global climate coupling by a thermal bipolar seesaw mechanism performed by the ocean circulation system (Stocker and Johnsen, 2003).

Such high-resolution correlations give important insight into the global mechanisms of earth's climate, but require exact matching or dating of the ice cores and complementary archives as e.g. marine sediment cores. Besides

counting of visual annual layers, which is possible down to the last glacial-interglacial transition at EDML, relative chronologies using the correlation of certain atmospheric records (e.g. methane used by Blunier and Brook, 2001) or the stratigraphic matching of volcanic events (Ruth et al., 2007) are used for dating. A further independent dating method is based on assumptions for modeling ice-sheet dynamics (Huybrechts et al., 2007).

## 4.1 Ice mechanical behaviour

The core of an ice-sheet flow model is based on Glen’s flow law (Huybrechts, 2007), which describes ice deformation on a macroscopic scale and was derived from laboratory deformation tests (Glen, 1955)

$$\dot{\epsilon} = B \cdot \exp(-Q/RT) \cdot \sigma^n \quad (4.1)$$

where  $\dot{\epsilon}$  is the minimum strain rate,  $\sigma$  is the applied stress and  $T$  the absolute temperature.  $R$  is the gas constant,  $B$ ,  $n$  and  $Q$  are constants. The deformation test conditions were those of secondary creep (Glen, 1955), because this is the only uniquely identifiable stage during creep of ice (e.g. Jacka, 1984). Nevertheless, ice sheets are supposed to deform in steady-state tertiary creep, because large strains prevail and preferred orientation fabrics evolve (Paterson, 1983; Budd and Jacka, 1989; Jacka et al., 2003). Thus the flow parameter  $B$  is modified to empirically fit to field data, because it depends on a variety of factors, such as hydrostatic pressure, crystal orientations, impurity contents, microstructures and perhaps others (e.g. Paterson, 1994). Therefore, the actual deformation processes in natural ice still have to be considered as poorly known.

Furthermore, it was repeatedly mentioned, that high-stress deformation is significantly different from low-stress deformation, e.g. that the stress exponent for high stresses is close to 3, whereas it is smaller under low-stress conditions prevailing in ice sheets (e.g. Pimienta and Duval, 1987; Duval et al., 2000; Montagnat and Duval, 2004). A direct proof of validation of Glen’s flow law, in the sense of similarity of deformation mechanisms in fast-creep experiments and ice-sheet flow, does not exist to date. These open questions raise another necessary focus and objective during ice-coring projects: to study the physics and mechanics of natural ice.

A material’s mechanical response to stress is a change in the shape of an object (deformation), quantified as strain. After a reversible part of deformation (elastic deformation), the material deforms plastically (ductile deformation) until it fractures (brittle deformation), where the exact stress (tensile

strength) and time for the failure point mainly depend on strain rate, temperature and confining pressure (e.g. Evans et al., 1990).

While in the inner, i. e. main part of the large ice sheets the natural deformation is ductile flow, brittle behaviour plays an important role in the crevasse areas of especially outflow glaciers, ice streams and ice shelves. Technically, it has an important impact on the artificial ice-core-drilling process. After cutting a ring into the ice, the inner remaining cylinder is held by three core catchers (Fig. 1 in Publication VI - App. F), which pull the core until it breaks (Publication VI - App. F). Under such tensile conditions the behaviour is controlled by nucleation and propagation of cracks (Schulson et al., 1984; Schulson, 1999). Core-break data collected during drilling of the EDML core provide an empirical equation for the fracture-stress temperature dependence of ice (Publication VI - App. F) under high strain rates ( $\gg 10^{-5}\text{s}^{-1}$ ), which fits well with a theory of crack nucleation (Schulson, 1987). In the following, only ductile, plastic deformation is considered.

#### 4.1.1 Creep deformation of ice

Although the hexagonal ice is, compared to other solids, a rather brittle and hard material (Frost and Ashby, 1982), the natural deformation of ice sheets under gravitational flow is ductile. This is mainly due to the large time scales and thus low strain rates, but also due to the high homologous temperatures (absolute temperature divided by melting-point temperature) for ice masses on earth. The plasticity of ice is characterized by an unusually strong anisotropy of the monocrystal. It readily experiences deformation if a component of shear stress acts on the basal plane (easy glide orientation), whereas deformation parallel to the non-basal planes (Fig. 4.1) is much more difficult (hard glide orientation) (e.g. Nakaya, 1958; Hobbs, 1974). As a consequence of this single-crystal anisotropy in ice, in a polycrystal, c-axes rotate during deformation towards the compression axis and away from the extension axis with increasing strain (e.g. Jacka and Maccagnan, 1984; Azuma and Higashi, 1985). Hence preferred crystal-orientation fabrics evolve with depth in the ice sheets (e.g. Gow and Williamson, 1976; Herron and Langway, 1982; Alley, 1988; Lipenkov et al., 1989; Thorsteinsson et al., 1997; Azuma et al., 2000; Wang et al., 2003; DiPrinzio et al., 2005) affecting the viscosity in certain stress configurations and thus the hardness of the ice in certain depths. Such information is essential for ice-sheet flow models (e.g. Azuma, 1994; Placidi et al., 2004; Gillet-Chaulet et al., 2005; Thorsteinsson, 2006; Faria, 2006; Pettit et al., 2007). As ice cores are only few discrete spots, but ice sheet modeling is performed over large spaces, interpolation of the crystal-orientation data is necessary. A possibility to improve this interpolation in

some regions is shown in Publication VII (App. G). The anisotropy of the crystal results in different dielectric properties along the  $c$ -axis and in the basal plane of  $\Delta\epsilon' = \epsilon'_{\parallel} - \epsilon'_{\perp} \approx 0.035$ , which is roughly 1% of the permittivity of ice (Fujita et al., 2000). Thus, a change in crystal-orientation fabric has the potential to generate reflections detected by radio-echo sounding (RES). For the first time, a sharp change in the crystal orientation distribution from a vertical girdle fabric to a single maximum fabric as observed in EDML between  $\sim 2020$  m and  $\sim 2030$  m depth (Fig. 3 and 4 in Publication VII - App. G) could be directly evidenced to cause a RES peak, which cannot be explained by density or conductivity measured by dielectric profiling (DEP). Such RES horizons can be used in future to extrapolate the extent of the girdle/single maximum transition along radar profiles to characterize the ice flow.

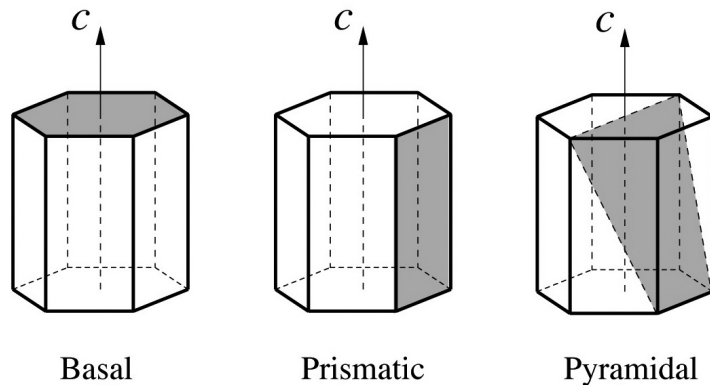


Figure 4.1: *Ice crystal schematized as a hexagonal prism with crystallographic planes indicated.*

## 4.2 Study of deformation-related recrystallization by analysis of microstructures

The evolution of a preferred crystal-orientation fabric is a mesoscopic indicator of plastic deformation accomplished by intracrystalline slip (Azuma and Higashi, 1985). As this intracrystalline slip is assumed to be the main deformation mechanism in ice (e.g. Duval et al., 1983; Pimienta and Duval, 1987; Duval et al., 2000; Montagnat and Duval, 2000), the actual deformation processes are acting below the grain scale, on the atomic scale. Thus, they are difficult to observe directly. However, these processes leave behind

traces observable with an optical microscope, if certain techniques are applied (Chap. 3). Investigations on this high resolution usually lack the overview necessary to obtain statistics over a significant ice volume (Montagnat et al., 2003a,b). The microstructure mapping method offers both, insight into small scale structures at high resolutions and overview over a considerable amount of material (Publication IV - App. D). Some data obtained with this method in samples from the EDML ice core (Publication II - App. B) and from creep tests with artificial ice (Publication I - App. A) are shown and compared in the following. Further data and explanations can be found in Publication I (App. A), Publication II (App. B) and Publication III (App. C).

#### 4.2.1 Subgrain boundaries, Grain boundaries and their interaction/controlled by deformation

**Subgrain-boundary occurrence** Grain substructures are formed by *polygonization* (after Poirier, 1985): under the action of localized stresses, some grains are divided into two or more parts. This process forms slightly misoriented subgrains separated by dislocation walls and is the beginning stage and basis for *rotation recrystallization*, a continuous dynamic recrystallization process (Humphreys and Hatherly, 2004), which is active during deformation in the whole volume of material. The division starts by alignment and arrangement of dislocations into walls forming subgrain boundaries (Weertman and Weertman, 1992), which may slowly develop into new grain boundaries.

How many grains undergo subgrain-boundary formation in the EDML ice core is revealed by statistics on the occurrence of grains with subgrain boundaries (Fig. 2a in Publication II - App. B). The data show that the majority of all grains have subgrain boundaries or dislocation walls and therefore support that polygonization indeed plays an important role in ice-sheet deformation. Subgrain boundaries have been described and attributed to rotation recrystallization in  $\sim 700$  m depth at Vostok (Lipenkov in Duval, 2000), in  $\sim 1300$  m at Dome Fuji (Azuma et al., 2000) and in  $\sim 380$  m depth at GRIP (Thorsteinsson et al., 1997). High amounts (half of all grains) of subgrain boundaries have been described in Dome Concordia ice core for  $\sim 150$  m depth (Wang et al., 2003). Although subgrain boundaries in ice have been observed and described before, a conclusive study focusing on subgrain boundaries, their statistical occurrence or detailed analysis on their geometry is still missing. The different observations in different ice cores probably result from different observation methods: if crossed polarizers are used to reveal subgrain boundaries, only some highly developed subgrain boundaries can be seen depending on the polarizers and grain orientation.

The sublimation method reveals a much greater number of less developed subgrain boundaries with smallest misorientations ( $\ll 0.5^\circ$ , verified by X-ray Laue measurements (Miyamoto and Hamann, unpublished data, June 2007)).

As another parameter to describe the occurrence of subgrain boundaries, a subgrain-boundary density is defined as the total subgrain-boundary length per area (Chap. 3.5). Subgrain-boundary densities in the EDML ice core also reveal that subgrain formation is active in all depths (Fig. 4.2 d) (Publication II - App. B). This finding contradicts the classical recrystallization regime concept: Three recrystallization regimes in the ice sheets have been described as occurring in a sequence with depth. Normal grain growth in the upper part of the ice sheet (grain-boundary energy driven, static recrystallization) is followed by rotation recrystallization in the middle (continuous dynamic recrystallization) and migration recrystallization in the lowermost layers (discontinuous dynamic recrystallization) (e.g. Pimienta and Duval, 1989; Alley, 1992; Duval and Castelnau, 1995; De La Chapelle et al., 1998; Duval, 2000; Montagnat and Duval, 2000). As subgrain boundaries are formed in all depths in EDML, neither the normal grain growth regime nor a distinct rotation recrystallization regime was detected (Publication II - App. B).

Microstructural investigations of experimentally deformed ice samples show that subgrain-boundary formation in creep tests is correlated to strain during primary creep stage. Primary creep terminated at  $\sim 1$  to 2% (Fig. 2 in Publication I - App. A) indicated by the minimum strain rate where concurrently a steady value of subgrain-boundary density is reached (Fig. 4.2 c). Thus, crystal-substructure evolution is connected with isotropic hardening (Publication I - App. A), which is the non-reversible component of strain during transient creep ascribed by Duval et al. (1983) to a period of zero strain rate during stress-drop experiments. The dislocation walls and subgrain boundaries act as obstacles for dislocations due to short-range interactions between dislocations, which is demonstrated by the increasing subgrain-boundary density during primary creep. As the production of obstacles and thus the hindering of dislocation motion is increasing, the strain rate decreases until a steady density of obstacles is reached at minimum strain rate.

**Grain-boundary morphology** Grain-boundary morphology is affected by grain-boundary migration. In the static case, without deformation, the grain-boundary surface energy drives the motion, which intends to minimize the grain-boundary area, thus to flatten the grain boundaries. As a consequence they move towards the center of its curvature and, as a boundary between two grains is concave towards the smaller grain, small grains shrink and disappear leading to *normal grain growth* (e.g. Alley et al., 1995;

Thorsteinsson, 1996; Humphreys and Hatherly, 2004). Therefore, normal grain growth leads to straight grain boundaries, regular grains and triple junctions of  $\sim 120^\circ$ , sometimes called *foam texture*, because it resembles a soap-cell network, which is a famous example of a wide variety of minimum-surface patterns in natural science (Weary and Rivier, 1984).

In the dynamic case when deformation is applied to the polycrystal, defects such as dislocations, dislocation walls and subgrain boundaries are introduced and thus internal strain energy accumulates. Grain-boundary migration tends to eliminate these defects and to reduce the strain energy by sweeping away dislocations which are located in front of a moving grain boundary (e.g. Passchier and Trouw, 1996; Humphreys and Hatherly, 2004; Duval and Montagnat, 2006). This process (*strain induced boundary migration - SIBM*), which belongs to discontinuous dynamic recrystallization, can result in irregular, complex grain-boundary shapes (examples see Fig. 3.3, Fig. 4.2 e,f, Fig. 5 in Publication I - App. A) if the driving pressure by internal strain energy exceeds the driving pressure by grain-boundary curvature (e.g. Beck and Sperry, 1950; Humphreys and Hatherly, 2004; Rios et al., 2005). This delicate pressure balance can be used to estimate dislocation densities from grain-boundary curvatures and subgrain-boundary densities (Publication I - App. A).

A measure for the irregularity of grains is the perimeter ratio: the ratio of convex perimeter against real perimeter (see Fig. 1 in Publication I - App. A and Uthus et al. (2005)). A regular object (e.g. circle, ellipse or rectangle) has perimeter ratio =1. Lower values describe the degree of irregularity. The irregularity of grains in creep tests is clearly related to strain (Fig. 4.2 e) indicating the increasing internal strain energy from very small strains onward.

Grain-boundary shapes in EDML are complex and irregular as well (Fig. 3.3 c,d and Fig. 1 and 4 in Publication II - App. B). Similar to the subgrain-boundary density, the mean perimeter ratio does not change significantly with depth compared to the variation of data (Fig. 4.2 f). The irregularity of the shapes of grain boundaries suggests difficulties in order with grain boundary sliding as suggested as a deformation mechanism (Goldsby and Kohlstedt, 1997, 2001; Goldsby, 2006).

**Strain/Stress localization** Distributions of crystal substructures within grains are very similar in ice-core and in creep-test samples. In both cases subgrain boundaries are stronger and preferably accumulated close to grain boundaries forming a highly heterogeneous spacial distribution (e.g. Fig. 7 and 9 in Publication I - App. A and Fig. 1, 4 and 5 in Publication II -

App. B) with a highly deformed grain mantle and a less strained grain core (Publication IV - App. D). An observed increased subgrain-boundary density at prominent parts of complex grain-boundary geometries strikingly suggests, that strain accumulation is the rule rather than the exception in deforming ice in general. The frequent occurrence of grain-boundary curvatures and the surplus of subgrain boundaries on their convex sides (and hence the excess of driving pressure exerted by internal strain energy over driving pressure exerted by grain-boundary tension) indicates, that high dislocation densities can occur locally ((Fig. 10 and 11 in Publication I - App. A and Fig. 5 d in Publication II - App. B)). These complex grain geometries evolve due to bulging of grain boundaries in experimentally deformed ice as well as in polar ice (Publication II - App. B and Publication I - App. A). This is part of an intense feed-back process where complex geometries lead to complicated stress interaction at grain boundaries in polycrystalline ice, which lead to strain localization and localized dislocation formation exerting strain energy, that, in turn, restart again bulging of grain boundaries and SIBM.

### **Implications from comparison EDML data - creep-test data on micro-mechanisms**

Experiments have been conducted at stresses between 0.18 and 0.52 MPa (Publication I - App. A). Compared with the polar ice sheets, where driving stresses are typically lower than 0.1 MPa, deformation rates are rather high. Besides differences in strain rates, total strains in experiments reached a maximum of  $\sim 8.6\%$  only, whereas much higher deformation is expected in the ice core samples (Paterson, 1983; Budd and Jacka, 1989; Jacka et al., 2003). Furthermore, other possible variables influencing creep or deformation-related recrystallization (e.g. impurities, temperature, grain size, fabrics) cover a striking range of values along the ice core and in the samples. Therefore it is surprising that the mean subgrain-boundary density is of the same order in experiments ( $\sim 0$  to  $4 \text{ mm}^{-1}$ , see Fig. 4.2 c, Publication I - App. A) and in EDML ice core ( $\sim 1$  to  $3 \text{ mm}^{-1}$ , see Fig. 4.2 d, Publication II - App. B).

A slight difference in the scattering of measured values (0 to  $\sim 6 \text{ mm}^{-1}$  in creep-test samples,  $\sim 3 \text{ mm}^{-1}$  in EDML ice core, Fig. 4.2 c,d) and the slightly lower average values in ice deformed at low stresses in the ice sheet can be explained by processes which reduce the dislocation density (Publication III - App. C). They can act more extensively with the prolonged duration of creep in the slowly deforming ice sheet. Montagnat and Duval (2000) incorporated these processes into a deformation model. The two main processes are recovery and dynamic recrystallization which compete, because both are driven by the stored internal strain energy.

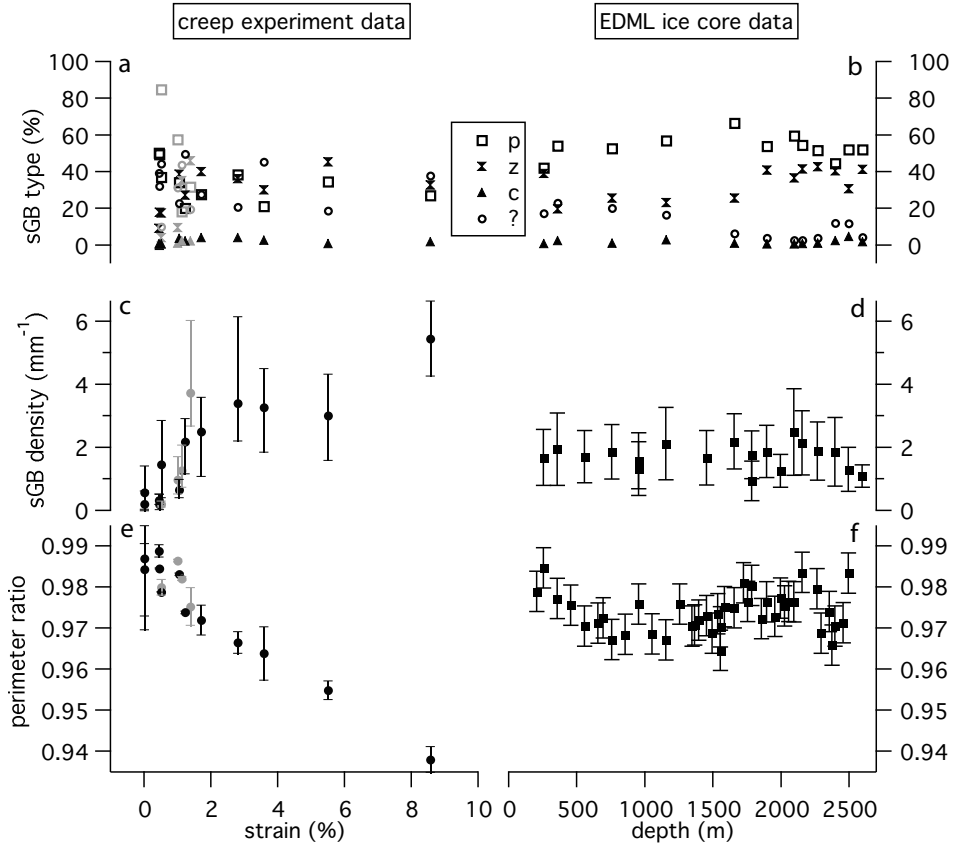


Figure 4.2: *Evolution of microstructure parameters. a and b: subgrain-boundary type frequency ( $p$ =parallel type,  $z$ =zigzag-type,  $c$ =classical polygonization type, as described by Nakaya (1958),  $?$ =ambiguous shape and arrangement). c and d: mean subgrain-boundary density. e and f: mean grain perimeter ratio indicating irregularity of grains (see text). Ordinate is identical in all graphs. Left: during creep experiments. Error bars indicate the scatter of data in four to six measured values. Black markers represent experiments at  $\sim -4.5^\circ\text{C}$ , grey markers represent  $\sim -23^\circ\text{C}$ . Right: EDML samples. Error bars give the standard deviation.*

Two primary processes are involved in recovery: annihilation of dislocations and rearrangement of dislocations (Humphreys and Hatherly, 2004). Annihilation can remove dislocations by connecting two dislocations of opposite signs and is therefore dependent on the ease of operation of climb and cross slip (Föll, 2000). The low stacking fault energy of ice (Hondoh, 2000), which leads to wide dissociation of dislocations in the basal plane, hinders climb and cross slip (Humphreys and Hatherly, 2004). However, it was observed to occur with aging (Higashi et al., 1988) and may thus play some role in the ice sheet, but not in the high-stress creep tests.

The second recovery process, the rearrangement of dislocations, creates lower energy configurations and leads to formation of dislocation walls and subgrain boundaries (*polygonization*). Further gathering of dislocations leading to *rotation recrystallization*, converts subgrain boundaries into grain boundaries. Therefore the higher subgrain-boundary density values in experimentally deformed samples than in EDML samples (Fig. 4.2 c,d) does not necessarily suggest a higher amount of rearrangement of dislocations during creep tests, because dislocations in the ice sheet can just "join" an existing dislocation wall, instead of forming a new one. However, misorientation data of EDML samples do not prove intensive further gathering of dislocations and subsequent subgrain rotation, because a surplus of small-angle misorientations of neighbouring grains with respect to random grain-pair misorientations was not found (Fig. 3 in Publication II - App. B).

As another process, *SIBM* restores the material properties more efficiently than recovery, because it can remove dislocations effectively by eliminating many dislocation all at once. This is possible due to the fact that they are typically accumulated locally close to grain boundaries (Publication II - App. B and Publication I - App. A, examples see Fig. 3.3, Fig. 7 in Publication I - App. A) caused by strain localization (Wilson and Zhang, 1994; Zhang and Wilson, 1997; Mansuy et al., 2000). The difference between experimentally-deformed and ice-core samples in terms of the degree of irregularity of grains (defined in Fig. 1 in Publication I - App. A) gives insight into the delicate balances of the competing recovery and SIBM under slow and fast deformation: Irregularity during creep tests clearly increases with strain (Fig. 4.2 e), which directly reflects the dislocation production. Compared to the values of grain irregularities from ice core samples they exhibit extreme values (Fig. 4.2 e,f). In these high-stress regimes, recovery seems to be relatively unimportant compared to the generation of defects by deformation. During application of low stresses, grains are still significantly irregular (Fig. 4.2 f), but as total accumulated strains should be higher in the ice sheet than in experiments, recovery, which also reduces dislocation density, seems to inhibit the evolution of highest irregularities of grains (Fig. 4.2 e,f) by SIBM.

Microstructure data indicate that the relation of dislocation-production rate to dislocation-reduction rate is significantly higher in experimentally deformed samples, which leads to more extreme values for subgrain-boundary density and grain-boundary irregularity (Fig. 4.2 c-f). The comparison of the two data sets indicates, that the reason for different high-stress and low-stress behaviour might be, that recovery is mainly time dependent, whereas dislocation production is deformation dependent. Natural polar ice does not completely work harden, namely accumulate as many dislocations as the creep-test samples and reach maximum subgrain-boundary density as it seems to be the case in creep tests. Thus, processes reducing the dislocation density are clearly counterbalancing dislocation production and strain hardening in the natural ice. From the microstructural point of view, the findings might be interpreted, that slow deforming ice sheet ice can be regarded as more or less permanently being at the transition from primary creep to secondary creep. This supports the assumption, that Glen's flow law can be used for ice sheet modeling. However, the evolution of an anisotropic crystal-orientation distribution was not yet included in this discussion and further investigations to cover the plurality of probable variables (e.g. impurities) influencing these processes are necessary.

#### 4.2.2 Subgrain-boundary types

Considering the significantly different formation and deformation conditions in terms of e.g. temperature, impurities, grain size, strain and strain rate of the observed ice samples it is surprising at first sight that the same types of subgrain boundaries (Fig. 6 a in Publication II - App. B) were found in experimentally deformed ice as well as in natural ice. These characteristic types can be distinguished by their shapes and arrangements (Fig. 3.3) and with respect to the crystal lattice orientation (Fig. 4.3). It is known from other materials that the orientation of subgrain boundaries depends on the orientation of slip systems of dislocations accumulating in the grain (Trepied et al., 1980). As detailed observation and analysis of these characteristic arrangements can be useful to study dislocation action in polycrystalline ice, the observed types shall be described here in detail. This at-hand thesis describes and characterizes different types of subgrain boundaries for the first time.

The subgrain-boundary formation in single crystal ice was first described by Nakaya (1958). Bending of the basal plane in the direction of the c-axis, rearrangement of basal edge dislocations into walls and subsequent splitting of the grain lead to formation of subgrain boundaries (Weertman and Weertman, 1992; Hull and Bacon, 2001). This process produces straight subgrain

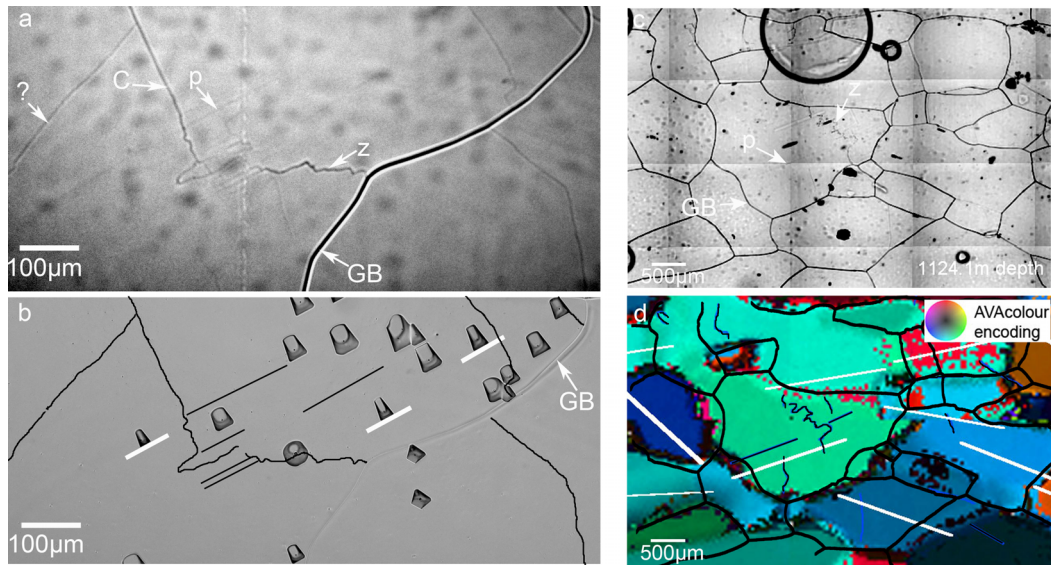


Figure 4.3: *Subgrain-boundary types and crystal orientation. a: Creep-test sample. b: Same section as a, after application of etch-pit method. Subgrain boundaries (thin black lines) are redrawn after a. Basal plane traces (white bars) are drawn after etch pits (see Fig. 3.4). c: EDML sample. d: AVA image (Achsenverteilungsanalyse) of c-axes of the same section as c (legend as stereographic projection see white box) measured with automatic fabric analyzer (Wilson et al., 2003). Subgrain boundaries (thin black lines) and grain-boundary network (thick black lines) are drawn after c. Differences in fit of grain-boundary network with AVA-image is due to oblique grain boundaries. Basal plane traces (white bars) are drawn after c-axes measurements. (GB=grain boundary, p=parallel type subgrain boundary, z=zigzag type subgrain boundary, c=classical polygonization type subgrain boundary as described by Nakaya (1958)). Further examples can be seen in Fig. 6 in Publication II - App. B.*

boundaries perpendicular to the basal plane, which cross the grain. Such arrangement of subgrain boundaries can indeed be observed in the sublimation grooves revealed by microstructure mapping (see example in Fig. 3.4 and 4.3 a, b) and are called c-type subgrain boundaries indicating the resemblance of Nakaya's "classical" description. First X-ray Laue measurements confirm that the majority of subgrain boundaries arranged in this configuration indicate a misorientation obtained by rotation around one a-axis (Miyamoto and Hamann, unpublished data, June 2007). They are interpreted as basal tilt boundaries (Fig. 6 b in Publication II - App. B and Publication I - App. A). Actually this type of subgrain boundaries is most rare in artificial creep test samples as well as in polar ice (Fig. 4.2 a,b). Characteristically, c-type subgrain boundaries pass into another type characterized by its irregular, usually zig-zag shape.

Subgrain boundaries of this related zigzag or step shape (called z-type) are also arranged at an angle to the basal plane, with short segments running parallel to this plane (see example in Fig. 4.3). Typically, z-subgrain boundaries do not cross a grain completely but fade out with some distance to the high angle grain boundary. They can be interpreted as a sequence of boundaries with a diversity of dislocation types involved (e.g. basal edge and non-basal edge dislocations) (Publication I - App. A). Clearly further investigations with high resolution full crystal orientation methods (Montagnat et al., 2003a,b; Iliescu et al., 2004; Miyamoto et al., 2005; Obbard et al., 2006b) are necessary.

The third distinguishable type is called p-type subgrain boundary, because it appears in swarms exactly parallel to each other. Besides the alignment in swarms, its parallel arrangement with respect to the basal plane of the crystal lattice is remarkable (Fig. 4.3). Considering their arrangement and shape, three possible explanations can be given: basal twist boundaries, non-basal tilt boundaries or micro-shear zones (Publication I - App. A, Publication II - App. B and Publication V - App. E). Basal twist boundaries are composed of screw dislocations in the basal plane (Fig. 6 b in Publication II - App. B). The commonness of this dislocation type in ice has been shown (e.g. in Higashi et al., 1988; Hondoh, 2000; Montagnat et al., 2003b). Basal twist boundaries produce misorientations which can be described by rotation around the c-axis. First X-ray Laue measurements have confirmed their existence (Miyamoto and Hamann, unpublished data, June 2007).

Non-basal tilt boundaries can be imagined as a pile-up of non-basal edge dislocations. They have been confirmed by preliminary X-ray Laue measurements as well (Miyamoto and Hamann, unpublished data, June 2007), indicating a rotation around one a-axis. The typical macroscopic anisotropy of ice deformation is thought to be caused by peculiar properties of the dis-

locations, viz. that non-basal dislocations do not contribute significantly to the deformation of ice, because they occur as short segments due to the strong tendency of ice dislocations to dissociate into partials due to its small stacking fault energy (Hondoh, 2000). The process producing such a high amount of non-basal dislocations to build up subgrain boundaries is still not fully understood and will be topic of further investigations.

The alternative explanation as micro-shear zones describes shearing-off of a prominent part of a grain, which is penetrating a neighbour (Fig. 6 c in Publication II - App. B). This shear occurs along the basal plane that is aligned parallel to long grain boundary chains. This process was observed during the deformation of octachloropropane (Bons and Jessell, 1999) and considered as a possible cause for sudden change in ice softness in the depth range 2385 m to  $\sim$ 2575 m of EDML (Publication V - App. E).

At this point shall be called to mind that the arrangement and shapes of sublimation grooves along subgrain boundaries described above is most easily observable if the sublimation surface is within  $\sim 30^\circ$  to the *c*-axis (Chap. 3.5). Thus a considerable amount of unidentifiable types is observed (Fig. 4.2 a,b), which, in the case of ice core samples decreases with depth (Fig. 4.2 b), as fabric enhancement enables vertical sections with many grains "nicely" oriented for sublimation.

### **Implications from subgrain-boundary types on micromechanisms**

As mentioned above, it is interesting that the types of observed grain substructures are the same in deformed artificial ice and ice from the EDML ice core. It is especially interesting, as the experiments reached at most secondary creep whereas polar ice is supposed to deform in steady-state tertiary creep. First of all, the similarity in subgrain-boundary observations directly proves the relevance of dislocation creep in polar ice (supporting Duval et al., 1983; Pimienta and Duval, 1987; Montagnat and Duval, 2000) and under the chosen experimental conditions.

Moreover, due to the observation of the similarity of grain substructures and the high mechanical anisotropy of ice it can be assumed that these structures indeed are characteristic traces of deformation processes, displaying a material peculiarity in its response to creep. If the resolved shear stress is not exactly parallel to the *c*-axis, which is unlikely in the highly complex stress situation for grains in polycrystals, ice responds in all other stress configurations firstly by the activation of the dominant slip system, the basal plane. Other slip systems should contribute much less to ice deformation (Hondoh, 2000), because of the peculiar properties of dislocations in ice. However, non-basal slip has been proposed before as a basal-slip-accommodating process

(Hutchinson, 1977; Duval et al., 1983; Castelnau et al., 1996, 1997), which is necessary to provide strain compatibility among neighbouring grains, to avoid the occurrence of microcracks and voids. The significant occurrence of subgrain boundaries, which cannot only be explained by arrangement of basal dislocations (p and maybe z in Fig. 4.2 a,b), gives first experimental evidence of the importance of non-basal glide also in slowly deforming natural ice. Further investigations including subgrain-boundary lengths of all types and full crystal-misorientation measurements can bring clarity on which amount non-basal glide is possible or necessary under different deformation conditions.

# 5

## Conclusions

Systematic analysis of deformation effects by microstructure mapping along the whole length of the EPICA Dronning Maud Land ice core reveal discrepancies with the standard recrystallization model describing three recrystallization regimes with increasing depth (Normal Grain Growth, Rotation Recrystallization and Migration Recrystallization). Instead, subgrain formation and strain induced boundary migration indicate, that both dynamic recrystallization processes (rotation and migration) occur concurrently in all depths of the ice sheet.

The microstructures used as evidences for the dynamic recrystallization (subgrain boundaries, grain morphology) have been tested to indeed originate from deformation by reproducing them artificially in creep tests. This independent method affirms the value of the structures under flow conditions. Besides, a correlation of substructure evolution and strain hardening was shown, which can now explain the previously described macroscopic behaviour of ice during primary creep. The grain-size reducing effect of deformation could be proven unambiguously.

The consistency in grain-substructure observations in experimentally deformed and Antarctic ice identify dislocation creep as deformation process. The more moderate values and scatters of subgrain-boundary densities and grain-boundary irregularities in ice sheets indicate, that dislocation density-decreasing processes (recovery and dynamic recrystallization) play a far more important role under low-stress conditions. Recovery by rearrangement of dislocations can be identified in subgrain-boundary formation. The delicate interplay of dislocation production, recovery and dynamic recrystallization controls the degree of work hardening and therefore the softness of the material, apart from fabric evolution.

According to macroscopic observations, the population of non-basal dislocations should be much smaller than that of basal dislocations, which are

responsible for dislocation creep of ice. However, significant amounts of non-basal dislocations, enough even to form subgrain boundaries have to be taken into account, to explain all the observed subgrain-boundary types.

## 6

# Outlook

Further investigations with high-resolution crystallographic methods (X-ray Laue diffractometry and Elektron Backscatter diffractometry) promise further characterization and quantification of subgrain boundary types, their formation processes and role during deformation of polycrystalline polar ice. Insight into the activation of dislocation types, which can be obtained by these measurements, contributes to our understanding of the mechanical peculiarities of ice.

The finding about the single dynamic recrystallization regime will be processed in theoretical and numerical modeling with ELLE ([www.materials-knowledge.org/elle](http://www.materials-knowledge.org/elle)) to eventually develop a new recrystallization- and grain-growth theory for ice sheets.

The ongoing measurements and processing of crystal-orientation fabrics data in association with mesoscopic (stratigraphic layering recorded by linescanning method, [http : //doi.pangaea.de/10.1594/PANGAEA.208005](http://doi.pangaea.de/10.1594/PANGAEA.208005)) and microscopic structures (grain shapes obtained from microstructure mapping) promise insight into stress configurations and deformation states in the bottom part of the EDML ice core.

# References

- Alley, R., Gow, A., and Meese, D. (1995). Mapping c-axis fabrics to study physical processes in ice. *J. Glaciol.*, 41(137):197–203.
- Alley, R. B. (1988). Fabrics in polar ice sheets: Development and prediction. *Science*, 240:493–495.
- Alley, R. B. (1992). Flow-law hypotheses for ice-sheet modelling. *J. Glaciol.*, 38:245–256.
- Alley, R. B., Clark, P. U., Huybrechts, P., and Joughin, I. (2005). Ice-sheet and sea-level changes. *Science*, 310:456–460.
- Azuma, N. (1994). A flow law for anisotropic ice and its application to ice sheets. *Earth Planet. Sci. Lett.*, 128:601–614.
- Azuma, N. and Higashi, A. (1985). Formation processes of ice fabric pattern in ice sheets. *Ann. Glaciol.*, 6:130–134.
- Azuma, N., Wang, Y., Yoshida, Y., Narita, H., Hondoh, T., Shoji, H., and Watanabe, O. (2000). Crystallographic analysis of the Dome Fuji ice core. In Hondoh, T., editor, *Physics of Ice Core Records*, pages 45–61, Sapporo. Hokkaido University Press.
- Beck, P. A. and Sperry, P. R. (1950). Strain induced grain boundary migration in high purity aluminium. *J. Appl. Phys.*, 21(2):150–152.
- Bindoff, N., Willebrand, J., Artale, V., Cazenave, A., Gregory, J., Gulev, S., Hanawa, K., Quere, C. L., Levitus, S., Nojiri, Y., Shum, C., Talley, L., and Unnikrishnan, A. (2007). Observations: Oceanic climate change and sea level. In Solomon, S., Qin, D., Manning, M., Chen, Z., Marquis, M., Averyt, K., Tignor, M., and Miller, H., editors, *Climate Change 2007: The Physical Science Basis. Contribution of Working Group I to the Fourth Assessment Report of the Intergovernmental Panel on Climate Change*, pages 385–432. Cambridge University Press, Cambridge, United Kingdom and New York, NY, USA.

- Blunier, T. and Brook, E. J. (2001). Timing of Millennial-Scale Climate Change in Antarctica and Greenland During the Last Glacial Period. *Science*, 291(5501):109–112.
- Bons, P. D. and Jessell, M. W. (1999). Micro-shear zones in experimentally deformed OCP. *J. Struct. Geol.*, 21:323–334.
- Budd, W. F. and Jacka, T. H. (1989). A review of ice rheology for ice sheet modelling. *Cold Reg. Sci. Technol.*, 16:107–144.
- Castelnau, O., Canova, G., Lebensohn, R., and Duval, P. (1997). Modelling viscoplastic behavior of anisotropic polycrystalline ice with a self-consistent approach. *Acta Mater.*, 45(11):4823–4834.
- Castelnau, O., Duval, P., Lebensohn, R., and Canova, G. R. (1996). Viscoplastic modeling of texture development in polycrystalline ice with a self-consistent approach: Comparison with bound estimates. *J. Geophys. Res.*, 101(B6):13,851–13,868.
- Dansgaard, W., Johnsen, S. J., Clausen, H. B., Dahl-Jensen, D., Gundestrup, N. S., Hammer, C. U., Hvidberg, C. S., Steffensen, J. P., Sveinbjornsdottir, A. E., Jouzel, J., and Bond, G. (1993). Evidence of general instability of past climate from a 250-kyr ice-core record. *Nature*, 364:218–220.
- De La Chapelle, S., Castelnau, O., Lipenkov, V., and P., D. (1998). Dynamic recrystallization and texture development in ice as revealed by the study of deep ice cores in antarctica and greenland. *J. Geophys. Res.*, 103(B3):5,091–5,106.
- DiPrinzio, C. L., Wilen, L. A., Alley, R. B., Fitzpatrick, J. J., Spencer, M. K., and Gow, A. J. (2005). Fabric and texture at Siple Dome, Antarctica. *J. Glaciol.*, 51(173):281–290.
- Duval, P. (2000). Deformation and dynamic recrystallization of ice in polar ice sheets. In Hondoh, T., editor, *Physics of Ice Core Records*, pages 103–113, Sapporo. Hokkaido University Press.
- Duval, P., Arnaud, L., Brissaud, Montagnat, M., and De La Chapelle, S. (2000). Deformation and recrystallization processes of ice from polar ice sheets. *Ann. Glaciol.*, 30:83–87.
- Duval, P., Ashby, M. F., and Andermann, I. (1983). Rate-controlling processes in the creep of polycrystalline ice. *J. Phys. Chem.*, 87:4066–4074.

- Duval, P. and Castelnau, O. (1995). Dynamic recrystallisation of ice in polar ice sheets. *J. Physique*, 5:197–205.
- Duval, P. and Montagnat, M. (2006). Physical deformation modes of ice in glaciers and ice sheets. In Knight, P. G., editor, *Glacier Science and Environmental Change*, pages 303–308. Blackwell Publishing.
- EPICA community members (2004). Eight glacial cycles from an antarctic ice core. *Nature*, 429:623–628.
- EPICA community members (2006). One-to-one coupling of glacial climate variability in greenland and antarctica. *Nature*, 444:195–198.
- European Science Foundation (1998). European project for ice coring in antarctica (EPICA). <http://www.esf.org/activities/research-networking-programmes/life-earth-and-environmental-sciences-lesc/completed-esf-research-networking-programmes-in-life-earth-and-environmental-sciences/european-project-for-ice-coring-in-antarctica-epica-page-1/more-information.html>.
- Evans, B., Fredrich, J. T., and Wong, T.-F. (1990). The brittle-ductile transition in rocks. In Duba, A. G., Durham, W. B., Handin, J. W., and Wang, H. F., editors, *Geophysical Monograph*, volume 56, pages 1–20. Am. Geophys. Union.
- Faria, S. (2006). Creep and recrystallization of large polycrystalline masses. Part III: Continuum theory of ice sheets. *Proc. Roy. Soc. London*, A462(2073):2797–2816.
- Faria, S. H., Kipfstuhl, S., Kuhs, W. F., Freitag, J., Hamann, I., Azuma, N., Murshed, M. M., and Klein, H. (2007). Multiscale structures in the antarctic ice sheet part i: Inland ice. In Hondoh, T., editor, *Physics of Ice Core Records*, volume 2, page 23. submitted.
- Fischer, H., Fundel, F., Ruth, U., Twarloh, B., Wegner, A., Udisti, R., Becagli, S., Castellano, E., Morganti, A., Severi, M., Wolff, E., Littot, G., Röthlisberger, R., Mulvaney, R., Hutterli, M. A., Kaufmann, P., Federer, U., Lambert, F., Bigler, M., Hansson, M., Jonsell, U., de Angelis, M., Boutron, C., Siggaard-Andersen, M.-L., Steffensen, J. P., Barbante, C., Gaspari, V., Gabrielli, P., and Wagenbach, D. (2007). Reconstruction of millennial changes in dust emission, transport and regional sea ice coverage using the deep epica ice cores from the atlantic and indian ocean sector of antarctica. *Earth Planet. Sci. Lett.*, 260:340–354.

- Föll, H. (2000). Defects in crystals. *Hyperscript*. <http://www.techfak.uni-kiel.de/matwis/amat/defen/index.html>.
- Frost, H. J. and Ashby, M. F. (1982). *Deformation mechanism maps - The plasticity and creep of Metals and Ceramics*. Pergamon Press.
- Fujita, S., Matsuoka, T., Ishida, T., Matsuoka, K., and Mae, S. (2000). A summary of the complex dielectric permittivity of ice in the megahertz range and its application for radar sounding of polar ice sheets. In Hondoh, T., editor, *Physics of Ice Core Records*, pages 185–212. Hokkaido University Press.
- Gillet-Chaulet, F., Gagliardini, O., Meyssonier, J., Montagnat, M., and Castelnau, O. (2005). A user-friendly anisotropic flow law for ice-sheet modelling. *J. Glaciol.*, 51(172):3–14.
- Glen, J. W. (1955). The creep of polycrystalline ice. *Proc. Roy. Soc. London*, A228:519–538.
- Goldsby, D. L. (2006). Superplastic flow of ice relevant to glacier and ice-sheet mechanics. In Knight, P. G., editor, *Glacier Science and Environmental Change*, pages 308–314. Blackwell Publishing.
- Goldsby, D. L. and Kohlstedt, D. L. (1997). Grain boundary sliding in fine-grained Ice I. *Scripta Mat.*, 37(9):1399–1406 (8).
- Goldsby, D. L. and Kohlstedt, D. L. (2001). Superplastic deformation of ice: experimental observations. *J. Geophys. Res. (Solid Earth)*, 106(B6):11,017–11,030.
- Gow, A. J. and Williamson, T. (1976). Rheological implications of the internal structure and crystal fabrics of the West Antarctic ice sheet as revealed by deep core drilling at Byrd Station. *CRREL Rep.*, 76(35):1665–1677.
- GRIP Project Members (1993). Climate instability during the last interglacial period recorded in the GRIP ice core. *Nature*, 364:203–207. Please be aware that these conclusions have been modified in the light of later findings. Please see later papers for more details.
- Grotes, P., Stuiver, M., White, J., Johnsen, S., and Jouzel, J. (1993). Comparison of oxygen isotope records from the GISP2 and GRIP Greenland ice cores. *Nature*, 366:552–554.

- Herron, S. L. and Langway, C. C. (1982). A comparison of ice fabrics and textures at Camp Century, Greenland and Byrd Station, Antarctica. *Ann. Glaciol.*, 3:118–124.
- Higashi, A., (editor), Fukuda, A., Shoji, H., Oguro, M., Hondoh, T., and Goto-Azuma, K. (1988). *Lattice defects in ice crystals*. Hokkaido University Press, Sapporo, Japan.
- Higuchi, K. (1958). The etching of ice crystals. *Acta Metall.*, 6:636–642.
- Hobbs, P. V. (1974). *Ice Physics*. Oxford University Press.
- Hondoh, T. (2000). Nature and behaviour of dislocations in ice. In Hondoh, T., editor, *Physics of Ice Core Records*, pages 3–24, Sapporo. Hokkaido University Press.
- Hull, D. and Bacon, D. (2001). *Introduction to Dislocations*. Elsevier.
- Humphreys, F. J. and Hatherly, M. (2004). *Recrystallization and Related Annealing Phenomena*. Elsevier.
- Hutchinson, J. W. (1977). Creep and plasticity of hexagonal polycrystals as related to single crystal slip. *Metallurgical and Materials Transactions A*, 8(9):1465–1469.
- Huybrechts, P. (2007). Ice Sheet Modeling. In Riffenburgh, B., editor, *Encyclopedia of the Antarctic*, pages 514–517. Routledge, New York and London.
- Huybrechts, P., Rybak, O., Pattyn, F., Ruth, U., and Steinhage, D. (2007). Ice thinning, upstream advection, and non-climatic biases for the upper 89% of the EDML ice core from a nested model of the Antarctic ice sheet. *Clim. Past*, 3:577–589.
- Iliescu, D., Baker, I., and Chang, H. (2004). Determining the orientations of ice crystals using electron backscatter patterns. *Microscopy Res. Tech.*, 63:183–187.
- IPCC (2007). Summary for Policymakers. In Solomon, S., Qin, D., Manning, M., Chen, Z., Marquis, M., Averyt, K., M. Tignor, and Miller, H., editors, *Climate Change 2007: The Physical Science Basis. Contribution of Working Group I to the Fourth Assessment Report of the Intergovernmental Panel on Climate Change*. Cambridge University Press, Cambridge, United Kingdom and New York, NY, USA.

- Jacka, T. and Maccagnan, M. (1984). Ice crystallographic and strain rate changes with strain in compression and extension. *Cold Reg. Sci. Technol.*, 269-286(3):8.
- Jacka, T. H. (1984). The time and strain required for development of minimum strain rates in ice. *Cold Reg. Sci. Technol.*, 8(3):261–268.
- Jacka, T. H., Donoghue, S., Li, J., Budd, W. F., and Anderson, R. M. (2003). Laboratory studies of the flow rates of debris-laden ice. *Ann. Glaciol.*, 37.
- Lemke, P., Ren, J., Alley, R., Allison, I., Carrasco, J., Flato, G., Fujii, Y., Kaser, G., Mote, P., Thomas, R., and Zhang, T. (2007). Observations: Changes in snow, ice and frozen ground. In Solomon, S., Qin, D., Manning, M., Chen, Z., Marquis, M., Averyt, K., Tignor, M., and Miller, H., editors, *Climate Change 2007: The Physical Science Basis. Contribution of Working Group I to the Fourth Assessment Report of the Intergovernmental Panel on Climate Change*, pages 337–383. Cambridge University Press, Cambridge, United Kingdom and New York, NY, USA.
- Lipenkov, V. Y., Barkov, N. I., Duval, P., and Pimienta, P. (1989). Crystalline texture of the 2083 m ice core at Vostok station, Antarctica. *J. Glaciol.*, 35(121):392 – 398.
- Lorius, C., Merlivat, Jouzel, J., and Pourchet (1979). A 30,000-yr isotope climatic record from Antarctic ice. *Nature*, 280:644–648.
- Mansuy, P., Philip, A., and Meyssonier, J. (2000). Identification of strain heterogeneities arising during deformation of ice. *Ann. Glaciol.*, 30:121–126.
- Matsuda, M. (1979). Determination of axis orientations of polycrystalline ice. *J. Glaciol.*, 22(86):165–169.
- Miyamoto, A., Shoji, H., Hori, A., Hondoh, T., Clausen, H., and Watanabe, O. (2005). Ice fabric evolution process understood from anisotropic distribution of a-axis orientation on the GRIP (Greenland) ice core. *Ann. Glaciol.*, 42:47–52.
- Montagnat, M. and Duval, P. (2000). Rate controlling processes in the creep of polar ice, influence of grain boundary migration associated with recrystallization. *Earth Planet. Sci. Lett.*, 183:179–186.
- Montagnat, M. and Duval, P. (2004). The viscoplastic behaviour of ice in polar ice sheets: experimental results and modelling. *C. R. Physique*, 5(7):699–708.

- Montagnat, M., Duval, P., Bastie, P., and Hamelin, B. (2003a). Strain gradients and geometrically necessary dislocations in deformed ice single crystals. *Scripta Mat.*, 49:411–415.
- Montagnat, M., Duval, P., Bastie, P., Hamelin, B., and Lipenkov, V. Y. (2003b). Lattice distortion in ice crystals from the Vostok core (Antarctica) revealed by hard X-ray diffraction; implication in the deformation of ice at low stresses. *Earth Planet. Sci. Lett.*, 214:369–378.
- Mullins, W. W. (1957). Theory of thermal grooving. *J. App. Phys.*, 28(3):333–339.
- Nakaya, U. (1958). Mechanical properties of single crystal of ice. Part I. Geometry of deformation. *US Army Snow Ice and Permafrost Research Establishment, Research Report*, 28.
- Nishida, K. and Narita, H. (1996). Three-dimensional observations of ice crystal characteristics in polar ice sheets. *J. Geophys. Res.*, 101(D16):21,311–21,317.
- North Greenland Ice Core Project members (2004). High-resolution record of northern hemisphere climate extending into the last interglacial period. *Nature*, 431:147–151.
- Obbard, R., Baker, I., and Iliescu, D. (2006a). Grain boundary grooving in ice in a scanning electron microscope. correspondence. *J. Glaciol.*, 52(176):169–172(4).
- Obbard, R., Baker, I., and Sieg, K. (2006b). Using electron backscatter diffraction patterns to examine recrystallization in polar ice sheets. *J. Glaciol.*, 52(179):546–557.
- Oerter, H., Wilhelms, F., Jung-Rothenhäusler, F., Göktas, F., Miller, H., Graf, W., W., and Sommer, S. (2000). Accumulation rates in Dronning Maud Land, Antarctica, as revealed by dielectric-profiling measurements of shallow firn cores. *Ann. Glaciol.*, 30:27–34.
- Passchier, C. W. and Trouw, R. A. J. (1996). *Microtectonics*. Springer Verlag.
- Paterson, W. (1983). Deformation within polar ice sheets: An analysis of the Byrd station and Camp Century borehole-tilting measurements. *Cold Reg. Sci. Technol.*, 8(2):165–179.
- Paterson, W. S. B. (1994). *The physics of glaciers*. Butterworth-Heinemann, Elsevier, third edition.

- Petit, J. R., Basile, I., Leruyet, A., Raynaud, D., Lorius, C., Jouzel, J., Stievenard, M., Lipenkov, V. Y., Barkov, N. I., Kudryashov, B. B., Davis, M., Saltzman, E., and Kotlyakov, V. (1997). Four climate cycles in Vostok ice core. *Nature*, 387:359–360.
- Petit, J. R., Jouzel, J., Raynaud, D., Barkov, N. I., Barnola, J.-M., Basile, I., Bender, M., Chappellaz, J., Davis, M., Delaygue, G., Delmotte, M., Kotlyakov, V. M., Legrand, M., Lipenkov, V. Y., Lorius, C., Pepin, L., Ritz, C., Saltzman, E., and Stievenard, M. (1999). Climate and atmospheric history of the past 420,000 years from the Vostok ice core, Antarctica. *Nature*, 399:429–436.
- Petrenko, V. F. and Whitworth, R. W. (1999). *Physics of ice*. Oxford University Press.
- Pettit, E., Thorsteinsson, T., Jacobson, H., and Waddington, E. (2007). The role of crystal fabric in flow near an ice divide. *J. Glaciol.*, 53(181):277–288.
- Pimienta, P. and Duval, P. (1987). Rate controlling processes in the creep of polar glacier ice. *J. Physique*, C1(3):243 – 248.
- Pimienta, P. and Duval, P. (1989). Rheology of polar glacier ice. *Ann. Glaciol.*, 12:206–207.
- Placidi, L., Faria, S., and Hutter, K. (2004). On the role of grain growth, recrystallization and polygonization in a continuum theory for anisotropic ice sheets. *Ann. Glaciol.*, 39:49–52.
- Poirier, J.-P. (1985). *Creep of crystals*. Cambridge University Press.
- Rios, P. R., Jr, F. S., Sandimc, H. R. Z., Plaut, R. L., and Padilhad, A. F. (2005). Nucleation and growth during recrystallization. *Materials Research*, 8(3):225–238.
- Russ, J. C. (2002). *The Image Processing Handbook*. CRC Press, fourth edition.
- Russell-Head, D. (2004). *Fabric Analyser System - Investigator - Version 1.12*. <http://www.earthsci.unimelb.edu.au/facilities/analyser>.
- Ruth, U., Barnola, J. M., Beer, J., Bigler, M., Blunier, T., Castellano, E., Fischer, H., Fundel, F., Huybrechts, P., Kaufmann, P., Kipfstuhl, S., Lambrecht, A., Morganti, A., Oerter, H., Parrenin, F., Rybak, O., Severi, M., Udisti, R., Wilhelms, F., and Wolff, E. (2007). EDML1: A chronology for

- the EPICA deep ice core from Dronning Maud Land, Antarctica, over the last 150 000 years. *Clim. Past*, 3:475–484.
- Saylor, D. M. and Rohrer, G. S. (1999). Measuring the influence of grain-boundary misorientation on thermal groove geometry in ceramic polycrystals. *J. Am. Ceram. Soc.*, 82:1529–36.
- Schulson, E. (1987). The fracture of ice. *J. de Physique, Colloque C1*, 48:207–220.
- Schulson, E. M. (1999). The structure and mechanical behaviour of ice. *JOM*, 51(2):21–27.
- Schulson, E. M., Lim, P. N., and Lee, R. W. (1984). A brittle to ductile transition in ice under tension. *Phil. Mag.*, A49(3):353–363.
- Steinemann, S. (1958). Experimentelle Untersuchungen zur Plastizität von Eis. *Beiträge zur Geologie der Schweiz, Hydrologie*, 10:72.
- Stocker, T. F. and Johnsen, S. J. (2003). A minimum thermodynamic model for the bipolar seesaw. *Paleoceanography*, 18(4):1087.
- Taylor, K. C., Hammer, C. U., Alley, R. B., Clausen, H. B., Dahl-Jensen, D., Gow, A. J., Gundestrup, N. S., J., K., Moore, J. C., and Waddington, E. D. (1993). Electrical conductivity measurements from the GISP2 and GRIP Greenland ice cores. *Nature*, 366:549–552.
- Thorsteinsson, T. (1996). Textures and fabrics in the grip ice core, in relation to climate history and ice deformation. *Ber. Polarforsch.* 205, Alfred-Wegener-Institut für Polar- und Meeresforschung. ISSN 0176 - 5027.
- Thorsteinsson, T. (2006). Anisotropy and flow of ice. In Knight, P., editor, *Glacier Science and Environmental Change*, pages 315–317. Blackwell Publishing.
- Thorsteinsson, T., Alley, R. B., Gow, A. J., Johnsen, S. J., Kipfstuhl, J., and Meese, D. A. (1995). Comparison of deep ice cores. *Nature*, 373:393–394.
- Thorsteinsson, T., Kipfstuhl, J., and Miller, H. (1997). Textures and fabrics in the GRIP ice core. *J. Geophys. Res.*, 102(C12):26,583–26,599.
- Trepied, L., Doukhan, J. C., and Paquet, J. (1980). Subgrain boundaries in quartz theoretical analysis and microscopic observations. *Phys. Chem. Min.*, 5(3):201–218.

- Uthus, L., Hoff, I., and Horvli, I. (2005). Evaluation of grain shape characterization methods for unbound aggregates. In *Seventh International Conference on the Bearing Capacity of Road*, Trondheim. Railways and Airfields (BCRA).
- Vaughan, D. and Arthern, R. (2007). Why is it hard to predict the future of ice sheets? *Science*, 315:1503–1504.
- Wang, Y., Kipfstuhl, S., Azuma, N., Thorsteinsson, T., and Miller, H. (2003). Ice-fabrics study in the upper 1500 m of Dome C (East Antarctica) deep ice core. *Ann. Glaciol.*, 37:97–104.
- Weary, D. and Rivier, N. (1984). Soap, cells and statistics - random patterns in two dimensions. *Contemp. Phys.*, 25(1):59–99.
- Weertman, J. and Weertman, J. R. (1992). *Elementary Dislocation Theory*. Oxford University Press.
- Wilson, C. J. L., Russell-Head, D. S., and Sim, H. M. (2003). The application of an automated fabric analyzer system to the textural evolution of folded ice layers in shear zones. *Ann. Glaciol.*, 37:7–17.
- Wilson, C. J. L. and Zhang, Y. (1994). Comparison between experiment and computer modelling of plane-strain simple-shear ice deformation. *J. Glaciol.*, 40(134):46–55.
- Zhang, Y. and Wilson, C. J. L. (1997). Lattice rotation in polycrystalline aggregates and single crystals with one slip system: a numerical and experimental approach. *J. Struct. Geol.*, 19(6):875–885.

# Appendix A

## Publication I - Evolution of ice crystal microstructure during creep experiments

Hamann, I., Weikusat, Ch., Azuma, N., Kipfstuhl, S. (2007)  
Journal of Glaciology, Vol. 53, No. 182, pp. 479-489.

# Evolution of ice crystal microstructure during creep experiments

Ilka HAMANN,<sup>1,2</sup> Christian WEIKUSAT,<sup>1\*</sup> Nobuhiko AZUMA,<sup>1</sup> Sepp KIPFSTUHL<sup>2</sup>

<sup>1</sup>*Department of Mechanical Engineering, Nagaoka University of Technology, 1603 Kamitomioka, Nagaoka 940-2188, Niigata, Japan*

<sup>2</sup>*Alfred Wegener Institute for Polar and Marine Research, Columbusstrasse, D-27568 Bremerhaven, Germany  
E-mail: ilka.hamann@awi.de*

**ABSTRACT.** Results of laboratory uniaxial compression tests over the stress range 0.18–0.52 MPa and the strain range 0.5–8.6% at approximately –5 and –20°C are presented. Grain-size analysis and comparisons with annealing tests confirm that grain-growth reducing processes are active during deformation. Microstructural observations reveal that subgrain-rotation recrystallization and grain-shape changes due to strain-induced grain-boundary migration are the causes of the grain-growth deceleration. Further results from microstructural observations show that obstacle formation by dislocation walls and subgrain boundaries is the reason for isotropic hardening during creep. Subgrain-boundary types that are likely to be relevant for studies on the activity of different dislocation types are described.

## INTRODUCTION

The study of deformation mechanisms and their links to the crystal texture evolution of polycrystalline ice is of growing interest, as knowledge of the mechanical properties of ice in polar ice sheets is vitally important for the interpretation of ice-core records and modelling ice-sheet flow.

The flow of polycrystalline ice has been studied for many decades. Creep experiments on ice produce creep curves showing the primary, secondary and tertiary stages typical for many polycrystalline materials (e.g. Budd and Jacka, 1989; Paterson, 1994; Petrenko and Whitworth, 1999; Hooke, 2005). Processes which control the plasticity of ice in the different creep stages were reviewed by Duval and others (1983) using classical strain test parameters which describe the reaction of a test specimen to deformation. Although tertiary creep is more significant in glaciology (e.g. Budd and Jacka, 1989; Paterson, 1994; Petrenko and Whitworth, 1999), Glen's law describing the strain-rate–stress relation in secondary creep (Glen, 1955) is widely applied in glacier studies. This secondary creep stage attracted particular interest because it is identified as a unique point on the ice creep curve (Jacka, 1984). The strain test parameters are not easy to obtain in ice sheets. However, as ice is a highly anisotropic material, due to its hexagonal crystal system, various processes (e.g. dislocation climb and glide and diffusional processes) compete during deformation. These processes act on the atomic scale and are therefore difficult to observe directly in deforming polycrystalline samples. Nonetheless, they leave behind certain structures on the grain and subgrain scale indicating deformation mechanisms, so microstructures can be used to study these processes. Single mechanisms, such as grain rotation or grain-boundary sliding, can be observed by studying the evolution of *c* axes (e.g. Azuma and Higashi, 1985), grain size (e.g. Goldsby and Kohlstedt, 1997) and other microstructural properties. Recently, high-resolution crystallographic analysis has provided new information that

improves our understanding of recrystallization processes (Montagnat and others, 2003; Miyamoto and others, 2005; Obbard and others, 2006b). For statistical observations at high spatial resolution, a new microstructure-mapping method (Kipfstuhl and others, 2006) allows more direct and easily obtainable observations of features produced by the deformation-related processes. In the future, comparing data obtained using this method for ice-core samples, with unknown deformation conditions, with data obtained in the same way for experimentally deformed ice, with well-known deformation conditions, may add to our understanding of flow laws in ice sheets.

One important aspect of the structures of polycrystalline ice is the grain-size evolution. It is well established that the temperature-dependent normal grain growth with time (e.g. Gow, 1969) can be disturbed in natural ice (e.g. Gow and Williamson, 1976; Duval and Lorius, 1980; Thorsteinsson and others, 1995). Explanations for this grain-growth reduction have been discussed for many years (e.g. Gow and Williamson, 1976; Duval and Gac, 1980; Paterson, 1994), but there is, as yet, no consistent understanding to be found in the literature. In laboratory ice deformation experiments Jacka and Li (1994) found a steady-state crystal size with the tertiary creep stage. Examination of microstructures can help to understand the physical processes leading to grain-growth reduction and to evaluate whether these processes could be the cause of grain-size variations in ice sheets.

This work presents, for the first time, laboratory experimental studies on microstructural features that are clearly related to deformation. The aim is to give evidence for, and discuss processes leading to, the grain-growth reducing effect of deformation indicated by microstructural observations. These studies are used to clarify the processes leading to strain hardening during primary creep.

## METHODS

### Experimental procedures

In order to obtain bubble-free samples with a small grain size and without initial deformation features, samples were

\*Present address: Institute of Mineralogy, Ruprecht-Karls-University of Heidelberg, Im Neuenheimer Feld 236, D-69120 Heidelberg, Germany.

**Table 1.** Overview of the experimental conditions. Test samples were cylindrical with diameter 13–19 mm and length 14–38 mm. Temperatures are means over the duration of the experiment. In some cases it is not clear whether final strain rate is the minimum strain rate

Experiment	$T$ °C	Stress MPa	Approx. time days	Strain %	Final strain rate $s^{-1}$	Min. strain rate $s^{-1}$	Mean grain size $mm^2$	Mean initial grain size $mm^2$
4–5	–4.5	0.16	8	0.45	$2.34 \times 10^{-9}$		3.98	0.12
5–5	–4.5	0.35	10	2.8	$2.08 \times 10^{-8}$		2.93	0.29
6	–4.5	0.35	3	1.7	$4.11 \times 10^{-8}$		2.25	0.59
7	–4.2	0.35	25	5.5	$1.91 \times 10^{-8}$		10.98	0.85
9	–4.7	0.35	1.5	0.51	$2.04 \times 10^{-8}$		1.07	0.27
10	–4.8	0.35	3	1.22	$2.06 \times 10^{-8}$		2.04	0.14
11	–4.9	0.35	0.5	0.44	$2.38 \times 10^{-8}$		1.48	0.25
12	–4.7	0.18	13	1.04	$4.29 \times 10^{-9}$		3.45	0.22
14	–4.9	0.52	3	3.58	$8.66 \times 10^{-8}$	$6.24 \times 10^{-8}$	1.43	0.08
15	–4.8	0.52	8	8.56	$9.01 \times 10^{-8}$	$8.58 \times 10^{-8}$	1.31	0.20
4–23	–23.5	0.20	10	0.51	$1.43 \times 10^{-9}$		0.07	0.08
5–23	–23	0.35	35	1.38	$2.29 \times 10^{-9}$		1.31	0.28
8	–23	0.35	28	1	$1.10 \times 10^{-9}$		0.65	0.27
13	–22.5	0.52	31	1.12	$2.34 \times 10^{-9}$		0.85	0.18

produced using large-grained bubble-free ice obtained by slow freezing of pure water under vibration that were then exposed to a phase transition at  $\sim 300$  MPa,  $\sim 233$  K. This procedure enables us to produce small-volume samples (cylindrical:  $\sim 15$ – $20$  mm diameter,  $\sim 50$  mm length) with small grain sizes (mean diameter  $\sim 0.6$  mm) due to nucleation/recrystallization processes during the phase change from ice II to ice Ih. In contrast to standard sample production procedures, which usually include pressure sintering, our samples are bubble-free, and do not exhibit deformational microstructures.

Samples were rounded using a lathe. Top and bottom surfaces were cut parallel with a microtome (cylindrical: 13–19 mm diameter, and 14–38 mm length). The creep machines we used consist of a basal plate, which is situated in a silicon oil bath and a loading stage lead by vertical guide rails. The silicon oil bath is used to prevent the deforming sample from sublimation and to keep the temperature constant during the test. A displacement sensor is attached to the loading stage, which moves down as the sample is compressed, and measures the shortening of the sample. Table 1 gives an overview of all experiments conducted during the study.

For reference, concurrent annealing of a small section cut from the initial samples was conducted in the same silicon oil bath used for creep experiments.

### Observation methods

Thin sections were prepared according to standard procedures, allowing the surfaces to sublimate and reveal (sub)grain boundaries as etch grooves (Kipfstuhl and others, 2006). For each sample, at least two sections, one cut horizontally and the other vertically, were prepared. Microstructures were mapped afterwards with a manual XY-stage and a differential interference microscope (Olympus B  $\times$  51 differential interference contrast (DIC),  $10\times$  lens). Two to six sectors ( $\sim 5$  mm by 6 mm) of each section, usually chosen close to the centre of the sample and not disturbed by, for example, bad sublimation regions, were photographed with  $\sim 25$  images to get a representative overview of the sample. Grain size and shape were

determined from overview pictures of the whole sample between crossed polarizers (Stereoscope 12,  $6\times$  to  $64\times$ ,  $1\times$  objective).

### Measurement methods

Subgrain-boundary statistics were obtained from photomicrographs using digital image analysis. Microstructure maps were assembled from microscopic mosaic images and used to measure total subgrain-boundary length in the grain assemblage presented in the map. This had to be done manually, as subgrain boundaries, in contrast to grain boundaries, appear only as thin faint lines in the images which are difficult to extract automatically. The area of the microstructure map was measured and the subgrain-boundary density calculated. Subgrain-boundary density is defined as the sum of all subgrain-boundary lengths per area. Possible interrelations between subgrain-boundary density and the sample cutting scheme (i.e. horizontally or vertically cut) were investigated by systematically changing cutting schemes. These types of observations have not been reported before; this may be because, apart from the time-consuming measurements and analysis processes, standard sample production procedures include pre-deformation due to non-hydrostatic pressure (e.g. Jacka and Lile, 1984; Goldsby and Kohlstedt, 1997) which means deformation microstructures are present in initial samples. Our samples have no such initial deformation features.

Grain parameters were derived from crossed-polarizer pictures which were segmented using an edge filter, revealing the basic network of grain boundaries (Gay and Weiss, 1999). Artefacts were removed manually. The grain-boundary network pictures were analyzed with image-processing software to obtain grain-size (area, perimeter) data by pixel counting. The software assumes an ellipse of the same area as each grain. Using the length of the major and minor axes of this ellipse, grain-elongation data and the aspect ratio of each grain can be derived.

The ratio of convex perimeter to real perimeter (Fig. 1) called ‘perimeter ratio’ has been adopted to describe the morphology of the grains. This parameter, used here for the first time to describe the grain shape in polycrystalline ice,

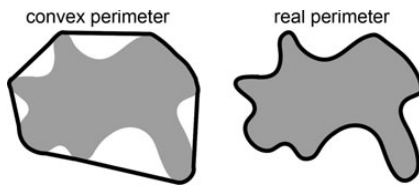


**Fig. 1.** Schematic illustration of the definition of convex perimeter and real perimeter measured by Image-Pro. The ratio is used as a measure of the irregularity of grains.

can be measured using Image-Pro Plus (Media Cybernetics). It was used in a similar way to measure the roughness of grains in unbound aggregates of gneiss forming a base course in road surfaces. A grain with straight boundaries has a perimeter ratio of 1; the value decreases as the irregularity becomes more complex.

**EXPERIMENTAL RESULTS**

This study combines observations of creep, in terms of displacement, strain and strain rate, with observations of the microstructure of the sample before and after deformation. The microstructure observations are focused on grain size, grain shape and subgrain-boundary evolution with time and creep. As the total strains were low, most samples did not appear to be macroscopically deformed – they did not show macroscopic strain localization such as bending of the whole sample or cracking.

**Creep data**

Experiments were conducted to reach strains of 0.4–8.6% at ~-5°C and 0.5–1.4% at ~-23°C. Greater strains were not attempted as the apparatus was only available for a limited time. Only two of the experiments clearly reached minimum isotropic creep. In the highest-strain experiments, strain rate usually stopped decreasing at ~1–2% strain (Fig. 2).

**Grain-size data**

Mean grain size increased during almost all our creep tests (Table 1). Comparisons with data derived from grain-growth experiments at -5°C (Nishimura, 2004) using the same sample type, produced by phase transition, indicate significantly faster increases in grain size when no stress is applied (Fig. 3). A striking difference was found between samples deformed at ~-5°C and at ~-23°C (Fig. 3).

**Grain-shape data**

Elongation, and therefore mean grain aspect ratio, slightly increases with increasing strain (Fig. 4a). At the highest strains a steady aspect ratio of ~1.7 was reached. Importantly, no difference in mean grain aspect ratio could be found between vertically and horizontally cut sections. The orientation of the majority of the grain elongations does not change significantly and no preferred grain-elongation direction could be observed.

We also investigated the detailed irregularity of the grains. Polygonal and regular-shaped grains, isometric with straight grain boundaries and triple-junction angles close to 120°, were observed in samples before deformation and in samples which had been annealed (Fig. 5a). Deformed samples show irregular grains with bulging and curved grain boundaries,

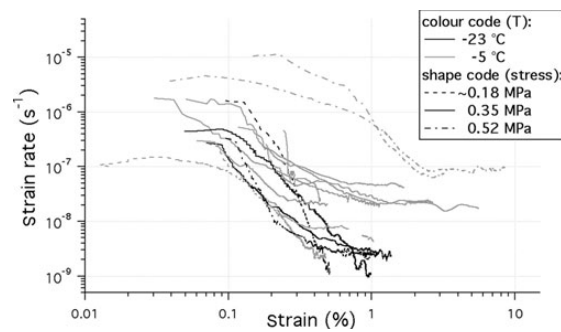


**Fig. 2.** Strain rate vs strain for all experiments.

extending into neighbouring grains to produce an interlocking texture (Fig. 5b). With increasing strain the grains become increasingly irregular. Perimeter ratio values slightly below 1 are obtained for the highly regular grains in initial and annealed samples. With increasing strain the increasing bulging of the grain boundaries and increasing localized curvature radii decrease the perimeter ratio (Fig. 4b).

**Subgrain boundaries and subgrain-boundary density**

Kipfstuhl and others (2006) showed that subgrain boundaries are revealed as grooves under controlled sublimation conditions. The dependence of sublimation/thermal grooving on misorientation was described generally by Mullins (1957) and by Saylor and Rohrer (1999) for ceramic polycrystals. Recently Obbard and others (2006a) described a model for preferred sublimation and some special aspects of grain-boundary grooving for ice. As the transition from subgrain boundaries to grain boundaries is gradual, a clear definition or critical value to distinguish between the two is difficult. In materials science the transition is typically taken as between 10° and 15° (see, e.g., Humphreys and Hatherly, 2004, p. 92) and in geology as <5° (see, e.g., Passchier and Trouw, 1996, p. 265). For ice, Montagnat and Duval (2000) used 5° as the critical value for the transformation. Preliminary results of X-ray Laue diffractometry (personal communication from A. Miyamoto, 2007) reveal typical misorientations for strong grooves of ~3°. Faint sublimation grooves, although clearly visible, cannot be easily detected by X-ray measurements, indicating a very small misorientation (<<0.5°). Therefore it is probably correct to call some

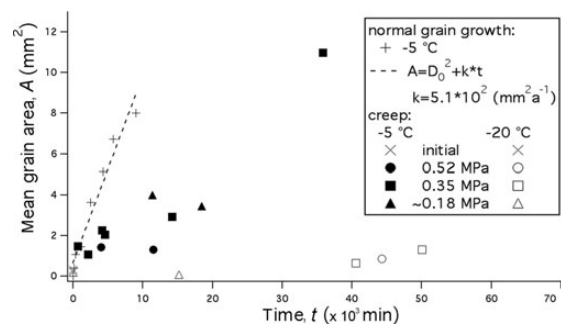


**Fig. 3.** Grain-size evolution during creep tests and Nishimura's (2004) grain-growth experiment.

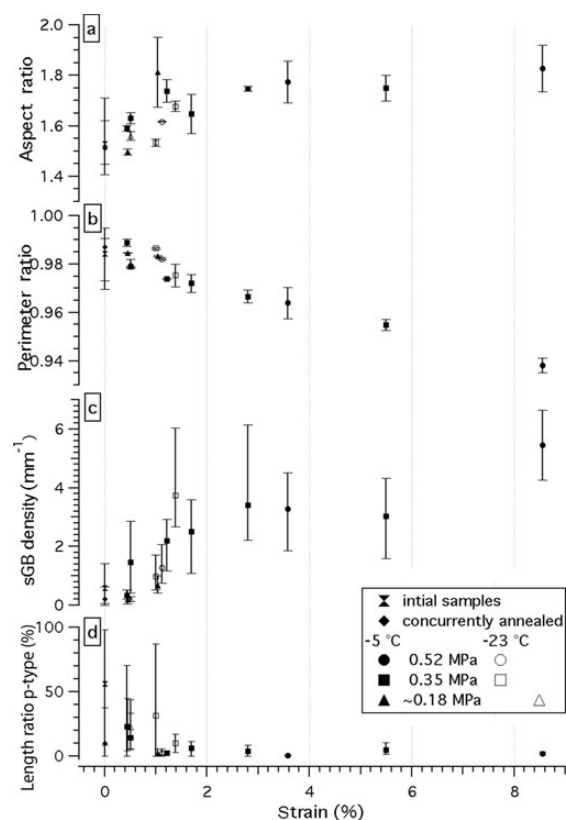


**Fig. 4.** Microstructural evolution in creep experiments with increasing strain. (a, b) Grain aspect ratio (a); grain perimeter ratio (see Fig. 1 and text for definition) (b). Mean derived from vertical and horizontal sections. (c, d) Subgrain-boundary (sGB) density (c); frequency of parallel-type subgrain boundaries (ratio of the total length of parallel-type subgrain boundaries to total length of all subgrain boundaries) (d). Mean over four to six selected regions (area:  $\sim 5 \text{ mm} \times \sim 6 \text{ mm}$ ) in a section. Bars indicate variability.

of these sublimation grooves dislocation walls rather than subgrain boundaries. The distinction is not made here, because of the gradual transition from dislocation walls to subgrain boundaries to grain boundaries. High-resolution misorientation measurements can be performed using hard X-ray equipment (Montagnat and others, 2003), useful for

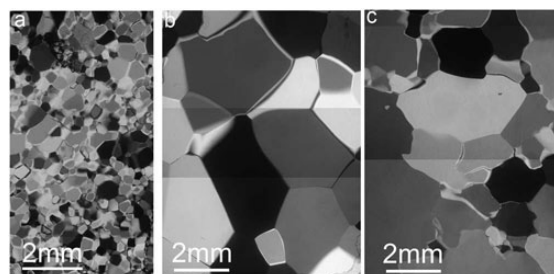


**Fig. 5.** Composite photomicrographs taken between crossed polarizers. (a) Initial sample. (b, c) After 3 days at  $-4.9^\circ\text{C}$ : annealing only (b); creep test at 0.52 MPa and 3.58% total strain (c).

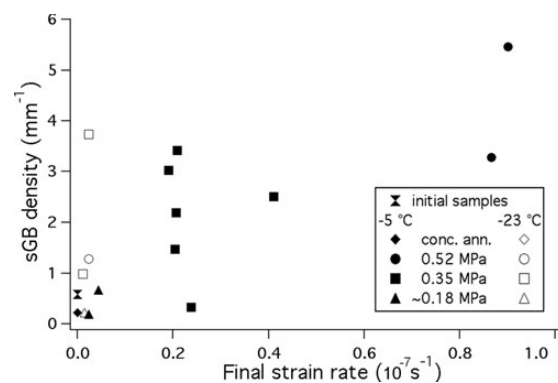


**Fig. 6.** Mean subgrain-boundary density against final strain rate. Mean over four to six selected regions (area:  $\sim 5 \text{ mm} \times 6 \text{ mm}$ ) in a section. Further experiments are required.

distinguishing these features, but the sample sizes are tiny and neither geometric arrangement nor statistics on substructures can be obtained.

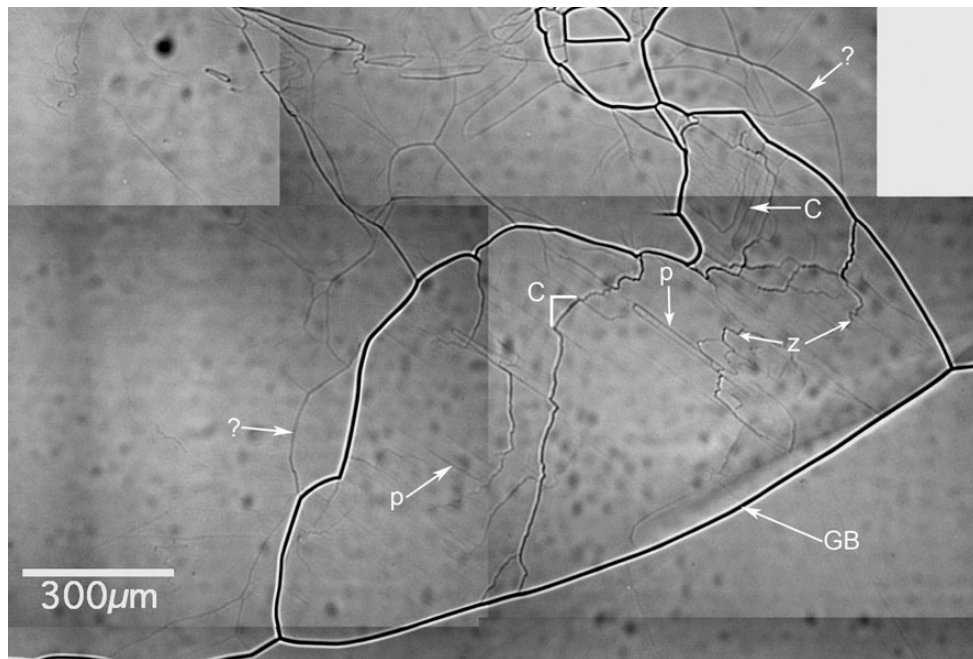
The systematic study of subgrain-boundary density during creep tests reveals it evolves with strain (Fig. 4c). Mean subgrain-boundary density increases with strain (Fig. 4c) from  $\sim 0.5\%$  up to  $\sim 2\%$ . For strains larger than 2–3% the increase stops at a value of  $\sim 3.5 \text{ mm}^{-1}$ . No systematic difference in subgrain-boundary density or grain size was observed between horizontally and vertically cut sections. Values plotted in Figure 4c are mean values of at least four individual measurements, each determined for one microstructure map ( $\sim 5 \text{ mm} \times 6 \text{ mm}$  of a sample surface). Particularly for strains higher than 1%, the individual measurements have a large scatter (bars in Fig. 4c), reflecting a heterogeneous distribution of deformation over the section. Figure 4c shows that the range of variability is approximately similar in all samples,  $\sim 3 \text{ mm}^{-1}$  above 1% strain, which indicates that our analysis of four microstructure maps is representative. As experiments at lower temperatures take much longer, only a few data are so far available, though these agree well with the above finding.

Figure 6 illustrates the subgrain-boundary density with final strain rates measured for the experiments. Although a clear correlation cannot yet be shown, subgrain-boundary density seems to increase with strain rate. Further experiments are required to investigate the relation between subgrain evolution and strain rate.

### Subgrain-boundary types

Different subgrain-boundary types classified by shape, and very similar to those found in Antarctic ice (data will be presented elsewhere), have been observed. The appearance of subgrain boundaries is manifold (Fig. 7). Variations occur in shape and intensity (i.e. greyscale value). The subgrain-boundary shapes vary from regular straight (rare) to regular bowed (often) and irregular zigzag or step-shaped (very often). The latter sometimes build conspicuous networks. Straight, exactly parallel groups of subgrain boundaries are striking, often appearing faint and light grey.

The shapes of subgrain boundaries have been investigated with respect to crystal orientation using a combination of microstructure mapping and etch-pit analysis (Fig. 8), which enables a more definite classification of



**Fig. 7.** Types of subgrain boundaries in a vertical section ( $-4.8^{\circ}\text{C}$ ,  $0.52\text{ MPa}$ ,  $8.56\%$  total strain). GB – grain boundary; p – parallel subgrain boundary; ? – not yet classified subgrain boundary; c – classical polygonization type subgrain boundary.

three subgrain-boundary types: parallel subgrain boundaries are not only exactly parallel to others in the swarm, but are also parallel to the trace of the basal plane (type p – parallel); zigzag or step-shaped subgrain boundaries usually run in one reticulate direction parallel and in the other at a high angle to the basal plane (type z – zigzag); regular, more-or-less straight subgrain boundaries with the classical polygonization orientation (perpendicular to the basal plane) have also been observed (c – classical polygonization type), but almost always change into the zigzag type at one end (Figs 7 and 8). Bowed subgrain boundaries and those without any distinct shape usually do not seem to correspond with the crystal orientation and cannot be classified.

Due to the striking and easily recognizable nature of parallel subgrain boundaries, statistics on their occurrence have been calculated (Fig. 4d). The fraction of the length of parallel subgrain boundaries over total subgrain boundaries, and the variability, is highest in undeformed samples, because the few subgrain boundaries occurring in initial samples are often parallel. In slightly deformed samples (up to 1% strain) the parallel type represents  $\sim 20\text{--}30\%$  of the total subgrain-boundary length, but for strains above 2% this frequency decreases rapidly to only several per cent.

#### Distribution of subgrain boundaries within grains

Subgrain boundaries are not randomly distributed within the grain. They accumulate along grain boundaries, i.e. they usually start somewhere along a grain boundary and fade out towards the crystal core. However, the distribution along the grain boundaries is not homogeneous. Accumulation of subgrain boundaries in some regions of grains, preferentially at edges or necks, has been observed (Fig. 9). The heterogeneous distribution can be described as a ‘core and mantle’

structure (Kipfstuhl and others, 2006); a mantle describing the rim of the crystal with high subgrain-boundary density and the core defined by low subgrain-boundary density in the middle of a grain. This description holds for most grains.

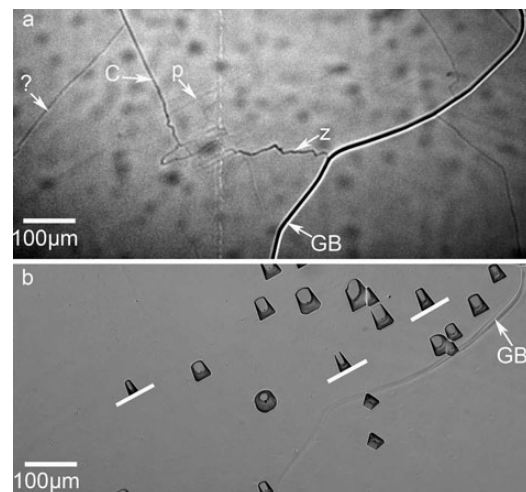


**Fig. 8.** Combination of microstructure mapping and etch-pit method. Example of vertical section ( $-4.8^{\circ}\text{C}$ ,  $0.35\text{ MPa}$ ,  $1.22\%$  strain). (a) Sublimated surface showing grain boundaries (GB) and different types of subgrain boundaries (p – parallel; z – zigzag; c – classical polygonization type; ? – not identified). (b) Etch pits produced on same sector as (a). Short white bars indicate trace of basal plane in cutting surface according to etch-pit shape. Note: parallel type is parallel to basal plane trace; classical polygonization type is perpendicular to basal plane trace.

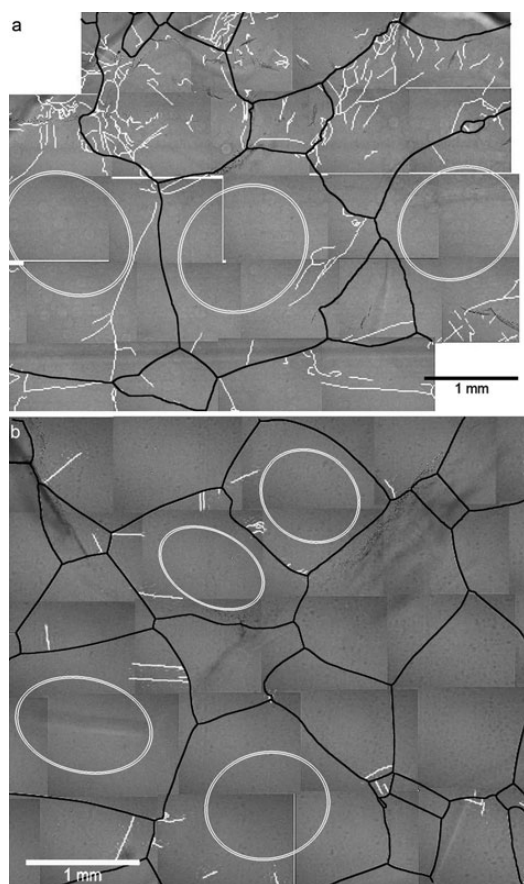


**Fig. 9.** Distribution of subgrain boundaries (marked as lines). Most subgrain boundaries are attached or close to a grain boundary (black), forming a subgrain-boundary-free core (approximately indicated by ellipses), which is not sharply defined. (a) Horizontal section ( $-4.8^{\circ}\text{C}$ ,  $0.35\text{ MPa}$ ,  $1.22\%$  total strain). (b) Horizontal section ( $-4.9^{\circ}\text{C}$ ,  $0.35\text{ MPa}$ ,  $0.44\%$  total strain). Note: Distribution inside grain is highly heterogeneous, e.g. areas of higher subgrain-boundary density (top of (a)).

Detailed measurements of subgrain-boundary density give values two to five times higher near to grain boundaries ( $1\text{--}36\text{ mm}^{-1}$ ; see Fig. 10), compared to the mean subgrain-boundary density ( $3$  and  $6\text{ mm}^{-1}$ ; see Fig. 4c). This difference clearly indicates the heterogeneity of the subgrain-boundary distribution within grains. Detailed subgrain-boundary density was measured choosing curved grain boundaries. An additional observation was that the majority of curved grain boundaries have more subgrain boundaries on their convex side than on the concave side (Fig. 10b).

## INTERPRETATION AND DISCUSSION

### Creep behaviour and substructure evolution

At  $\sim 2\%$  strain (i.e. at minimum strain rate; Fig. 2) a steady value of mean subgrain-boundary density is reached (Fig. 4c). This finding indicates that strain hardening during primary creep corresponds to the evolution of the substructure of the crystal. Duval and others (1983) suggest the

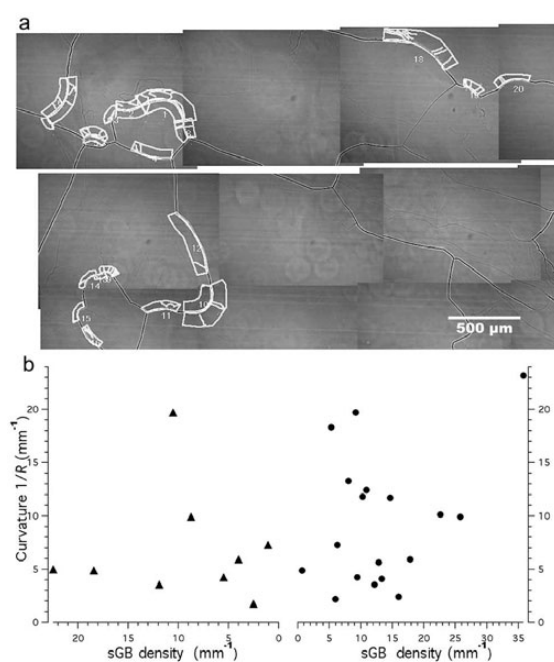


**Fig. 10.** Subgrain-boundary density in the vicinity of curved grain boundaries ( $-4.8^{\circ}\text{C}$ ,  $0.52\text{ MPa}$ ,  $8.56\%$  total strain). (a) Schematic showing how subgrain-boundary density was determined with measured areas, subgrain boundaries and curvatures. Numbers refer to the measurement. (b) Curvatures against subgrain-boundary densities. Areas on convex ( $\bullet$ ) and concave ( $\blacktriangle$ ) sides of the curve are shown separately.

decrease in creep rate during this stage is due to two different hardening processes: kinematic hardening and isotropic hardening. Kinematic hardening is evidenced by partly recoverable deformation during transient strain, due to non-uniform distribution of long-range internal stresses caused by different orientations of grains which favour or hinder basal slip in the individual grain.

Isotropic hardening is the non-reversible component of strain during transient creep ascribed by Duval and others (1983) to a period of zero strain rate during stress-drop experiments. The processes leading to isotropic strain hardening can be observed directly using subgrain-boundary density data. Dislocations which accomplish plastic creep (e.g. Duval and others, 2000; Montagnat and Duval, 2000, 2004) form dislocation walls and subgrain boundaries. The synchrony of achievement of minimum strain rate and steady subgrain-boundary density suggests that the cause for this part of strain hardening is the production of obstacles which hinder the motion of dislocations. The most common obstacles for dislocations in ice are dislocation walls and subgrain boundaries. As the production of such obstacles and the prevention of dislocation motion is increased, the deformation rate keeps decreasing until a steady density of obstacles is reached. This coincides with attaining the maximum value of the subgrain-boundary density.

When an obstacle is encountered, dislocations cannot move freely and stress must accumulate. It is plausible that this stress accumulation leads to locally increased dislocation production due to sources for dislocations at nodes or

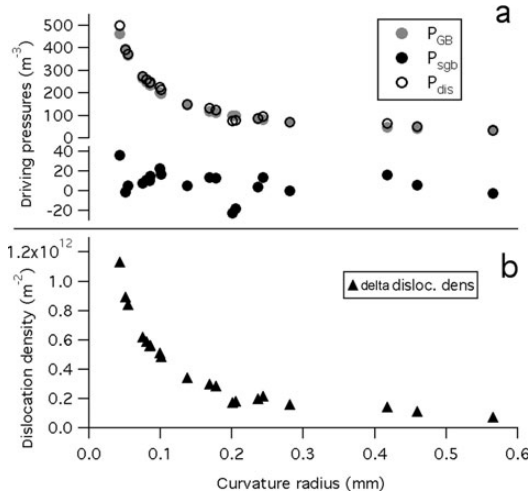


**Fig. 11.** (a) Driving pressures on the convex sides of the curved grain boundaries calculated from curvature radii ( $P_{GB}$ ) and subgrain-boundary density measurements ( $P_{sGB}$ ) (Fig. 10). Minimum driving pressures by dislocations to keep these curvature radii are also given ( $P_{dis}$ ). Note the second y axis with a larger scale for ( $P_{sGB}$ ). (b) Minimum dislocation density excess which has to be larger on the convex side for the radius of curvature to remain stable, estimated from minimum driving pressures by dislocations.

steps formed by obstacles in the glide plane (Ahmad and others, 1986) and increased subgrain-boundary formation by dislocation pile-up. Three observations indeed reveal significant deformation inhomogeneity inside the sections and even inside the grains: (i) the high variability of single measurements (bars in Fig. 4c); (ii) the qualitatively observable heterogeneous distribution of subgrain boundaries (Fig. 9); and (iii) the difference between mean subgrain-boundary densities (up to  $\sim 5.5 \text{ mm}^{-1}$ ; see Fig. 4c) and the locally measured subgrain-boundary density (up to  $36 \text{ mm}^{-1}$ ; see Fig. 10). Not only is the internal stress of the non-uniform state due to resistance to creep between basal and other planes (Duval and others, 1983), but also the deformation within the grains is not homogeneous. This finding is in general accordance with strain gradients in ice described by Montagnat and others (2003) and interpreted, following Ashby (1970), as being associated with the storage of geometrically necessary dislocations.

Subgrain-boundary obstacles lead to a higher strain-energy accumulation than expected under the assumption that dislocations cross the whole grain, reach grain boundaries and are absorbed by them (Pimienta and Duval, 1987). This non-uniform state of strain energy within grains can be studied in the vicinity of grain-boundary curves. These areas are chosen because the existence of ‘bulges’ indicates a difference in energy across the boundary (e.g. Duval and others, 1983; Barber, 1990).

The energy change,  $\Delta E$ , across a migrating grain boundary is given by

$$\Delta E = \Delta E_{GB} + \Delta E_{sGB} + \Delta E_{dis}, \quad (1)$$

where  $\Delta E_{GB}$  is due to grain-boundary area change,  $\Delta E_{sGB}$  is due to subgrain-boundary area change and  $\Delta E_{dis}$  is a consequence of removal of dislocations by the passage of grain boundaries.

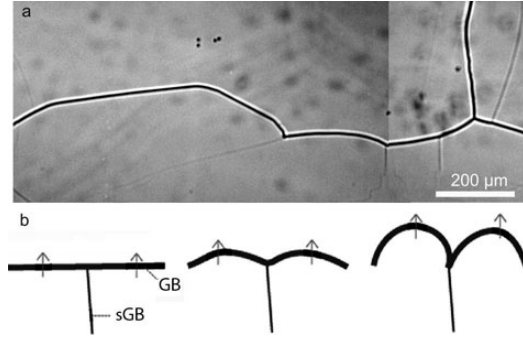


**Fig. 12.** Extensive interaction of subgrain boundaries with grain boundaries. (a) The geometry indicates pinning of a moving grain boundary by the subgrain boundary ( $-4.5^\circ\text{C}$ ,  $0.35 \text{ MPa}$ ,  $2.8\%$  total strain). (b) Conceptual model; the grain boundary is moving towards the top of the picture (arrows indicate direction of movement) and the subgrain boundary pins it where they meet, in a similar way to particle-pinning of grain boundaries.

This energy change exerts a driving stress,  $P$ , on the grain boundary:

$$P = \pm P_{GB} + P_{sGB} + P_{dis}. \quad (2)$$

The driving pressure on the convex side of the curved grain boundary,  $P_{GB} = (2\gamma_{GB})/R$ , is acting against motion to the convex side and is therefore subtracted. The grain-boundary energy,  $\gamma_{GB}$ , is  $\sim 10^{-2} \text{ J m}^{-2}$  ( $4.2 \times 10^{-2} \text{ J m}^{-2}$ ; Petrenko and Whitworth, 1999;  $6.5 \times 10^{-2} \text{ J m}^{-2}$ ; Ketcham and Hobbs, 1969; Hobbs, 1974). The curvature radii,  $R$  ( $\sim 0.05\text{--}0.3 \text{ mm}$ ; Fig. 10), are significantly smaller than values usually considered, which use mean grain size for such estimations.

Driving stress due to subgrain-boundary removal by sweep of grain boundaries is  $P_{sGB} = \gamma_{sGB} \Delta \rho_{sGB}$ , with  $\gamma_{sGB}$  being the subgrain-boundary energy ( $\sim \gamma_{GB}/10$ ; Humphreys and Hatherly, 2004) and  $\Delta \rho_{sGB}$  the subgrain-boundary density difference across the grain boundary.

$P_{GB}$  and  $P_{sGB}$  can be calculated using data shown in Figure 10. Values for  $P_{sGB}$  (Fig. 11a) are negative or positive depending on the subgrain boundary frequency on the convex and concave sides of the grain boundary. Although  $P_{sGB}$  is usually positive,  $P_{GB}$  reaches much higher values (by two orders of magnitude) due to the very small curvature radii compared to the maxima of  $P_{sGB}$ . This estimate shows that the internal strain energy contributed by the subgrain boundaries is not enough to produce the observed curvature radii. Grain-boundary motion is not affected by subgrain boundaries themselves, although frequently observed pinning of grain boundaries at intersections with subgrain boundaries (Fig. 12) indicates there are exceptions. As dislocations collected in subgrain boundaries or dislocation walls do not provide enough internal strain energy to produce the observed curvatures, internal energy exerted by more randomly distributed dislocations must be operating (also estimated in Fig. 11a). Thus subgrain-boundary occurrence indicates a higher dislocation density accumulated around them by acting as obstacles.

The driving pressure caused by removal of dislocations other than those which comprise dislocation walls or subgrain boundaries is  $P_{dis} = 0.5 \Delta \rho_{dis} G b^2$  (e.g. Duval, 1985; Humphreys and Hatherly, 2004), where  $\Delta \rho_{dis}$  is the

minimum dislocation density excess which has to be larger on the convex side for the radius of curvature to remain stable,  $G$  is the shear modulus ( $35.2 \times 10^8 \text{ N m}^{-2}$ ; Petrenko and Whitworth, 1999) and  $b$  is the Burgers vector of a perfect dislocation in the basal plane ( $\sim 0.5 \text{ nm}$ ; Hondoh, 2000). Considering motion of the grain boundary to the convex side as indicated by the bulging,  $P$  in Equation (2) must be positive ( $P \geq 0$ ).  $\Delta\rho_{\text{dis}}$  can then be estimated (Fig. 11b). Minimum dislocation densities reach values of  $10^{12} \text{ m}^{-2}$ , one to two orders of magnitude higher than previously estimated (Duval, 1985) or modelled (Montagnat and Duval, 2000) for bulk ice samples. Dislocation densities locally increased by subgrain boundaries acting as obstacles can produce enough internal energy to initiate strain-induced grain-boundary migration during the early stages of creep.

### Grain-growth reduction during deformation

The parabolic growth law which describes the grain growth of ice crystals in firn (Gow, 1969), and which is widely applied to ice in ice sheets,

$$A = D_0^2 + kt, \quad (3)$$

can be applied to grain-growth experiments with no applied stress ( $k \approx 5.1 \times 10^2 \text{ mm}^2 \text{ a}^{-1}$ ; Fig. 3). The growth rate,  $k$ , is temperature-dependent.

Grain-size data from creep experiments indicate that grains grow during deformation, but growth is significantly slower than during grain growth with no loading at the same temperature (Fig. 3). We observe an influence of temperature on grain-size evolution during primary/secondary creep (Fig. 3). Jacka and Li (1994) suggest the dependence of grain-size evolution on stress during steady-state tertiary creep is largely independent of temperature. Although creep clearly reduces grain growth during creep tests, we cannot find an explicit dependence on stress. An explanation might be that due to the fact that our experiments do not represent the tertiary creep stage, the measured grain sizes can be regarded as intermediate stages moving towards the steady-state crystal size described by Jacka and Li (1994). Creep experiments at conditions chosen here indicate both temperature and stress dependence of grain-size evolution. This suggests that primary and secondary creep provide a transition between the dependence of grain size on temperature and its dependence on stress.

During experiments which take place at annealing conditions, static grain growth influences grain size and grains can grow according to the grain-growth constant,  $k$ , for a given temperature following Equation (4). Additional processes affecting grain size take place during creep (Gow and Williamson, 1976). Whether these effects compete with or support normal grain growth probably depends on initial grain size, and possibly on other factors such as stress and, eventually, strain rate. Our experimental conditions enable processes which reduce grain-growth rates. As grain size moves towards a stress-dependent tertiary steady-state value, the reducing effect of deformation on grain growth is expected to be small with small stress (fig. 3 in Jacka and Li, 1994). Experiments conducted at 0.18 MPa clearly show the reduction of grain growth by creep (Fig. 3). However, further experiments are required to clarify whether a threshold stress is needed for the competing processes in grain growth at very small stresses (i.e.  $<0.18 \text{ MPa}$ ).

In the following we consider three micro-processes that could be responsible for the grain-growth reduction:

(1) effects of soluble and insoluble impurities on mobility of grain boundaries and driving stresses; (2) splitting of grains by subgrain-rotation recrystallization (polygonization); and (3) migration recrystallization by locally very high grain-boundary migration rates and/or by nucleation of new strain-free grains.

(1) The inhibition of grain growth by impurities and particles that is often seen (Alley and others, 1986; Thorsteinsson and others, 1995) can be excluded here, because pure-water ice has been used to produce the samples. Therefore the grain-growth reduction, observed in these experiments, must be caused by deformation, even though only low total strains are reached.

(2) Although significant fabric change and intense grain rotation are not expected at these low strains (Azuma and Higashi, 1985), subgrain-boundary formation takes place; it is the first stage of splitting of grains by subgrain-rotation recrystallization. Unfortunately fabric data could not be obtained systematically due to the small sample size with relatively small crystal numbers per thin section after tests and problems with application of the etch-pit method. However, the extent to which subgrain boundaries contribute to grain-growth reduction depends on the development into high-angle grain boundaries. Further rotation of subgrains and therefore further deformation is needed. Additionally, removal of subgrain boundaries by grain-boundary migration needs to be considered. Providing a first stage of polygonization, subgrain boundaries contribute to grain-growth reduction. However, a direct correlation between higher subgrain-boundary density and smaller grain size during or after deformation cannot be shown.

(3) Migration recrystallization is described typically as the nucleation of new strain-free grains and the fast migration of grain boundaries (e.g. Duval and Castelnau, 1995), including two phenomena (strain-induced grain-boundary migration (SIGBM) and recrystallization with nucleation) whose main characteristics are alike in that internal strain energy and relatively high temperatures are needed. Nucleation easily decelerates grain growth by production of small grains. However, this explanation is unlikely because true nucleation textures or grain nucleation near grain boundaries, which are visible in high-resolution microstructure maps of sublimation features, are not observed in our experiments. The spontaneous nucleation process is difficult to achieve, requiring very high internal strain energies and high temperatures and, possibly, preferably oriented nucleation seeds. If one of these conditions is not adequately fulfilled, dynamic recrystallization always starts with SIGBM. Although usually described as causing high mean grain size due to the very high grain-boundary migration rate, SIGBM can reduce grain growth. SIGBM is evidenced by irregular grains (Fig. 5) with curves of grain boundaries producing interlocking textures (Duval and Castelnau, 1995; Goldsby and Kohlstedt, 2002). The bulging grain-boundary curves can be cut off from the parent grain by further grain-boundary motion, to build a new, small grain with a similar orientation to the parent (Humphreys and Hatherly, 2004, p.251). Additionally, SIGBM can lead to apparent grain-growth reduction by three-dimensional duplication effects

(studied in detail by Nishida and Narita, 1996) emerging only with interlocking textures: a single grain appears plurally in one section due to its multiple protuberances. It is inevitably counted and measured as two or more grains and therefore significantly decreases the measured mean grain size (also discussed by Gow, 1969; Alley and Woods, 1996). The occurrence of SIGBM is measured in creep samples using the perimeter ratio (Fig. 4b) and has been shown by estimates of local dislocation densities and observations of bulging grain boundaries. Irregularity is dependent on strain and indicates that the contribution of SIGBM to the deceleration of grain growth during deformation is important in these strain regimes.

### Implications for subgrain-boundary-formation processes

It is known from other materials that the orientation of subgrain boundaries depends on the orientation of slip systems of dislocations accumulating in the grain (Trépiéd and others, 1980). As the dominant slip system in ice lies in the basal plane and other slip systems contribute much less to ice deformation (Hondoh, 2000), the different orientations and arrangements of subgrain boundaries give insights into basic considerations about how they are formed. Clearly these thoughts need to be inspected in more detail using full crystal orientation measurements, which are now becoming available (Montagnat and others, 2003; Miyamoto and others, 2005; Obbard and others, 2006b).

The type-c subgrain boundary (straight and basal plane orthogonal) can be explained by considering the classical, and so far only, formation process described in ice (Nakaya, 1958). A tilt boundary is built by pile-up and alignment of edge dislocations gliding on the basal plane during bending of the crystal.

Type-p subgrain boundaries (regular, straight and parallel to the basal plane) cannot be formed by bending of basal planes, but might be explained by analogy with the tilt boundary, i.e. as pile-up and accumulation of screw dislocations (Weertman and Weertman, 1992). The occurrence of this dislocation type in ice was shown by Montagnat and others (2003). A second possible interpretation for p-type subgrain boundaries might be micro-shear zones, which have been observed by Bons and Jessell (1999) in a rock-analogue material. In shear zones (of micrometres to kilometres) observed in rocks, a distinct package of material undertakes a high portion of the total strain of the bulk sample. In contrast to normal slip on basal planes accomplished by dislocations, a wider region of atomic layers consisting of several tens of layers is deformed while the bulk above and below the shear zone remains relatively undeformed. In our experimentally deformed samples, this type of subgrain boundary is quite unlikely, because a distinct grain geometry is needed for micro-shear zones (Bons and Jessell, 1999). However it has been observed in Antarctic ice (S. H. Faria and others, [http://www.mis.mpg.de/preprints/2006/prepr2006\\_33.html](http://www.mis.mpg.de/preprints/2006/prepr2006_33.html)).

Type-z subgrain boundaries (zigzag or step-like) probably consist of tilt boundaries formed by edge dislocations on basal and non-basal planes. As most grains are not oriented to preferably build one type of dislocation, they probably form several dislocation types which align to type-z subgrain boundaries. However, motion of dislocations in many directions (climb and glide) is necessary to obtain sections of

relatively pure tilt or twist boundary. Preliminary X-ray Laue measurements confirm the existence of tilt and twist boundaries (personal communication from A. Miyamoto, 2007).

The rapidly decreasing frequency of type-p subgrain boundaries (Fig. 4d) shows that they are not produced under our conditions and suggests that it is the other types (c and z) that are produced in our experiments.

### Outlook: similarity of high- and low-stress microstructures

Experiments have been conducted at stresses between 0.18 and 0.52 MPa. Compared with the polar ice sheets, where driving stresses are typically <0.1 MPa, measured deformation rates are very high. It is interesting, then, that observed ice substructures are very similar in deformed artificial ice and ice from deep Antarctic ice cores, especially as the experiments reached only secondary creep whereas polar ice deforms, predominantly, in near-steady-state tertiary creep.

As mentioned above, the typical shapes and arrangements of subgrain-boundary types found in the experimentally deformed ice have been characterized in an Antarctic ice core (EDML; data will be presented elsewhere). Due to this observation and the high mechanical anisotropy of ice it can be assumed that these structures are, indeed, characteristic traces of deformation processes displaying the material's response to creep. The similarity between the subgrain-boundary types can be explained by the preponderance of internal dislocation slip for the deformation of polar and artificial ice (Duval and others, 1983; Montagnat and Duval, 2000). A difference might be found in the fraction of the different subgrain-boundary types. In our experiments the fraction of parallel-type subgrain boundaries decreases rapidly with strain, yet this is the most common kind found throughout the deep ice core. This finding suggests further studies are necessary to learn about the activity of dislocation types in low- and high-stress regimes. Furthermore, distributions of subgrain boundaries inside grains are very similar. In both cases, substructures are observed close to grain boundaries forming a 'core and mantle' structure. The accumulation at protruding parts of grains strikingly indicates that strain accumulation is the rule rather than the exception in deforming ice in general. The preponderance of subgrain boundaries on the convex side of grain-boundary curves (Fig. 10) has also been observed in ice sheets, suggesting that local dislocation-density peaks can also occur in ice at low stresses. Most surprising is that mean subgrain-boundary density is of the same order in high-stress experiments ( $\sim 4 \text{ mm}^{-1}$ ; see Fig. 4c) and in the EDML ice core ( $\sim 2 \text{ mm}^{-1}$ ). The slightly lower values in ice deformed at low stresses can be explained by recovery processes which can act with the prolonged duration of creep.

Alongside other similarities in substructure observed in experiments and in ice cores, the evolution of grain growth and especially its dependence on creep should be investigated. This requires further examination of strain-rate effects, impurity effects and other possible factors. In experiments the grain-growth reduction is already significant at low strains. At the higher strains in polar ice it is possible that strain inhomogeneities in layers of the ice sheet lead to significant differences in grain size; further work is required to clarify this. However, deformation needs to be considered as a possible cause for grain-size variation in ice cores.

## CONCLUSIONS

Observations of microstructure evolution during creep experiments have been presented which provide new information about deformation processes at the subgrain scale.

Deformation can significantly reduce grain growth without the presence of solutes or particles. Even at low strains, <10%, subgrain-rotation recrystallization and strain-induced grain-boundary migration lead to less grain growth than under unstrained conditions. Local strain inhomogeneities in polar ice sheets have to be considered when studying sudden grain-size changes in ice cores.

The creep experiments demonstrate the connection between isotropic hardening during primary creep and substructure evolution. The hardening is due to the production and interaction of dislocation walls and subgrain boundaries which act as obstacles for dislocation movement. Strain heterogeneities observed inside grains lead to locally high dislocation densities ( $10^{12} \text{ m}^{-2}$ ), which can cause SIGBM. Similarities in substructure observations indicate similar processes in polar ice.

Different types of subgrain boundaries indicate several formation processes in which several types of dislocations must be involved. The described substructures are indicative of the deformation of ice because they have been observed in artificial and polar ice due to the preponderance of intracrystalline slip.

## ACKNOWLEDGEMENTS

This work was supported by a Grant-in Aid for Science Research (No. 16104006) from the Ministry of Education, Culture, Sports, Science and Technology, Japan. Travel funding was received from the German Academic Exchange Service (DAAD). We thank T. H. Jacka for inspiring discussions, laboratory members (M. Takada, A. Shigekuni, Y. Oba, T. Kokure, T. Nakamura, K. Oba, K. Anno, H. Kobayashi and many others) who helped in many ways and two anonymous reviewers for helpful comments.

## REFERENCES

- Ahmad, S., M. Ohtomo and R.W. Whitworth. 1986. Observation of a dislocation source in ice by synchrotron radiation X-ray topography. *Nature*, **319**(6055), 659–660.
- Alley, R.B. and G.A. Woods. 1996. Impurity influence on normal grain growth in the GISP2 ice core, Greenland. *J. Glaciol.*, **42**(141), 255–260.
- Alley, R.B., J.H. Perepezko and C.R. Bentley. 1986. Grain growth in polar ice: I. Theory. *J. Glaciol.*, **32**(112), 415–424.
- Ashby, M.F. 1970. The deformation of plastically non-homogeneous materials. *Philos. Mag.*, **21**(8), 399–424.
- Azuma, N. and A. Higashi. 1985. Formation processes of ice fabric pattern in ice sheets. *Ann. Glaciol.*, **6**, 130–134.
- Barber, D.J. 1990. Regimes of plastic deformation processes and microstructures: an overview. In Barber, D.J. and P.G. Meredith, eds. *Deformation processes in minerals, ceramics and rocks*. London, Unwin Hyman, 138–178.
- Bons, P.D. and M.W. Jessell. 1999. Micro-shear zones in experimentally deformed octachloropropane. *J. Struct. Geol.*, **21**(3), 323–334.
- Budd, W.F. and T.H. Jacka. 1989. A review of ice rheology for ice sheet modelling. *Cold Reg. Sci. Technol.*, **16**(2), 107–144.
- Duval, P. 1985. Grain growth and mechanical behaviour of polar ice. *Ann. Glaciol.*, **6**, 79–82.
- Duval, P. and O. Castelnau. 1995. Dynamic recrystallization of ice in polar ice sheets. *J. Phys. IV [Paris]*, **5**, 197–205. (Supplément au 3.)
- Duval, P. and H.I. Gac. 1980. Does the permanent creep-rate of polycrystalline ice increase with crystal size? *J. Glaciol.*, **25**(91), 151–157.
- Duval, P. and C. Lorius. 1980. Crystal size and climatic record down to the last ice age from Antarctic ice. *Earth Planet. Sci. Lett.*, **48**(1), 59–64.
- Duval, P., M.F. Ashby and I. Anderman. 1983. Rate-controlling processes in the creep of polycrystalline ice. *J. Phys. Chem.*, **87**(21), 4066–4074.
- Duval, P., L. Arnaud, O. Brissaud, M. Montagnat and S. de la Chapelle. 2000. Deformation and recrystallization processes of ice from polar ice sheets. *Ann. Glaciol.*, **30**, 83–87.
- Gay, M. and J. Weiss. 1999. Automatic reconstruction of polycrystalline ice microstructure from image analysis: application to the EPICA ice core at Dome Concordia, Antarctica. *J. Glaciol.*, **45**(151), 547–554.
- Glen, J.W. 1955. The creep of polycrystalline ice. *Proc. R. Soc. London, Ser. A.*, **228**(1175), 519–538.
- Goldsby, D.L. and D.L. Kohlstedt. 1997. Grain boundary sliding in fine-grained ice I. *Scripta Mater.*, **37**(9), 1399–1406.
- Goldsby, D.L. and D.L. Kohlstedt. 2002. Reply to comment by P. Duval and M. Montagnat on 'Superplastic deformation of ice: experimental observations'. *J. Geophys. Res.*, **107**(B11). (10.1029/2002JB001842.)
- Gow, A.J. 1969. On the rates of growth of grains and crystals in South Polar firn. *J. Glaciol.*, **8**(53), 241–252.
- Gow, A.J. and Williamson, T. 1976. Rheological implications of the internal structure and crystal fabrics of the West Antarctic ice sheet as revealed by deep core drilling at Byrd Station. *CRREL Rep.* 76, 1665–1677.
- Hobbs, P.V. 1974. *Ice physics*. Oxford, etc., Clarendon Press.
- Hondoh, T. 2000. Nature and behavior of dislocations in ice. In Hondoh, T., ed. *Physics of ice core records*. Sapporo, Hokkaido University Press, 3–24.
- Hooke, R.LeB. 2005. *Principles of glacier mechanics. Second edition*. Upper Saddle River, NJ, Prentice Hall.
- Humphreys, F.J. and M. Hatherly. 2004. *Recrystallization and related annealing phenomena. Second edition*. Oxford, etc., Pergamon Press.
- Jacka, T.H. 1984. The time and strain required for development of minimum strain rates in ice. *Cold Reg. Sci. Technol.*, **8**(3), 261–268.
- Jacka, T.H. and J. Li. 1994. The steady-state crystal size of deforming ice. *Ann. Glaciol.*, **20**, 13–18.
- Jacka, T.H. and R.C. Lile. 1984. Sample preparation techniques and compression apparatus for ice flow studies. *Cold Reg. Sci. Technol.*, **8**(3), 235–240.
- Ketcham, W.M. and P.V. Hobbs. 1969. An experimental determination of the surface energies of ice. *Philos. Mag.*, **19**(162), 1161–1173.
- Kipfstuhl, S. and 6 others. 2006. Microstructure mapping: a new method for imaging deformation-induced microstructural features of ice on the grain scale. *J. Glaciol.*, **52**(178), 398–406.
- Miyamoto, A., H. Shoji, A. Hori, T. Hondoh, H. Clausen and O. Watanabe. 2005. Ice fabric evolution process understood from anisotropic distribution of a-axis orientation on the GRIP (Greenland) ice core. *Ann. Glaciol.*, **42**, 47–52.
- Montagnat, M. and P. Duval. 2000. Rate controlling processes in the creep of polar ice: influence of grain boundary migration associated with recrystallization. *Earth Planet. Sci. Lett.*, **183**(1–2), 179–186.
- Montagnat, M. and P. Duval. 2004. The viscoplastic behaviour of ice in polar ice sheets: experimental results and modelling. *C. R. Phys.*, **5**(7), 699–708.
- Montagnat, M., P. Duval, P. Bastie and B. Hamelin. 2003. Strain gradients and geometrically necessary dislocations in deformed ice single crystals. *Scripta Mater.*, **49**(5), 411–415.
- Mullins, W.W. 1957. Theory of thermal grooving. *J. Appl. Phys.*, **28**(3), 333–339.

- Nakaya, U. 1958. Mechanical properties of single crystals of ice. Part 1. Geometry of deformation. *SIPRE Res. Rep.* 28.
- Nishida, K. and H. Narita. 1996. Three-dimensional observations of ice crystal characteristics in polar ice sheets. *J. Geophys. Res.*, **101**(D16), 21,311–21,317.
- Nishimura, K. 2004. The effect of impurities on grain growth rate on ice of Antarctic ice cores. (Master's thesis, Nagaoka University of Technology.)
- Obbard, R., I. Baker and D. Iliescu. 2006a. Correspondence. Grain boundary grooving in ice in a scanning electron microscope. *J. Glaciol.*, **52**(176), 169–172.
- Obbard, R., I. Baker and K. Sieg. 2006b. Using electron backscatter diffraction patterns to examine recrystallization in polar ice sheets. *J. Glaciol.*, **52**(179), 546–557.
- Passchier, C.W. and R.A.J. Trouw. 1996. *Microtectonics*. Berlin and Heidelberg, Springer-Verlag.
- Paterson, W.S.B. 1994. *The physics of glaciers. Third edition*. Oxford, etc., Elsevier.
- Petrenko, V.F. and R.W. Whitworth. 1999. *Physics of ice*. Oxford, etc., Oxford University Press.
- Pimienta, P. and P. Duval. 1987. Rate controlling processes in the creep of polar glacier ice. *J. Phys. [Paris]*, **48**, Colloq. C1, 243–248. (Supplément au 3.)
- Saylor, D.M. and G.S. Rohrer. 1999. Measuring the influence of grain-boundary misorientation on thermal groove geometry in ceramic polycrystals. *J. Am. Ceram. Soc.*, **82**(6), 1529–1565.
- Thorsteinsson, T., J. Kipfstuhl, H. Eicken, S.J. Johnsen and K. Fuhrer. 1995. Crystal size variations in Eemian-age ice from the GRIP ice core, central Greenland. *Earth Planet. Sci. Lett.*, **131**(3–4), 381–394.
- Trépiéd, L., J.C. Doukhan and J. Paquet. 1980. Subgrain boundaries in quartz theoretical analysis and microscopic observations. *Phys. Chem. Mineral.*, **5**(3), 201–218.
- Weertman, J. and J.R. Weertman. 1992. *Elementary dislocation theory*. Oxford, etc., Oxford University Press.

*MS received 4 January 2007 and accepted in revised form 12 May 2007*

# Appendix B

## Publication II - Subgrain boundaries in EPICA-Dronning Maudland (EDML) deep ice core

Hamann, I., Kipfstuhl, S., Faria, S. H., Azuma, N., Miyamoto, A.  
(subm. October 2007)

Submitted to Journal of Glaciology on October 12<sup>th</sup> 2007.

## Subgrain boundaries in EPICA-Dronning Maud Land (EDML) deep ice core

Ilka HAMANN,<sup>1\*</sup> Sepp KIPFSTUHL,<sup>1</sup> Sérgio H. FARIA,<sup>2</sup> Nobuhiko AZUMA,<sup>3</sup> Atsushi MIYAMOTO,<sup>4</sup>

<sup>1</sup>Alfred Wegener Institute Foundation for Polar and Marine Research, Columbusstrasse, D-27568 Bremerhaven, Germany

<sup>2</sup>University of Göttingen, GZG, Sect. of Crystallography, Goldschmidtstr. 1, D-37077 Göttingen, Germany

<sup>3</sup>Department of Mechanical Engineering, Nagaoka University of Technology, 1603- Kamitomioka, Nagaoka 940-2188, Japan

<sup>4</sup>Institute of Low Temperature Science, Hokkaido University, Kita 19-jo Nishi 8-chome, Kita-ku, Sapporo 060-0819, Japan

**ABSTRACT.** Subgrain boundaries which are revealed as shallow sublimation grooves are a direct and easily observable feature of intracrystalline deformation. Data obtained from an Antarctic deep ice core (EDML) cannot detect a distinct depth region of increased subgrain boundary formation compared to other depths, which would indicate a polygonization regime and therefore cannot support the classical model of recrystallization regimes. Several shapes of subgrain boundaries reflecting the high mechanic anisotropy in combination with crystal-orientation analysis enable characterization of different subgrain-boundary types.

### INTRODUCTION

The dynamics of glaciers and polar ice sheets play an important role for the impact ice masses have on climate. Models of ice sheet flow help to understand these influences. The flow law commonly used in these models and originally formulated by Glen (1955) contains parameters involving mostly unknown effects of impurities and microstructures (Paterson, 1994; Petrenko and Whitworth, 1999). Anisotropic flow laws have been developed to include the crystal-orientation distributions as a fundamental component of ice structures (e.g. Gillet-Chaulet and others, 2005; Faria, 2006; Placidi and Hutter, 2006; Thorsteinsson, 2006; Pettit and others, 2007). Comprehension of microstructural features can help to improve our understanding about the flow of ice.

The deformation of polar ice sheets is brought about by several processes on the atomic scale, like dislocation motion and diffusion, which are difficult to observe directly. As grain-size evolution and crystal-orientation fabric development are easier to observe they are preferably described for ice cores to infer the microscopic processes operating (e.g. Gow and Williamson, 1976; Alley, 1992; Thorsteinsson and others, 1997; Azuma and others, 1999; Wang and others, 2003; DiPrinzio and others, 2005). However, traces of deformation on the direct, microscopically visible scale are, besides others, subgrain boundaries. They result from microscopic processes during creep: the bending and splitting of grains into smaller pieces, often called polygonization or rotation recrystallization (e.g. Poirier, 1985).

Subgrain boundaries have been widely studied in material- and geosciences for a considerable time (e.g. Sedlacek and others, 2002; Humphreys and Hatherly, 2004; Bestmann and others, 2005, and references therein). In the case of ice, they mainly have been described in experimentally deformed specimens (Nakaya, 1958; Wilson and others, 1986; Barrette and Sinha, 1994; Hamann and others, 2007) and ideas from metallic and geologic materials have been applied. For naturally deformed ice, like polar ice sheets or glaciers, a conclusive study focusing on subgrain boundaries, their statistical oc-

currence or detailed analysis on their geometry is still missing. According to Nakaya (1958), who deformed single crystals of ice from the Mendenhall Glacier and described their emergence in ice for the first time, the polygonization process starts with formation of slip lines, which become visible after bending the ice crystal just a few minutes of arc. This first stage is followed by the formation of multiple subgrain boundaries in regions of stress/strain concentration changing the bow-shaped curving of the slip bands to a more angular-shaped slip-band geometry due to dislocation rearrangement along a wall. Thus, the subgrain boundaries border regions of slightly different misorientations. Further deformation and bending of the grain leads to an increase of misorientation and therefore to the strengthening of one subgrain boundary and finally to the splitting of the grain.

Extracted from the glaciology literature the following is the standard model of recrystallization processes: following a normal grain growth regime, polygonization leading to rotation recrystallization dominates the microstructural evolution in a typical depth range (several hundreds of meters depth down to depths reaching  $-10^{\circ}\text{C}$  temperature) and is followed by a migration recrystallization regime (e.g. Duval and Castelnau, 1995; Alley and others, 1995; Duval, 2000).

Although the occurrence of grain substructures has been noted in some studies (e.g. Lipenkov in Thorsteinsson and others, 1997; Duval, 2000; Wang and others, 2003) there is still no conclusive work on subgrain boundaries as a direct effect of rotation recrystallization which proves or disproves the classical model. As polygonization is assumed to play some role for the evolution of the crystal-orientation fabrics in deeper ice, it gained attention among the subgrain-boundary formation processes in ice-related studies (Alley and others, 1995; Mansuy and others, 2000; Faria and Kipfstuhl, 2004; Placidi and others, 2004).

In other materials different evolution mechanisms of subgrain boundaries have been described by Means and Ree (1988) and are mentioned for completeness. Experiments with a rock-analogue material (octachloropropane) revealed seven types of subgrain boundaries including the classical polygonization. Furthermore evolution from former grain bound-

\*E-mail: ilka.hamann@awi.de

aries by reduction of misorientation has been found, as well as formation by coalescence or impingement due to moving (sub)grain boundaries, and several types describing the migration of subgrain boundaries. Especially in the deeper parts of ice sheets, where strong lattice preferred orientations occur (girdle or single maximum fabrics) due to the reduction of c-axes misorientations, small angle grain boundaries might evolve from reduction of misorientation along former high angle grain boundaries. Also in the deeper parts of ice sheets, in regions close to the bedrock with higher temperature, where grain boundaries are thought to be more mobile, even evolution by impingement could become possible. Means and Ree (1988) observed that the main portion of subgrain boundaries for which a formation process could be determined was built by splitting of grains in a polygonization process.

The aim of this work is to show that in polar ice apart from classical polygonization (sketched by e.g. Nakaya, 1958; Alley and others, 1995) other subgrain boundary formation processes must be active and that the subdivision of grains occurs in all depths. We present statistical data on subgrain boundaries observed in samples of the EPICA (European Project for Ice Coring in Antarctica) deep ice core drilled in Dronning Maud Land, Antarctica (EDML ice core).

## METHOD

Ice-thick sections (50 x 100 x 5 mm) cut vertically along the ice core were prepared by carefully microtoming both surfaces. Thermal etching by sublimation reveals grain boundaries and subgrain boundaries as grooves on the surfaces (e.g. Nishida and Narita, 1996; Obbard and others, 2006a). The section frozen on a glass plate is then mapped in microscopic resolution (1pix=3.5 $\mu$ m) (Kipfstuhl and others, 2006). The surface of the whole sample is reconstructed by 1200 up to 1800 photomicrographs to a mosaic image. The majority of observations have been performed on site, mostly 1 to 2 days after drilling.

From the mosaic images statistical data about the occurrence of subgrain boundaries, their frequencies in individual grains, their shape and location were derived manually by image analysis. In contrast to the deep grooves produced by grain boundaries, subgrain-boundary grooves are shallow (Saylor and Rohrer, 1999), have varying depths and appear as light to middle dark grey lines in the photographs. They are difficult to extract automatically as varying depths of grooves and varying background grey values do not allow global thresholds to segment these features from the images. Subgrain-boundary number and types occurring in each grain have been counted and the corresponding grain area was measured by automatic image analysis. Approximately one hundred grains per sample have been examined in 18 different depths equally distributed along the core length.

Additionally, four thin sections were prepared to derive crystal-orientation fabric data as well as microstructures measured by mapping of sublimation features on the same surface, in order to characterize different types of subgrain boundaries according to their shapes and arrangement with respect to the crystallographic orientation. Further crystal-orientation data, processed as nearest neighbour misorientations, are used for this study. The c-axis measurements have been conducted with an automatized fabric analyser system (Wilson and others, 2003). Investigator v1.12 (Russell-Head, 2004) was used to determine misorientation angles. The complete crystal-

orientation fabric data set for the whole length of the core shall be presented elsewhere. Fabric data for some selected depths can be seen in Eisen and others (2007).

First X-ray Laue measurements of full crystallographic orientation were used to confirm that shallow sublimation grooves indeed represent all subgrain boundaries (unpublished data, June 2007). Details concerning the method can be found in (Miyamoto and others, 2005). Comparing the sublimation grooves along subgrain boundaries with respect to the crystal orientations the quality (intensity or depth) of sublimation grooving turned out to depend on orientation. Therefore the typical shapes are most easily observable, if the sublimation surface is within  $\approx 30^\circ$  to the c-axis. Higher angles between c-axis and sublimation surface lead to fainter, less well defined lines in the microstructure map, which might lead to errors in recognition of the features. The reason for this dependence of sublimation on cutting-orientation is probably due to the fact that the best thermal grooving can be obtained if the boundary is perpendicular to the surface, whereas an oblique intersection of boundary and surface produces oblique and shallow grooves. Therefore a considerable amount of unidentifiable subgrain boundaries can occur in grains "badly" oriented for sublimation grooving. With increasing depth, as crystal-orientation fabric evolution enables sample cutting with many grains "nicely" oriented for sublimation, this effect is decreasing. This leads to an underestimation of subgrain-boundary frequencies in shallower depth samples. The data presented in this paper have been obtained from section images without any correction of dependence on crystal orientation or correction of 3D-effects.

## RESULTS

Subgrain boundaries separate parts of a grain with slightly different orientations. They are common features in the EDML ice core, and are observed in all depths, and appear in different shapes and intensities or depths of sublimation grooves. Typical subgrain boundaries encountered in the EDML core are shown in Fig. 1.

Most subgrain boundaries occur in networks or intricate patterns (e.g. Fig. 1c). Only few, generally the stronger ones, cross grains completely. The shallow sublimation grooves have low misorientations, though they are qualitatively visible and traceable between crossed polarizers under high resolution (in Kipfstuhl and others, 2006, Fig. 6). These findings are consistent with preliminary results from the EPICA Dome C ice core (in Wang and others, 2003, Fig. 4) and X-ray Laue measurements, which verify that even very low misorientation boundaries ( $\ll 0.5^\circ$ ) can be detected by sublimation method (unpublished data, June 2007). Such features are probably dislocation walls rather than subgrain boundaries and may be transient structures (see interpretation and discussion below). For the sake of simplicity the distinction between subgrain boundaries and transient dislocation walls will not be made in the following, so that all weak, shallow sublimation grooves will be called subgrain boundaries. On the other hand, the most trivial ideal of a single subgrain boundary describing division of a grain into two clearly distinguishable parts (e.g. Fig. 1b) is actually *not* the most frequent one. Typically, maximum misorientations of sublimation grooves classified as strong subgrain boundaries in this study are  $\approx 3$  to  $4^\circ$  (unpublished data, June 2007).

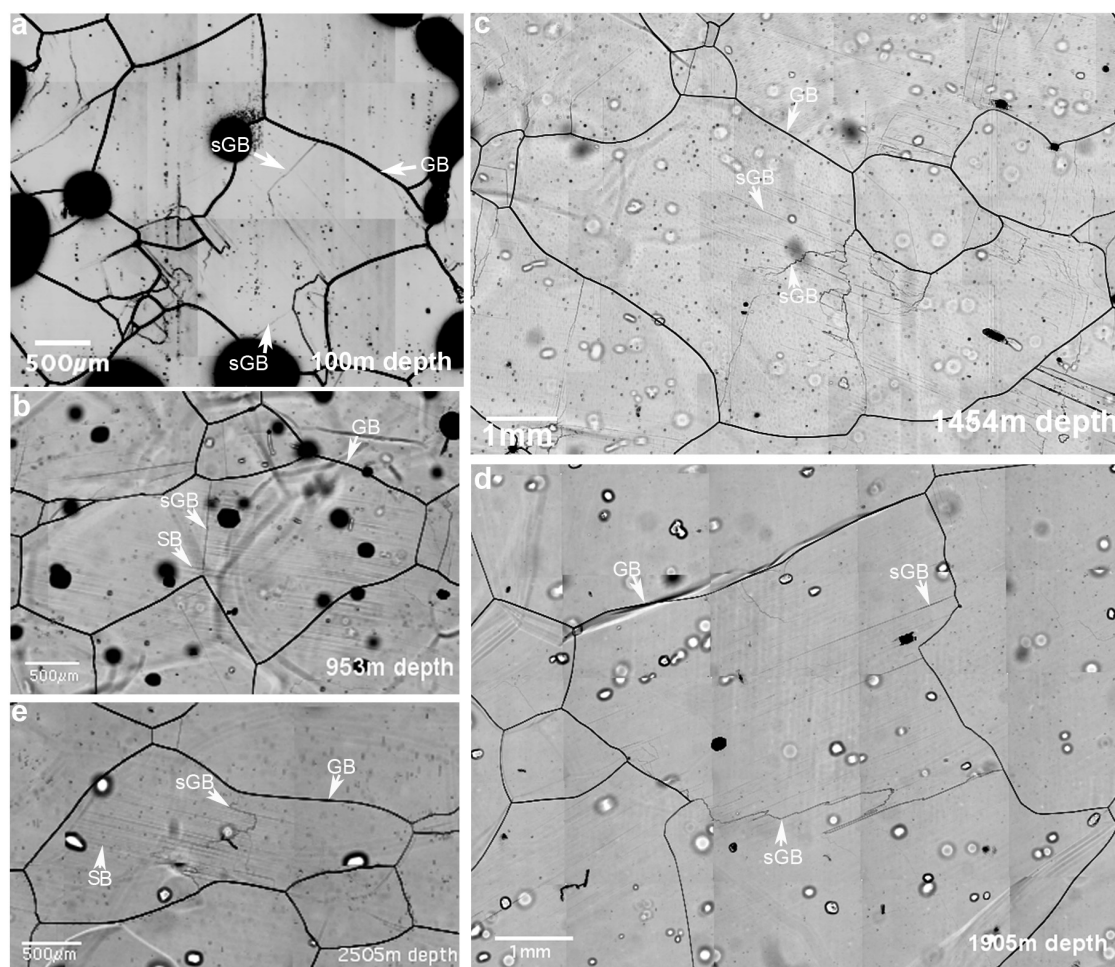


**Fig. 1.** Photomicrographs from different depths. Grain boundaries (GB), slip bands (SB) and subgrain boundaries (sGB) are indicated. The different grey values of the lines (in the same picture) are related to the depths of the respective etch grooves produced by sublimation. Different grey values in different pictures are due to changes in light conditions and capturing settings.

### Subgrain-boundary occurrence

The frequency of grains with subgrain boundaries versus depth (Fig. 2a) reveals that in any depth these occur between 36% and 86% of all examined grains. The record shows that the concentration of subgrain boundaries does not change much with depth. Starting with  $\approx 65\%$  grains with subgrain boundaries at the most shallow depths a slight increase to  $\approx 80\%$  at 1800m depth seems to occur (Fig. 2a). Though, it has to be taken into account that the data have not been corrected for the above mentioned dependence of grooving on crystal orientation and sublimation-surface orientation. With more depth, a preferred lattice orientation evolves: the c-axis orientations develop from a uniform (isotropic) distribution in shallow depths to an alignment in a plane (girdle fabric from  $\approx 600m$  to 2000m depth) and along the vertical core axis (single maximum fabric) in the deepest samples (below 2030m)(unpublished data shall be presented elsewhere, first results in Eisen and others, 2007). Although a relative fit-

ting of core breaks was attempted, loss of core orientation lead to changing angles between girdle plane and sublimation surface: samples used for subgrain-boundary studies with a rather weak but strengthening girdle ( $\approx 600m$  to 1650m) are cut in an angle of  $\approx 45^\circ$  to the girdle plane, whereas below ( $\approx 1650m$  to 2030m) the girdle plane is identical to the sublimation surface. The latter and the single maximum fabric configuration provide more grains well oriented for sublimation in vertical sections. Therefore the data in the shallower depths are probably somewhat underestimated, which suggests, that this increase is smaller or might even be an artefact of the sublimation method and the fabric evolution. In the deepest examined depths between 1800m and 2600m the fraction of grains with subgrain boundaries is decreasing to  $\approx 50\%$  again. However, the relevance is not clear as the scatter of data is rather high.

The effect of grain size is displayed in Fig. 2b. Samples with larger grains include more grains showing subgrain bound-

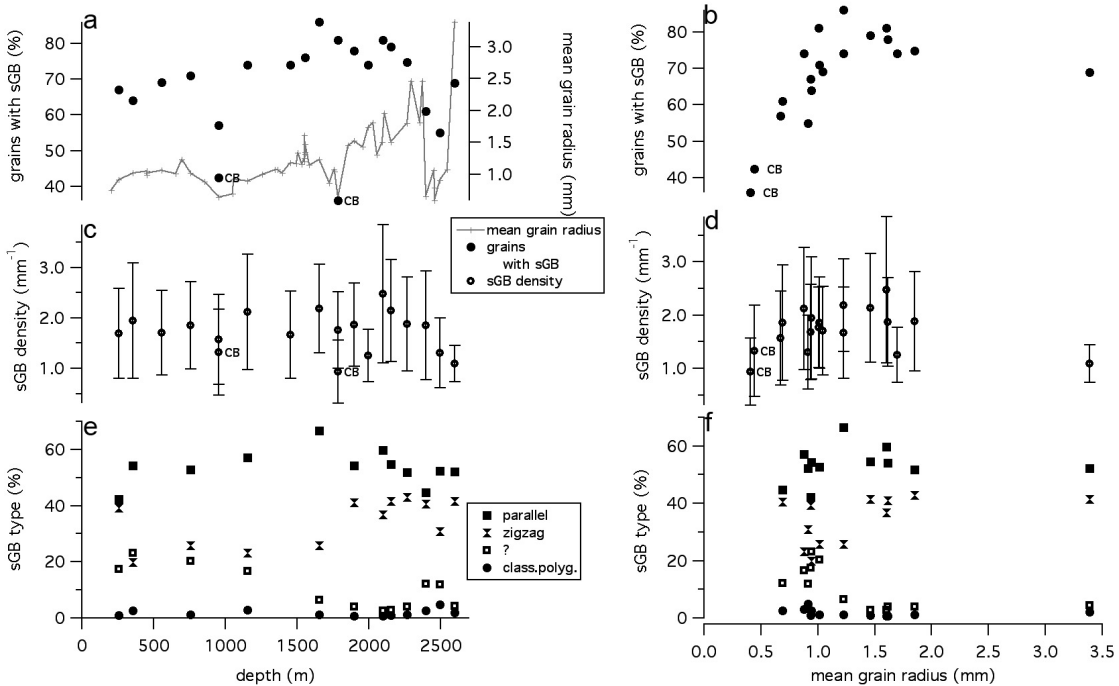


**Fig. 2.** Subgrain boundary frequencies versus drilling depth and mean grain radius, respectively. (Grain radii were calculated from area-equivalent circles for each grain.) a&b: Fraction of grains with subgrain boundaries (Line: grain size for comparison in a). c&d: Average values of subgrain boundary density (See text for further explanation. Error bars: standard deviation.) e&f: Fraction of subgrain boundary types. (CB = cloudy band)

aries (up to 80% of all grains) whereas small-grain-size samples in cloudy bands exhibit only 30% grains with subgrain boundaries. Interesting is the comparison of the statistics of small and large grains within the same sample (10cm length), which means small- and large-grain-size ice have the same age, bulk deformation and thermal history. This is possible in samples from the last glacial period, where clear ice and cloudy bands are found in the same sample. Cloudy band ice is characterized by significantly smaller grain size and higher impurity concentration. It bears significantly less grains undergoing subgrain-boundary formation than clear, large-grain-size ice. For example, the section from  $\approx 1800m$  depth shows the highest values in the clear-ice part and in the cloudy ice the lowest. The highest amounts of grains with subgrain boundaries (75 to 80%) can be observed in samples with a mean grain radius of  $\gtrsim 1mm$ . This mean grain radius of  $\approx 1mm$  seems to indicate a critical value for grains undergoing a maximum amount of subgrain-boundary formation in the observed samples (Fig. 2b).

To assess the grain-size influence in the subgrain-boundary occurrence from our data we define the subgrain-boundary density as total subgrain-boundary length per area. Since subgrain boundaries could not be automatically detected in a reliable way via image analysis, the total subgrain-boundary length within a grain has been determined by time consuming and tedious manual measurements. Therefore, a true subgrain-boundary density from exactly measured lengths was determined for three depths only. The values displayed in Fig. 2c,d are simplified subgrain-boundary densities estimated as fol-

lows. For all examined depths, we calculated an assessed total subgrain-boundary density from subgrain-boundary numbers per grain by assuming that the average subgrain-boundary length is the radius of the grain. This is a reasonable estimate because most subgrain boundaries do not cross the grain completely, but start at the grain boundary and fade out towards the centre of the grain. By comparison with the exactly measured value in the three depths results the fact that, this assessed subgrain-boundary density underestimates the true value by  $\approx 25\%$ . This underestimation is probably due to the fact that many subgrain boundaries are not straight but shaped irregularly. Therefore, finally a correction was applied which was obtained from the power-law correlation of true subgrain-boundary densities with the assessed densities leading to the mean simplified subgrain-boundary densities in Fig. 2c,d.

Subgrain-boundary-density data, which smoothen the grain-size effect on subgrain-boundary statistics confirm that there is no clear correlation with depth (Fig. 2c). Values are changing only within the range of the scattering of data. However, a distinct depth region of significantly higher subgrain-boundary formation cannot be detected.

### Misorientation data

For subgrain-boundary types, which involve c-axes misorientation, the role of sub-division of grains for grain-size evolution can be evaluated using misorientation data extracted from fabric measurements as suggested by Alley and others (1995). Misorientations of neighbouring grains and randomly chosen

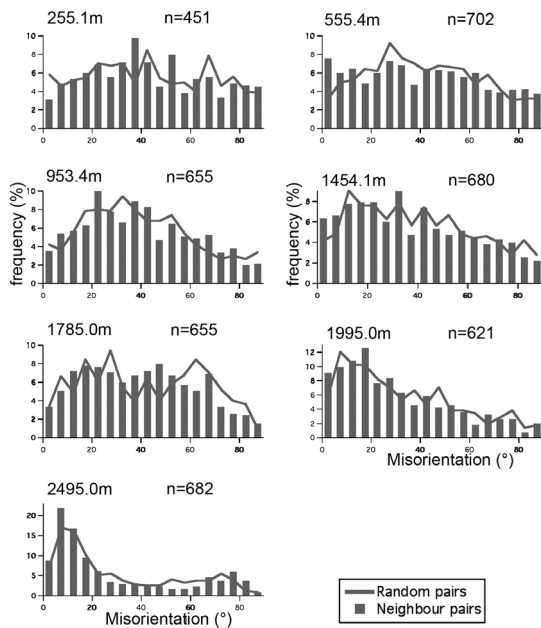


**Fig. 3.** C-axes misorientation distribution histograms. Bin width is  $5^\circ$ . Line: random grain pairs, selected automatically from whole sample c-axis data (500 pairs per section). Bars: neighbour grain pairs, selected manually (number of pairs given as  $n$ ).

grains are compared in Fig. 3. Both data sets are dominated by the influence of the above mentioned fabric evolution with depth (unpublished data shall be presented elsewhere, first results in Eisen and others, 2007). This leads to accumulation of smaller misorientation angles ( $10 - 15^\circ$ ) with depth (visible in 1995m and 2495m depth) as most c-axes become aligned along the vertical axis in both, random and neighbouring grain pairs. Although a slightly higher frequency of the smallest nearest-neighbour misorientations ( $0 - 10^\circ$ ) can be observed at 555.4m, the discrepancy as to random-pair misorientations is not significantly larger than for other angles in this depth. Therefore the analysis of neighbour-grain misorientations does not provide evidence that a significant amount of subgrain boundaries turns into grain boundaries at some particular depth. This is contrary to previous expectations (e.g. Alley and others, 1995; Azuma and others, 2000) and supports Wang and others (2003) results.

### Distribution of subgrain boundaries within grains

Subgrain boundaries are not distributed homogeneously inside the ice crystallites (Fig. 1 and 4). Generally, they occur more frequently, stronger and darker at the grain boundaries and become lighter and fewer towards the center of the grain (e.g. Fig. 1c,d) (Kipfstuhl and others, 2006). Furthermore, high-resolution subgrain-boundary distribution is clearly related to and seems affected by the grain-boundary morphology and grain shapes, which are irregular and complex from shallow depths on (examples see Fig. 1) (Kipfstuhl and others, 2007a,b), because accumulation of subgrain boundaries

occurs especially at sites with a complex part of grain boundary where a grain e.g. is penetrating into a neighbour (Fig. 4). Approximately 20 to 40% of all grains show these geometry-related effects on subgrain boundary distribution.

The interactions of grain-boundary morphology with subgrain boundaries can be distinguished by the shape of their intersection. Sharply edge-shaped connections seem to indicate that subgrain boundaries sometimes hold or are held by the grain boundary, as well as to separate a prominent part from the grain (Fig. 4b).

Besides such sharply edged junctions, smooth grain boundary curvatures can be observed in most grains. These curved grain-boundary segments are often bowed toward the part of a grain, which shows subgrain boundaries (examples see Fig. 5a-c). Statistics on grain-boundary curvatures reveal, that the majority show higher subgrain-boundary density on their convex sides (Fig. 5d). The amount of cases, where a difference of subgrain-boundary numbers on both sides cannot be detected, or where no subgrain boundaries visible in the vicinity of the grain-boundary curvature are, however, still very high in all samples. Nevertheless, the fraction of bulges towards the side with higher subgrain-boundary density shows a significant surplus of convex-side types in all examined depths.

### Subgrain-boundary types

Three types of subgrain boundaries can be distinguished according to their shapes and arrangement with respect to the basal plane (Fig. 6a). Two of them occur at high angle or orthogonal and the third parallel to the basal plane.

The most common type (p-type) of subgrain boundaries is regular and straight and occurs parallel to slip bands, the traces of the basal plane, which can be observed by c-axes measurements in combination with microstructure mapping (Fig. 6f,d). This parallel arrangement to the basal plane was confirmed by preliminary X-ray Laue measurements (unpublished data, June 2007). Often, the p-type appears in peculiar swarms of multiple subgrain boundaries parallel to each other. The second common type (z-type) appears irregular (zigzag or step-like shape, Fig. 6d) and often in networks. The latter is usually rather short, not crossing the grain completely, becoming less dark and fading out. The third type is more straight and orthogonal or nearly orthogonal to the basal planes (Fig. 6e). Its shape and arrangement regarding the crystal orientation resembles best the classical conception of a grain undergoing polygonization as described by (Nakaya, 1958) (see also e.g. Fig. 2 in Alley and others, 1995). Therefore it will also be called "classical" polygonization type (c-type) in the following. In some cases subgrain boundaries of this type are connected to a z-type subgrain boundary and the z- and the c-types are both perpendicular or at some high angle to the basal plane (Fig. 6d,e), which makes distinction difficult. Frequently, all three subgrain types occur together in the same grain.

The above described types are best developed and recognizable in grains where the c-axis has an angle to the sublimation surface within  $\approx 30^\circ$ , because, as mentioned above, the sublimation quality is dependent on the sublimation surface orientation. In grains with other orientations these types are less developed or there occur subgrain boundaries with no specific shape (e.g. roundly bowed).

The evolution of frequencies of the types with depth are displayed in Fig. 2e,f. As already mentioned the most frequent

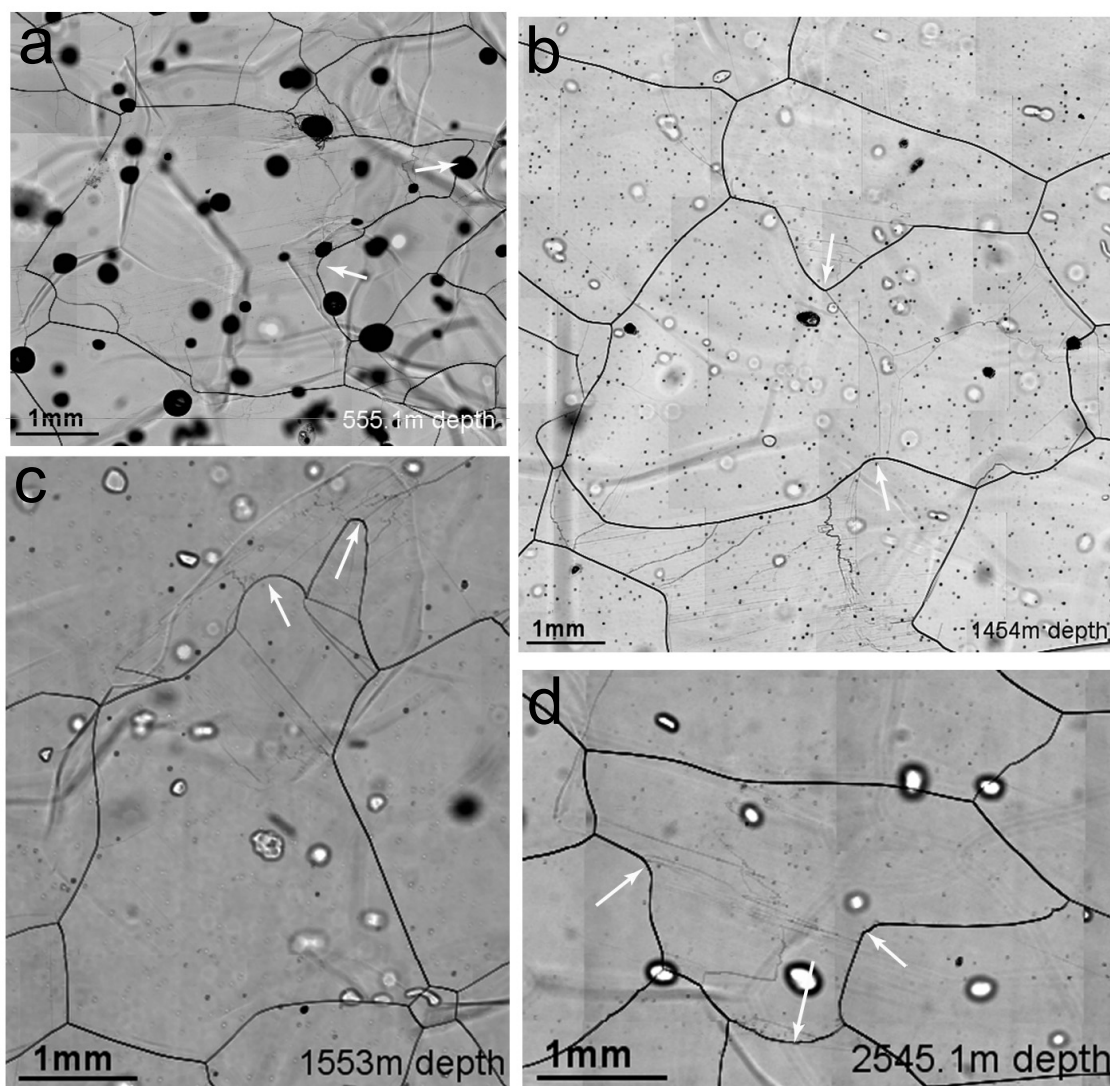


**Fig. 4.** Photomicrograph examples of typical interactions between grain and subgrain boundaries at several depths. Subgrain boundaries occur preferably at protruding geometries of grain boundaries where a grain is penetrating into a neighbour. Examples of such protrusions are indicated by arrows. a: 555.1m b: 1454m c: 1553m d: 2545.1m.

type is the parallel one, followed by the irregular type, and the type resembling best the classical polygonization is quite rare. This is the case in all depths. A considerable amount of subgrain boundaries was observed where a classification of shape was difficult. The frequencies of types are not changing significantly with depth. Only the amount of unidentifiable subgrain-boundary types decreases, probably due to fabric enhancement, which enables vertical sections with many grains oriented for best sublimation conditions.

## DISCUSSIONS

### Implications on recrystallization processes in ice sheets

Dynamic recrystallization processes induce changes in the preferred crystal-orientation fabrics and therefore are important for the modeling of the flow of ice sheets (Budd and Jacka, 1989; Duval and Castelnau, 1995; Thorsteinsson, 2006). Three recrystallization regimes in the ice sheets have been described as occurring in a sequence with depth: normal grain growth (grain-boundary energy driven, static recrystallization), rotation recrystallization (continuous dynamic recrystallization) and migration recrystallization (discontinuous dynamic recrystallization) (e.g. Pimienta and Duval, 1989; Al-

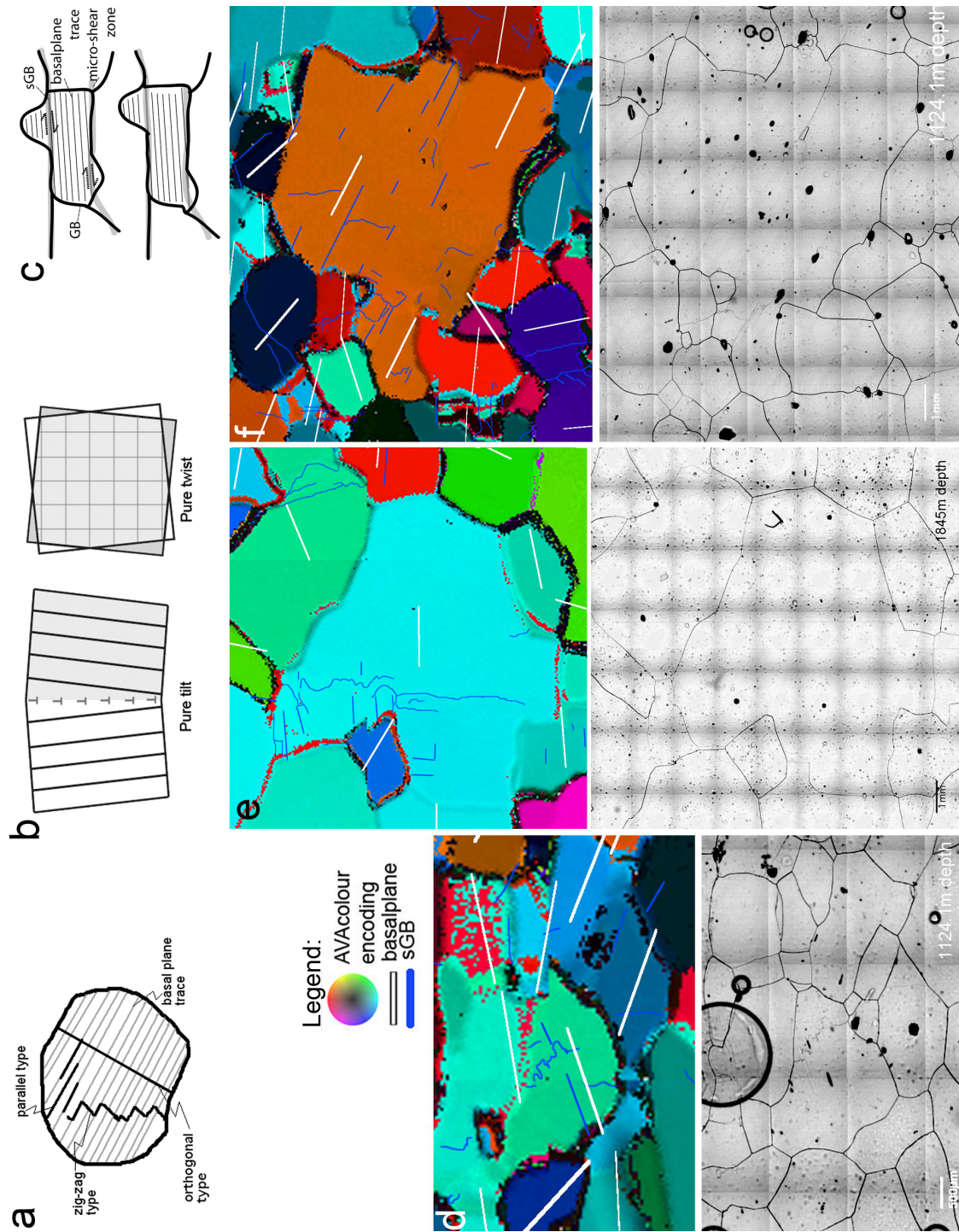


**Fig. 6.** a: Schematic illustration of subgrain-boundary types b: Possible formation processes involving easiest dislocation conceptions (after Föll, 2000) c: Possible formation process involving micro shear (after Bons and Jessell, 1999) d-f: Combination of microstructure mapping (lower pictures) and c-axis measurements with trace of basal plane (white bars) drawn after AVA-image and subgrain boundaries drawn after photomicrograph (lower pictures)

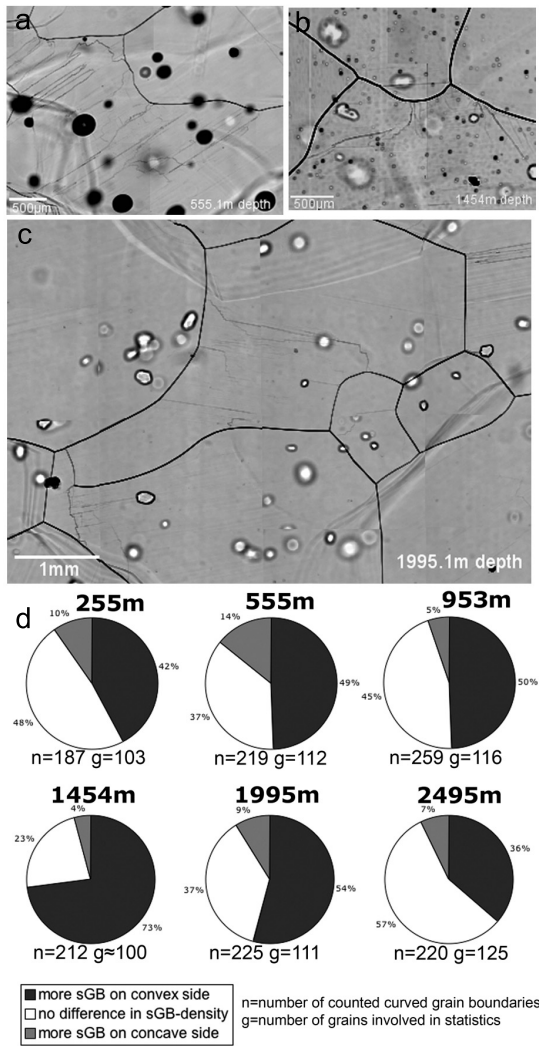


**Fig. 5.** a-c: Photomicrograph examples of grain boundary bulging. a: 555.1m b: 1454m c: 1995.1m. d: Frequency diagrams of the subgrain density at each side of the bulge, for different depths.

ley, 1992; Duval and Castelnau, 1995; De La Chapelle and others, 1998; Duval, 2000; Montagnat and Duval, 2000).

#### Rotation recrystallization

A small effect on fabric evolution is caused by rotation recrystallization by which, under the action of localized stresses, some grains are divided into two or more subgrains. This process forms slightly misoriented subgrains (referred to as polygonization after Poirier (1985)) separated by dislocation walls. Polygonization leads to subgrain-boundary formation, splitting of grains and thus to a reduction of grain size indicated by the higher frequency of grains with subgrain boundaries in larger grain-size samples than in smaller ones (Fig. 2b). Larger grains tend to split easier than smaller grains, which

is likely to be the case during polygonization. This is the beginning stage and basis for rotation recrystallization, a continuous dynamic recrystallization process (Humphreys and Hatherly, 2004) acting during deformation in the whole volume of material. The division starts by alignment and arrangement of dislocations into walls forming subgrain boundaries (Weertman and Weertman, 1992), which may slowly develop into new grain boundaries. How many grains undergo subgrain-boundary formation is revealed by statistics on the occurrence of grains with subgrain boundaries (Fig. 2a). The data presented here show that the majority of all grains have subgrain boundaries or dislocation walls and therefore support that polygonization indeed plays an important role in ice-sheet deformation.

According to the current belief (e.g. Duval and Castelnau, 1995; De La Chapelle and others, 1998; Duval and others, 2000) rotation recrystallization should set in at depths, typically in a few hundred meters, where normal grain growth, characterized by continuously increasing grain size, ceases. The reason for this belief is that, polygonization tends to split grains and consequently subgrain boundaries should occur in this depth. The levelling of the grain-size curve with depth were used as markers for the change in dominance from normal grain growth to polygonization (e.g.  $\approx 400m$  at Bird Station (e.g. Gow and Williamson, 1976; Alley and others, 1995) and  $\approx 700m$  at GRIP (Castelnau and others, 1996; Thorsteinsson and others, 1997)).

Also in the EDML ice core, grain size increases slightly in the firn and the most shallow 100m (Fig. 2a), but is almost constant in Holocene (down to  $\approx 700m$  depth), and only starts to increase below LGM ice (below  $\approx 1000m$  depth). However, the observed subgrain-boundary occurrence prohibit the current standard interpretation: they are found from very shallow depths onward (Fig. 1a) (Kipfstuhl and others, 2007a) indicating the splitting of grains taking place there. Previously, first subgrain boundaries have been described and attributed to rotation recrystallization in  $\approx 700m$  depth at Vostok (Lipenkov in Duval and others, 2000), in  $\approx 1300m$  at Dome Fuji (Azuma and others, 2000) and in  $\approx 380m$  depth at GRIP (Thorsteinsson and others, 1997). Even high amounts (half of all grains) of subgrain boundaries have been described in Dome Concordia ice core already for  $\approx 150m$  depth (Wang and others, 2003). The different observations in different ice cores probably result from different observation methods: if crossed polarizers are used to reveal subgrain boundaries, only some highly developed subgrain boundaries can be seen depending on the polarizers and grain orientation. The sublimation method reveals a much greater number of less developed subgrain boundaries with smallest misorientations ( $\ll 0.5^\circ$ , verified by X-ray Laue measurements, unpublished data, June 2007).

Further gathering of dislocations leads to subsequent subgrain rotation, and thus gives way to continuous dynamic recrystallization, and finally converts subgrain boundaries into grain boundaries. The question how many of these features truly develop into grain boundaries cannot easily be answered. A small misorientation subgrain boundary may represent a transient stage of subgrain-boundary formation, more precisely called dislocation walls, as a generic expression for the prototype of any subgrain boundary under formation. Some of these dislocation walls probably are transient structures, because it is not known if they develop into higher misorientation boundaries by gathering of more dislocations or disap-

pear, as they are e.g. consumed by a migrating grain boundary. Such transient dislocation walls should have been treated separately as they will not contribute to the grain-size evolution. Considering the problem how many subgrain boundaries reach a certain misorientation to develop into grain boundaries, neighbour misorientation studies can be used. If rotation recrystallization dominates a certain region a surplus of small misorientations between nearest neighbours compared to random pair grains can be expected (e.g. Alley and others, 1995; Azuma and others, 2000; Wang and others, 2003). In EDML samples random and nearest neighbour c-axes misorientation distributions (Fig. 3) do not show a clear excess of small angles in neighbour misorientations in a certain depth range and therefore do not provide evidence that most observed subgrain boundaries turn into grain boundaries at some particular depth.

Due to the observations of grain size and subgrain-boundary occurrence evolution together with neighbour-misorientation data the idea that polygonization is dominant in a particular depth range cannot be confirmed. Rather, we argue that subgrain boundary formation and polygonization occurs in all depths of the EDML ice core.

#### *Strain induced boundary migration*

A second dynamic recrystallization process (discontinuous (Humphreys and Hatherly, 2004)) has been assumed to take place in the lower-most part of the ice sheet (deepest hundreds of meters) where the temperature exceeds  $-10^{\circ}\text{C}$  (e.g. Duval and others, 2000). This process, migration recrystallization, is usually described in the glaciological literature as nucleation of new grains and rapid migration of grain boundaries between dislocation-free nuclei and deformed grains (e.g. Duval and Castelnau, 1995). According to Humphreys and Hatherly (2004) discontinuous dynamic recrystallization can be identified by bulging of grain boundaries or lattice rotation of small material volumes at (sub)grain boundaries. The latter effect describes directly the classical nucleation of dislocation-free grains (Fig. 15e in Kipfstuhl and others, 2007b), due to fluctuations, which does, however, not work well for solid-state recrystallization (Rios and others, 2005).

The bulging of grain boundaries describes a relatively rapid grain boundary migration into a grain with higher internal strain energy caused by higher dislocation density. This strain induced boundary migration (SIBM) can also lead to another kind of nucleation if a bulging part is separated, e.g. bridged by subgrain boundaries cutting off this part and subsequent rotation occurs (Fig. 15b,c in Kipfstuhl and others, 2007b). The effect on fabric evolution by this nucleation process is rather small and similar to the effect of rotation recrystallization on fabric evolution. However, SIBM does not necessarily include the formation of new nuclei (Beck and Sperry, 1950), but can initiate recrystallization due to difference of internal strain energy in adjacent grains already present in the structure.

Observations on subgrain-boundary - grain-boundary interactions at grain-boundary curvatures indicate that the majority of grain boundaries bow towards the side of higher subgrain-boundary density (Fig. 5). The bulging requires a locally high dislocation-density gradient across a grain boundary (Hamann and others, 2007) and produces characteristic smoothly-rounded grain-boundary curvatures (Fig. 4c, 5a,b,c). Besides the described round curvatures sharp edges of grain boundaries held by subgrain boundaries can be frequently

observed pointing to the opposite direction than the bulges (e.g. Fig. 4c). To explain this phenomenon one can imagine that in an advanced stage of recovery, which allows a rearrangement of dislocations, most dislocations should be accumulated in subgrain boundaries whereas in an early state of recovery many dislocations are still dispersedly distributed (Passchier and Trouw, 1996). In the advanced state, one or few strong subgrain boundaries survive and develop further and therefore contain most dislocations of one grain (grain B in Fig. 7c), leaving the rest of its volume with a low density of dislocations. This can lead to a difference in stored energy with respect to a neighbouring grain with a higher density of statistically distributed dislocations (grain A in Fig. 7c), and consequently leads to migration of the grain boundary toward grain A with higher dislocation density. In this case, the well-developed subgrain boundaries seem to pin the grain boundary during their motion in a similar way as described for solid particles (e.g. Drury and Urai, 1990). Hindering the motion of the grain boundary the subgrain boundary slows down the migration of the grain boundary in their connecting point. On the other hand, subgrain boundaries in a less advanced stage occur as multiple subgrain boundaries, still collecting dislocations, and many dislocations are still distributed in the grain matrix, being not yet part of a subgrain boundary. The two recovery stages are characterized by a difference in stored energy, which can explain the above described two types of irregular grain-boundary geometries, the edge-shape type pinned by a subgrain boundary, and the bow-shaped type attracted by "young" subgrain boundaries and randomly distributed dislocations in the grain (Fig. 7). As a consequence, grain boundaries bow towards these regions of higher dislocation density, producing curvatures with many subgrain boundaries on their convex side. The interplay between bulging grain-boundary segments and pinned grain-boundary segments leads to complex grain geometries. The bulging mechanism does of course not always necessarily include pinning by a well-developed subgrain boundary, but may occur as simple bulging of high angle grain boundaries. Pinning is just a helpful effect to recognize and demonstrate migration of grain boundaries. These findings thus provide evidences that grain-boundary migration in such cases is driven by strain energy rather than grain-boundary curvatures, even in the most shallow depths (Kipfstuhl and others, 2007a).

The irregularity of grain boundaries (examples see Fig. 1, 4, 5a-c) and the interaction of grain boundaries and subgrain boundaries (Fig. 5, 7) observed in all depth ranges implies that SIBM is taking place in all depths. Even at low temperatures, where grain-boundary mobility is low and migration supposed to be slow, internal strain energy is locally high enough to activate migration recrystallization. Discontinuous dynamic recrystallization, not necessarily including nucleation, is therefore not restricted to the lowermost depth of the ice sheet

#### **Implications on subgrain-boundary formation processes and dislocations**

Subgrain boundaries are frequent and variable features providing information about the deformation of individual grains in a polycrystal. Owing to the strong anisotropy of ice crystals to deform mainly by dislocation glide on the basal plane (e.g. Hobbs, 1974), the deformation is expected to be rather heterogeneous (Wilson and Zhang, 1994; Zhang and Wilson, 1997; Mansury and others, 2000), which enables strain lo-

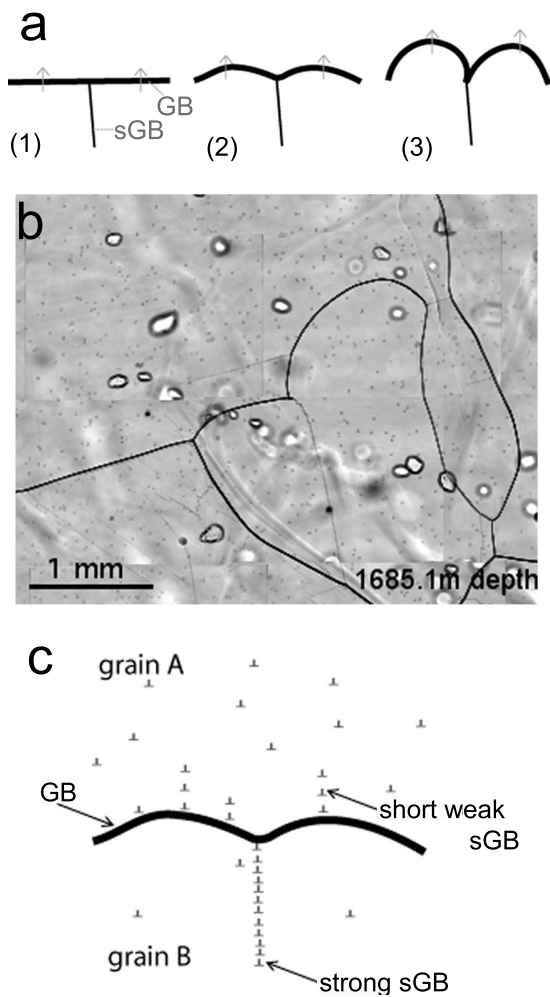


**Fig. 7.** a: Schematic illustration of grain-boundary pinning by a sub-grain boundary. Arrows give direction of moving GB b: Microphotograph example where the formation process described in a is likely. Please note the different shapes of the "free" part of the grain boundary and the part held by the sub-grain boundary. c: Schematic illustration of different dislocation distribution which can possibly explain pinning.

calization and consequently dislocation alignment. Subgrain boundaries and dislocation walls are built up by arrays of dislocations. The complex properties of dislocations in ice (reviewed by Hondoh (2000)) with its well-known predominant basal slip system (Duval and others, 1983) control the formation and evolution of the substructures. Complicated geometries and characteristics can be expected and are observed, but are still not understood completely with respect to the peculiar nature of ice dislocations. However, the most typical arrangements and shapes of subgrain boundaries shall be discussed here briefly regarding basic considerations on formation processes, although further investigations are required. Especially full crystal-orientation studies which are becoming available recently (Montagnat and others, 2003; Iliescu and

others, 2004; Miyamoto and others, 2005; Obbard and others, 2006b) promise insight into dislocation processes. Additionally, subgrain-boundary arrangement and shape observations are useful, because geometrical characteristics depend upon the orientations of glide systems which have been activated (Trepied and others, 1980; Lloyd and others, 1997).

Three different types of subgrain boundaries were classified according to their shape and orientation in the crystal: one parallel to the c-axis, another parallel to the basal plane, and a third zig-zag-shaped perpendicular or at high angle to the basal plane. The same types have been observed in experimentally deformed artificial ice (Hamann and others, 2007), in Arctic polar ice and in Alpine glacier ice (Kipfstuhl, unpublished data, June 2007). In the following we try to demonstrate possible formation processes by simplified considerations and explanations.

The usually described mechanism for ice subdivision (e.g. Alley, 1992) includes bending of the basal plane and glide of basal edge dislocations to form arrays parallel to the c-axis (Nakaya, 1958). This process was identified in the straight subgrain boundaries arranged orthogonal to the basal plane (Fig. 6e) indicating basal tilt boundaries (Fig. 6b, left).

The arrangement of the subgrain-boundary type parallel to the basal plane cannot be explained by the accumulation of basal edge dislocation. Correspondingly they may be twist boundaries consisting of basal screw dislocations (Fig. 6b, right) described by Montagnat and others (2003) and Higashi and others (1988). Certainly, further interpretations are possible and high resolution crystallographic investigation are necessary to further characterize them. An other interpretation for the parallel type is a micro-shear zone along the basal plane which arises from observations of this type of subgrain boundaries cutting off protrudes or prominently shaped parts of an irregular grain (Fig. 4b,d). This process has been proposed by (Bons and Jessell, 1999) for experimentally deformed octachloropropane. A typical microstructure called slanted brick wall structure shows the importance of this mechanism below  $\approx 2300m$  depth, where an enhanced creep indicates the importance of such a subgrain-boundary formation process (S. H. Faria and others, [http://www.mis.mpg.de/preprints/2006/prepr2006\\_3.html](http://www.mis.mpg.de/preprints/2006/prepr2006_3.html)).

The third zigzag-shaped type is probably in a stage under development. As the orientation of the grains in a polycrystal is seldom perfectly adjusted with the stress configuration to produce only one type of dislocations, several mixtures of dislocation types (e.g. basal and non-basal) may form boundaries.

Other possible subgrain-boundary evolution processes, such as reduction of misorientation on grain boundaries and impingement of moving (sub)grain boundaries are not yet considered here. However they might as well explain some of the observed subgrain-boundary patterns. Reduction of misorientation on grain boundaries could become important with strengthening of the single maximum fabric (below 2030m depth, unpublished data). All these additional formation processes may be significant in the lower part of the ice core, where no increased subgrain-boundary frequency is observed (Fig. 2).

## CONCLUSIONS

Subgrain boundaries are common features in ice samples from deep ice cores. The analysis of subgrain boundaries along the EDML ice core leads to the following conclusions:

a) The presence of subgrain boundaries in most grains of all examined samples directly identifies dislocation creep as a main deformation process.

b) Subgrain formation is active in all depths of the EDML ice core. A distinct rotation recrystallization regime was not detected.

c) Subgrain-boundary - grain-boundary interactions and grain irregularities indicate that, even in shallow depths, grain-boundary migration is driven by internal strain energy differences, thus grain-boundary migration recrystallization is not restricted to the lower-most depth of the ice sheet.

d) Conclusions a and b indicate that the recrystallization regime model with 1. Normal grain growth, 2. Polygonization/subgrain rotation recrystallization, 3. Migration recrystallization, is not easily applicable to the EDML ice core and has to be reconsidered. Rather, all processes affecting the microstructure and physical properties of ice, like deformation, grain boundary migration and recrystallization occur in all depths simultaneously, compete and interact with each other. In samples obtained from deep ice cores we see the frozen-in state of deformation in an ice sheet at certain, partly unknown creep conditions, containing the present state but also information about the strain history.

e) The very detailed studies about subgrain boundaries gave some insight about deformation in natural ice. They reveal the subgrain-boundary arrangement with respect to the crystal orientation, which shows: apart from the classical bending process described by Nakaya (1958), leading to basal tilt subgrain boundaries, different subgrain-boundary formation processes must be active. As dislocation walls parallel to the basal plane cannot be build up by basal edge dislocations other processes (e.g. basal twist and/or micro-shear, non-basal dislocations) have to be considered to be active in the deep ice core.

f) The finding that subgrain boundaries parallel to the basal plane are similar or even more frequent than subgrain boundaries parallel to the c-axes indicates that basal edge dislocations do not play alone a role in grain subdivision processes, as widely argued. Further investigations including high resolution full crystal-orientation analysis promise new insight into possible dislocation type activity.

g) Strain/stress localization seems to be the rule rather than an exception. Considerable differences in deformation can occur within very localized regions; namely inside single grains, indicated by heterogeneous distribution of subgrain boundaries in grains.

## ACKNOWLEDGMENTS

We thank Christian Weikusat for his help with image analysis and Christel Weikusat for proofreading. This work is a contribution to the European Project for Ice Coring in Antarctica (EPICA), a joint ESF (European Science Foundation)/EC scientific programme, funded by the European Commission and by national contributions from Belgium, Denmark, France, Germany, Italy, the Netherlands, Norway, Sweden, Switzerland and the United Kingdom. This is EPICA publication no. XXX.

## References

- Alley, R.B., A.J. Gow and D.A. Meese, 1995. Mapping c-axis fabrics to study physical processes in ice, *J. Glaciol.*, **41**(137), 197–203.
- Alley, R. B., 1992. Flow-law hypotheses for ice-sheet modelling, *J. Glaciol.*, **38**, 245–256.
- Azuma, N., Y. Wang, K. Mori, H. Narita, T. Hondoh, H. Shoji and O. Watanabe, 1999. Textures and fabrics in Dome F (Antarctica) ice core, *Ann. Glaciol.*, **29**, 163–168.
- Azuma, N., Y. Wang, Y. Yoshida, H. Narita, T. Hondoh, H. Shoji and O. Watanabe, 2000. Crystallographic analysis of the Dome Fuji ice core, Hondoh, T., ed., Physics of ice core records, Hokkaido University Press, Sapporo, 45–61.
- Barrette, P. D. and N. K. Sinha, 1994. Lattice misfit as revealed by dislocation etch pits in a deformed ice crystal, *J. Mat. Sci. Lett.*, **13**, 1478–1481.
- Beck, P. A. and P. R. Sperry, 1950. Strain Induced Grain Boundary Migration in High Purity Aluminium, *J. Appl. Phys.*, **21**(2), 150–152.
- Bestmann, M., S. Piazzolo, C. J. Spiers and D. J. Prior, 2005. Microstructural evolution during initial stages of static recovery and recrystallization: new insights from in-situ heating experiments combined with electron backscatter diffraction analysis, *J. Struct. Geol.*, **27**, 447–457.
- Bons, P. D. and M. W. Jessell, 1999. Micro-shear zones in experimentally deformed OCP, *J. Struct. Geol.*, **21**, 323–334.
- Budd, W. F. and T. H. Jacka, 1989. A review of ice rheology for ice sheet modelling, *Cold Reg. Sci. Technol.*, **16**, 107–144.
- Castelnaud, O., P. Duval, R.A. Lebensohn and G. R. Canova, 1996. Viscoplastic modeling of texture development in polycrystalline ice with a self-consistent approach: Comparison with bound estimates, *J. Geoph. Res.*, **101**(B6), 13,851–13,868.
- De La Chapelle, S., O. Castelnaud, V. Lipenkov and Duval P., 1998. Dynamic recrystallization and texture development in ice as revealed by the study of deep ice cores in Antarctica and Greenland, *J. Geophys. Res.*, **103**(B3), 5,091–5,106.
- DiPrinzio, C. L., L. A. Wilen, Richard B. Alley, J. J. Fitzpatrick, M. K. Spencer and A. J. Gow, 2005. Fabric and texture at Siple Dome, Antarctica, *J. Glaciol.*, **51**(173), 281–290.
- Drury, M. R. and J. L. Urai, 1990. Deformation-related recrystallization processes, *Tectonophys.*, **172**, 235–253.
- Duval, P., 2000. Deformation and dynamic recrystallization of ice in polar ice sheets, Hondoh, T., ed., Physics of ice core records, Hokkaido University Press, Sapporo, 103–113.
- Duval, P., L. Arnaud, Brissaud, M. Montagnat and S. De La Chapelle, 2000. Deformation and recrystallization processes of ice from polar ice sheets, *Ann. Glaciol.*, **30**, 83–87.
- Duval, P., M. F. Ashby and I. Andermann, 1983. Rate-Controlling Processes in the Creep of Polycrystalline Ice, *J. Phys. Chem.*, **87**, 4066–4074.
- Duval, P. and O. Castelnaud, 1995. Dynamic recrystallisation of ice in polar ice sheets., *J. Physique*, **5**, 197–205.
- Eisen, O., I. Hamann, S. Kipfstuhl, D. Steinhage and F. Wilhelms, 2007. Direct evidence for radar reflector originating from changes in crystal-orientation fabric, *The Cryosphere Discussions*, **1**, 1–16.

- Faria, S.H. and S. Kipfstuhl, 2004. Preferred slip band orientations and bending observed in the Dome Concordia ice core, *Ann. Glaciol.*, **39**, 38–390.
- Faria, S. H., 2006. Creep and recrystallization of large polycrystalline masses. III. Continuum theory of ice sheets, *Proc. Roy. Soc.*, **A462**, 2797–2816.
- Föll, H., 2000. Defects in Crystals, *Hyperscript*, [http : //www.tech.fak.uni - kiel.de/matwis/amat/def.n/index.html](http://www.tech.fak.uni-kiel.de/matwis/amat/def.n/index.html).
- Gillet-Chaulet, F., O. Gagliardini, J. Meyssonier, M. Montagnat and O. Castelnaud., 2005. A user-friendly anisotropic flow law for ice-sheet modelling, *J. Glaciol.*, **51**(172), 3–14.
- Glen, J. W., 1955. The creep of polycrystalline ice, *Proc. Roy. Soc. London*, **A228**, 519–538.
- Gow, A. J. and T. Williamson, 1976. Rheological implications of the internal structure and crystal fabrics of the West Antarctic ice sheet as revealed by deep core drilling at Byrd Station, *CRREL Rep.*, **76**(35), 1665–1677.
- Hamann, I., Weikusat Ch. and N. Azuma, 2007. Evolution of ice crystal microstructures during creep experiments, *J. Glaciol.*, **53**(183), 479–489.
- Higashi, A., A. Fukuda, H. Shoji, M. Oguro, T. Hondoh and K. Goto-Azuma, 1988. Lattice defects in ice crystals, Hokkaido University Press, Sapporo, Japan.
- Hobbs, P. V., 1974. *Ice Physics*, Oxford University Press.
- Hondoh, T., 2000. Nature and behaviour of dislocations in ice, Hondoh, T., ed., *Physics of ice core records*, Hokkaido University Press, Sapporo, 3–24.
- Humphreys, F. J. and M. Hatherly, 2004. *Recrystallization and Related Annealing Phenomena*, Elsevier.
- Iliescu, D., I. Baker and H. Chang, 2004. Determining the Orientations of Ice Crystals Using Electron Backscatter Patterns, *Microscopy Res. Tech.*, **63**, 183–187.
- Kipfstuhl, S., N. Azuma, S.H. Faria, J. Freitag, I. Hamann, P. Kaufmann, H. Miller, H. Oerter, K. Weiler and F. Wilhelms, 2007a. Evidence of dynamic recrystallization in polar firn, *in prep. for J. Glaciol.*, **August**.
- Kipfstuhl, S., N. Azuma, S. H. Faria, I. Hamann and F. Wilhelms, 2007b. Deformation and recrystallization in polar ice sheets - observations on the grain scale, Hondoh, T., ed., *Physics of Ice Core Records*, vol. 2, submitted.
- Kipfstuhl, S., I. Hamann, A. Lambrecht, J. Freitag, S. H. Faria, D. Grigoriev and N. Azuma, 2006. Microstructure mapping: a new method for imaging deformation induced microstructural features of ice on the grain scale, *J. Glaciol.*, **52**(178), 398–406.
- Lloyd, G. E., A. B. Farmer and D. Mainprice, 1997. Misorientation analysis and the formation and orientation of subgrain and grain boundaries, *Tectonophysics*, **279**, 55–78.
- Mansuy, P., A. Philip and J. Meyssonier, 2000. Identification of strain heterogeneities arising during deformation of ice, *Ann. Glaciol.*, **30**, 121–126.
- Means, W. D. and J. H. Ree, 1988. Seven types of subgrain boundaries in OCP, *J. Struct. Geol.*, **10**(7), 765–770.
- Miyamoto, A., H. Shoji, A. Hori, T. Hondoh, H.B. Clausen and O. Watanabe, 2005. Ice fabric evolution process understood from anisotropic distribution of a-axis orientation on the GRIP (Greenland) ice core, *Ann. Glaciol.*, **42**, 47–52.
- Montagnat, M. and P. Duval, 2000. Rate controlling processes in the creep of polar ice, influence of grain boundary migration associated with recrystallization, *Earth Planet. Sci. Lett.*, **183**, 179–186.
- Montagnat, M., P. Duval, P. Bastie and B. Hamelin, 2003. Strain gradients and geometrically necessary dislocations in deformed ice single crystals, *Scripta Mat.*, **49**, 411–415.
- Nakaya, U., 1958. Mechanical properties of single crystal of ice. Part I. Geometry of deformation, *US Army Snow Ice and Permafrost Research Establishment, Research Report*, **28**.
- Nishida, K. and H. Narita, 1996. Three-dimensional observations of ice crystal characteristics in polar ice sheets, *J. Geophys. Res.*, **101**(D16), 21,311–21,317.
- Obbard, Rachel, Ian Baker and Daniel. Ilescu, 2006a. Grain boundary grooving in ice in a scanning electron microscope. Correspondence, *J. Glaciol.*, **52**(176), 169–172(4).
- Obbard, R., I. Baker and K. Sieg, 2006b. Using electron backscatter diffraction patterns to examine recrystallization in polar ice sheets, *J. Glaciol.*, **52**(179), 546–557.
- Passchier, C. W. and R. A. J. Trouw, 1996. *Microtectonics*, Springer Verlag.
- Paterson, W. S. B., 1994. *The physics of glaciers*, Butterworth-Heinemann, Elsevier, third ed.
- Petrenko, V. F. and R. W. Whitworth, 1999. *Physics of ice*, Oxford University Press.
- Pettit, E.C., Th. Thorsteinsson, H.P. Jacobson and E.D. Waddington, 2007. The role of crystal fabric in flow near an ice divide, *J. Glaciol.*, **53**(181), 277–288.
- Pimienta, P. and P. Duval, 1989. Rheology of polar glacier ice, *Ann. Glaciol.*, **12**, 206–207.
- Placidi, L., S.H. Faria and K. Hutter, 2004. On the role of grain growth, recrystallization and polygonization in a continuum theory for anisotropic ice sheets, *Ann. Glaciol.*, **39**, 49–52.
- Placidi, L. and K. Hutter, 2006. An anisotropic flow law for incompressible polycrystalline materials, *Z. angew. Math. Phys.*, **57**, 160–181.
- Poirier, J.-P., 1985. *Creep of crystals*, Cambridge University Press.
- Rios, Paulo Rangel, Fulvio Siciliano Jr, Hugo Ricardo Zschommler Sandimc, Ronald Lesley Plaut and Angelo Fernando Padilhad, 2005. Nucleation and Growth During Recrystallization, *Materials Research*, **8**(3), 225–238.
- Russell-Head, D., 2004. *Fabric Analyser System - Investigator - Version 1.12*, <http://www.earthsci.unimelb.edu.au/facilities/analyser>.
- Saylor, D. M. and G. S. Rohrer, 1999. Measuring the Influence of Grain-Boundary Misorientation on Thermal Groove Geometry in Ceramic Polycrystals, *J. Am. Ceram. Soc.*, **82**, 1529–36.
- Sedlacek, R., W. Blum, J. Kratochvil and S. Forest, 2002. Subgrain formation during deformation: physical origin and consequences, *Met. and Mat. Trans.*, **A33**, 319–327.
- Thorsteinsson, Th., 2006. *Glacier Science and Environmental Change*, Knight, P.G. (ed.), Blackwell Publishing, chap. Anisotropy and flow of ice, 315–317.
- Thorsteinsson, Th., J. Kipfstuhl and H. Miller, 1997. Textures and fabrics in the GRIP ice core, *J. Geophys. Res.*, **102**(C12), 26,583–26,599.
- Trepied, L., J. C. Doukhan and J. Paquet, 1980. Subgrain boundaries in quartz theoretical analysis and microscopic observations, *Phys. Chem. Min.*, **5**(3), 201–218.
- Wang, Y., S. Kipfstuhl, N. Azuma, Th. Thorsteinsson and H. Miller, 2003. Ice-fabrics study in the upper 1500 m of Dome C (East Antarctica) deep ice core, *Ann. Glaciol.*, **37**, 97–104.
- Weertman, J. and J. R. Weertman, 1992. *Elementary Dislo-*

- cation Theory, Oxford University Press.
- Wilson, C. J. L., Burg and Mitchell, 1986. The origin of kinks in polycrystalline ice, *Tectonophys.*, **127**, 27–48.
- Wilson, C. J. L., D. S. Russell-Head and H. M. Sim, 2003. The application of an automated fabric analyzer system to the textural evolution of folded ice layers in shear zones, *Ann. Glaciol.*, **37**, 7–17.
- Wilson, C. J. L. and Y. Zhang, 1994. Comparison between experiment and computer modelling of plane-strain simple-shear ice deformation, *J. Glaciol.*, **40**(134), 46–55.
- Zhang, Y. and C. J. L. Wilson, 1997. Lattice rotation in polycrystalline aggregates and single crystals with one slip system: a numerical and experimental approach, *J. Struct. Geol.*, **19**(6), 875–885.

# Appendix C

## Publication III - Deformation microstructures in an Antarctic ice core (EDML) and in experimentally deformed artificial ice

Hamann, I., Kipfstuhl, S., Azuma, N., Faria, S. H., Miyamoto, A.  
(subm. August 2007)

Submitted to Physics of Ice Core Records, 2<sup>nd</sup> volume (T. Hondoh, ed.)  
on August 31<sup>st</sup> 2007.

# Deformation microstructures in an Antarctic ice core (EDML) and in experimentally deformed artificial ice

Ilka Hamann <sup>\*</sup>, Sepp Kipfstuhl <sup>\*</sup>, Nobuhiko Azuma <sup>\*\*</sup>, Sérgio H. Faria <sup>\*\*\*</sup> Atsushi Miyamoto <sup>\*\*\*\*</sup>

<sup>\*</sup> Alfred Wegener Institute, Bremerhaven, Germany, [ilka.hamann@awi.de](mailto:ilka.hamann@awi.de), [sepp.kipfstuhl@awi.de](mailto:sepp.kipfstuhl@awi.de)

<sup>\*\*</sup> Department of Mechanical Engineering, Nagaoka University of Technology, Nagaoka, Japan, [azuma@mech.nagaokaut.ac.jp](mailto:azuma@mech.nagaokaut.ac.jp)

<sup>\*\*\*</sup> GZG, Sect. of Crystallography, University of Göttingen, Göttingen, Germany, [sh.faria@geo.uni-goettingen.de](mailto:sh.faria@geo.uni-goettingen.de)

<sup>\*\*\*\*</sup> Institute of Low Temperature Science, Hokkaido University, Sapporo, Japan, [miyamoto@lowtem.hokudai.ac.jp](mailto:miyamoto@lowtem.hokudai.ac.jp)

**Abstract:** Deformation microstructures in an Antarctic ice core (EDML) and in experimentally deformed artificial ice, which together represent a plurality of conditions and parameters, are reconsidered and compared. Data presented here cover grain substructure and shape observations. Despite the different flow conditions surprising similarities in these observations indicate intracrystalline slip as the deformation carrier in natural as well as in experimentally deformed ice. Same subgrain-boundary shapes and arrangements in both cases indicate characteristic types, which suggest that non-basal dislocations may play a significant role in the deformation of ice. Subgrain-boundary density and grain-boundary shapes show that a difference between processes in creep tests and in the Antarctic ice sheet is the efficiency of recovery and dynamic recrystallization.

**Key words:** low angle grain boundary, creep test, dynamic recrystallization, recovery, sublimation grooves

## 1 Introduction

Studies on ice flow conditions and physical properties have been performed for several decades in natural ice from deep ice cores [e.g. 1, 2, 3] as well as in artificially produced and experimentally deformed ice [e.g. 4, 36, 6, 7]. Microstructure investigations in these works are usually concerned with the texture (grain size, grain morphology) and crystal orientation fabrics on the grain scale. However, as the preponderant deformation mechanism in ice is intracrystalline slip [e.g. 6, 8, 9], most deformation is indeed carried out on a smaller scale range, the subgrain scale within individual grains. Investigations on this high resolution usually lack the overview which enables statistics over a significant ice volume [10, 11]. The microstructure mapping method represents therefore a good compromise, by offering insight into small scale

structures at high resolutions over a considerable amount of material [12].

Microstructures provide evidences of recrystallization and deformation and therefore provide information on the operation of these processes. A sequence with depth of three recrystallization regimes is often proposed for polar ice sheets [e.g. 9, 13]. Deformation independent normal grain growth in the upper hundreds of meters is supposed to be followed by rotation recrystallization (continuous dynamic recrystallization) in the middle part of the ice sheet's depth and by discontinuous dynamic recrystallization (migration recrystallization) in the lowermost region. Rotation recrystallization results from progressive misorientation of grain fragments, which are formed by the so-called polygonization mechanism [e.g. 14]. This process divides grains under the action of localized stresses into two or more misoriented subgrains which are separated by dislocation walls. Thus, the rotation recrystallization process which should dominate the middle depth region of an ice sheet is highly correlated to subgrain-boundary formation processes. Therefore these features deserve special interest and investigation.

The aim of this article is to reconsider subgrain boundary data and grain substructure observations obtained from Antarctic ice as well as from deformed artificial samples [15, 16] and to try a first comparison to show evidences which microprocesses represent the different flow behaviour under high and low stresses. Arguments for the activity of intracrystalline slip in low and high stress regimes involving basal and maybe even non-basal glide can be given by subgrain-boundary observations.

## 2 Samples

Creep experiments using ice samples free of bubbles, impurities and deformation features have been conducted under uniaxial compression over the stress range 0.18 to 0.52MPa and the strain range 0.5 to 8.6% at approximately  $-5$  and  $-20^{\circ}\text{C}$  [15]. Initial samples were

isotropic and had small grain sizes ( $\approx 0.6\text{mm}^2$ ). Microstructures of deformed samples were examined by image analysis of microstructure maps [12] in which grain boundaries and subgrain boundaries are revealed as shallow sublimation grooves (examples see Fig. 1) by thermal etching [17].

This observation method was also used for natural ice core samples from  $\approx 2775\text{m}$  long EDML (EPICA Dronning Maud Land) acquired at Kohlen station ( $75^\circ00.104'S$ ,  $0^\circ04.07'E$ ) between 2001 and 2006. At this site the annual accumulation rate is  $64\text{kgm}^{-2}$  per year [18] and mean temperatures at the surface are  $\approx -45^\circ\text{C}$  and  $\approx -3^\circ\text{C}$  at the bore hole bottom [19]. Surface velocities are in the order of  $0.7\text{ma}^{-1}$  [20]. Variable grain sizes [16] and impurity contents [21] are observed along the ice core.

The microstructure discussions here are focused on grain shape and subgrain-boundary observations, because these are so far rarely considered.

### 3 Subgrain-boundary types

In consideration of the significantly different formation and deformation conditions in terms of e.g. temperature, impurities, grain size, strain and strain rate of the observed ice samples it is surprising at first sight that the same types of subgrain boundaries were found in experimentally deformed ice as well as in natural ice [15, 16]. These characteristic types can be distinguished after their shapes and arrangements (Fig. 1) and with respect to the crystal lattice orientation (Fig. 2). It is known from other materials that the orientation of subgrain boundaries depends on the orientation of slip systems of dislocations accumulating in the grain [22]. As detailed observation and analysis of these characteristic arrangements can be useful to study dislocation action in polycrystalline ice, the observed types shall be described here in detail.

The subgrain-boundary formation in ice was first described by Nakaya [23]. Bending of the basal plane in the direction of the c-axis, rearrangement of basal edge dislocations into walls and subsequent splitting of the grain lead to formation of subgrain boundaries [25, 26]. This process produces straight subgrain boundaries perpendicular to the basal plane, which cross the grain. Such arrangement of subgrain boundaries can indeed be observed in the sublimation grooves revealed by microstructure mapping (see example in Fig. 2a, b) and are called c-type subgrain boundaries indicating the resemblance of Nakaya's "classical" description. First X-ray Laue measurements confirm that the majority of subgrain boundaries arranged in this configuration indicate a misorientation obtained by rotation around one a-axis [27]. They are interpreted as basal tilt boundaries [15]. Actually this type of subgrain boundaries is most rare in artificial creep test samples as well as in polar ice (Fig. 3a,b). Characteristically c-type subgrain boundaries pass into another type characterized by its irregular, usually zig-zag shape.

Subgrain boundaries of this related zigzag or step

shape (z-type) are also arranged at an angle to the basal plane, with short segments running parallel to this plane (see example in Fig. 2). Typically z-subgrain boundaries do not cross a grain completely but fade out with some distance to the high angle grain boundary. They can be interpreted as a sequence of boundaries with a diversity of dislocation types involved (e.g. basal edge and non-basal edge dislocations) [15]. Clearly further investigations are necessary, which become available with high resolution full crystal orientation methods [10, 11, 28, 29, 30].

The third distinguishable type is called p-type subgrain boundary, because it appears in swarms exactly parallel to each other. Besides the alignment in swarms, its parallel arrangement with respect to the basal plane of the crystal lattice is remarkable (Fig. 2). In consideration of their arrangement and shape three possible explanations can be given: basal twist boundaries, non-basal tilt boundaries or micro-shear zones [15, 16, 31]. Basal twist boundaries are composed of screw dislocations in the basal plane. The commonness of this dislocation type in ice has been shown [e.g. in 10, 32, 33]. These subgrain boundary types produce misorientations which can be described by rotation around the c-axis. Indeed preliminary X-ray Laue measurements confirm their existence [27].

Non-basal tilt boundaries can be imagined as a pile-up of non-basal edge dislocations. They have been confirmed by preliminary X-ray Laue measurements as well [27], indicating a rotation around one a-axis. The process producing such a high amount of non-basal dislocations to build up subgrain boundaries is still not clear and will be topic of further investigations.

The alternative explanation as micro-shear zones describes shearing-off of a prominent part of a grain, which is penetrating a neighbour. This shear occurs along the basal plane that is aligned parallel to long grain boundary chains. This process was observed during the deformation of octachloropropane [34] and considered as a possible cause for sudden change in ice softness in the depth range  $2385\text{m}$  to  $\approx 2575\text{m}$  of EDML [31].

We have to mention that the arrangement and shapes of sublimation grooves along subgrain boundaries described above is most easily observable if the sublimation surface is almost parallel (within  $\approx 30^\circ$ ) to the c-axis. The reason for this dependence of sublimation on cutting orientation is probably due to the fact that best thermal grooving can be obtained if the boundary is perpendicular to the surface, whereas an oblique intersection of boundary and surface produces oblique and shallow grooves. Therefore a considerable amount of unidentifiable types is observed (Fig. 3a,b), which, in the case of ice core samples decreases with depth (Fig. 3b), as fabric enhancement enables vertical sections with many grains "nicely" oriented for sublimation.

#### 3.1 Implications on micromechanisms

As mentioned above, it is interesting that the types of observed ice substructures described above are the same in deformed artificial ice and ice from a deep Antarctic

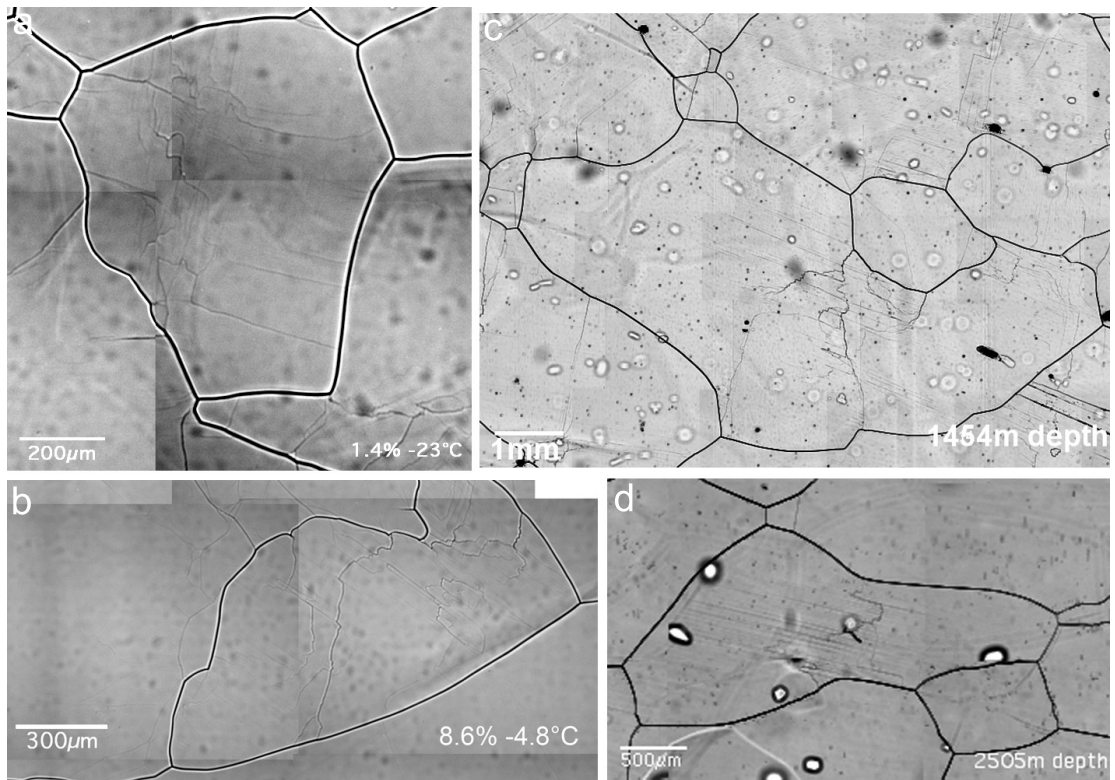


Figure 1: *Microstructure mapping examples from vertically cut thick sections. a & b: creep experiment samples. a: deformed at  $-23^{\circ}\text{C}$  with  $0.35\text{MPa}$  until  $1.4\%$  strain. b: deformed at  $-4.8^{\circ}\text{C}$  with  $0.52\text{MPa}$  until  $8.6\%$  strain. c & d: EDML ice core samples. Depths are given. Some photographs are reprinted from the *Journal of Glaciology* with permission of the International Glaciological Society.*

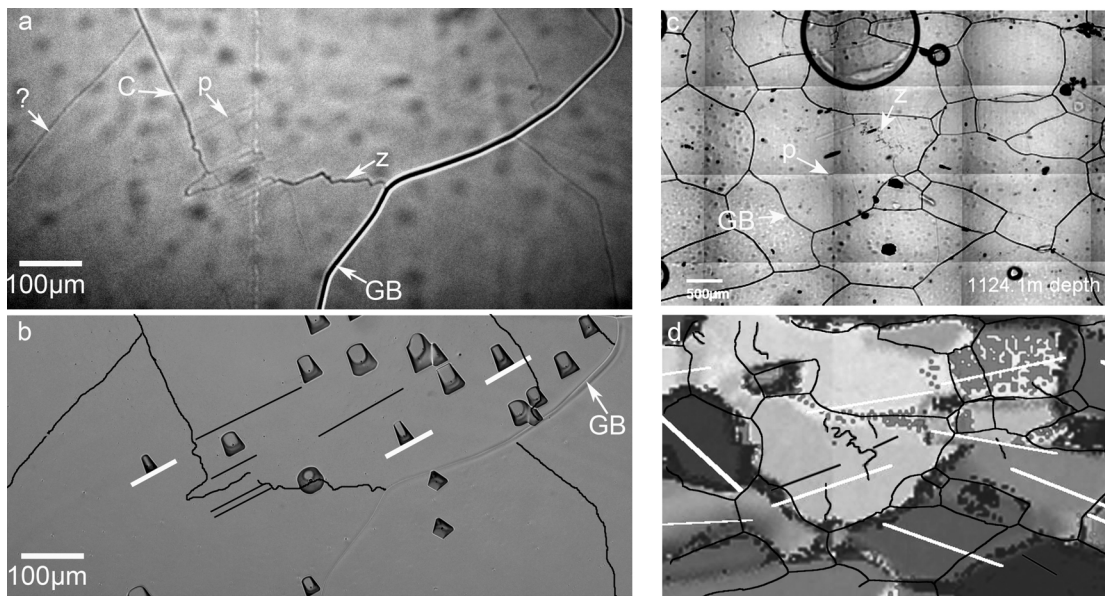


Figure 2: Subgrain-boundary types and crystal orientation. *a*: Creep-test sample. *b*: Same section as *a*, after application of etch pit method. Subgrain boundaries (black lines) are drawn after *a*. Basal plane traces (white bars) are drawn after etch pits. *c*: EDML sample. *d*: AVA image obtained of same section as *c*. Subgrain boundaries and grain-boundary network (black lines) are drawn after *a*. Rather bad fit of grain-boundary network with AVA-image is due to oblique grain boundaries. Basal plane traces (white bars) are drawn after *c*-axes measurements with automatic fabric analyzer [24]. (GB=grain boundary, p=parallel type, z=zigzag type, c=classical polygonization type subgrain boundary as described by Nakaya [23]). Some photographs are reprinted from the *Journal of Glaciology* with permission of the International Glaciological Society.

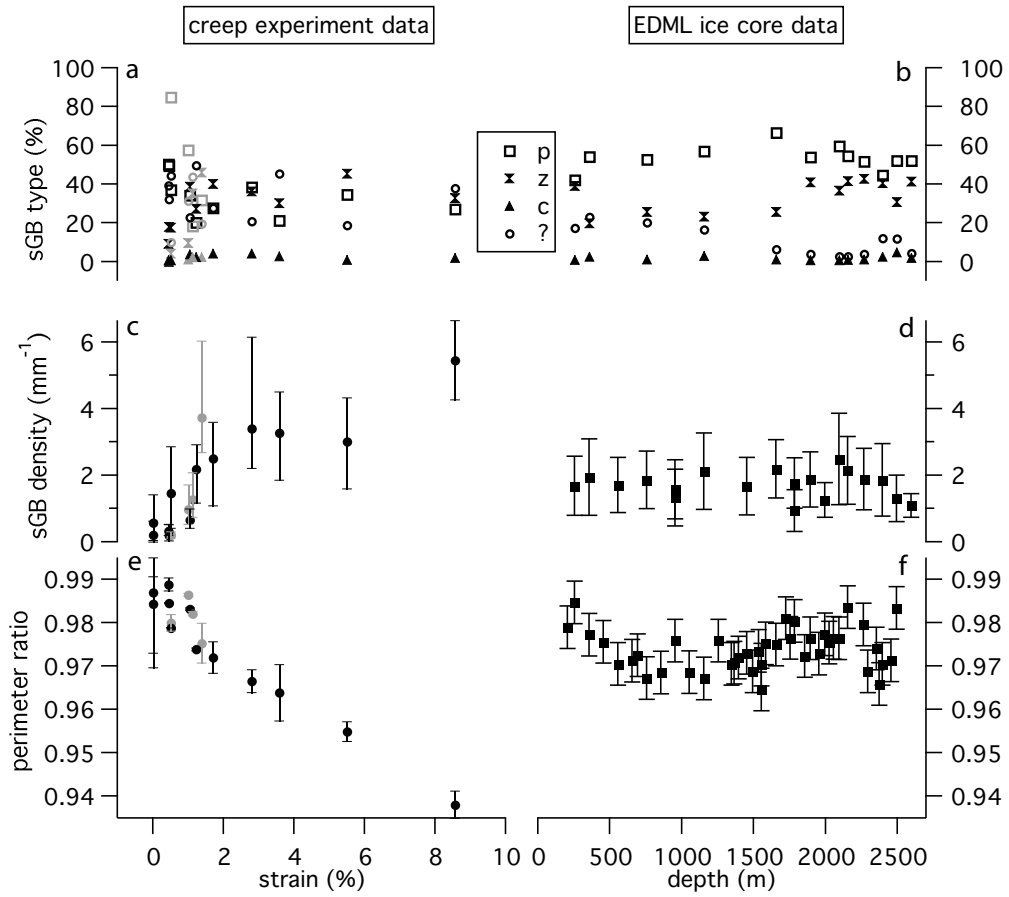


Figure 3: Evolution of microstructure parameters. a&b: subgrain-boundary type frequency (p=parallel type, z=zigzag-type, c=classical polygonization type, as described by Nakaya [23], ?=ambiguous shape and arrangement). c&d: mean subgrain-boundary density. e&f: mean grain perimeter ratio indicating irregularity of grains (see text). Ordinate is identical in all graphs. Left: during creep experiments. Error bars indicate the scatter of data in four to six measured values. Black markers represent experiments at  $\approx -4.5^\circ\text{C}$ , grey markers represent  $\approx -23^\circ\text{C}$ . Right: ice sheet samples (EDML). Error bars give the standard deviation. (Partly reproduced from the *Journal of Glaciology* with permission of the International Glaciological Society.)

ice core, especially as the experiments reached at most secondary creep whereas polar ice is supposed to deform in steady-state tertiary creep, because large strains prevail and preferred orientation fabrics evolve [35, 36, 37]. First of all, the similarity in subgrain-boundary observations prove directly the relevance of dislocation creep in polar ice [supporting 6, 8, 9] and under the chosen experimental conditions.

Moreover, due to the observation of the similarity of grain substructures and the high mechanical anisotropy of ice it can be assumed that these structures indeed are characteristic traces of deformation processes displaying a material peculiarity in its response to creep. If the resolved shear stress is not exactly parallel to the *c*-axis, which is unlikely in the highly complex stress situation for grains in polycrystals, ice responds in all other stress configurations firstly by the activation of the dominant slip system, the basal plane. Other slip systems should contribute much less to ice deformation [33], because of the peculiar properties of dislocations in ice. However, non-basal slip has been proposed before as a basal-slip-accommodating process [6, 38, 39, 40], which is necessary to provide strain compatibility among neighbouring grains, to avoid the occurrence of microcracks and voids. The significant occurrence of subgrain boundaries which cannot only be explained by arrangement of basal dislocations (*p* and maybe *z* in Fig. 3a,b) gives first experimental evidence of the importance of non-basal glide. Further investigations including subgrain-boundary lengths of all types and full crystal misorientation measurements can bring the question forward, how much non-basal glide is possible or necessary under different deformation conditions.

#### 4 Subgrain-boundary density, Grain-boundary morphology and Strain/Stress localization

The first characteristic similarities observed above encourage us to try a comparison of creep experiments and ice sheet samples with more parameters.

As a parameter to describe the occurrence of subgrain boundaries, a subgrain-boundary density is defined as the total subgrain-boundary length per area, which can be obtained by image analysis of the microstructure maps [12] (examples see Fig. 1). In experimentally deformed ice samples subgrain-boundary formation in creep tests is correlated to strain during primary creep stage which lasted until  $\approx 1$  to 2% strain (Fig. 3c) due to the production and interaction of dislocation walls and subgrain boundaries which act as obstacles for dislocation movement [15]. This demonstrates the connection of crystal-substructure evolution with isotropic hardening [15], which is due to short-range interactions between dislocations and represents the non-reversible component of strain during transient creep [6]. Microstructure mapping of EDML ice core thick sections reveals that subgrain formation is permanently active in all depths

(Fig. 3d) [16]. Therefore a distinct rotation recrystallization regime as expected by the classical recrystallization regime concept [e.g. 13] was not detected.

A measure for the irregularity of grains is the perimeter ratio: the ratio of convex perimeter against real perimeter (see Fig. 1 in [15]). A most regular object (e.g. circle, ellipse or rectangle) has perimeter ratio = 1. Lower values describe the degree of irregularity. The correlation of irregularity of grains with strain in creep tests (Fig. 3e) is clear. Compared to the values of grains from ice core samples they exhibit extremal values (Fig. 3e,f). Similar to subgrain-boundary density the mean perimeter ratio does not change significantly with depth compared to the variation of data.

Furthermore, distributions of subgrain boundaries inside grains are very similar. In both cases crystal substructures are more strong and preferably accumulated close to grain boundaries forming a highly heterogeneous substructure distribution [15, 16]. The accumulation at prominent parts of complex grain-boundary geometries observed in ice sheets and creep test samples strikingly suggests that strain accumulation is the rule rather than the exception in deforming ice in general. The frequent occurrence of grain-boundary curvatures and the surplus of subgrain boundaries on their convex side and hence the excess of driving pressure exerted by internal strain energy over driving pressure exerted by grain-boundary tension indicates that locally high dislocation densities can occur [15].

#### 4.1 Implications on micromechanisms

Experiments have been conducted at stresses between 0.18 and 0.52 MPa. Compared with the polar ice sheets, where driving stresses are typically lower than 0.1 MPa, measured deformation rates are rather high. Besides differences in strain rates, total strains in experiments reached a maximum of  $\approx 8.6\%$  only, whereas much higher deformation is expected in the ice core samples. Furthermore other possible variables influencing creep or deformation related recrystallization (e.g. impurities, temperature, grain size, fabrics) cover a striking range of values along the ice core and in the samples. Therefore it is most surprising that mean subgrain boundary density is of the same order in experiments ( $\approx 0$  to  $4\text{mm}^{-1}$ , see Fig. 3c) and in EDML ice core ( $\approx 1$  to  $3\text{mm}^{-1}$ , see Fig. 3d). The appearance of subgrain boundaries proves the important role of dislocation creep under the range of deformation conditions, because subgrain boundaries are composed of arrays of dislocations [25, 26]. The irregularity of the shapes of grain boundaries suggest difficulties to carry out grain boundary sliding.

A slight difference can be observed in the scattering of measured values. While the subgrain-boundary density data from creep experiments cover a range of  $\approx 6\text{mm}^{-1}$ , the data from the EDML ice core vary only within  $\approx 3\text{mm}^{-1}$  (Fig. 3c,d). However, here a statistical effect cannot be excluded definitely as the creep test samples are smaller and therefore the examined area was

smaller than in ice core samples.

Together with the slightly lower average values in ice deformed at low stresses in the ice sheet the data-scattering difference can be explained by processes which reduce the dislocation density. They can act more extensively with the prolonged duration of creep in the slowly deforming ice sheet. Montagnat and Duval [8] incorporated these processes in a deformation model. The two main processes are recovery and dynamic recrystallization which compete, because both are driven by the stored internal strain energy. Dynamic recrystallization can be defined as a "*deformation-induced reworking of the grain sizes, shapes or orientations*" [see 14, p. 179]. Conversely, recovery takes place at a smaller scale within individual ice grains.

Two primary processes are involved in recovery: annihilation of dislocations and rearrangement of dislocations [41]. Annihilation can remove dislocations by connecting two dislocations of opposite signs. The rate of dislocation annihilation is dependent on the ease of operation of climb and cross slip, because two dislocations with the same Burgers and line vectors but opposite signs have to share identical glide planes to meet and annihilate [42]. However, the low stacking fault energy of ice [33], which leads to wide dissociation of dislocations in the basal plane, hinders climb and cross slip [41].

Rearrangement of dislocations creates lower energy configurations and leads to formation of dislocation walls and subgrain boundaries (polygonization). This process is very active in ice as can be observed by the frequent occurrence of subgrain boundaries. Further gathering of dislocations leading to subsequent subgrain rotation, and thus giving way to continuous dynamic recrystallization, converts subgrain boundaries into grain boundaries. Therefore the higher subgrain-boundary density values in experimentally deformed samples than in EDML samples (Fig. 3c,d) does not necessarily suggest higher amount of rearrangement of dislocations during creep tests. However, misorientation data of EDML samples cannot proof intensive further gathering of dislocations and subsequent subgrain rotation, because a surplus of small angle misorientations of neighbouring grains with respect to random grain-pair misorientations was not found [16]. Ice sheet ice does not completely work harden, viz. reach maximum subgrain-boundary density (Fig. 3c,d).

As another important process, which heals the material from dislocations, grain boundary migration plays an important role. Grain boundaries can sweep away dislocations and subgrain boundaries which are located in front of a moving grain boundary [43]. This process is less subtle and restores the materials properties more efficiently than recovery, because it can remove dislocations effectively which are typically accumulated locally due to strain localization [10, 15, 16]. That this strain induced grain boundary migration (SIGBM as one mode of dynamic recrystallization) indeed plays an important role can easily be observed by the irregularity of grains (examples see Fig. 1, Fig. 3e,f). These complex

grain geometries evolve due to bulging of grain boundaries in experimentally deformed ice as well as in polar ice [15, 16]. This is part of an intense feed-back process where complex geometries lead to complicated stress interaction at grain boundaries in polycrystalline ice, which lead to strain localization and localized dislocation formation; that restart again bulging of grain boundaries. The difference between experimentally-deformed and ice core samples in terms of the degree of irregularity of grains (Fig. 3e,f) gives insight in the delicate balances of the competing recovery and SIGBM under slow and fast deformation. Irregularity during creep tests clearly increases with strain (Fig. 3e), which reflects the dislocation production directly. In these high stress regimes recovery seems to be relatively slow compared to the generation of defects by deformation. During application of low stresses grains are still significantly irregular (Fig. 3f), but as total accumulated strains should be higher in the ice sheet than in experiments, recovery, which reduces dislocation density without SIGBM, seems to inhibit the evolution of highest irregularities of grains (Fig. 3e,f).

Microstructure data indicate that the relation of dislocation-production rate to dislocation-reduction rate is significantly higher in experimentally deformed samples, which leads to more moderate values for subgrain-boundary density and for grain-boundary irregularity (Fig. 3c-f). The comparison of the two data sets indicates that the reason for different high-stress and low-stress behaviour might be, that recovery is mainly time dependent, whereas dislocation production is deformation dependent. Annihilation, which is difficult to carry out in ice, also occurs with aging [32] and may thus play some role in the ice sheet. However, further investigations to cover the plurality of probable variables (e.g. impurities) influencing these processes are necessary.

## 5 Conclusions

Studies on grain substructures in deformed ice samples reveal the effects and impact of intracrystalline deformation processes. The similarities in grain substructure observations in experimentally deformed and Antarctic ice identify dislocation creep as a deformation carrier, whereas the more moderate values and scatters of subgrain-boundary densities and grain-boundary irregularities in ice sheets indicate that dislocation density-decreasing processes (recovery and dynamic recrystallization) play a far more important role under low-stress conditions. Recovery by rearrangement of dislocations can be identified in subgrain-boundary formation. Among dynamic recrystallization mechanisms, strain-induced grain boundary migration can be detected by bulging grain boundaries and the degree of irregularity of the grains. The delicate interplay of dislocation production, recovery and dynamic recrystallization controls the degree of work hardening and therefore the softness of the material, apart from fabric evolution.

The population of non-basal dislocations should be much smaller than that of basal dislocations, which are responsible for dislocation creep of ice, but significant amounts of non-basal dislocations, enough even to form subgrain boundaries have to be taken into account, to explain all the observed subgrain-boundary types.

## References

- [1] Gow, A. J. and T. Williamson, "Rheological implications of the internal structure and crystal fabrics of the West Antarctic ice sheet as revealed by deep core drilling at Byrd Station", *CRREL Rep.*, 76(35), 1976, pp. 1665-1677.
- [2] Thorsteinsson, Th., J. Kipfstuhl and H. Miller, "Textures and fabrics in the GRIP ice core", *J. Geophys. Res.*, 102(C12), 1997, pp. 26,583-26,599.
- [3] Azuma, N., Y. Wang, Y. Yoshida, H. Narita, T. Hondoh, H. Shoji and O. Watanabe, "Crystallographic analysis of the Dome Fuji ice core", T. Hondoh (ed.), *Physics of ice core records*, Hokkaido University Press, Sapporo, 2000, pp. 45-61.
- [4] Glen, J. W., "The creep of polycrystalline ice", *Proc. Roy. Soc. London*, A228, 1955, pp. 519-538.
- [36] Jacka, T. H., "The time and strain required for development of minimum strain rates in ice", *Cold Reg. Sci. Technol.*, 8(3), 1984, pp. 261-268.
- [6] Duval, P., M. F. Ashby and I. Andermann, "Rate-Controlling Processes in the Creep of Polycrystalline Ice", *J. Phys. Chem.*, 87, 1983, pp. 4066-4074.
- [7] Steinemann, S., "Experimentelle Untersuchungen zur Plastizität von Eis", *Beiträge zur Geologie der Schweiz, Hydrologie*, 1958, 10, pp. 72.
- [8] Montagnat, M. and P. Duval, "Rate controlling processes in the creep of polar ice, influence of grain boundary migration associated with recrystallization", *Earth Planet. Sci. Lett.*, 183, 2000, pp. 179-186.
- [9] Alley, R.B., "Flow-law hypotheses for ice-sheet modelling", *J. Glaciol.*, 1992, 38, pp. 245-256.
- [10] Montagnat, M., P. Duval, P. Bastie and B. Hamelin, "Strain gradients and geometrically necessary dislocations in deformed ice single crystals", *Scripta Mat.*, 49, 2003, pp. 411-415.
- [11] Montagnat, M., P. Duval, P. Bastie, B. Hamelin and V.Y. Lipenkov, "Lattice distortion in ice crystals from the Vostok core (Antarctica) revealed by hard X-ray diffraction; implication in the deformation of ice at low stresses", *Earth Planet. Sci. Lett.*, 214, 2003, pp. 369-378.
- [12] Kipfstuhl, S., I. Hamann, A. Lambrecht, J. Freitag, S. H. Faria, D. Grigoriev and N. Azuma, "Microstructure mapping: a new method for imaging deformation induced microstructural features of ice on the grain scale", *J. Glaciol.*, 52(178), 2006, pp. 398-406.
- [13] Duval, P., "Deformation and dynamic recrystallization of ice in polar ice sheets", T. Hondoh (ed.), *Physics of ice core records*, Hokkaido University Press, Sapporo, 2000, pp. 103-113.
- [14] Poirier, J.-P., "Creep of crystals", Cambridge University Press, 1985.
- [15] Hamann, I., Ch. Weikusat and N. Azuma, "Evolution of ice crystal microstructures during creep experiments", *J. Glaciol.*, acc. 12th May, 2007, (07J001).
- [16] Hamann, I., S. Kipfstuhl, S. H. Faria and N. Azuma, "Subgrain boundaries in EPICA-Dronning Maudland (EDML) deep ice core", in preparation for *J. Glac.*, August 2007.
- [17] Saylor, D. M. and G. S. Rohrer, "Measuring the Influence of Grain-Boundary Misorientation on Thermal Groove Geometry in Ceramic Polycrystals", *J. Am. Ceram. Soc.*, 82, 1999, pp. 1529-36.
- [18] Oerter, H., F. Wilhelms, F. Jung-Rothenhäusler, F. Göktas, H. Miller, W. Graf, W. and S. Sommer, "Accumulation rates in Dronning Maud Land, Antarctica, as revealed by dielectric-profiling measurements of shallow firn cores", *Ann. Glaciol.*, 30, 2000, pp. 27-34.
- [19] Wilhelms, F., S. G. Sheldon, I. Hamann, S. Kipfstuhl, "Implications for and findings from deep ice core drillings - An example: The ultimate tensile strength of ice at high strain rates", W. F. Kuhs (ed.), *Physics and Chemistry of Ice*, Royal Society of Chemistry, 2007.
- [20] Wesche, Ch., O. Eisen, H. Oerter, D. Schulte, D. Steinhage, "Surface topography and ice flow in the vicinity of the EDML deep-drilling site", *J. Glaciol.*, acc., 2007, (06J101)
- [21] Fischer, H., F. Fundel, U. Ruth, B. Twarloh, A. Wegner, R. Udisti, S. Becagli, E. Castellano, A. Morganti, M. Severi, E. Wolff, G. Littot, R. Rthlisberger, R. Mulvaney, M. Hutterli, P. Kaufmann, U. Federer, F. Lambert, M. Bigler, M. Hansson, U. Jonsell, M. de Angelis, C. Boutron, M.-L. Siggaard-Andersen, J. P. Steffensen, C. Barbante, V. Gaspari, P. Gabrielli, D. Wagenbach, "Reconstruction of millennial changes in dust transport, emission and regional sea ice coverage using the deep EPICA ice cores from the Atlantic and Indian Ocean sector of Antarctica", *Earth Planet. Sci. Lett.*, 260, 2007, pp. 340-354.
- [22] Trepied, L., J. C. Doukhan and J. Paquet, "Subgrain boundaries in quartz - theoretical analysis and microscopic observations", *Phys. Chem. Miner.*, 5(3), 1980, pp. 201-218.

- [23] Nakaya, U., "Mechanical properties of single crystal of ice. Part I. Geometry of deformation", US Army Snow Ice and Permafrost Research Establishment, Research Report, 28, 1958.
- [24] Wilson, C. J. L., D. S. Russell-Head and H. M. Sim, "The application of an automated fabric analyzer system to the textural evolution of folded ice layers in shear zones", *Ann. Glaciol.*, 37, 2003, pp. 7-17.
- [25] Weertman, J. and J. R. Weertman, "Elementary Dislocation Theory", Oxford University Press, 1992.
- [26] Hull, D. and D. Bacon, "Introduction to Dislocations", Elsevier, 2001.
- [27] Miyamoto, A. and I. Hamann, unpublished data, June 2007.
- [28] Miyamoto, A., H. Shoji, A. Hori, T. Hondoh, H.B. Clausen and O. Watanabe, "Ice fabric evolution process understood from anisotropic distribution of a-axis orientation on the GRIP (Greenland) ice core", *Ann. Glaciol.*, 42, 2005, pp. 47-52.
- [29] Obbard, R., I. Baker and K. Sieg, "Using electron backscatter diffraction patterns to examine recrystallization in polar ice sheets", *J. Glaciol.*, 52(179), 2006, pp. 546-557.
- [30] Iliescu, D., I. Baker and H. Chang, "Determining the Orientations of Ice Crystals Using Electron Backscatter Patterns", *Microscopy Res. Tech.*, 63, 2004, pp. 183-187.
- [31] Faria, S., I. Hamann, S. Kipfstuhl and H. Miller, "Is Antarctica like a birthday cake?", Preprint no. 33/2006 of the Max Planck Institute for Mathematics in the Sciences, Leipzig, 2006.
- [32] Higashi, A., A. Fukuda, H. Shoji, M. Oguro, T. Hondoh and K. Goto-Azuma, "Lattice defects in ice crystals" Higashi, A. (ed.), Hokkaido University Press, Sapporo, Japan, 1988.
- [33] Hondoh, T. "Nature and behavior of dislocations in ice". T. Hondoh (ed.), *Physics of ice core records*, Hokkaido University Press, Sapporo, 2000, pp. 324.
- [34] Bons, P. D. and M. W. Jessell, "Micro-shear zones in experimentally deformed OCP", *J. Struct. Geol.*, 21, 1999, pp. 323-334.
- [35] Jacka, T.H., S. Donoghue, J. Li, W. F. Budd, and R. M. Anderson, "Laboratory studies of the flow rates of debris-laden ice", *Ann. Glaciol.*, 37, 2003, pp. 108-112.
- [36] Jacka, T. and M. Maccagnan, "Ice crystallographic and strain rate changes with strain in compression and extension", *Cold Reg. Sci. Tech.*, 8, 1984, pp. 269-286.
- [37] Paterson, W. "Deformation within polar ice sheets: An analysis of the Byrd station and Camp Century borehole-tilting measurements", *Cold Reg. Sci. Tech.*, 8, 1983, pp. 165-179.
- [38] Hutchinson, J. W., "Creep and plasticity of hexagonal polycrystals as related to single crystal slip", *Metallurgical and Materials Transactions A*, 8, 1977, pp. 1465-1469.
- [39] Castelnau, O., P. Duval, R. Lebensohn and G. R. Canova, "Viscoplastic modeling of texture development in polycrystalline ice with a self-consistent approach: Comparison with bound estimates", *J. Geoph. Res.*, 101, 1996, pp. 13,851-13,868.
- [40] Castelnau, O., G. Canova, R. Lebensohn and P. Duval, "Modelling viscoplastic behavior of anisotropic polycrystalline ice with a self-consistent approach", *Acta Mater.*, 45, 1997, pp. 4823-4834.
- [41] Humphreys, F. J. and M. Hatherly, "Recrystallization and Related Annealing Phenomena", Elsevier, 2004.
- [42] H. Föll, "Defects in Crystals", Hyperscript, 2004, [www.tf.uni-kiel.de/matwis/amat/defen/index.html](http://www.tf.uni-kiel.de/matwis/amat/defen/index.html).
- [43] Duval, P. and M. Montagnat, "Physical deformation modes of ice in glaciers and ice sheets", Knight, P. G. (ed.), *Glacier Science and Environmental Change*, Blackwell Publishing, 2006, pp. 303-308

## Appendix D

### Publication IV - Microstructure mapping: a new method for imaging deformation-induced microstructural features of ice on the grain scale

Kipfstuhl, S., Hamann, I., Lambrecht, A., Freitag, J., Faria, S. H., Grigoriev, D., Azuma, N. (2006)  
Journal of Glaciology, Vol. 52, No. 178, pp. 398-406.

# Microstructure mapping: a new method for imaging deformation-induced microstructural features of ice on the grain scale

Sepp KIPFSTUHL,<sup>1</sup> Ilka HAMANN,<sup>1,2</sup> Anja LAMBRECHT,<sup>1,3</sup> Johannes FREITAG,<sup>1</sup>  
Sérgio H. FARIA,<sup>1,4</sup> Dimitri GRIGORIEV,<sup>5</sup> Nobuhiko AZUMA<sup>2</sup>

<sup>1</sup>Alfred Wegener Institute for Polar and Marine Research, Columbusstrasse, D-27568 Bremerhaven, Germany  
E-mail: kipfstuhl@awi-bremerhaven.de

<sup>2</sup>Department of Mechanical Engineering, Nagaoka University of Technology, Kamitomioka cho 1603-1,  
Nagaoka 940-2188, Japan

<sup>3</sup>Institute for Geodesics and Geophysics, Technical University of Vienna, Gusshausstrasse 27–29/1282,  
A-1040 Vienna, Austria

<sup>4</sup>GZG, Department of Crystallography, University of Göttingen, Goldschmidtstrasse 1, D-37077 Göttingen, Germany

<sup>5</sup>Department of Earth Sciences, University College London, Gower Street, London WC1E 6BT, UK

**ABSTRACT.** This work presents a method of mapping deformation-related sublimation patterns, formed on the surface of ice specimens, at microscopic resolution ( $3\text{--}4\ \mu\text{m pixel}^{-1}$ ). The method is based on the systematic sublimation of a microtomed piece of ice, prepared either as a thick or a thin section. The mapping system consists of an optical microscope, a CCD video camera and a computer-controlled  $xy$ -stage. About 1500 images are needed to build a high-resolution mosaic map of a  $4.5 \times 9\ \text{cm}$  section. Mosaics and single images are used to derive a variety of statistical data about air inclusions (air bubbles and air clathrate hydrates), texture (grain size, shape and orientation) and deformation-related features (subgrain boundaries, slip bands, subgrain islands and loops, pinned and bulged grain boundaries). The most common sublimation patterns are described, and their relevance for the deformation of polar ice is briefly discussed.

## 1. INTRODUCTION

The microstructure of a rock is understood as the small-scale arrangement of geometric elements within it (Hobbs and others, 1976). Ice (and firn) in the cold and dry plateaus of polar ice sheets is a monomineralic rock and, as such, it has many geometric elements which can be observed using an optical microscope (e.g. grain and subgrain boundaries, slip bands, pores and air inclusions (air bubbles, air clathrate hydrates and plate-like inclusions), to mention the most common). Ice also contains traces of insoluble impurities, typically solid particles like mineral dust and volcanic ash, but only occasionally are such particles deposited in high enough amounts to form visible layers (e.g. Fujii and others, 1999; Svensson and others, 2005).

Over 20 years ago, Wilson (1986) noted a paucity of data on ice microstructure evolution with progressive deformation, as well as a lack of studies on slip bands in naturally deformed ice. Although dislocation glide is widely accepted as the dominant deformation mechanism in polar ice, there is still considerable debate on the role of grain boundary sliding (Goldsby and Kohlstedt, 2001, 2002; Duval and Montagnat, 2002). Detailed observation of deformation-induced microstructural features of polar ice, which are characteristic of the deformation mechanisms active in situ, may contribute to solving this debate.

There is a long list of questions which motivates the mapping of the microstructure of firn and ice in microscopic resolution. For instance, in order to properly discriminate the factors influencing the microstructure properties, like global and local climate conditions (impurity load, accumulation rate, insolation, etc.), depositional characteristics (finer or coarser grains) and the regimes of deformation and recrystallization, it is essential

to analyze the microstructural features of ice through an annual layer (whose typical thickness on the dry plateaus of polar ice sheets ranges between 3 and 20 cm of ice equivalent). In combination with fabric measurements (Wang and Azuma, 1999; Azuma and others, 2000; Wilen, 2000; Wilson and others, 2003) data about grain size and shape have been derived (Svensson and others, 2003), but we are aware of no study investigating the microstructure of ice by mapping as many features in a section as possible by means of digital-imaging techniques. Arnaud and others (1998) used a classic still camera to photograph the microstructure of firn and bubbly ice in coaxial reflected light. Nishida and Narita (1996) reconstructed the three-dimensional shape of ice grains using similar methods. Both used classic still cameras, and were not able to instantaneously control the image quality (contrast, resolution, etc.). They developed negative films, digitized the negatives and finally processed the resulting digital images in a computer, although computer-based image-processing systems were already described at that time (Perovich and Hirai, 1988; Eicken, 1993). Likewise, optical microscopes have been used to derive statistical data about air bubbles and hydrates (Uchida and others, 1994; Pauer and others, 1999; Lipenkov, 2000; Kipfstuhl and others, 2001), but no systematic mapping or image processing was performed during such investigations.

In the past decade, computing power and digital-imaging techniques have progressed rapidly and modern digital cameras have attained such high image quality that they can, in most cases, successfully replace classic film still cameras. It is possible today to set up a mapping environment consisting of commercially available components, like a charge-coupled device (CCD) video or digital camera, a computer-controlled  $xy$ -stage and an optical microscope or

similar lens system, that can be operated under cold room conditions down to  $-30^{\circ}\text{C}$  and even below without major problems.

While the NorthGRIP deep ice core (North Greenland Ice Core Project members, 2004) was being drilled in Greenland, we began to set up and test a computer-controlled microscopic imaging system, which could replace the tedious and time-consuming manual counting of air inclusions (see, e.g., Kipfstuhl and others, 2001). The idea was to automate the microscopic observation as much as possible, through the scanning of a thin or thick section of ice (typical dimensions: 5–10 cm by 10 cm) and the production of digital images at microscopic resolution in a reasonable time (about an hour), while drilling was ongoing. The processing of the images could then be done at a more convenient time. While testing this equipment for air-bubble and hydrate studies, we found it was also suitable for recording grain boundaries and a wide variety of deformation-induced microstructural features, among them slip bands and subgrain boundaries, which have received little attention to date. Some of these features (e.g. grain and subgrain boundaries) were revealed by sublimation of the exposed ice surface, which became an essential part of the method. In this paper, we describe the computer-imaging environment which has been used in Antarctica within the EPICA–DML (European Project for Ice Coring in Antarctica–Dronning Maud Land) microstructure mapping project. We describe the procedures used to obtain good optical images and the microstructural features seen in naturally deformed ice. We first present results demonstrating that careful preparation and adequate observation techniques reveal a wide spectrum of deformation-induced microstructural features which may help us to better understand the recrystallization processes taking place in ice sheets.

## 2. METHODS

The NorthGRIP and EPICA cutting plans dedicate the top 10 mm of the 98 mm diameter core for the study of physical properties (EPICA community, 2004; NorthGRIP members, 2004). From 9 or 10 cm long vertical sections, with the long axis parallel to the vertical axis of the ice core, another section about 6 mm thick is cut (Fig. 1, grey-shaded region). The dimensions of a section used for mapping are typically 40–50 mm wide, 90–110 mm long and 4–5 mm thick.

### 2.1. Sample preparation

Samples are prepared according to the standard procedures used for the production of thin sections for fabric and texture analysis (e.g. Uchida and others, 1994; Pauer and others, 1999). We use band-saws for cutting and microtomes for polishing. Clear surfaces are achieved by exposing the polished section to the free atmosphere. Sublimation of an ice surface works like chemical or thermal etching, a method widely employed in materials science to produce etch pits and grooves on the surfaces of metal, mineral and ceramic samples (Mullins, 1957; Kuroiwa and Hamilton, 1963; Hobbs, 1974; Nishida and Narita, 1996; Arnaud and others, 1998). During sublimation, the scratches produced by the microtome blades disappear, while certain characteristic patterns, called sublimation ‘grooves’, ‘lines’ and ‘pits’, start to develop at the sites where grain/subgrain boundaries (as well as other energetically unfavourable structures) meet the surface. We wait between half an hour and half a day to

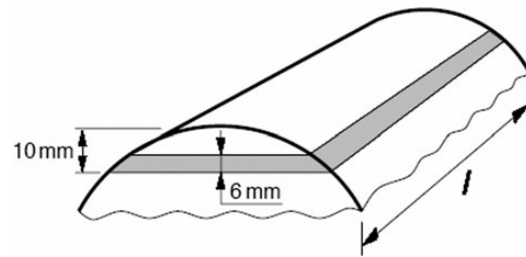


**Fig. 1.** Cutting scheme. From the top piece of a 98 mm diameter ice core the lower half (grey shaded) is used for crystal studies and microstructure mapping. The length,  $l$ , is 55 cm for the EDC (EPICA Dome C) core and 100 cm for the EDML (EPICA Dronning Maud Land) core.

obtain a clear surface, with well-developed grain-boundary grooves. The sublimation time depends very much on temperature, temperature gradient, humidity and air movement or wind above the sample. Sublimation is accelerated when the ice section lies under a light bulb, in direct sunlight and wind, (and probably also in a vacuum chamber, not yet tested). In general, the drier the air, the more distinct and clear the surface.

After the first (lower) surface of the sample is sufficiently clear, it is sealed off with a thin film of silicon oil ( $10^{-4} \text{ m}^2 \text{ s}^{-1}$ ). Thus protected against over-sublimation, the section is frozen onto a glass plate. The second (upper) surface is treated in the same manner. However, because of the better contrast of a pristine surface (no silicon oil and no cover glass), we seal off this surface just after the first mapping run is completed.

### 2.2. Mapping system

The system used to map the samples consists of an optical microscope (Leica DMLM), a CCD video camera (Hamamatsu C5405), a frame grabber (SCION LG3) and an  $xy$ -stage (Märzhäuser XY100). Images are usually taken in transmission. The process of image acquisition, i.e. the positioning of the sample on the  $xy$ -stage and subsequent image capture, is controlled by the public domain NIH Image software (developed at the US National Institutes of Health and available on the internet at <http://rsb.info.nih.gov/nih-image/>) together with the LG3 frame grabber, both running on an Apple G3 computer. As colour cameras offer no advantage for our purposes, all images are acquired in grey value. Black-and-white cameras give better contrast and sensitivity than colour cameras, and they produce fewer data (resolution: 1 byte or 256 grey values). The standard size chosen for a single image is 2.5 by 1.8 mm, but this can be changed depending on the lenses used in the microscope. Consecutive images are taken every 2 mm in the  $x$  direction. An overlapping of 0.5 mm is helpful for the later reconstruction of the full mosaic figure, giving us some freedom to find the best match between neighbouring images. A series of about 1500 images is needed to map a section 45 by 90 mm. The whole scan takes about 1 hour. The mapping system described above has been used at Dome C and in Dronning Maud Land during five field seasons. The main problem encountered so far is the alignment (matching) of the individual images as we deal with four pairs of horizontal axes: one pair for the camera (image), one for the  $xy$ -stage,

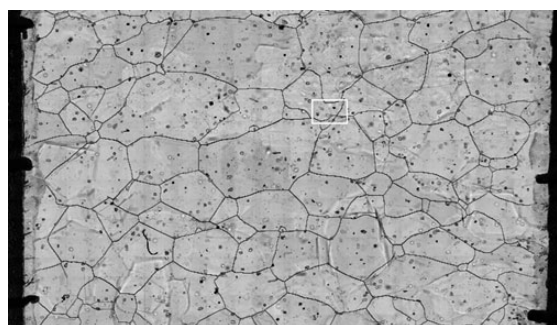


**Fig. 2.** A mosaic of about 300 images showing a 2 by 4.5 cm section from the Dome C ice core (depth 1291 m). Dark lines are high-angle grain boundaries, while dark and black spots or rings are air hydrates. Also visible are internal grain boundaries (blurred, dark lines). The thick, black ticks on both sides of the sample are ~1 cm apart and indicate the scale. The white rectangle marks a single microphotograph (image number 749, 2.5 by 1.7 mm). For comparison, this microscopic image is shown in full resolution in Figure 3.

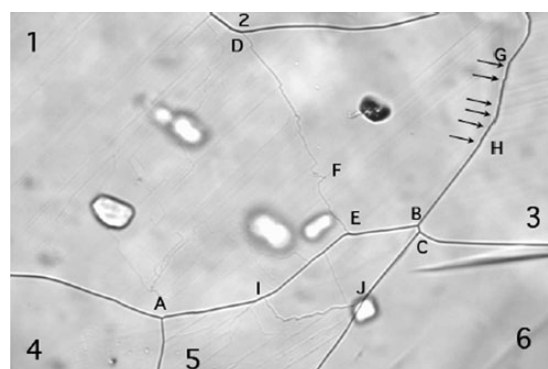


**Fig. 3.** Microphotograph marked in Figure 2 in full resolution. Subgrain boundaries, irregular sublimation groove patterns, slip bands and air hydrates (the single black inclusion is a decomposing air hydrate) are visible at this higher magnification. Labelled features are described in the text. (EDC ice core, depth 1291 m, width 2.5 mm.)

one for the glass plate and another for the sample itself. These four pairs of axes should match as exactly as possible to avoid time-consuming corrections later. Another problem is the large size of the reconstructed images, of the order of 400 MB. For example, to extract grain sizes using NIH Image's particle analysis routines we have to scale the images down to 25%.

Information about the *c*-axis orientation of grains and subgrains is essential for the understanding of deformation on the grain scale. However, the fabric analyzers currently available (Wang and Azuma, 1999; Wilson and others, 2003) do not have the necessary resolution.

### 3. RESULTS OF MICROSTRUCTURE MAPPING

In this section we compare the features which can be observed at different resolution levels, from a single microscopic image up to a mosaic in standard magnification for common texture and fabric analyses. This should give an idea of the degree of detail, and consequently the amount of new, relevant information on the polar ice microstructure, which can be obtained with this method.

#### 3.1. Low-resolution (mesoscopic) view

A mosaic of the EDC (EPICA Dome C) core from 1291 m depth, 2 cm high and 4.5 cm wide, composed of about 300 images, is shown in Figure 2. It is just a quarter of the entire thick section (9 cm high and 4.5 cm wide), which encompasses 1280 images (20 images per row and 64 rows). The mosaic in Figure 2 demonstrates that grain boundaries and air inclusions are detected by microstructure mapping when the microscope is focused on the surface of the section. Notice that this sample comes from a depth where all air bubbles have already transformed into clathrates (i.e. air hydrates), which are seen as 'little rings', deeper in the section. Dark or black spots are defocused or decomposing air hydrates partly filled with gas. The ticks on the left and right margins, approximately 1 cm apart, serve as benchmarks to locate interesting features within the image or section, respectively. The outermost margins of the sections,

over about the length of the ticks (1–2 mm), are often disturbed to such an extent that grain-boundary grooves and other interesting sublimation patterns have disappeared. Mosaic images like Figure 2 are the basis of all further analyses. Using image-processing software, we can determine the orientation of slip bands (Faria and Kipfstuhl, 2004), extract the grain boundary network to derive texture information like grain size and shape, and derive statistical data about the presence of sublimation grooves or subgrain boundaries within grains, air bubbles and air hydrates, as well as other visible features (work in progress).

When shown at low resolution (of the order of  $100 \mu\text{m pixel}^{-1}$ ), the grain-boundary network does not differ much from that extracted by other methods (Arnaud and others, 1998; Wang and Azuma, 1999). Therefore, there is no reason to discuss the low-resolution image in Figure 2 in detail: most grain boundaries look rather 'flat' and seem to manifest the characteristic features of a so-called 'foam texture', with straight and equiaxed boundaries. In contrast, it is shown in section 3.2 that at higher resolution a significant number of grains show irregular boundaries, indicating that other processes, as well as normal grain growth, are important.

#### 3.2. High-resolution (microscopic) view

Figure 3 illustrates how much detail is hidden in a mosaic image originally produced by mapping in microscopic resolution. We recognize many details and substructures not only within the ice matrix but also on grain boundaries (e.g. slip bands and grain-boundary steps). Most microstructural features shown in this figure can be observed in sections from any depth. For convenience, grains are numbered from 1 to 6 and interesting features are labelled with capital letters (A–J). Air inclusions and internal structures are not marked.

In the discussion below we concentrate on deformation- and grain-growth-related features. High-angle grain boundaries meet at three triple junctions (A, B and C). The parts of grains 2, 3, 4 and 6 visible in Figure 3 are free of sublimation

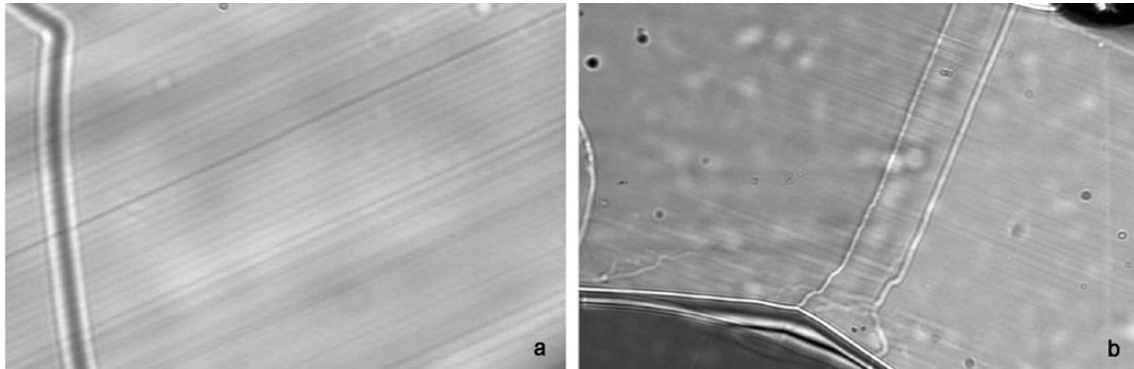


**Fig. 4.** (a) Straight and (b) kinked slip bands. Spacing of the bands ranges between  $\sim 10$  and  $20 \mu\text{m}$ . The misorientation in (b) is about  $2^\circ$ . White lines in (b) are the grooves of a tilt boundary visible on both surfaces of a thin section placed between crossed polarizers. Note that the left half of the grain is slightly darker than the right subgrain. Generally, slip bands are not evenly distributed in a grain. (EDC ice core, depth 1291 m (a) and 489 m (b), width  $600 \mu\text{m}$ .)

features. Grain 3 shows slip bands ending at the boundary with grain 1, which is divided into two subgrains by a developing subgrain boundary between D and E. The left subgrain contains slip bands overlain by an irregular network of very faint sublimation lines, with some sublimation lines parallel to the slip bands and others perpendicular to them. Subgrain boundary DE shows steps with straight segments. Other parts are quite irregular. Some of the steps are accompanied by more prominent slip bands and sublimation grooves. These last two features are often not easy to differentiate at first sight: we need to focus the microscope deeper into the sample to distinguish them, for sublimation grooves soon become defocused, whereas slip bands remain almost unaltered (since they are interior features; see section 4.1). This lack of distinction could, in principle, cause some difficulties in the interpretation of certain digital images, but fortunately this is not the case in practice: straight sublimation grooves, parallel to slip bands, are often related to the slip process itself, and they hide slip bands behind them (see section 4.2). As evidenced by grains 1 and 3, slip bands are, in general, not evenly distributed over grains and subgrains. A closer look at the grain boundary separating grain 3 and grain 1 reveals tiny steps between G and H (marked by arrows), in a region of grain 3 where strong slip bands are visible. The steps may be produced by intense basal slip deformation. Grain 5 is divided by a strong but irregular subgrain boundary, the upper subgrain once again by a weak, straight subgrain boundary. The interior of both upper subgrains is free of features. In contrast, the lower subgrain is covered by an irregular pattern of sublimation grooves, most of them parallel or of similar orientation. It seems that the irregular subgrain boundary, IJ, moved downwards into the lower subgrain, leaving behind a recovered, thus clear, upper subgrain.

One important finding from Figure 3 is that it documents the interaction of strong and weak sublimation grooves, i.e. the interaction of grain and subgrain boundaries. This is most clearly manifested in grain 1 at D and E, but also in grain 5 at I and J, where the high-angle boundaries bow towards the subgrain boundaries. An explanation for this apparent interaction may be that grain-boundary migration is driven in those particular sites by stored strain energy, and not by

grain-boundary curvature/interface energy, as expected to be the case during normal grain growth. We do not yet know the relevance of this apparent interaction. However, it indicates that the interaction between subgrain and high-angle grain boundaries has to be taken into account to understand grain-boundary migration in detail.

#### 4. INTERPRETATION

Sublimation features are marks on the surface of an ice specimen, which are caused by preferred vaporization. As a consequence, such superficial marks become blurred and fade out of view as the microscope is focused deeper into the sample. Slip bands, air bubbles and hydrates, dust and ash particles belong to another category of features, called 'interior', since they are located inside the material and are not produced by sublimation. In this section we discuss how to distinguish and interpret interior and sublimation (surface) features.

##### 4.1. Interior features

Figure 4 shows slip bands observed when the microscope is focused on the interior of the sample. At first sight it may be somewhat perplexing that the slip bands in Figure 4a seem to cross the grain boundary; but this is in reality just an illusion (a 'depth effect'), caused by the fact that the grain boundary is inclined enough to become invisible, so that only the defocused boundary groove on the surface is seen.

We studied two EPICA cores; in each we observe grains with straight, bent and polygonized (broken) slip bands. Frequently, coarse and fine slip occur in the same grain and the distribution of slip bands is then inhomogeneous (e.g. Figs 3 and 4). The spacing of the slip bands varies between 5 and  $20 \mu\text{m}$  for fine slip and 20 and  $100 \mu\text{m}$  for coarse slip. The spacing of the slip bands seems to be roughly independent of depth and pressure. A remarkably high number of bent and polygonized slip bands is found at shallow depths just below the firn-ice transition (about 100 m). Subgrain boundaries perpendicular to the slip bands, therefore probably tilt boundaries (i.e. boundaries made up of edge dislocations), are already visible in grains with slip bands bent more than  $1-2^\circ$  (Fig. 4b; see also fig. 5 in Wang and others, 2003).

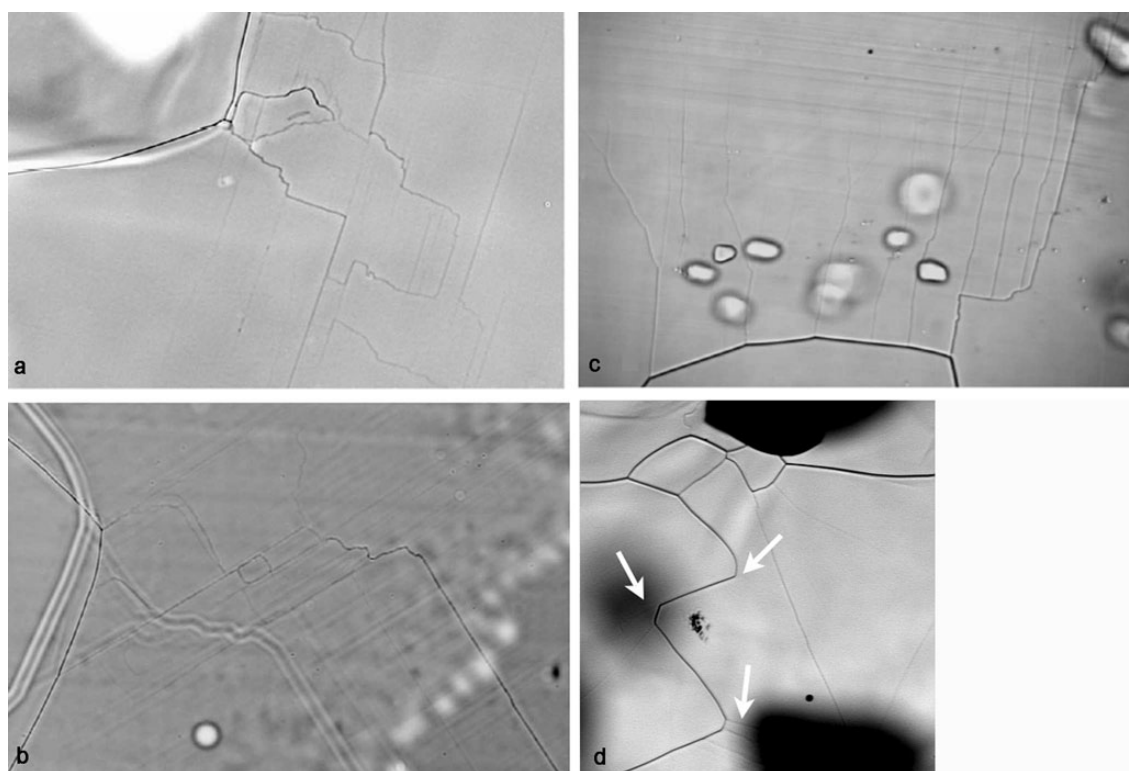


**Fig. 5.** Complex sublimation line patterns. The faint, parallel lines are slip bands and thus indicate the orientation of the basal planes. Notice that sublimation grooves occur only on the convex side of grain boundaries. (a) Complex patterns of sublimation grooves at a grain corner (EDC core, depth 768 m, width 600  $\mu\text{m}$ ). (b) Transition zone between a high-angle grain boundary (left) and a tilt boundary (right) in a thin section (EDC core, depth 150–200 m, exact depth not known, width 600  $\mu\text{m}$ ). Blurred, defocused sublimation lines correspond to grooves in the bottom surface, while the sharp, black lines are focused grooves on the top surface. It should be noted that the sublimation groove associated with the subgrain (tilt) boundary becomes weaker as it gets more irregular and dissociates into intricate patterns and loops. (c) Multiple tilt boundaries in a grain bent over a large area (EDML core, depth 2105 m, width 600  $\mu\text{m}$ ). (d) Irregular, wavy grain boundary (EDML core, depth 154 m, width 1.2 mm). Arrows point to weak sublimation lines.

In our thick/thin sections we observe some grains exhibit slip bands, while others do not. In principle, one could argue that those grains with no visible slip bands should be either unstrained or fully recovered/recrystallized, but this would be a hasty conclusion. In fact, experience shows that the *c*-axis orientation relative to the plane of observation is crucial for the detection of slip activity. In other words, slip bands fade out of view whenever the *c* axis is not nearly perpendicular to the viewing axis of the microscope. Tilting of the thick section about one axis (a four-axes universal stage was not available) showed that slip bands tilted more than about 5–10° fade out and disappear (*c* axis tilted <10° out of the sample plane). Consequently, slip band analysis via microstructure mapping must be restricted to those grains showing visible slip bands.

#### 4.2. Sublimation features

##### *Common sublimation patterns*

Figure 5 shows the most common types of sublimation features: complex patterns of sublimation grooves at corners of grains (Fig. 5a) and at transition zones between subgrain and high-angle grain boundaries (Fig. 5b), single or multiple subgrain and tilt boundaries perpendicular to slip bands (Fig. 5c) and wavy or irregular high-angle grain boundaries,

together with other complex sublimation line patterns. Noteworthy is that complex sublimation line patterns are strongly related to corners of high-angle grain boundaries, and also that they occur more frequently in the marginal area (the ‘mantle’) of the grains than in their central parts (the grain ‘core’). Typical of complex sublimation line patterns are series of parallel lines, often interrupted by several alternated steps at right angles (zigzag-like lines) finally continuing in the original direction. Sometimes, irregular sublimation lines meet straight lines, follow or cross them and form loops, often called ‘subgrain islands’ (Koo and others, 2000; Ryde and others, 2004). The complex patterns in Figure 5b, within the transition zone between the high-angle grain boundary and the well-developed subgrain boundary coming from the lower-right corner, may indicate that the best configuration for the new triple junction had not yet been achieved. Figure 5c is a good example for a grain bent over a wide bulge, where multiple subgrain boundaries develop as demonstrated by Nakaya (1958). The developing subgrain boundaries start at a high-angle grain boundary, but fade out in weaker branches, leaving the centre of the grain undisturbed. Interesting to note also is that in Figure 5a–c the sublimation line patterns are commonly found on the convex side of the grain boundaries, while the concave side appears

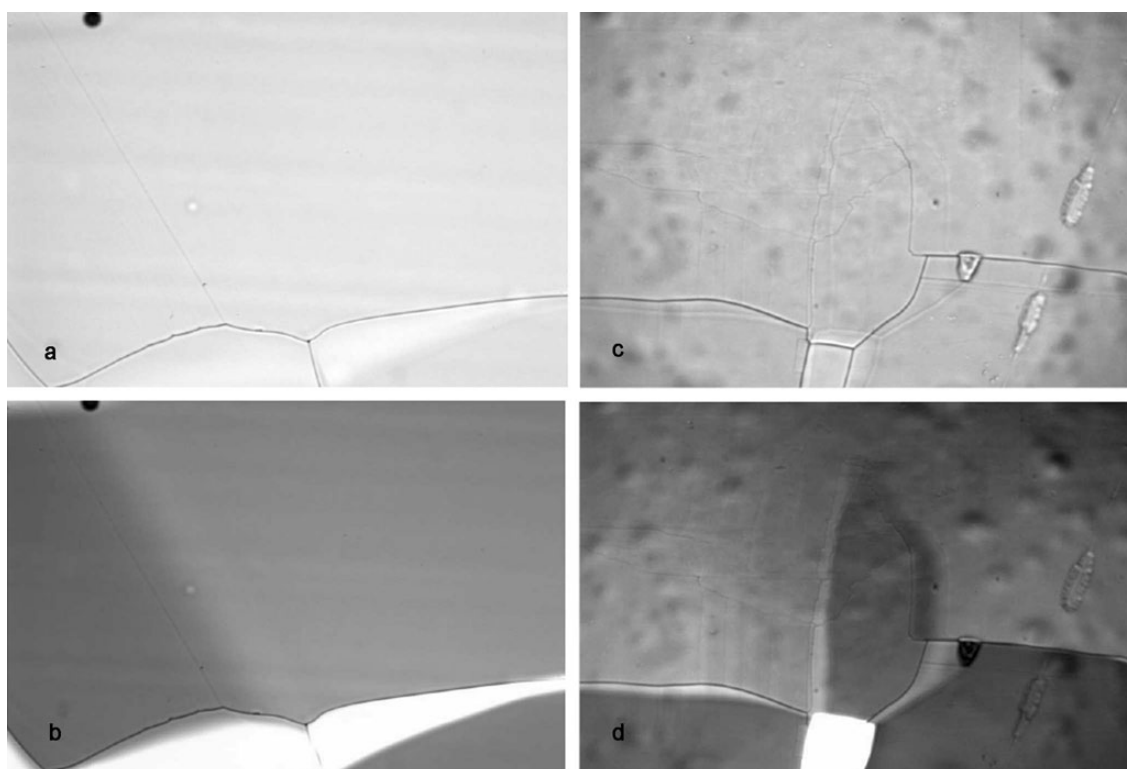


**Fig. 6.** Thin sections from two depths of the EDC ice core, illuminated with normal and polarized light. Slightly different orientations are indicated by contrasting shades of grey in (b) and (d). (a,b) Tilt boundary in a sample from  $\sim 150$ – $200$  m depth (exact depth not known), width  $600\ \mu\text{m}$ : (a) normal light; (b) polarized light. (c,d) Complex pattern of sublimation lines in a sample from  $1134.6$  m depth, width  $600\ \mu\text{m}$ : (c) normal light; (d) polarized light. Note the stepwise change in grey value on the left of the subgrain and several faint vertical subgrain boundaries.

free of any sublimation features. This behaviour is also typical for extremely irregular or wavy grain-boundary segments, as in Figure 5d.

#### *Subgrain boundaries*

Slip bands and subgrain boundaries result from shearing, bending, twisting and consequent subdivision of a grain or parts of a grain. The *c*-axis misorientation caused by bending is best observed in thin sections placed between crossed polarizers, where it is manifest as a change in colour or grey shade. Microphotographs of thin sections prepared as described in section 2.1 and illuminated with normal and polarized light are shown in Figure 6. In both sections we observe that the grey shade changes not only across high-angle grain boundaries (the wide dark lines) but also across the weak single line in Figure 6a and b and across the complex, weak line pattern in Figure 6c and d. This comparison proves that those weak sublimation grooves are indeed related to changes in orientation within a grain, and can therefore be interpreted as subgrain boundaries. Unfortunately, we cannot quantitatively estimate the misorientation angle directly from the difference in grey values. However, our observations of slip bands indicate that single, smooth/straight sublimation grooves like those shown in Figure 6a and b normally appear when the slip bands are tilted by just a few (one or two) degrees (Wang and others, 2003; Faria and Kipfstuhl, 2004). Additionally, in all mapped

sections we commonly observe a progressive change in the character of most sublimation lines, as we move our attention from the core towards the boundary of a given grain. Such a change is manifold, being characterized, for instance, by a gradual transition of the grey values of sublimation lines, ranging from very faint (hardly visible) in the core to weak and finally dark black at the boundary. Together with this transition in intensity there is also a change in shape, from more irregular (zigzag-like) to smoothly curved and straight lines. Further, we observe in thin sections between crossed polarizers that the grey shade difference across a sublimation line is proportional to the intensity and smoothness of the sublimation line. Therefore, the strength of a sublimation line in a mapped image can be used as a qualitative measure of the *c*-axis misorientation across it.

There is, however, a particular type of straight sublimation line that can be very intense, yet at the same time manifests no shade difference (and consequently no *c*-axis misorientation) across it. As a rule, such a sublimation line is parallel to slip bands (Fig. 5b). We suggest two possible explanations for its origin: it could indicate a rotation of the basal planes about the *c* axis of the grain, in which case it would denote a 'twist boundary', or it could be generated by a strong and localized process of micro-shear, as proposed for other geological materials by Bons (1999). It should be noted that neither twist boundaries nor micro-shear zones have been reported by Nakaya (1958), Wilson (1986) or Zhang and Wilson (1997).

### 4.3. Interpretation of sublimation line features

Nakaya (1958) showed that subgrain boundaries tend to develop in regions of maximum stress/strain concentration. As evidence for strain localization we consider our finding that sublimation line features occur preferably at corners or bulges of high-angle grain boundaries. From our observations, we believe that in ice, as in other creeping rocks, strain localization is the rule rather than the exception (Bons, 1999). In this sense, any apparent interaction between a subgrain boundary or sublimation line features and a high-angle grain boundary may express such strain localization. We assume this explains the observations in Figure 5, that sublimation features are found on the convex side of high-angle grain boundaries, while the concave sides appear free of sublimation features. High-angle grain boundaries probably migrate towards areas containing a higher density of deformation-related sublimation features (that is a higher density of stored strain energy, as sublimation lines indicate lattice defects) and leave undisturbed ice matrix behind them. Thus, grain-boundary migration may be driven in such cases by strain energy and not by grain-boundary curvature (surface tension/energy). It is surprising that the extremely wavy grain boundary from 154 m depth (Fig. 5d) also shows this behaviour, although it is generally argued that stored energy at such shallow depths should not be significant (Alley, 1992; Montagnat and Duval, 2000). However, there are good reasons to assume that stress and strain localization are particularly important at shallow depths, since the fabric there is isotropic, and consequently the grain-grain interaction should be strong, due to the difficult accommodation of intergranular incompatibility. Indeed, the most irregularly shaped grain boundaries are observed in the upper hundreds of metres. Strain localization is obviously an important aspect in the evolution of a single grain. What is remarkable is that the character of the observed patterns in individual grains does not change much down the core. Therefore, we are confident that concentration, strength and smoothness of sublimation grooves can be used to learn more about the deformation of a grain and finally to quantify the different processes controlling deformation and grain growth.

We assume that concentration, strength and smoothness of sublimation grooves reflect the evolution of the response of a grain to deformation. The more a grain or a part of a grain is strained, the more rich and intense sublimation patterns may be present. The most irregular patterns may characterize early stages of deformation, while a few strong and smooth lines correspond to stages of advanced recovery and annealing (e.g. subdivision of a grain). In this sense, microstructure mapping permits access to the deformation on the grain scale through optical microscopy. At this stage, the interpretations presented above should be regarded as preliminary, since statistical studies needed to draw firm conclusions are still in progress and the information about *c*-axis orientation is not yet available at the required resolution.

## 5. DISCUSSION

The step forward with automated mapping is that digital images of entire sections in microscopic resolution are produced and the relevance of features can be investigated. Quantitative data about the occurrence of subgrain boundaries, slip lines and other microstructural features, like subgrain boundary loops or four junctions, become readily

available and allow us to characterize the evolution of the microstructure on the grain scale.

As it is impossible to study the microstructure of polar ice under the conditions prevailing in the interior of an ice sheet, we have studied ice samples immediately after core extraction. We then repeated the mapping some time (hours and days) later. These analyses convinced us that there are only minor changes within the first hours and some days up to a few weeks after core extraction. It is very unlikely that the observed grain/subgrain-boundary patterns could be created during the less than 3–5 hours needed to prepare the fastest samples. Admittedly, there is a short period (of less than an hour) while the core is being pulled up from the borehole at  $1 \text{ m s}^{-1}$  and the pressure is dropping at a typical rate of  $\sim 1 \text{ kPa s}^{-1}$ . Nevertheless, we can hardly imagine that all mapped microstructural features are artefacts produced within this short time, seeing that most features are characteristic of *slow* deformation. Firm-core studies support this view. All microstructural features seen in deep ice cores are already present in firm and shallow ice cores, where the influence of the pressure release on the evolution of the microstructure should be negligible.

Now, if the visible sublimation line patterns are related to deformation, then microstructure mapping provides valuable information about the intracrystalline response of ice grains to deformation over a wide range of stages. Microstructure mapping can therefore fill the gap between observations on the 'macroscale', represented by classic texture and fabric studies, and those on the lattice scale, accessible only by electron microscopy (SEM/EBSD) and gamma-/X-ray diffraction studies (GRD/XRD). Provided that our interpretation of Figure 6 is correct, that is that the occurrence of sublimation line patterns on the convex side of grains is evidence of strain-induced boundary migration, then microstructure mapping may offer a means of characterizing and quantifying grain growth. The mosaic images contain all the necessary information to derive statistical data for investigating the role of strain-induced boundary migration, polygonization (subdivision of grains) and grain-boundary sliding. New phenomena, like subgrain islands, two-sided grains, twist boundaries and micro-shear, invariably call our attention to new views of the fundamental processes behind grain growth and inter-/intracrystalline deformation. For the first time, layering and the effect of impurity load on grain growth and deformation can be studied at the grain scale. This is important for ice containing cloudy bands, where grain size also appears banded and switches with the cloudiness in ice.

Currently, a serious technical difficulty is the coupling of microstructure mapping data with *c*-axis orientation. High-resolution fabric data are needed to investigate how the features described above and the underlying processes are related to lattice orientation. Also mechanical tests (although performed at much higher deformation rates than *in situ*) are needed to investigate and compare the evolution of microstructural features of naturally and artificially deformed ice.

## 6. CONCLUSION

Through the method of microstructure mapping described here, imperfections of the ice matrix become optically visible on the surface when an ice specimen is carefully prepared and sublimated. We can distinguish not only grain

and subgrain boundaries, but also more complex line patterns, probably related to various stages of deformation. Slip bands and other kinds of visible inclusions (ash particles, air bubbles and air clathrate hydrates) can also be observed.

Microstructure mapping is a tool not only to derive statistical data about inclusions, but also to study deformation on the grain scale and the interaction between neighbouring grains or within ensembles of a few tens/hundreds of grains. From the reconstructed mosaic images, qualitative and quantitative information can be derived to characterize the diverse deformation and recrystallization processes taking place in an ice sheet. Microstructure mapping should thus fill the gap between classic texture and fabric studies, where grain ensembles are treated statistically, and SEM/EBSD/GRD/XRD observations with extremely high resolution but very limited spatial range.

The method described in this work has been successfully applied to ice samples of the EPICA Microstructure Mapping Project, where it proved itself to be a fast means of documenting the microstructure of fresh ice-core samples during drilling. Our preliminary results suggest that intracrystalline deformation is highly inhomogeneous and all sublimation line patterns occur more or less independent of depth. This implies, for example, that stress/strain localization has to be taken into consideration to understand grain growth. Unfortunately, a coupling of these results to high-resolution *c*-axis analysis on the grain and subgrain scale is not yet available.

## ACKNOWLEDGEMENTS

F. Valero Delgado wrote the NIH Image macros. This work is a contribution to the European Project for Ice Coring in Antarctica (EPICA), a joint European Science Foundation/European Commission scientific programme, funded by the European Union and by national contributions from Belgium, Denmark, France, Germany, Italy, the Netherlands, Norway, Sweden, Switzerland and the United Kingdom. The main logistic support was provided by Institut Polaire Français-Émile Victor (IPEV) and Programma Nazionale di Ricerche in Antartide (PNRA) (at Dome C) and the Alfred Wegener Institute for Polar and Marine Research (AWI) (at Dronning Maud Land). This is EPICA publication No. 158.

## REFERENCES

- Alley, R.B. 1992. Flow-law hypotheses for ice-sheet modeling. *J. Glaciol.*, **38**(129), 245–256.
- Arnaud, L., M. Gay, J.M. Barnola and P. Duval. 1998. Imaging of firn and bubbly ice in coaxial reflected light: a new technique for the characterization of these porous media. *J. Glaciol.*, **44**(147), 326–332.
- Azuma, N. and 6 others. 2000. Crystallographic analysis of the Dome Fuji ice core. In Hondoh, T., ed. *Physics of ice core records*. Sapporo, Hokkaido University Press, 45–61.
- Bons, P.D. 1999. Micro-shear zones in experimentally deformed octachloropropane. *J. Struct. Geol.*, **21**, 323–334.
- Duval, P. and M. Montagnat. 2002. Comment on 'Superplastic deformation of ice: experimental observations' by D.L. Goldsby and D.L. Kohlstedt. *J. Geophys. Res.*, **107**(B4), 2082. (10.1029/2001JB000946.)
- Eicken, H. 1993. Automated image analysis of ice thin sections – instrumentation, methods and extraction of stereological and textural parameters. *J. Glaciol.*, **39**(132), 341–352.
- EPICA community. 2004. Eight glacial cycles from an Antarctic ice core. *Nature*, **429**(6992), 623–628.
- Faria, S.H. and S. Kipfstuhl. 2004. Preferred slip-band orientations and bending observed in the Dome Concordia (East Antarctica) ice core. *Ann. Glaciol.*, **39**, 386–390.
- Fujii, Y. and 8 others. 1999. Tephra layers in the Dome Fuji (Antarctica) deep ice core. *Ann. Glaciol.*, **29**, 126–130.
- Goldsby, D.L. and D.L. Kohlstedt. 2001. Superplastic deformation of ice: experimental observations. *J. Geophys. Res.*, **106**(B6), 11,017–11,030.
- Goldsby, D.L. and D.L. Kohlstedt. 2002. Reply to comment by P. Duval and M. Montagnat on 'Superplastic deformation of ice: experimental observations'. *J. Geophys. Res.*, **107**(B11), 2313. (10.1029/2002JB001842.)
- Hobbs, B.E., W.D. Means and P.F. Williams. 1976. *An outline of structural geology*. New York, John Wiley and Sons.
- Hobbs, P.V. 1974. *Ice physics*. Oxford, Clarendon Press.
- Kipfstuhl, S., F. Pauer, W.F. Kuhs and H. Shoji. 2001. Air bubbles and clathrate hydrates in the transition zone of the NGRIP deep ice core. *Geophys. Res. Lett.*, **28**(4), 591–594.
- Koo, J.B., D.Y. Yoon and M.F. Henry. 2000. Island grains of low misorientation angles formed during abnormal grain growth in Cu. *Metall. Mater. Trans.*, **31A**(5), 1489–1491.
- Kuroiwa, D. and W.L. Hamilton. 1963. Studies of ice etching and dislocation etch pits. In Kingery, W.D., ed. *Ice and snow: properties, processes, and applications*. Cambridge, MA, MIT Press, 34–55.
- Lipenkov, V.Y. 2000. Air bubbles and air-hydrate crystals in the Vostok ice core. In Hondoh, T., ed. *Physics of ice core records*. Sapporo, Hokkaido University Press, 327–358.
- Montagnat, M. and P. Duval. 2000. Rate controlling processes in the creep of polar ice: influence of grain boundary migration associated with recrystallization. *Earth Planet. Sci. Lett.*, **183**(1–2), 179–186.
- Mullins, W.W. 1957. Theory of thermal grooving. *J. Appl. Phys.*, **28**(3), 333–339.
- Nakaya, U. 1958. Mechanical properties of single crystals of ice. Part 1. Geometry of deformation. *SIPRE Res. Rep.* 28.
- Nishida, K. and H. Narita. 1996. Three-dimensional observations of ice crystal characteristics in polar ice sheets. *J. Geophys. Res.*, **101**(D16), 21,311–21,317.
- North Greenland Ice Core Project (NorthGRIP) members. 2004. High-resolution record of Northern Hemisphere climate extending into the last interglacial period. *Nature*, **431**(7005), 147–151.
- Pauer, F., J. Kipfstuhl, W.F. Kuhs and H. Shoji. 1999. Air clathrate crystals from the GRIP deep ice core: a number-, size- and shape-distribution study. *J. Glaciol.*, **45**(149), 22–30.
- Perovich, D.K. and A. Hirai. 1988. Microcomputer-based image-processing system. *J. Glaciol.*, **34**(117), 249–252.
- Ryde, L., B. Hutchinson and T. Kumano. 2004. Grain boundaries with high misorientation and low mobility. *Mater. Sci. Forum*, **467–470**, 739–744.
- Svensson, A. and 6 others. 2003. Properties of ice crystals in NorthGRIP late- to middle-Holocene ice. *Ann. Glaciol.*, **37**, 113–122.
- Svensson, A. and 7 others. 2005. Visual stratigraphy of the North Greenland Ice Core Project (NorthGRIP) ice core during the last glacial period. *J. Geophys. Res.*, **110**(D2), D02108. (10.1029/2004JD005134.)
- Uchida, T., T. Hondoh, S. Mae, V.Y. Lipenkov and P. Duval. 1994. Air-hydrate crystals in deep ice-core samples from Vostok Station, Antarctica. *J. Glaciol.*, **40**(134), 79–86.
- Wang, Y. and N. Azuma. 1999. A new automatic ice-fabric analyzer which uses image-analysis techniques. *Ann. Glaciol.*, **29**, 155–162.
- Wang, Y., S. Kipfstuhl, N. Azuma, T. Thorsteinsson and H. Miller. 2003. Ice fabrics study in the upper 1500 m of the Dome C (East Antarctica) deep ice core. *Ann. Glaciol.*, **37**, 97–104.

- Wilén, L.A. 2000. A new technique for ice-fabric analysis. *J. Glaciol.*, **46**(152), 129–139.
- Wilson, C.J.L. 1986. Deformation induced recrystallization of ice: the application of in situ experiments. In Hobbs, B.E. and H.C. Heard, eds. *Mineral and rock deformation: laboratory studies – the Paterson Volume*. Washington, DC, American Geophysical Union, 213–232. (Geophysical Monograph 36.)
- Wilson, C.J.L., D.S. Russell-Head and H.M. Sim. 2003. The application of an automated fabric analyzer system to the textural evolution of folded ice layers in shear zones. *Ann. Glaciol.*, **37**, 7–17.
- Zhang, Y. and C.J.L. Wilson. 1997. Lattice rotation in polycrystalline aggregates and single crystals with one slip system: a numerical and experimental approach. *J. Struct. Geol.*, **19**(6), 875–885.

*MS received 2 November 2005 and accepted in revised form 15 June 2006*

# Appendix E

## Publication V - Is Antarctica like a birthday cake?

**Faria, S. H., Hamann, I., Kipfstuhl, S., Miller, H. (2006)**

Preprint No. 33/06 of the MPI für Mathematik in den Naturwissenschaften,  
Leipzig. [www.mis.mpg.de/preprints/2006/prepr2006\\_33.html](http://www.mis.mpg.de/preprints/2006/prepr2006_33.html)

# Is Antarctica like a birthday cake?

Sérgio H. Faria,<sup>1,2\*</sup> Ilka Hamann,<sup>1†</sup> Sepp Kipfstuhl,<sup>1</sup> Heinz Miller<sup>1</sup>

<sup>1</sup>Alfred Wegener Institute for Polar and Marine Research,  
Columbusstr., D-27515 Bremerhaven, Germany,

<sup>2</sup>Max Planck Institute for Mathematics in the Sciences,  
Inselstr. 22, D-04103 Leipzig, Germany

\*Corresponding author. E-mail: [faria@mis.mpg.de](mailto:faria@mis.mpg.de)

†Temporary address: Department of Mechanical Engineering, Nagaoka University  
of Technology, 16031 Kamitomioka, Nagaoka, 940-2188 Niigata, Japan

*One-sentence summary:* **In this report, submitted directly from the EPICA (European Project for Ice Coring in Antarctica) drilling camp in Dronning Maud Land (DML), Antarctica, we describe the microstructure of deep layers of soft ice in the EPICA–DML ice core.**

*Abstract:* **A peculiarity of the EPICA–DML drilling camp in Antarctica has been the establishment of a subterranean laboratory for ice microscopy on site. There we performed the first microscopic observations of soft ice strata in the EPICA–DML deep ice core. Contrary to common expectations, the softening is not produced by preferred orientations of the ice lattice (fabric), but rather by dynamic grain boundary structures formed by microshear under conditions of high temperature, moderate stress, small grain size and high impurity content. Evidently, the existence of layers of soft ice has serious implications for ice core dating and related paleoclimatic studies.**

Thanks to the modern globalization of culture (and sad as it may be), the contemporary idealization of a birthday cake is roughly the same throughout the world: a pile of sweet bread pieces separated by layers of soft (usually creamy) filling. The prospect that the stratigraphy of the Antarctic ice sheet could resemble the structure of such a birthday cake —namely, strata of soft ice sandwiched between layers of normal (harder) ice— has been the fear of many glaciologists and climate scientists. The reasons for such a worry are indeed justified: the overburden pressure of the ice sheet may squeeze soft ice faster than normal ice, invalidating standard models of ice dating based on the premise of monotonic layer thinning. Evidently, errors in ice core dating imply uncertainties in climatic records. Furthermore, soft ice strata may produce layers of enhanced deformation, which are particularly susceptible to flow instabilities that disrupt the temporal stratification of the ice core and consequently destroy its climatic records.

Despite several evidences for soft ice layers derived from tunnel and borehole closure/tilting rates in polar regions (1–4), the causes of such enhanced flows have been poorly investigated, remaining a matter of speculation. Certain is only the fact that all soft ice strata reported so far coincide with layers of high impurity content and small grain sizes. Presently, the most accepted explanation for the formation of soft strata in ice sheets is related to the preferred lattice orientations of the ice grains, often called fabric. According to this conjecture (4), a soft ice stratum should be characterized by an exceptionally strong fabric, produced by some unspecified effect of high impurity concentration and small grain sizes. The strong fabric so generated should be compatible with the stress acting on that layer, in the sense that ice with such a fabric would be softer (for that particular stress state) than isotropic ice.

Accidentally, we have had in the current season (Antarctic summer 2005/06) the opportunity to discover our own evidences for soft ice layers at the EPICA–DML drilling camp in Antarctica (5). An insufficient amount of densifier in the borehole fluid, used to counterbalance

the closing pressure on the hole walls, gave rise to a noticeable closure (diameter reduction by about five millimeters) in a deeper part of the hole, namely from 2385 m down to the final depth reached in the former drilling season (2565 m depth, Antarctic summer 2003/04). Unfortunately, no correlation between closure and tilt of the hole was possible, due to problems with the inclinometer. Most interesting is that the closure occurs quite abruptly with depth. This fact has attracted our attention to the existence of a remarkable softening effect in the deep ice.

In contrast to former investigations of soft ice layers, we did not have solely the fabric and stratigraphic (linescanner) data, but also a detailed microscopic mapping of the whole ice core, mostly prepared in our on-site laboratory (6). We started, however, with a standard fabric analysis. To our surprise, we found no noticeable difference between the fabrics in the soft stratum and in the surrounding ice (Fig. 1). However, as in other accounts of soft ice layers, we observed from stratigraphic and chemical data a precise correlation between borehole closure, high impurity content and small grain sizes (5, 7). The unchanged fabric lead us to conclude that the softening should not be associated to an enhancement of dislocation glide by impurities, since an increase in glide activity would certainly affect the fabric. In order to corroborate this hypothesis, we decided to analyze ice core photomicrographs made on site, with the hope of finding in subgrain boundaries and slip bands some hint about changes in the dislocation activity of ice. Nevertheless, no noticeable change in the structure of slip bands and subgrain boundaries was visible: dislocation glide seemed not strongly affected by impurities. Additionally, we found also no indication of intense deformation by diffusion (Nabarro–Herring/Cobble creep), which should be revealed by zones of clean ice near grain boundaries.

Notwithstanding, the micrographs revealed something unexpected. The upper image in Fig. 1 illustrates the usual grain boundary structure of polar ice from the EPICA–DML site (2185 m depth). Similar structures have been also observed in ice from Dome C (Antarctica), GRIP and NorthGRIP (Greenland) (6, 8, 9). There is no identifiable pattern in that sample,

just an irregular network of grain boundaries. In contrast, the lower images in Fig. 1 show the typical grain boundary structure within the EPICA–DML soft ice layer (2385 m and 2395 m depth): there is a conspicuous pattern of aligned grains, with most grain boundaries oriented in two preferred directions and having a strong tendency to produce long, unbroken chains nearly parallel to the local stratigraphy (see also Fig. 2). Such a “*slanted brick wall pattern*” is particularly evident in the depth range 2385–2405 m, although its presence can be continually identified in all ice core samples down to 2575 m depth.

As the current data on impurity content and borehole closure end at the depth reached in the former drilling season (2565 m depth, Antarctic summer 2003/04), we have no direct indication of the precise depth where the soft ice layer ceases. Nevertheless, from the grain size data and the persistence of the slanted brick wall pattern —both extracted from on-site microstructure mapping— we estimate that the soft ice layer at the EPICA–DML site should lie between 2385 m and  $2575 \pm 5$  m depth. If this depth range corresponds to a single soft ice layer, 190 m thick, or if it is composed of a series of thinner strata, is still not certain.

Now, what is the relation between the observed “slanted brick wall pattern” of the microstructure and the softening of ice evidenced by the closure of the EPICA–DML borehole? The answer can be found in a careful analysis of the high-resolution micrographs, which reveal a frequent arrangement of subgrain boundaries, as illustrated in Fig. 2: most subgrain boundaries tend to act as “bridges” connecting the detached parts of long chains of grain boundaries. Grains containing such subgrain boundaries appear to be “sheared off” by the grain boundary chains crossing them. This kind of microscopic deformation mechanism is known as *microstructural shear*, or simply *microshear* (10, 11). It has often been studied in laboratory experiments (where a corresponding pattern, called “tabular-grain structure”, is frequently generated), but its observation in naturally deformed rocks has been so far inhibited by extensive grain boundary migration and recrystallization. The reason why we are able to identify microshear in the polar

ice samples shown in Figs. 1 and 2 is an exceptional combination of high temperature (approx.  $> -15^{\circ}\text{C}$ , i.e.  $> 94\%$  of melting temperature) and moderate stresses—both occasionally found in the lower depths of ice sheets— with a high impurity content that hinders recrystallization and reduces the migration rate of grain boundaries (indeed, this is one reason why small grain sizes correlate so well with high impurity content in all polar ice core records).

The manner in which microshear produces and maintains the slanted brick wall pattern is explained in Fig. 2. It is clear that a certain amount of sliding along grain boundary chains is necessary to produce the microshear zones shown in Fig. 2. However, in contrast to those deformation mechanisms usually subsumed under the names “grain boundary sliding” and “superplasticity”, in which each grain slides past its neighbors, the sliding by microshear is chiefly restricted to zones containing long grain boundary chains (several grains in size) and such zones can make their way also through grains, when suitable. As the grain boundary network evolves by deformation and grain boundary migration, new microshear zones may come into existence, while older ones are deactivated. As a result, at any instant the dislocation creep by basal glide is enhanced by transient, localized zones of microshear.

Even though the eventual displacement within a single microshear zone usually corresponds only to a fraction of the average grain size (i.e. up to several hundreds of microns in the EPICA–DML soft ice layer), extensive strain can be accumulated in a relatively short period of time if a large number of active microshear zones is sustained. It should be emphasized, however, that microshear does not replace the standard deformation mechanism in polar ice by dislocation glide. Rather, both processes must be complementary. More precisely, the natural deformation of normal (“clean”) polar ice should indeed be entirely caused by dislocation glide, whereas certain deep layers of “warm” polar ice with high impurity content (like the one reported here) may deform in situ by a *combination* of dislocation glide *and* microshear. This combination renders the material softer than clean ice with the same fabric and deformed under the same

conditions.

How and which impurities may affect the viscosity of the grain boundaries of polar ice (as well as the diffusive mass transfer needed to accommodate sliding along trijunctions and small grain boundary irregularities) remains a matter of future study, as the chemical properties of the EPICA–DML ice core are still under investigation (5, 7). Certain is that temperature should play a decisive role in the activation of microshear in ice, seeing that its competing mechanisms of promotion (grain boundary sliding, self-diffusion, subgrain formation) and inhibition (recrystallization, recovery, grain growth) are all thermally activated.

The discovery of cloudy ice layers softened by microshear in deep Antarctic ice has serious consequences not only to ice core dating and paleoclimate records, as already discussed, but also for rock mechanics and geology. Indeed, to the knowledge of the present authors this is the first observation of microshear in naturally deformed rocks, a deformation mechanism proposed since many years to be active in tectonites, but never observed in situ because of its concealing by recrystallization effects. Therefore, the current results prove that polar ice can serve very well as a geophysical model material.

A fundamental question which remains open is if the flow enhancement by microshear could be intense enough to generate *extrusion* of the soft ice stratum (somewhat like the extrusion of the soft filling of a birthday cake, when you warm it up) or even the mixing of distinct age layers. In principle, the microstructure of the soft ice layer is indeed compatible with extrusion flow, even though no pronounced change in the fabrics is visible. Nevertheless, a tangible corroboration of the extrusion conjecture would require the knowledge of the relation between shearing orientation and ice flow direction with depth. The problem is that such an information seems impossible to be obtained for the time being, as the relative orientation of the ice core—achieved by fitting its pieces, since the fabrics in that depth range have rotational symmetry with respect to the core axis (cf. Fig. 1)—has repeatedly been lost. This last issue obviates

the need for drilling devices that can track the orientation of the ice core. As long as such an equipment is not available, we may be losing essential information about the ice sheet dynamics of Antarctica and Greenland.

## References and Notes

1. G. K. Swinzow, *J. Glaciol.* **4**, 215 (1962).
2. N. S. Gundestrup, B. L. Hansen, *J. Glaciol.* **30**, 282 (1984).
3. D. M. Etheridge, *Ann. Glaciol.* **12**, 46 (1989).
4. W. S. B. Paterson, *The Physics of Glaciers* (Pergamon, Oxford, 1994), third edn.
5. F. Wilhelms, *et al.*, *in preparation* (empty).
6. S. Kipfstuhl, *et al.*, *Submitted to J. Glaciol.* .
7. EPICA community members, *in preparation* (empty).
8. S. H. Faria, S. Kipfstuhl, *Ann. Glaciol.* **39**, 386 (2004).
9. I. Hamann, *et al.*, *in preparation* (empty).
10. M. R. Drury, F. J. Humphreys, *J. Struct. Geol.* **10**, 83 (1988).
11. P. D. Bons, M. W. Jessel, *J. Struct. Geol.* **21**, 323 (1999).
12. This work is a contribution to the European Project for Ice Coring in Antarctica (EPICA), a joint European Science Foundation/European Commission scientific program, funded by the EU and by national contributions from Belgium, Denmark, France, Germany, Italy, the Netherlands, Norway, Sweden, Switzerland and the United Kingdom. This is EPICA publication no. XX.

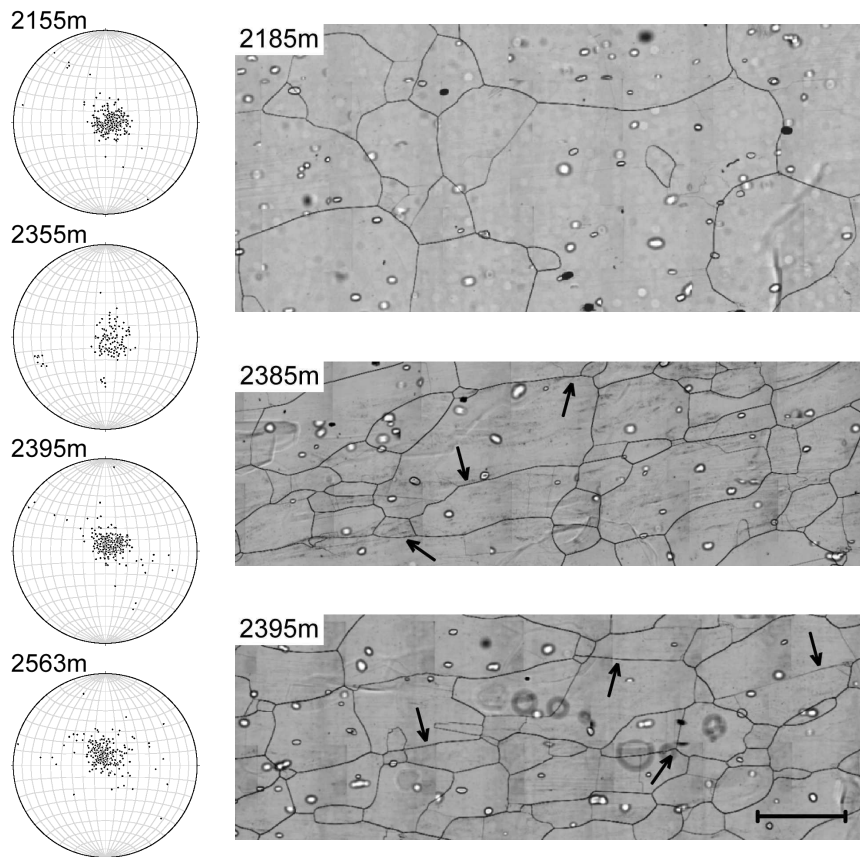


Figure 1: Microstructure of the EPICA–DML soft ice layer and its surroundings. **(Left)**: Equal area fabric diagrams of four distinct borehole depths. There is no noticeable difference between the distributions of lattice orientations outside (2155 m and 2355 m depth) and inside (2395 m and 2563 m depth) the soft ice layer. **(Right)**: Microstructure mapping micrographs of normal (“clean”) polar ice (2185 m depth) and of ice from the soft layer (2385 m and 2395 m depth). Thick and thin lines denote grain and subgrain boundaries, respectively, bright and dark spots correspond to air hydrates, while the grey circles in the lowest picture are just bubbles in the silicone oil film that protects the ice surface. No peculiar pattern can be found in the grain boundary structure of normal polar ice (2185 m depth), whereas the lowest two pictures (2385 m and 2395 m depth) clearly show the slanted brick wall pattern and the long chains of grain boundaries (marked by arrows) characteristic of the soft ice stratum. All micrographs have the same magnification, the scale bar in the lowest picture has 2 mm.

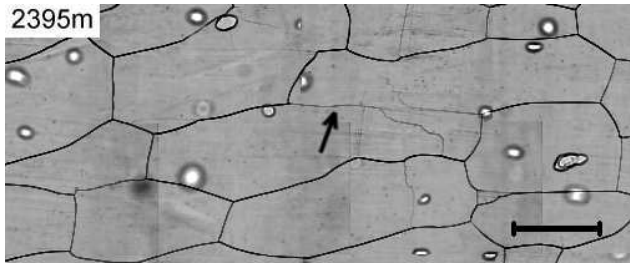
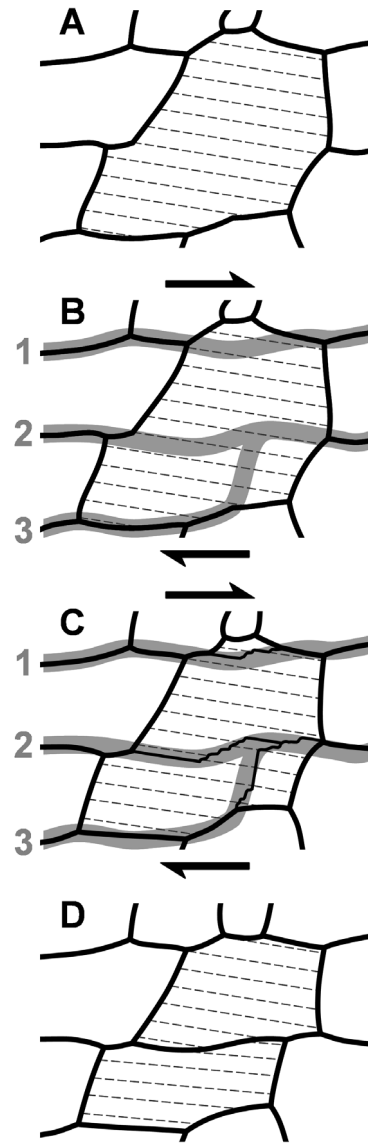


Figure 2: Relation between microshear and the “slanted brick wall pattern”. **(Left)**: Typical layered structure of grains in the soft ice stratum of the EPICA–DML ice core. The basic features of the micrograph follow the description given in Fig. 1; the scale bar stands here for 1 mm. Many grains are S-shaped, with most boundaries oriented nearly parallel or orthogonal to the local stratigraphy. Long chains of grain boundaries following the local stratigraphy are also quite common, being frequently connected by subgrain boundary “bridges” (as indicated by the arrow). **(Right)**: Pattern formation via microshear. Suppose that a certain grain (A) is corrupting the layered structure of the slanted brick wall pattern. Natural deformation of the ice sheet produces microshear zones along grain boundary chains (B), following the local stratigraphy. Such microshear zones can cross an obstructing grain in several ways, e.g. by cutting off its edges and protrusions (1), or by dividing it in two parcels (2), else by branching towards more active grain boundary chains (3). In any case, subgrain boundaries are formed (C). It should be remarked that dislocation activity within the grain is essential for subgrain formation. Finally, cut fragments are slowly consumed by grain boundary migration and the slanted brick wall pattern of the grain boundary network is improved (D). Evidently, such a layered structure promotes a positive feedback for further microshear.



## Appendix F

### Publication VI - Implications for and findings from deep ice core drillings - An example: the ultimate tensile strength of ice at high strain rates

Wilhelms, F., Sheldon, S. G., Hamann, I., Kipfstuhl, S. (2007)

Physics and Chemistry of Ice (The proceedings of the International Conference on the Physics and Chemistry of Ice held at Bremerhaven, Germany on July 23<sup>rd</sup>-28<sup>th</sup> 2006) The Royal Society of Chemistry Special Publication No. 311, pp. 635-639.

# IMPLICATIONS FOR AND FINDINGS FROM DEEP ICE CORE DRILLINGS — AN EXAMPLE: THE ULTIMATE TENSILE STRENGTH OF ICE AT HIGH STRAIN RATES

Frank Wilhelms<sup>1</sup>, Simon G. Sheldon<sup>2</sup>, Ilka Hamann<sup>1</sup> and Sepp Kipfstuhl<sup>1</sup>

<sup>1</sup>Alfred-Wegener-Institute for polar and marine research, Columbusstraße, D-27568 Bremerhaven, Germany, E-mail: fwilhelm@awi-bremerhaven.de

<sup>2</sup>Ice & Climate Group, Department of Geophysics, Niels Bohr Institute, Juliane Maries Vej 30, DK-2100 Copenhagen Ø, Denmark

## 1 INTRODUCTION

At present, several deep ice core drilling operations have just been finished and new ventures are in the planning phase. In this paper we discuss ice properties related data attained when drilling the Dronning Maud Land (DML) deep ice core<sup>1</sup> in the framework of the European Project for Ice Coring in Antarctica (EPICA). The drill site is located<sup>2</sup> in East Antarctica at 75° S, close to the Greenwich meridian. The pull force rating of the winch to break the core at the end of a drill run is one of the key design parameter for ice coring winches. Amongst drilling personnel it is common knowledge that core breaks are getting harder in warm ice. However this has never been quantified, but is consistent with the experience based on safety tests for ice-screws. The engineers of the German Alpine Club's security-council quote the warm ice (just below the melting point) to be tougher and attribute this to its "more plastic behaviour"<sup>3</sup>. When designing heating for railway switches, engineers want to estimate under which conditions the frozen blade can be ripped from the track. The literature on tensile strength of ice suggests a decrease with increasing temperature for low strain rates<sup>4,5</sup> (in the order of  $10^{-6}$  ...  $10^{-5}$  s<sup>-1</sup>), however the latest review of all compiled data suggests that for low strain rates the tensile strength of ice is independent from temperature<sup>6</sup>, but for high strain rates this might be completely different as crack healing acts or cracks become blunt<sup>7</sup>. The core breaks presented here represent much higher strain rates and should be well in a crack-nucleation regime<sup>8</sup>. On the other hand we frequently observed refrozen water on the drill head, when drilling at temperatures above -10 °C. Liquid water at the cutters could either act as lubricant or even heal micro-cracks that were initiated by the cutting process. Both processes would lead to a reduction of the number of initial micro-cracks and thus strengthen the ice core. The remarkably smooth ice core surfaces we observed towards the bedrock at higher temperatures also suggest the presence of liquid water during the cutting process.

## 2 ICE CORE DRILLING PROCEDURE

### 2.1 Experimental setup

Deep ice cores are drilled by cutting a ring into the glacier. The inner remaining cylinder moves into a tube, the so called core barrel. After a certain depth increment, depending on the used drill system between about 0.8 m to more than 4 m, the cylindrical ice core is broken off from the bore-hole's bottom and hoisted to the surface. The drill system's layout is described elsewhere<sup>9,10</sup>. Figure 1 gives an overview about the drill system. During the breaking and hoisting process the core is held by the three core catchers (Figure 1a) and the force is applied by pulling with a winch (Figure 1b). Even though the core catchers are designed to introduce fracture into the core, they quite often abrade the core's surface and the abrasion wedges the core into the core barrel. Thus, the pulling force is in most core breaks applied to the core's entire cross section. The applied pulling force is measured with a strain gauge, calibrated in kilogramme (force), which is situated in the drill towers top pulley. When breaking the core, one spools in the cable with a speed of a few cm/s. The maximum tension is recorded automatically and is noted as "core break", as well as the final plumbing depth, for each respective drill run.

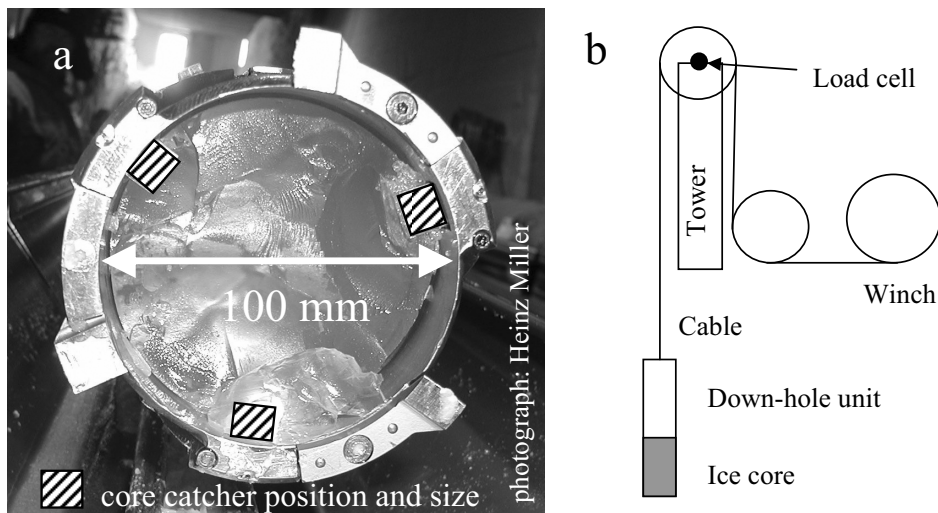


**Figure 1** *The experimental setup; a: Drill head with cutters and hatched core catcher area; b: The core catchers hold the core when pulling with the winch and recording the break force with the load cell.*

### 2.2 Core-break data treatment

From the recorded force data the cable and the drill's weight in the drilling liquid are subtracted and the data are converted into true force readings. The confinement pressure does not contribute to the net force, as the drill is permeable to fluid and thus the fluid can be easily displaced around the ice core. For each core break the cable depth plumbing is also recorded, so that one has a core break versus depth data set. In total there are about 1500 core breaks, so that on average there are about 40 core breaks in a depth interval of 50 m, which is used to average the data for further investigation. The core break errors are

the quadratic sum of 6 % systematic error from load cell calibration and the standard error of the mean of each depth interval.

### 2.3 Temperature and pressure logging of the hole

The bore-hole was logged several times with a logging tool, thus measuring temperature, pressure and the geometry of the bore-hole. The tool is described elsewhere<sup>11</sup>, relevant for the discussion here is the temperature measurement with an absolute precision of better than 50 mK. The pressure in the hole deviates by less than 500 kPa from the ice pressure over the whole range and can be calculated roughly from the given drilling depth by multiplying with the average drill liquid/ice density of  $0.92 \text{ Mgm}^{-3}$  and the acceleration of gravity of  $9.8 \text{ ms}^{-2}$ . It thus increases linear from about 0.1 MPa (atmospheric pressure) at the top of the hole to about 25 MPa at the bottom of the hole in 2774 m depth.

## 3 THE TEMPERATURE DEPENDENCE OF ICE'S ULTIMATE TENSILE STRESS

### 3.1 Ultimate tensile stress calculated from break strength

Figure 2 presents the dependence of break strength versus temperature for raw (grey dots) and averaged (error bars) data. As the ultimate tensile stress, or also called fracture stress, is the average force per area to break the sample, the fracture stress is strictly proportional to the break strength with the factor of inverse cores cross section  $1/(\pi (0.049 \text{ m})^2)$ . The right axis of the Figure is thus the fracture stress to break off the core. The top axis of the Figure presents the coincident depth and pressure for the respective ordinate temperature.

### 3.2 Comparison with published data and consistency check

As we present an increase of tensile fracture strength at high strain rates for the first time, we can not compare them directly to previously published data. But we can compare certain aspects of our data with the literature and thus check for consistency.

*3.2.1 Tensile fracture stress reading at a certain temperature.* For polycrystalline ice with a grain size of 10 mm one finds a fracture stress of about 800 kPa at  $-10 \text{ }^\circ\text{C}$  reported in the literature<sup>8</sup> for high strain rates. This finding is consistent with the observed fracture stress in this study of about 700 kPa at 263 K.

*3.2.2 Variation with crystal size.* The dependence of fracture stress on crystal size is well established in the literature<sup>8</sup>, thus one could argue that the observed temperature dependence is truly a change in crystal size? This kind of artefact can be excluded, as the fracture stress decreases with increasing grain size<sup>8</sup>. In deep ice cores in general and, also observed in the core from DML here, the grain size increases with depth and as temperature also increases with depth, one should expect a decrease of fracture stress with increasing temperature. The contrary is the case and the increase in fracture stress with temperature might even be stronger than observed here.

*3.2.3 Variation with crystal orientation fabrics.* One could also argue that the observed increase is an artefact due to a change in the fabric's crystal orientation of the ice core. For the DML core discussed here the fabric changes from a random orientation steadily to a girdle type fabric at a depth of about 1000 m and then quite suddenly within an interval of about 20 m around 2040 m to a single maximum type fabric, where it remains further down. Thus, in the interval of dramatic change, the fabric does not change

and has changed before without a significant change in fracture strength. Thus the textural and fabric changes that occur in an ice core can be excluded to be the source of our observed increase of fracture stress with depth.

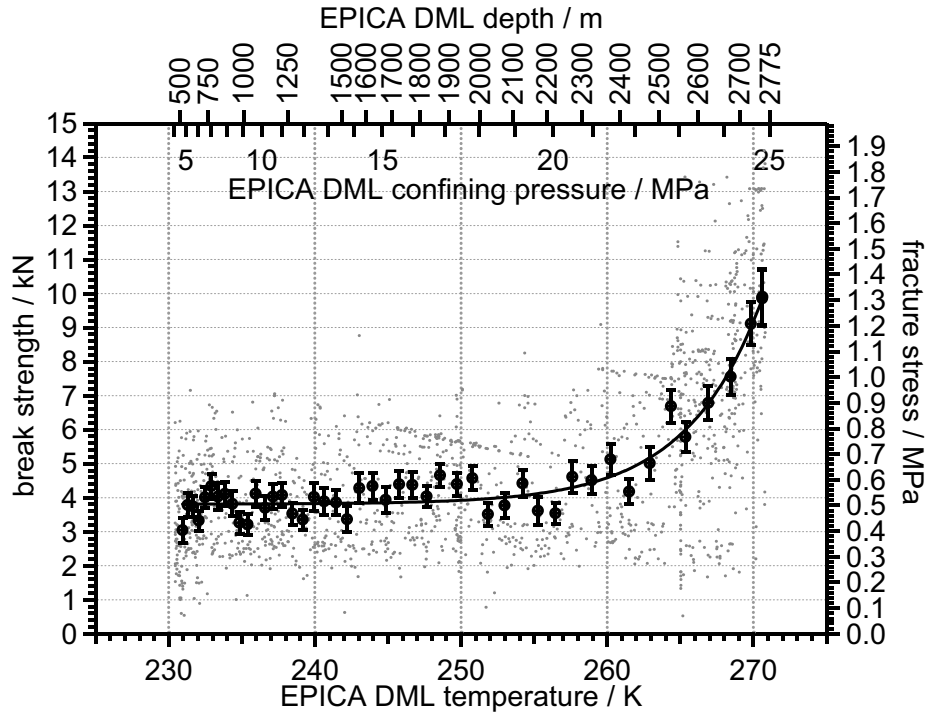


**Figure 2** *The fracture stress of polar ice under high strain rates; from the raw breaking strength (dots), averaged values with error bars (6% systematic error and standard error of the mean) have been calculated in 50 m intervals. By division with the cross section one yields the fracture stress of ice. The solid line is a least squares curve fit to the data.*

### 3.3 An empirical fit in the temperature range above 230 Kelvin

A more succinct description is given by an empirical curve to the averaged data. Fitting an exponential function by minimizing the  $\chi^2$ , yields a best fit for: (fracture stress)/kPa = 505 + 1.4E-20\*exp((absolute temperature)/5.17 K).

## 4 CONCLUSION

We report an effect quantitatively that seems to be well known in practical engineering, but is to our knowledge not yet described in the scientific literature. Astonishing is that the ordinate found in section 3.3 is the same as the ordinate in the theory to describe (fracture stress)/kPa = 510 + 30 (m/grain size)<sup>1/2</sup> in terms for crack nucleation<sup>8</sup>. This is consistent with the observation in the cited work, as at high strain rates the fracture stress is crack nucleation controlled. In the cited work Schulson explains the discrepancies to the

theoretical value for the grain size dependent factor with a thermally activated mechanism that relaxes the stress concentrated at the grain boundaries. A quasi liquid layer at the grain boundaries could help to relax piled dislocations. Liquid water in the bore hole could reduce the number of introduced cracks at the ice core surface or even heal cracks. At present, there seems to be no theory available to describe the fracture stress adequately. Thus our empirical fit will provide needed information to engineering branches, as e.g. railway engineers who required data on ultimate tensile stress of ice from us to estimate under which conditions frozen railway switches would simply break the ice freezing the blade to the track. These data will serve until systematic tests under laboratory conditions are available. If liquid water plays a significant role in the bore hole, the machining procedure of samples for stress tests should be addressed carefully. Machining at high temperatures to minimise the number of induced cracks at the sample surface should be considered.

### Acknowledgements

We thank Paul Duval for his fruitful questions and comments during the review process. This work is a contribution to the European Project for Ice Coring in Antarctica (EPICA), a joint European Science Foundation/European Commission scientific programme, funded by the EU and by national contributions from Belgium, Denmark, France, Germany, Italy, the Netherlands, Norway, Sweden, Switzerland and the United Kingdom. The main logistic support was provided by IPEV and PNRA (at Dome C) and AWI (at Dronning Maud Land). This is EPICA publication no. 163 and AWI publication awi-n16131.

### References

- 1 EPICA community members *One-to-one interhemispheric coupling of polar climate variability during the last glacial, accepted by Nature*, doi:10.1038/nature05301.
- 2 C. Drücker, F. Wilhelms, H. Oerter, A. Frenzel, H. Gernandt and H. Miller, *Mem. Natl Inst. Polar Res., Spec. Issue*, 2002, **56**, 302–312.
- 3 C. Semmel and D. Stopper, *DAV Panorama, ISSN 1437–5923*, 2005, **2**, 91–95.
- 4 T. R. Butkovich, *SIPRE Res. Rep.*, 1954, **11**, 12. (reproduced in P. V. Hobbs, Clarendon Press, Cambridge, 1974, 333.)
- 5 E. M. Schulson, P. N. Lim and R. W. Lee, *Philos. Mag. A*, 1984, **49**, 353–363.
- 6 E. M. Schulson, personal communication, 2006.
- 7 E. M. Schulson, S. G. Hoxie and W. A. Nixon, *Philos. Mag. A*, 1989, **59**, 303–311.
- 8 E. M. Schulson, *Journal de Physique, Colloque C1, supplément au n° 3*, **48**, 1987, C1-207–C1-220.
- 9 S. J. Johnsen, N. S. Gundestrup, S. B. Hansen, J. Schwander and H. Rufli, *Mem. Natl Inst. Polar Res., Spec. Issue*, 1994, **49**, 9–23.
- 10 L. Augustin and A. Antonelli, *Mem. Natl Inst. Polar Res., Spec. Issue*, 2002, **56**, 226–244.
- 11 N. S. Gundestrup, H. B. Clausen and L. B. Hansen, *Mem. Natl Inst. Polar Res., Spec. Issue*, 1994, **49**, 224–233.

# Appendix G

## Publication VII - Direct Evidence for Radar Reflector originating from Changes in Crystal-Orientation Fabric

Eisen, O., Hamann, I., Kipfstuhl, S., Steinhage, D., Wilhelms, F.  
(2007)

The Cryosphere, 1, pp. 1-10.

## Direct evidence for continuous radar reflector originating from changes in crystal-orientation fabric

O. Eisen, I. Hamann, S. Kipfstuhl, D. Steinhage, and F. Wilhelms

Alfred-Wegener-Institut für Polar- und Meeresforschung, Bremerhaven, Germany

Received: 23 May 2007 – Published in The Cryosphere Discuss.: 15 June 2007

Revised: 5 September 2007 – Accepted: 1 October 2007 – Published: 19 October 2007

**Abstract.** The origin of a strong continuous radar reflector observed with airborne radio-echo sounding (RES) at the EPICA deep-drilling site in Dronning Maud Land, Antarctica, is identified as a transition in crystal fabric orientation from a vertical girdle to an increased single-pole orientation seen along the ice core. The reflector is observed with a 60 ns and 600 ns long pulse at a frequency of 150 MHz, spans one pulse length, is continuous over 5 km, and occurs at a depth of about 2025–2045 m at the drill site. Changes in conductivity as reflector origin are excluded by investigating the ice-core profile, synthetic RES data, and a RES profile with different electromagnetic polarisation azimuths. The reflector's magnitude shows maximum values for polarisation parallel to the nearby ice divide and disappears for polarisation perpendicular to it, identifying the orientation of the girdle to lie in the vertical plane parallel to the ice divide. Observations allow us to extrapolate the crystal orientation feature along the reflector in space, with implications for ice-sheet dynamics and modeling.

tions depends on the degree of anisotropy within. The current demand for advanced modeling of ice sheets requires the incorporation of anisotropic properties of ice and the spatial distribution of these properties for unraveling ice sheet history and predicting the future development (ISMSS Committee, 2004). Various ways have been developed to treat anisotropic rheology, as, for instance, summarised by Marshall (2005). The correlation between fabric changes and climate transitions (e.g. Durand et al., 2007), moreover, emphasizes that valuable information is carried by vertical and lateral fabric distributions. However, information about the distribution of crystals within the ice, the crystal orientation fabric (COF), is mainly available from ice coring, and restricted, therefore, to point locations. No standard procedure exists to date to determine the spatial variation of COF within ice sheets on a routine basis. This is, however, a key to an improved understanding and modeling of ice-sheet behaviour. Here, we present direct evidence that radio-echo sounding (RES) provides a formidable tool to map strong fabric changes occurring over a few 10s of meters in the vertical, and, moreover, carries the potential to map the lateral distribution of COF continuously.

### 1 Introduction

Natural ice found in ice sheets and glaciers shows anisotropic behaviour in various physical parameters (Petrenko and Whitworth, 1999). A body of ice with anisotropic orientation of crystals responds differently to applied stresses compared with isotropic ice, for which ice crystals have a random orientation. For anisotropic ice, ice flow could be enhanced by about an order of magnitude if stresses act parallel to the crystals' basal planes, but flow could be reduced by an order of magnitude if stresses act perpendicular to the basal planes (Paterson, 1994). Consequently, the general flow of ice and the response of ice sheets to changing environmental condi-

Since the beginning of operational applications of RES in glaciological research three processes were suggested to cause continuous internal reflections from within the ice column (Bogorodsky et al., 1985; Dowdeswell and Evans, 2004): changes in density (Robin et al., 1969), conductivity (Paren and Robin, 1975), and changes in COF (Harrison, 1973). Whereas the isochronous property of reflection horizons originating from changes in density and conductivity is nowadays routinely exploited for a multitude of purposes, the detection and interpretation of reflections stemming from changes in the COF is still in the early stages. Partial reflection of a propagating radar pulse occurs where either the real ( $\epsilon'$ ) or imaginary part ( $\epsilon''$ ) of the complex dielectric constant ( $\epsilon$ ) changes. The possibility to detect fabric changes with RES arises from the anisotropy of permittivity

Correspondence to: O. Eisen  
(olaf.eisen@awi.de)

Published by Copernicus Publications on behalf of the European Geosciences Union.

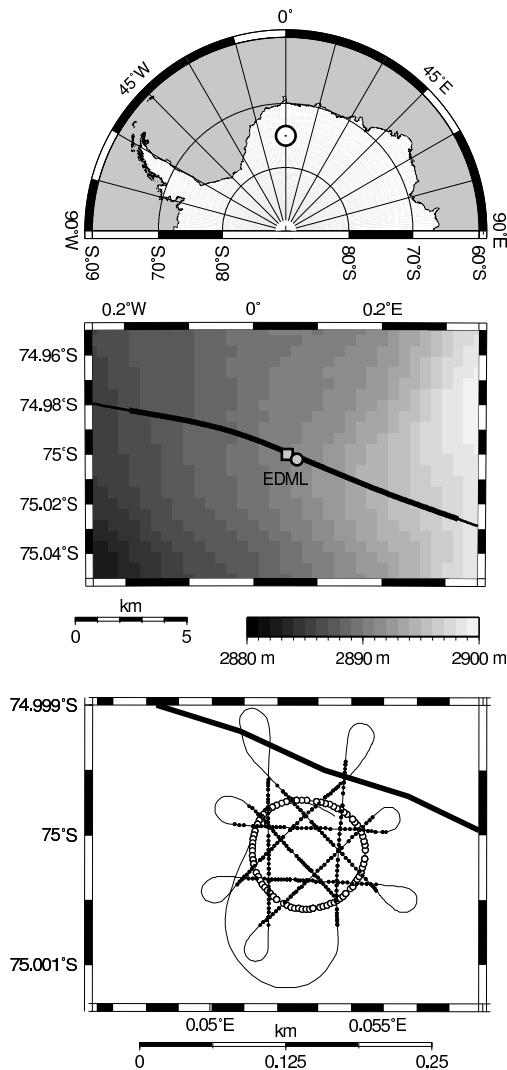


**Fig. 1.** Top: location of study area in Antarctica. Middle: location of EDML drill site (circle), RES flight line of profiles 022150/023150 (black line), and ground-based profile 033042 (square); bold black line: RES section shown in Fig. 2; grayscale: Radarsat Antarctic Mapping Project digital elevation model (Liu et al., 2001) on  $400 \times 400 \text{ m}^2$  raster (meter above sea level for WGS84 ellipsoid). Bottom: close-up of profile 033042 recorded with airplane on ground (thin line) and flight line of profiles 022150/023150 (thick line). Traces of the circle segment of profile 033042 are indicated by open circles, traces belonging to linear segments are shown as black dots.

in a pure ice crystal. The latest compilation of dielectric properties of ice (Fujita et al., 2000) provides an anisotropy in  $\epsilon'$  of  $\Delta\epsilon' = \epsilon'_{\parallel} - \epsilon'_{\perp} \approx 0.035$ , measured parallel and perpen-

dicular to the crystal c-axis at 1 MHz and 252 K. This value corresponds to little more than roughly 1% of the permittivity of ice, which is in the range of 3.1–3.2.  $\Delta\epsilon'$  is accurate to  $\sim 0.007$ , or 20% (Fujita et al., 2000, Fig. 3), and varies slightly with temperature and frequency, however insignificantly to be a concern in this study.

To discriminate reflections originating from changes in COF and conductivity, multi-frequency experiments can be utilized (Fujita et al., 1999). However, as ice is also a birefringent medium at radio frequencies (Hargreaves, 1978), multi-polarisation measurements are required to resolve ambiguities arising from anisotropic reflection and wave propagation (Doake et al., 2002; Fujita et al., 2003). With such experiments, Matsuoka et al. (2003) located high-scattering zones several hundred meters thick at depths around 1000–1500 m in East Antarctica. Based on the dependence of the reflection strength on the polarisation plane, the wide zones were interpreted as alternations in COF of adjacent ice layers (Matsuoka et al., 2004), induced by past and present ice flow. Fujita et al. (2006) determined the vertical evolution of the radar phase by combining ice-core profiles of COF with a matrix-model of radar-wave propagation at the sites where polarimetric radar studies were carried out. By comparison of COF data and model results with multi-polarisation/bi-frequency RES point data, they were able to separate the general contribution of anisotropic reflection from COF and birefringence to the observed signals. However, previous studies did not provide COF profiles from ice cores for direct comparison with continuous internal reflections in RES data and reflectivity.

In this work we extend previous findings by comparing RES data with ice-core profiles of COF, permittivity, and conductivity. Moreover, we use synthetic RES data to analyse the origin of RES signals. This leads to the novel observation that a sharp, continuous internal reflection horizon, trackable over several kilometers, is caused by an abrupt transition in crystal orientation fabric occurring over just a few tens of meters. Our deduction from these comparisons is supported by the analysis of the azimuth-dependence of reflection magnitude of the reflector of interest.

## 2 Data and methods

Data used in the present study were acquired within the European Project for Ice Coring in Antarctica (EPICA) at the deep drill site in Dronning Maud Land, Antarctica (EDML). The drill site is located at  $0.0684^\circ \text{ E}$ ,  $75.0025^\circ \text{ S}$  at 2891.7 m above sea level near a transient ice divide, characterised by along-flow compression and lateral extension, causing an overall vertical compression of the ice column (Wesche et al., 2007).

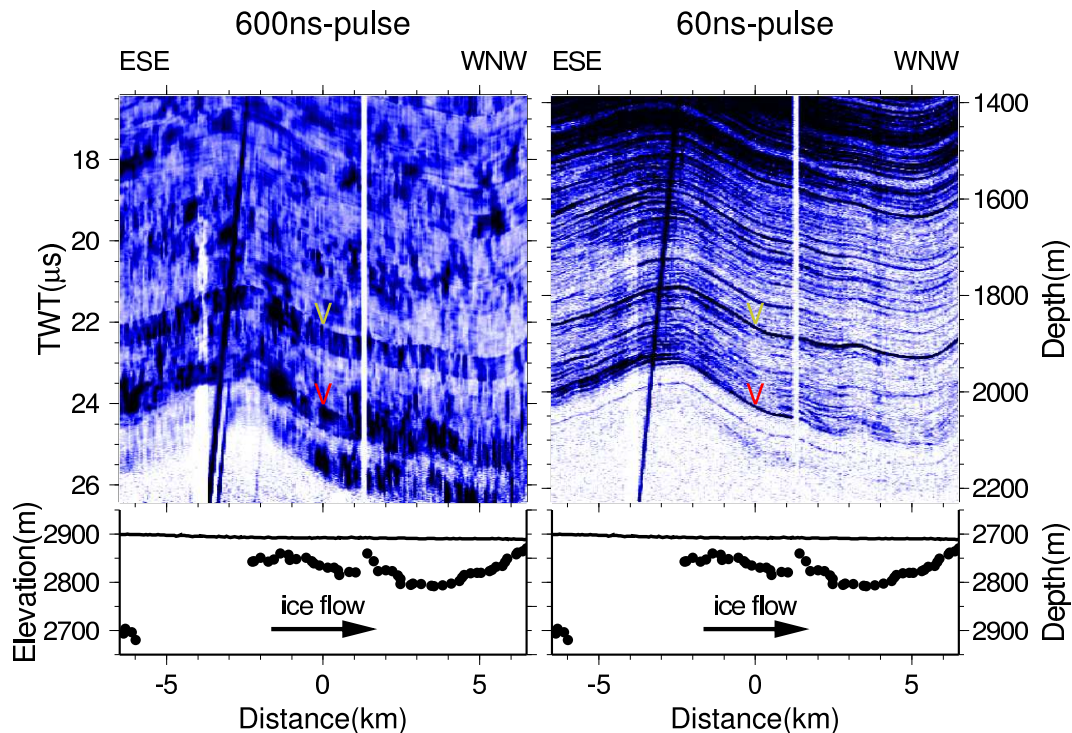


**Fig. 2.** Top: unfiltered 10-fold stack (65-m trace spacing) RES profile recorded with the 600-ns pulse (022150, left) and 60-ns pulse (023150, right); ordinates are the same for both panels: two-way travel time (TWT) on left ordinate is recording time corrected to the first break of surface reflection, right ordinate refers to depth below the surface for a mean wave speed of  $168.7 \text{ m } \mu\text{s}^{-1}$  from the surface to a 2100-m depth; color code indicates signal magnitude (increasing white-blue-black); first breaks of internal reflectors of interest are marked by yellow and red “V” at 0 km (drill site) at travel times of 22 and 24  $\mu\text{s}$ , respectively; dark diagonal line between  $-3.8$  and  $-2.3$  km is a hyperbola leg, caused by reflections from Kohlen station (located at 0 km); white vertical line at 1.3 km is caused by system dropout. Bottom: surface elevation above mean sea level (solid line, left axis) from airplane radar altimeter and depth of detected bedrock reflection below surface (black dots, right axes). The profile runs approximately parallel to a transient ice divide (ESE–WNW), arrow indicates ice flow from left to right.

## 2.1 Radio-echo sounding (RES)

We use data from the RES system on board the Dornier 228-101 aircraft Polar2, operated by the Alfred Wegener Institute (AWI). The system, with an overall sensitivity of 190 dB, generates 150-MHz bursts of 60 ns and 600 ns in duration, which are transmitted alternately. The receiver module rectifies and logarithmically compresses the signals, stacks 200 consecutive signals after analog-to-digital conversion, and stores the stack as a single trace on tape at sample intervals of 13.33 ns over a time window of 50  $\mu\text{s}$ . Data are normally acquired in-flight at an altitude of 450 m above ground at typical speeds of  $65 \text{ m s}^{-1}$  (130 knots), resulting in a trace spacing of the 200-fold stack of 6.5 m between equal pulses (Nixdorf et al., 1999). The airplane heading is equal to the polarisation of the electric field. Apart from static correction for

the first break of the surface reflection, no additional filtering or gain control is applied to the RES data used here. Conversion from recorded travel time to depth domain is performed with the calibration for pure-ice permittivity derived by Eisen et al. (2006), with a mean wave speed of  $168.7 \text{ m } \mu\text{s}^{-1}$  over the distance from the surface to 2100-m depth.

We use two types of RES data sets here (Fig. 1): (i) airborne data from the season 2002/03, with profiles 022150 (600 ns pulse) and 023150 (60 ns pulse) running along the ice divide (ESE–WNW direction), passing the EDML drill site about 100 m to the NNE (Fig. 2); (ii) data from profile 033042 (60 ns pulse) recorded in season 2003/04 with the airplane slowly moving on the ground about 500 m downstream from the drill site, first in a circle and then crossing the circle in linear segments in eight different orientations (N, NE, E, SE, S, SW, W, NW). The airborne data enable

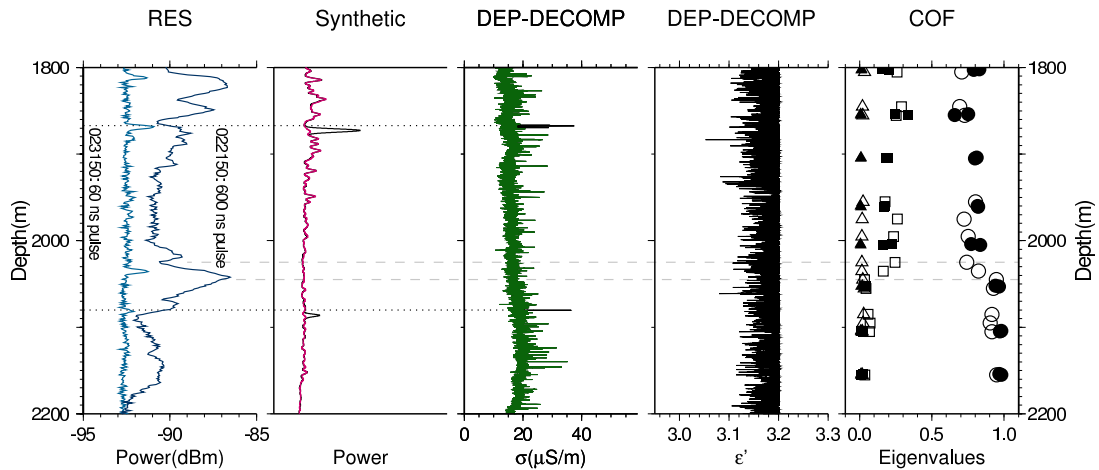


**Fig. 3.** Comparison of radar data and ice-core profiles at the EPICA-DML drill site. From left to right: RES signal power measured with two pulse widths for trace 4205 of profiles 022150 (600 ns pulse) and 023150 (60 ns pulse) with respect to 1 mW (dBm), representing a stack of 2000 recordings in total (200 pre-storage and 10 post-storage stacks) over a distance of 65 m; DEP-based synthetic RES trace for 60-ns pulse; DECOMP-corrected DEP conductivity ( $\sigma$ ); DECOMP-corrected DEP-permittivity ( $\epsilon'$ , with the permittivity of pure ice as upper bound); eigenvalues ( $\lambda_1$ : triangle,  $\lambda_2$ : square,  $\lambda_3$ : circle) of crystal orientation tensor along horizontal (filled symbols) and vertical core samples (open symbols). The black synthetic trace is based on original conductivity data (black  $\sigma$ -curve); on top the red synthetic trace is plotted, based on the DEP data with conductivity peaks removed (green  $\sigma$ -curve); peaks originating from conductivity thus appear black, emphasized by dotted horizontal lines; dashed horizontal lines connect the depth of the strong RES reflector with transition depth of changes in COF.

us to investigate the lateral extension of continuous internal reflections. For their subsequent analysis, we additionally stack 10 traces of each pulse width (resulting in a 65-m trace spacing in Fig. 2). The traces closest to the drill site are used later for comparison with ice-core data. They are referred to as the long and short pulse RES traces, respectively (Fig. 3). The ground-based data of profile 033042 provide insights into the dependence of reflected energy on polarisation azimuth. Along each of the eight linear segments of constant heading, we stack 70 consecutive traces to increase the signal-to-noise ratio. The data from the circle segment are used unstacked.

## 2.2 Ice-core permittivity and conductivity profiles

Dielectric profiling (DEP) at 250 kHz and  $\gamma$ -attenuation profiling, simultaneously carried out in the field after core retrieval, provide dielectric properties and density along the EDML ice core (see Eisen et al., 2006, for details). The calibrated DEP record is corrected for variations in core diameter and temperature. Unreliable data in the vicinity of the core breaks are removed. Effects of density and conductivity mixed complex-valued permittivity in the two-phase system ice–air are taken into account by applying an extended volumetric mixing model (DECOMP). Thus, contributions from density and conductivity in the complex permittivity are separated (Wilhelms, 2005).

## 2.3 Finite-difference forward modeling

The synthetic trace, adapted from Eisen et al. (2006), simulates the 60-ns pulse (Fig. 3). It is calculated by a one-dimensional finite-difference time-domain model of Maxwell's curl equations. Ice-core profiles of permittivity and conductivity serve as model input, separated using an inverse application of DECOMP at 250 kHz, conductivity linearly scaled to 150 MHz, and merged again with forward application of DECOMP. Conductivity is provided in 0.02-m resolution. Due to the strong influence of the DEP-measurement noise in permittivity on synthetic reflections, permittivity is smoothed over 20 m for forward modeling (Eisen et al., 2006). The synthetic trace thus only contains reflections which originate from changes in conductivity. Processing comprises a synchronization of the synthetic source signal to the RES first-break signal from the surface by a time shift of +0.1  $\mu$ s, application of a Hilbert magnitude transformation to obtain a signal envelope (i.e. mimic rectification), and a smoothing with a 0.1- $\mu$ s Gaussian running-mean filter. Details are presented in Eisen et al. (2006)

## 2.4 Determination of crystal-orientation fabric

Fabric data of the EDML deep ice core were measured down to a 2560-m depth in a coldroom at a temperature of  $-20^\circ\text{C}$  in 2005 at AWI (Bremerhaven, Germany). Ice-core sections

were drilled between 2001 and 2004 and have been stored at  $-30^{\circ}\text{C}$  after the transportation at  $-25^{\circ}\text{C}$  to AWI. Thin sections were prepared according to standard procedures using a microtome from horizontally ( $0.5 \times 50 \times 50 \text{ mm}^{-3}$ ) and vertically ( $0.5 \times 50 \times 100 \text{ mm}^{-3}$ ) cut samples. Orientations of  $c$ -axes were derived using an automatic fabric analyzer system (Wilson et al., 2003), which enables complete measurement of these samples in 15 to 30 min. Unfortunately, it is not yet possible to record the horizontal azimuth of the drilled core sections, so azimuth is not available for the thin sections. In addition to the Schmidt diagrams (mapping each measured crystal  $c$ -axis direction from a point on the hemisphere to a circular plane using an equal-area projection, Fig. 4), we present the data in terms of the eigenvalues  $\lambda_i$  of the orientation tensor (Wallbrecher, 1979). The eigenvalues (Fig. 3) represent the components along the orthogonal coordinate system  $\hat{e}_i$  of an ellipsoid, which best approaches the momentum of inertia of the  $c$ -axes distribution. Measurements of samples cut horizontally and vertically from the core are jointly displayed. From the distribution of all measurements along the whole core it is evident that the eigenvalues are accurate to about a value of  $\pm 0.1$ . This is partly explained by the physical variations in the distribution of crystals in each sample, but also partly by local effects attributed to the immaturity of the system. Nevertheless, the eigenvalues are considered reliable within this accuracy.

### 3 Results and discussion

Drilling at EDML finished in January 2006, reaching bedrock at a logged ice thickness of 2774.15 m. This corresponds well with the ice thickness determined by RES (Fig. 2). The RES profiles at both pulse widths show the common internal layering of ice sheets, which increasingly follows the bedrock topography at larger depth, especially evident for profile sections spanning several 10–100 km (not shown). A sudden decrease in reflected energy and the absence of any laterally continuous signals suggest that the echo-free zone is present in the lowest 500–800 m above bedrock, starting at about 2100 m at the drill site.

The 600 ns pulse spans some 50 m in ice and integrates over a much wider depth range than the short pulse, which covers only about 5 m. As would be expected, fewer layers are therefore visible in the profile recorded with the 600 ns pulse than in the one recorded with the 60 ns pulse (Fig. 2). Looking at single traces, it is evident that several distinct peaks in the short-pulse trace have nevertheless counterparts in the long-pulse trace. This is clearly the case for strong reflections at depths of 1810 and 2035 m, and less so at 1865 and 2080 m (Fig. 3). Dominant reflections of each pulse cover about one pulse length. The first break of the concurrent reflections appear at about the same depth, but the maximum power in the long pulse occurs about 10 m deeper than in the short pulse.

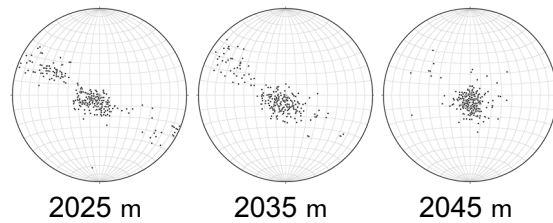


**Fig. 4.** Schmidt diagrams of vertical sections at three depths, showing the orientation of  $c$ -axes and the transition from vertical girdle-type to increased vertical single-maximum fabric. The orientations have been rotated into the horizontal  $xy$ -plane.

The comparison between the short pulse trace and the synthetic trace carried out by Eisen et al. (2006) demonstrates that a number of internal layers can be reproduced by forward modeling based on a conductivity profile. Removing dominant peaks by interpolation in the underlying conductivity profile causes a disappearance of the related reflections in the synthetic trace, as indicated for two cases at 1865- and 2080-m depth in Fig. 3 by the dotted line and the black peaks of the synthetic radargram. This demonstrates that these reflections originate from narrow peaks in conductivity, all less than about 0.5 m wide (Eisen et al., 2006). Interestingly, the strong signal in the short pulse at 2035 m is not reproduced in the synthetic data. The origin of this reflection and its characteristic properties will be investigated in detail in the remaining part of the paper.

#### 3.1 RES vs. ice-core data

In comparison to the reflection at 1865 m of the short pulse, which is caused by a peak with a maximum conductivity of  $38 \mu\text{S m}^{-1}$  on a background conductivity of  $15 \mu\text{S m}^{-1}$ , one would expect a conductivity peak of comparable size also at 2035 m. However, the conductivity profile merely displays a peak of  $24 \mu\text{S m}^{-1}$  on a background of  $17 \mu\text{S m}^{-1}$  at this depth. Peaks of this size appear regularly in the conductivity profile, without causing strong reflections, neither in the short pulse RES data nor in the synthetic trace. Missing data, rejected in the DEP quality check, could mask a prominent conductivity peak. Using 0.5 m as the upper limit for the width of strong conductivity peaks responsible for reflections, as identified by Eisen et al. (2006), the closest sections of data gaps  $>0.5$  m are located at 2026.26–2027.32, 2028.29–2028.81, 2038.90–2039.93, and 2040.03–2040.65 m. Each of these gaps is further away from the reflector's depth of origin than its depth accuracy of less than 1 m (Eisen et al., 2006). We therefore exclude the possibility that a single peak in conductivity causes the reflection in the short pulse trace at 2035 m.

Another possibility for the origin of the reflection at 2035-m depth would be that interference of partial reflections at

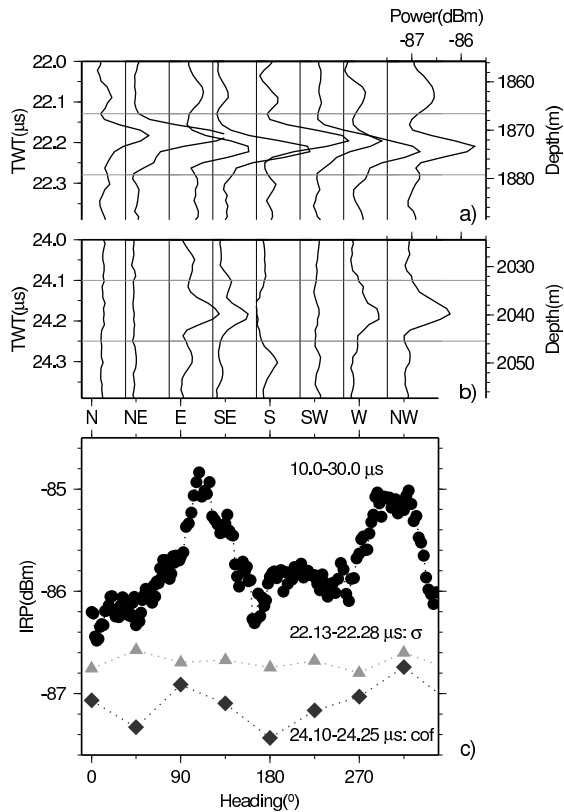


**Fig. 5.** Comparison of azimuth dependence for two reflectors originating from changes in (a) conductivity and (b) COF for eight airplane headings, which are equal to electric polarisation. Each trace in (a) and (b) is a stack of 70 traces along one of eight linear segments of profile 033042 (Fig. 1), recorded with the 60-ns pulse; power scale given for heading NW in a) applies for all traces; vertical baselines in (a) and (b) correspond to  $-87.5$  dBm; horizontal lines bound time windows used for calculation of internal reflection power (IRP) displayed in (c). (c) IRP as a function of azimuth and time window, calculated as the power average per sample over the respective time window. Triangles and diamonds: IRP over 150-ns time window (12 samples) of traces shown in (a) and (b), respectively; black circles: IRP over 10–30  $\mu$ s time window for unstacked traces of circle segment of profile. The ice divide runs along the ESE–WNW direction.

several conductivity peaks within one pulse length occurs. However, referring to the reflection's counterpart in the long-pulse data, it would be surprising that a series of small conductivity peaks of just  $5\text{--}10 \mu\text{S m}^{-1}$  above a background of  $15\text{--}20 \mu\text{S m}^{-1}$  would allow for coherent interference in both pulse lengths to produce the dominant reflections being one pulse width long. We therefore also exclude the possibility that the reflections at 2035 m in both RES traces are caused

by changes in conductivity, and thus the imaginary part  $\epsilon''$  of the dielectric constant.

The only other possibility for reflector origin is the real part  $\epsilon'$ . At these depths, changes in density are not present, as air bubbles already turned into air hydrates. As these have a very low volume density (Matsuoka et al., 2004), they hardly influence the bulk permittivity. One would consequently expect a profile of basically constant permittivity. The noise seen in the permittivity profile of about 0.05 on the sub-meter scale (Fig. 3) is attributed to measurement noise of the DEP bench. We therefore cannot use the permittivity profile to determine the reflection origin.

The remaining possibility to cause a change in  $\epsilon'$  are changes in COF. The Schmidt diagrams at 2025–2045-m depth in Fig. 4 show a transition from a vertical girdle-type to a single-maximum fabric with c-axes clearly concentrated around the vertical. The eigenvalues of the distribution of c-axes (Fig. 3) show this transition very clearly in the two largest components,  $\lambda_2$  and  $\lambda_3$ , which change by  $\sim 20\%$  over 20 m. A change from a vertical girdle-type fabric to a vertically concentrated fabric as reflector origin should result in an anisotropic response in the RES signals as a function of polarisation. This will be investigated next.

### 3.2 Analysis of RES polarisation azimuth

The RES data of profile 033042 were recorded with different airplane headings, and thus polarisation azimuths (Fig. 1). This data set provides an independent means to determine the origin of the internal reflections and enables us to fix the azimuth ambiguities of the COF measurements along the core.

For different time windows we calculate the internal reflection power (IRP, compare Gades et al., 2000), defined as the power average per sample (in dBm) within the time window. The azimuth dependence of the reflected energy from individual reflectors (i.e. for short time windows) is difficult to analyse for the circle segment, as the signal-to-noise ratio is very low and stacking is not feasible because of the different azimuths. However, IRP over the time window 10–30  $\mu$ s indicates that for the heading E to SE and W to NW the IRP is significantly higher than for other headings (Fig. 5). The maxima lie in the vertical plane along the ice divide (ESE–WNW).

Our explanation is as follows: c-axes orientations of all types (single maximum, girdle, ...) show small statistical variations around a mean distribution with depth. Thus, the dielectric properties also vary slightly with depth, causing some incoherent backscatter of a propagating radar signal. These variations have the largest effect on the radar backscatter if they occur in the vertical plane parallel to radar polarisation. At the present location, dominated by a girdle-type fabric between 450 and 2025-m depth, polarisation perpendicular to the ice divide results in an overall lower level of backscatter, whereas for polarisation parallel to the ice divide the level of backscatter is highest. We interpret this as

an indication that the girdle fabric lies in the vertical plane parallel to the ice divide, and that variations in the girdle fabric cause the higher backscatter in that plane. For later analysis, we define this as the  $yz$ -plane of an orthogonal coordinate system, with the horizontal coordinates  $x$  and  $y$  as the across-flow (NNE) and the along-flow (WNW) directions, respectively, and the vertical coordinate  $z$ .

We next look at the variation of reflected energy as a function of azimuths of the stacked linear segments. For the reflector originating at 1865-m depth at the drill site, both the display of the raw traces (Fig. 5a), as well as the IRP calculated over a 150-ns window containing the reflection (Fig. 5c) do not show any clear systematic variation in backscatter with azimuth. This isotropic pattern is expected for reflections stemming from changes in conductivity, as from the peak present at 1865 m in the ice-core data. At the depth of the change in COF at about 2035 m at the drill site, a reflection is visible for headings E and SE, and in the opposite directions W and NW. Along the other headings no reflection is visible (Fig. 5b). The IRP, again calculated for a 150-ns time window at these depths, likewise shows maxima for the headings which also show a reflection (Fig. 5c). We interpret this to be caused by the change in COF from the anisotropic distribution of  $c$ -axes of the girdle-type fabric, which has an isotropic distribution in the horizontal plane, to the vertically concentrated fabric. If the electric polarisation is parallel to the plane in which  $c$ -axes change, i.e. parallel to the ice divide in the  $yz$ -plane, permittivity changes as well, and a reflection occurs. If, in contrast, the electric polarisation is perpendicular to the plane containing the  $c$ -axes, then any changes in COF in the  $yz$ -plane will not influence the radar wave. We therefore take the azimuth-dependence of reflectivity as an independent confirmation that the reflector at 2035 m indeed originates from the changes in COF observed in the ice core.

### 3.3 Reflectivity from ice-core COF

The distribution of  $c$ -axes allows us to calculate the permittivity components. Following Fujita et al. (2006), the effective permittivity in the direction of the ellipsoid's principle components  $\hat{e}_i$  can be determined from the eigenvalue  $\lambda_i$  by  $\varepsilon'_i = \varepsilon'_\perp + \Delta\varepsilon'\lambda_i$ . In the present case, the principle component  $\hat{e}_3$  is very close to the vertical below 1700-m depth (Fig. 4), and  $\hat{e}_{1,2}$  lie in the horizontal  $xy$ -plane. Although borehole logging indicated that the core axis has a possible deviation of 1–2° from the vertical, we consider this negligible for the following analysis, as the accuracy of the fabric analyzer is on the same order of magnitude. This is moreover justified by the width of the distribution of  $c$ -axes of some tens of degrees, even for the vertically highly concentrated fabric. The results above with azimuth dependence of backscatter from the circle profile indicate that  $\hat{e}_1$  corresponds to the  $x$ -direction, and  $\hat{e}_2$  to the  $y$ -direction. The principle compo-

nents  $\hat{e}_i$  are therefore approximately aligned with the orthogonal coordinates  $x, y, z$ .

The change in COF between depths  $z_1=2025$  and  $z_2=2045$  m results in a change in the permittivity components  $\delta\varepsilon'_i = \varepsilon'_i|_{z_1} - \varepsilon'_i|_{z_2} = \Delta\varepsilon'(\lambda_i|_{z_1} - \lambda_i|_{z_2})$ . Using the eigenvalues determined in the vertical sections yields  $\delta(\varepsilon'_x, \varepsilon'_y, \varepsilon'_z) = \Delta\varepsilon'(0.6, 21.1, -20.5)10^{-2} = (0.2, 7.4, -7.2)10^{-3}$ . This change occurs over 20 m, well within the width covered by the long pulse. The radar wave propagates in the vertical direction, so only  $\delta\varepsilon'_{x,y}$  can cause a reflection. Using the approximation from Paren (1981) to determine the power reflection coefficient for a two-layer interface with differing permittivities,  $|R| = (\delta\varepsilon'/(4\varepsilon))^2$ , the change in  $\delta\varepsilon'_x$  corresponds to a reflection coefficient  $R_x = -96.1$  dB, and the change  $\delta\varepsilon'_y$  yields  $R_y = -64.6$  dB. The measurement error of 20% in  $\Delta\varepsilon' = 0.035$  results in an uncertainty of less than 1 dB of  $R_x$  and  $R_y$ . Whereas  $R_x$  is very small, likely too small to result in a sufficiently large reflection,  $R_y$  seems to be large enough to detect a related reflection at the surface. These reflection coefficients explain the above observation that the reflection at 2035 m only appears for polarisation in  $y$ -direction (parallel to the ice divide, Fig. 5b), but not in the  $x$ -direction (perpendicular to the ice divide).

The nearby reflections at 2080 m, appearing for both pulse lengths, provide a qualitative plausibility check for the hypothesis that the change in COF in the  $yz$ -plane is indeed strong enough to cause reflections. As shown by the synthetic trace, the reflections' origin is the conductivity peak at 2080 m with a height of  $37 \mu\text{S m}^{-1}$ . The reflection coefficient corresponding to this conductivity peak (Paren, 1981) results as  $-75.7$  dB at 150 MHz, only a few dB smaller than the reflection coefficients  $R_y$  resulting from the change in COF. The smaller reflection coefficient is consistent with the fact that the reflections' maximum peak power at 2080 m for both pulses are smaller than those at 2035 m. We can therefore indeed attribute the origin of the observed reflections at 2035 m to the change in COF, which is strong enough and occurs over a short enough distance to cause the strong reflections in the short and long pulse data.

### 3.4 Distribution of reflector from COF

Laterally, the reflector from COF (red "V" in Fig. 2) is quasi-parallel to other internal layers, e.g. the reflectors from conductivity at a depth of 1865 m (yellow "V") and 2080 m at the drill site, but displays stronger variations in reflection magnitude. Although the 600-ns pulse radargram contains more noise (in terms of clutter or speckle) than the 60-ns data, the reflector from conductivity at 1865 m is clearly dominant. Both reflectors from conductivity can clearly be tracked over the whole section of the 60-ns pulse in Fig. 2. The reflector from COF seems to be continuous over the whole section in the 600-ns data as well, although of very low quality. In contrast, it can only be tracked between  $-3$  km and  $2.5$  km in the 60-ns data. It is very strong on the downstream

(right) side of the anticline between  $-3$  and  $1.5$  km. Further upstream (to the left) from the anticline, it fades away, with several strong reflectors appearing within  $20$  m above it. Downstream from the drill site, it starts to fade away at  $1.5$  km, and is interrupted and lost in the syncline starting around  $3$  km. The different characteristics of the  $60$  ns and  $600$  ns emphasize that care has to be exercised when interpreting long-pulse radar data, as reflector characteristics and mechanisms could change within the pulse length without resulting in obvious changes in the reflection magnitude or depth. The variation of reflection magnitude of the reflector from COF suggests that fabric changes are less continuous than conductivity characteristics, as they are susceptible to variations of internal stresses, e.g. between upstream and downstream sides of subglacial bedrock variations.

### 3.5 Reflectors from COF – frequent or uncommon?

Whereas certain flow regimes are necessary for sharp transitions in COF to occur, changes in conductivity are not constrained by comparable ice-dynamic conditions. We therefore expect that continuous internal reflectors from COF do occur less often than reflectors from conductivity. It is commonly expected that changes in conductivity cause isotropic reflectors. Reflections from COF, instead, can be anisotropic or isotropic. Anisotropic reflections only occur if the underlying change in COF patterns is also anisotropic in the horizontal plane. This is usually the case in flow regimes with significant lateral strain (e.g. Fujita et al., 2003), as is the case at the EDML drilling site. In contrast, analyses at Dome Fuji down to a depth of  $2500$  m (about  $83\%$  ice thickness) by Fujita et al. (2006) indicate that isotropic reflections with birefringent effects prevail. They explain this by the horizontally-symmetric pattern in COF in the same depth range, caused by symmetric divide flow at the dome. Any potential reflections from changes in COF therefore also show an isotropic pattern at Dome Fuji.

Observations of either type of reflector, conductivity- or COF-based, are likely biased, as data acquisition required for ice-core analyses are more intensive for detection of COF-type reflectors. The same holds true for the type of RES measurements required to indirectly identify the reflector origin from RES measurements alone. Reflections from conductivity are independent of polarisation plane. Reflectors from COF can only be identified by azimuth-dependent polarisation measurements at a single location in the case of anisotropic reflections, or a combination with multi-frequency measurements in the case of isotropic reflections. As azimuths-dependent RES measurements require more time than simple straight RES profiles (especially if only airborne systems are available), they are carried out less often.

To date, the reflector discussed here is the only one at EDML that can be clearly attributed to changes in COF. In contrast,  $13$  strong internal reflectors were identified to

originate from changes in conductivity at the same location (Eisen et al., 2006). However, with more COF data emerging, it might be possible that some reflectors appear to be of a mixed type, with their origin being partly from changes in COF, partly from conductivity. For instance, the reflector only present in the  $600$ -ns pulse data at  $1850$ -m depth could be caused by the series of conductivity peaks (Fig. 3), but it could also stem from slight changes in COF, or both. Further refinement of the COF data in at least  $10$ -m resolution is necessary to answer this question conclusively.

Some of the few ice cores from deep-drilling sites currently available display transitions from COF patterns which are anisotropic in the horizontal plane (e.g. girdle-type), to highly concentrated single-maximum fabrics in the lower part of the ice column, as at NorthGRIP (Wang et al., 2002) or Vostok (Obbard and Baker, 2007). However, only for some of the deep-drilling ice cores are profiles of COF available in high enough resolution to search for potential reflectors from COF directly. Another promising site to identify reflections from COF is the Siple Dome. The COF data, measured in  $20$ -m intervals, show a sharp transition from an elongated to a highly concentrated fabric between  $685$  and  $700$ -m depth, with the largest eigenvalue of the COF distribution changing from  $0.75$  to  $0.95$  (DiPrinzio et al., 2005, Fig. 3). RES data from the Siple Dome (e.g. Gades et al., 2000, Fig. 3) indicate a strong continuous internal reflector at about the same depth (based on the travel time depth conversion of Gades et al., 2000). In analogy to the findings developed here, this reflector thus bears the potential to stem from an abrupt change in COF.

Ice-core deep drillings are mostly carried out at such divide or dome locations as Dome Fuji or Siple Dome. Paleoclimatic interpretation of ice-core records usually incorporates ice-flow modeling. Recent modeling studies of ice flow at Siple Dome emphasize the significance of changes in COF for ice flow. Pettit et al. (2007) implemented fabric properties from borehole measurements in an anisotropic nonlinear flow law as part of an ice-sheet flow model. They found that the band of highly vertically concentrated COF in the lower  $20$ – $30\%$  of the ice column causes concentrated bed-parallel shearing  $300$  m above the bed. Moreover, compared to an isotropic fabric, the anisotropy considerably increases the size of the isochrone arch underneath the Siple Dome divide, and thus strongly influences the age–depth distribution. Pettit et al. (2007) assumed that the COF-profile is only a function of normalized depth with respect to ice thickness. The method presented here to identify continuous reflectors from changes in COF provides a way to improve this assumption. If a reflector is identified to originate from changes in COF, its true depth tracked in RES profiles could be used as a proxy for the spatial distribution of the change in COF, instead of extrapolating its normalized depth as observed in boreholes or ice cores.

#### 4 Conclusions

The combination of ice-core profiles of COF and the conductivity with RES data of different pulse lengths in our approach identifies the origin of a defined continuous internal reflector as a sharp transition in COF, from a girdle-type to a single-maximum fabric over just a few tens of meters. This finding goes beyond the previous analyses, which related RES signals to flow-induced COF, but did not provide a direct comparison of continuous internal layers in RES data with nearby in-situ data of COF. We showed that, even at short pulse lengths, the width of the COF-related reflector is comparable to reflectors stemming from conductivity peaks, limited by the RES pulse length. The spatial variation of the reflector from COF in depth is parallel to other internal reflectors, but less continuous. However, we emphasize that we have no evidence whether the reflector from COF is an isochrone or not. These observations imply that care has to be taken when correlating ice-core data with internal reflectors, if only single-frequency single-polarisation RES data are available, as these cannot pin down the reflector origin unambiguously.

The identification of a single change in COF as the origin of a strong individual internal reflector opens new possibilities for understanding and modeling ice dynamics. The fabric properties can be extrapolated along the reflector, as long as it is continuously trackable in the RES profile. Determination of the internal distribution of stresses can thus go beyond the point information provided by ice cores. Ice-dynamic models can utilize the reflector as an ancillary condition. As the rheology of a girdle-type fabric differs from those of a single-maximum fabric, the reflector indicates a boundary of different ice-flow properties above and below the reflector within the ice sheet. A remaining challenge lies in exclusively using remote-sensing data, like RES or seismics, to discriminate physical properties from the ice sheet's surface, without requiring in-situ information from ice cores. By providing characteristic observations of the forward relation of changes in COF and reflectivity, this study provides another step towards solving the inverse problem, which should eventually be used to determine the continuous profiles of vertical and lateral physical properties within the ice sheet.

*Acknowledgements.* This work is a contribution to the European Project for Ice Coring in Antarctica (EPICA), a joint European Science Foundation/European Commission scientific programme, funded by the EU and by national contributions from Belgium, Denmark, France, Germany, Italy, the Netherlands, Norway, Sweden, Switzerland and the United Kingdom. The main logistic support was provided by IPEV and PNRA (at Dome C) and AWI (at Dronning Maud Land). This is EPICA publication no. 186. Preparation of this work was supported by an "Emmy Noether"-scholarship of the Deutsche Forschungsgemeinschaft grant EI 672/1 to O. Eisen.

Edited by: J. L. Bamber

www.the-cryosphere.net/1/1/2007/

#### References

- Bogorodsky, V. V., Bentley, C. R., and Gudmandsen, P. E.: Radioglaciology, D. Reidel Publishing Company, Dordrecht, Holland, 1985.
- DiPrinzio, C. L., Wilen, L. A., Alley, R. B., Fitzpatrick, J. J., Spencer, M. K., and Gow, A. J.: Fabric and texture at Siple Dome, Antarctica, *J. Glaciol.*, 51, 281–290, 2005.
- Doake, C. S. M., Corr, H. J. F., and Jenkins, A.: Polarization of radio waves transmitted through Antarctic ice shelves, *AG*, 34, 165–170, 2002.
- Dowdeswell, J. A. and Evans, S.: Investigations of the form and flow of ice sheets and glaciers using radio-echo sounding, *Rep. Prog. Phys.*, 67, 1821–1861, 2004.
- Durand, G., Gillet-Chaulet, F., Svensson, A., Gagliardini, O., Kipfstuhl, S., Meyssonier, J., Parrenin, F., Duval, P., and Dahl-Jensen, D.: Change of the ice rheology with climatic transitions – implications for ice flow modelling and dating of the EPICA Dome C core, *Clim. Past*, 3, 155–167, 2007, <http://www.clim-past.net/3/155/2007/>.
- Eisen, O., Wilhelms, F., Steinhage, D., and Schwander, J.: Improved method to determine RES-reflector depths from ice-core profiles of permittivity and conductivity, *J. Glaciol.*, 52, 299–310, 2006.
- Fujita, S., Maeno, H., Uratsuka, S., Furukawa, T., Mae, S., Fujii, Y., and Watanabe, O.: Nature of radio echo layering in the Antarctic ice sheet detected by a two-frequency experiment, *J. Geophys. Res.*, 104, 13 013–13 024, 1999.
- Fujita, S., Matsuoka, T., Ishida, T., Matsuoka, K., and Mae, S.: A summary of the complex dielectric permittivity of ice in the megahertz range and its application for radar sounding of polar ice sheets, in: *The Physics of Ice Core Records*, edited by: Hondoh, T., pp. 185–212, Hokkaido University Press, 1 edn., 2000.
- Fujita, S., Matsuoka, K., Maeno, H., and Furukawa, T.: Scattering of VHF radio waves from within an ice sheet containing the vertical-girdle-type ice fabric and anisotropic reflection boundaries, *Ann. Glaciol.*, 37, 305–316, 2003.
- Fujita, S., Maeno, H., and Matsuoka, K.: Radio-wave depolarization and scattering within ice sheets: a matrix-based model to link radar and ice-core measurements and its application, *J. Glaciol.*, 52, 407–424, 2006.
- Gades, A., Raymond, C., Conway, H., and Jacobel, R.: Bed properties of Siple Dome and adjacent ice streams, West Antarctica, inferred from radio-echo sounding measurements, *J. Glaciol.*, 46, 88–94, 2000.
- Hargreaves, N. D.: The radio-frequency birefringence of polar ice, *J. Glaciol.*, 21, 301–313, 1978.
- Harrison, C. H.: Radio echo sounding of horizontal layers in ice, *J. Glaciol.*, 12, 383–397, 1973.
- ISMAL Committee: Recommendations for the collection and synthesis of Antarctic Ice Sheet mass balance data, *Global Planet. Change*, 42, 1–15, 2004.
- Liu, H., Jezek, K., Li, B., and Zhao, Z.: Radarsat Antarctic Mapping Project digital elevation model version 2, Digital media, National Snow and Ice Data Center, Boulder, CO, USA, 2001.
- Marshall, S. J.: Recent advances in understanding ice sheet dynamics, *E. Plan. Sci. Lett.*, 240, 191–204, doi:10.1016/j.epsl.2005.08.016, 2005.
- Matsuoka, K., Furukawa, T., Fujita, S., Maeno, H., Uratsuka, S., Naruse, R., and Watanabe, O.: Crystal orientation fabrics within

The Cryosphere, 1, 1–10, 2007

- the Antarctic ice sheet revealed by a multipolarization plane and dual-frequency radar survey, *J. Geophys. Res.*, 108(B10), 2499, doi:10.1029/2003JB002425, 2003.
- Matsuoka, K., Uratsuka, S., Fujita, S., and Nishio, F.: Ice-flow induced scattering zone within the Antarctic ice sheet revealed by high-frequency airborne radar, *J. Glaciol.*, 50, 382–388, 2004.
- Nixdorf, U., Steinhage, D., Meyer, U., Hempel, L., Jenett, M., Wachs, P., and Miller, H.: The newly developed airborne RES-system of the AWI as a glaciological tool, *Ann. Glaciol.*, 29, 231–238, 1999.
- Obbard, R. and Baker, I.: The microstructure of meteoric ice from Vostok, Antarctica, *J. Glaciol.*, 53, 41–62, 2007.
- Paren, J. G.: PRC at a dielectric interface, *J. Glaciol.*, 27, 203–204, 1981.
- Paren, J. G. and Robin, G. de Q.: Internal reflections in polar ice sheets, *J. Glaciol.*, 14, 251–259, 1975.
- Paterson, W. S. B.: *The physics of glaciers*, 3rd edition, Oxford, New York, Tokyo, Pergamon, ix, 480 pp., ISBN 0-08037944 3, 1994.
- Petrenko, V. F. and Whitworth, R. W.: *Physics of Ice*, Oxford University Press, 1999.
- O. Eisen et al.: Internal RES reflector originating from COF
- Pettit, E. C., Thorsteinsson, T., Jacobson, H. P., and Waddington, E. D.: The role of crystal fabric in flow near an ice divide, *J. Glaciol.*, 53, 277–288, 2007.
- Robin, G. de Q., Evans, S., and Bailey, J. T.: Interpretation of radio echo sounding in polar ice sheets, in: *Philosophical Transactions of the Royal Society of London*, vol. 146 of A, pp. 437–505, Royal Society of London, 1969.
- Wallbrecher, E.: Methoden zum quantitativen Vergleich von Regelungsgraden und Formen strukturgeologischer Datenmengen mit Hilfe von Vektorstatistik und Eigenwertanalyse, *N. JB. Geol. Paläontol. Abh.*, 159, 113–149, 1979.
- Wang, Y., Thorsteinsson, T., Kipfstuhl, J., Miller, H., Dahl-Jensen, D., and Shoji, H.: A vertical girdle fabric in the NorthGRIP deep ice core, North Greenland, *Ann. Glaciol.*, 35, 515–520, 2002.
- Wesche, C., Eisen, O., Oerter, H., Schulte, D., and Steinhage, D.: Surface topography and ice flow in the vicinity of EDML deep-drilling site, *J. Glaciol.*, 53(182), 442–448, 2007.
- Wilhelms, F.: Explaining the dielectric properties of firm as a density and conductivity mixed permittivity (DECOMP), *Geophys. Res. Lett.*, 32, L16 501, doi:10.1029/2005GL022808, 2005.
- Wilson, J., Russell-Head, D. S., and Sim, H. M.: The application of an automated fabric analyzer system to the textural evolution of folded ice layers in shear zones, *Ann. Glaciol.*, 37, 7–17, 2003.

# Appendix H

## Publication VIII - One-to-one coupling of glacial climate variability in Greenland and Antarctica

EPICA Community Members, Fischer, H., Freitag, J., Frenzel, A., Fritzsche, D., Fundel, F., Gersonde, R., Hamann, I., Huybrechts, P., Kipfstuhl, S., Lambrecht, A., Meyer, H., Miller, H., Oerter, H., Ruth, U., Rybak, O., Schmitt, J., Valero-Delgado, F., Wegner, A., Wilhelms, F.(2006)

Nature, 444, pp. 195-198, doi:10.1038/nature05301.

# One-to-one coupling of glacial climate variability in Greenland and Antarctica

EPICA Community Members\*

Precise knowledge of the phase relationship between climate changes in the two hemispheres is a key for understanding the Earth's climate dynamics. For the last glacial period, ice core studies<sup>1,2</sup> have revealed strong coupling of the largest millennial-scale warm events in Antarctica with the longest Dansgaard–Oeschger events in Greenland<sup>3–5</sup> through the Atlantic meridional overturning circulation<sup>6–8</sup>. It has been unclear, however, whether the shorter Dansgaard–Oeschger events have counterparts in the shorter and less prominent Antarctic temperature variations, and whether these events are linked by the same mechanism. Here we present a glacial climate record derived from an ice core from Dronning Maud Land, Antarctica, which represents South Atlantic climate at a resolution comparable with the Greenland ice core records. After methane synchronization with an ice core from North Greenland<sup>9</sup>, the oxygen isotope record from the Dronning Maud Land ice core shows a one-to-one coupling between all Antarctic warm events and Greenland Dansgaard–Oeschger events by the bipolar seesaw<sup>6</sup>. The amplitude of the Antarctic warm events is found to be linearly dependent on the duration of the concurrent stadial in the North, suggesting that they all result from a similar reduction in the meridional overturning circulation.

The glacial climate in the North Atlantic region is characterized by rapid shifts from cold stadial to warmer interstadial conditions<sup>3,4,9</sup>. Greenland temperatures during these Dansgaard–Oeschger (D–O) events rise by 8–16 °C (refs 10, 11) within a few decades followed by a less rapid temperature decline back to stadial conditions. In contrast, glacial climate in the circum-Antarctic region exhibits slower millennial changes with smaller temperature amplitudes of only 1–3 °C (refs 1, 12, 13). After synchronization of Greenland and Antarctic ice core records<sup>1,2</sup> using the global atmospheric change in CH<sub>4</sub> concentrations, a conspicuous phase relationship between the largest Antarctic warmings (A1–A7; ref. 1) and the longest D–O events was observed with the south warming during the stadial conditions in the north, and starting to cool as soon as the D–O warming set in. This bipolar seesaw pattern was explained by changes in the heat and freshwater flux connected to the Atlantic Meridional Overturning Circulation (MOC), where a stronger MOC leads to increased drainage of heat from the Southern Ocean heat reservoir<sup>6,7</sup>.

In principle, an interhemispheric climate coupling by the bipolar seesaw should also apply for all the short D–O events. However, to what extent this concept is also able to explain the higher-frequency climate variability in Antarctic ice cores remained unclear (as discussed for example, in ref. 14 and references therein). Here we report

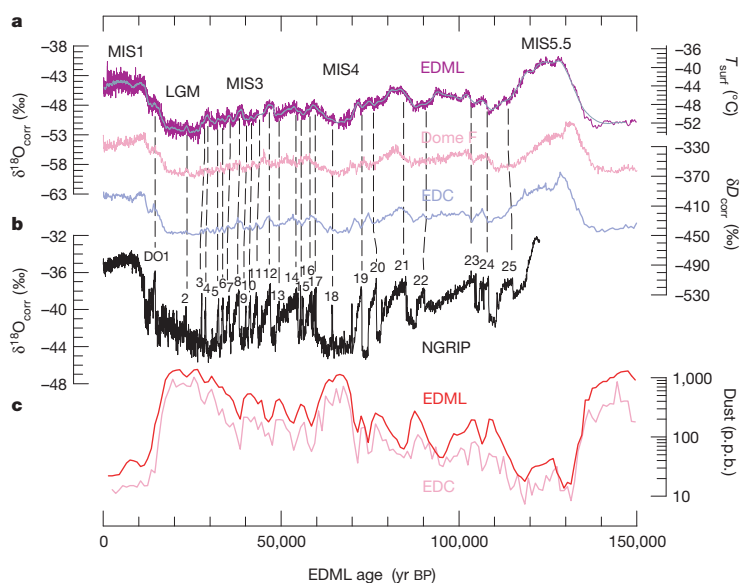


**Figure 1** | Antarctic stable isotope records show synchronous millennial variations during the last glacial, whereas rapid variations are encountered in Greenland. **a**, EDML  $\delta^{18}\text{O}$  record (purple, 0.5-m resolution; grey, 15-m running mean) after sea level and upstream correction (see Supplementary Information) over the past 150 kyr. The record shows features similar to those of the EDC<sup>12</sup> (blue) and the Dome F<sup>13</sup> (pink) isotope records but with more fine structure during MIS3 and MIS4. We note that EDML and EDC are plotted on the new common EDC3 timescale (see Supplementary Information) while Dome F is plotted on its individual timescale. The temperature axis on the right side indicates approximate surface temperatures at EDML as derived from the spatial  $\delta^{18}\text{O}$ /temperature gradient (see Supplementary Information). **b**,  $\delta^{18}\text{O}$  record of the NGRIP ice core (grey)<sup>9</sup>. **c**, Mineral dust records of the EDML (red) and EDC<sup>12</sup> (pink) ice cores at 1,000-yr resolution; these dust records were used for synchronization of the cores.

\*A full list of authors and their affiliations appears at the end of the paper.

on the climate record over the last glacial cycle from a new ice core drilled within the European Project for Ice Coring in Antarctica (EPICA) in the interior of Dronning Maud Land, hence denoted EDML, at 75° S, 0° E, 2,892 m.a.s.l. (metres above sea level), with a recent accumulation rate of 6.4 cm water equivalent (w.e.) per year<sup>15</sup>. This site was chosen to complement the long EPICA Dome C (EDC, 75° S, 123° E, 3,233 m.a.s.l., 2.5 cm w.e. yr<sup>-1</sup>) record<sup>12</sup>, because EDML is the first deep ice core in the Atlantic sector of the Southern Ocean region<sup>16</sup> and thus located near the southern end of the bipolar seesaw. The snow accumulation at EDML is two to three times higher than at other deep drilling sites on the East Antarctic plateau, so higher-resolution atmosphere and climate records can be obtained for the last glacial period, making the EDML core especially suitable for studying decadal-to-millennial climate variations in Antarctica.

In Fig. 1 the EDML  $\delta^{18}\text{O}$  record as proxy for local temperature on the ice sheet is shown in 0.5-m resolution (equivalent to 15–30 yr during the marine isotope stage MIS3 and 100–150 yr during MIS5) after correction for upstream and glacial–interglacial ice sheet altitude effects (see Supplementary Information). The overall pattern closely resembles that recorded in most Antarctic ice cores previously covering this time period<sup>12,13,17</sup>. Also, very similar dust profiles (Fig. 1) are encountered at EDML and EDC, related to parallel changes in climate conditions in the Patagonian dust source region common to both cores<sup>18</sup>. Despite the high correlation of the EDML  $\delta^{18}\text{O}$  and the EDC  $\delta D$  record over the last 150,000 yr ( $r^2 = 0.94$  for 250-yr averages) some distinct differences exist. In the penultimate warm period (MIS5.5) the EDML  $\delta^{18}\text{O}$  record indicates temperatures about 4–5 °C higher than those of the Holocene, in line with other ice cores from the East Antarctic plateau<sup>12,13,17</sup>. However,  $\delta^{18}\text{O}$  at EDML exhibits persistently higher  $\delta^{18}\text{O}$  values over the entire duration of MIS5.5 while other ice cores on the East Antarctic plateau show a substantial drop after an initial climate optimum<sup>12,13</sup>. We note that this difference is not due to the altitude corrections applied to the EDML  $\delta^{18}\text{O}$  record (see Supplementary Information), because a similar temporal evolution during MIS5.5 is also seen in the uncorrected data. Instead, a smaller cooling at EDML in the course of MIS5.5 compared to EDC and Dome Fuji is consistent with marine sediment records from the Atlantic sector of the Southern Ocean revealing persistently warmer summer sea surface temperatures

and a reduced winter sea ice cover throughout MIS5.5 (ref. 19). This suggests that there were regional differences in temperature and sea ice evolution during this period for the Atlantic and Indian Ocean sector.

The most outstanding feature of the high-resolution EDML record is the pronounced millennial variability during the glacial. As indicated by the dashed lines in Fig. 1 each of the warming episodes in Antarctica can be related to a corresponding D–O event, but only synchronization of the age scales allows us to assign them unambiguously and to pinpoint the phase relationship between climate changes in Greenland and Antarctica. To do this, the EDML core has been synchronized (see Supplementary Information) to the layer counted NGRIP ice core<sup>20,21</sup> over MIS3, using high-resolution  $\text{CH}_4$  profiles over the last 55 kyr from the NGRIP, GRIP and GISP2 ice cores<sup>11</sup>. The synchronized  $\delta^{18}\text{O}$  records are shown in Fig. 2. Also plotted is the  $\text{CH}_4$  synchronized  $\delta^{18}\text{O}$  record from the Byrd ice core<sup>1</sup> and new high-resolution  $\delta D$  data from EDC<sup>22</sup> which closely resemble the temperature variability found at EDML during MIS3 and support an Antarctic-wide interpretation of these fluctuations. The higher glacial snow accumulation at EDML ( $\sim 3$  cm w.e. yr<sup>-1</sup>) compared to that at EDC, Dome Fuji or Vostok ( $\sim 1.4$  cm w.e. yr<sup>-1</sup>) implies a  $\text{CH}_4$  synchronization two to three times better than at those sites. The synchronization uncertainty for MIS3 ranges from 400 to 800 yr for all events in the EDML record, making the synchronization error for EDML always much smaller than the duration of the events themselves.

This is important, because this allows an unequivocal one-to-one assignment not only of the well-known large warm events in Antarctica (A1, A2 and so on) but of each single isotope maximum indicated in Fig. 2 with a corresponding D–O event in the north. Although the exact timing of the temperature maxima relative to the stadial/interstadial transitions cannot be discerned more precisely than the synchronization error, it is evident that each Antarctic warming starts significantly before the respective D–O event. In addition, a synchronization of the stable water isotope records of the GRIP and EDC ice cores using the <sup>10</sup>Be production anomaly around 41,000 yr BP, which constrains the in-phase relationship of the onset of D–O 10 and the respective Antarctic  $\delta D$  maximum to better than 200 yr (ref. 23), supports our  $\text{CH}_4$  match. Accordingly, we suggest a new Antarctic Isotope Maximum (AIM) nomenclature in Fig. 2

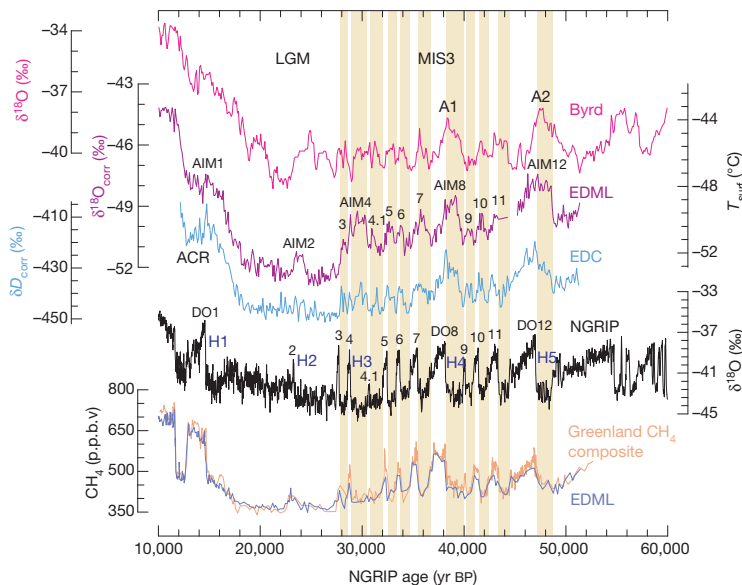


**Figure 2 | Methane synchronization of the EDML and the NGRIP records reveals a one-to-one assignment of each Antarctic warming with a corresponding stadial in Greenland.** Displayed are 100-yr averages during MIS3 in the EDML, EDC<sup>26</sup> and Byrd<sup>1</sup> ice core for the time interval 10–60 kyr BP in comparison with the NGRIP  $\delta^{18}\text{O}$  record from Northern Greenland<sup>9</sup>. All records are  $\text{CH}_4$  synchronized and given on the new GICC05 age scale for the NGRIP ice core, which has been derived by counting annual layers down to 41 kyr and by a flow model for older ages<sup>9,21</sup>. Yellow bars indicate the Greenland stadial periods that we relate to respective Antarctic temperature increases. The approximate timing of Heinrich layers in North Atlantic sediments is indicated as well<sup>27</sup>. The y axis on the right side indicates approximate temperature changes at EDML based on the modern spatial gradient between  $\delta^{18}\text{O}$  and temperature.

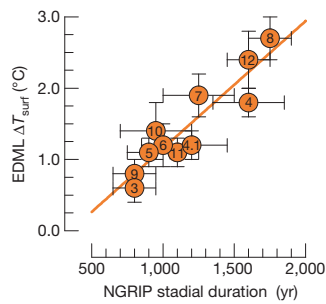


**Figure 3 | Amplitudes of Antarctic warmings show a linear relationship ( $r^2 = 0.85$ ) with the duration of the accompanying stadal in Greenland during MIS3.** The amplitude was determined from the Antarctic  $\delta^{18}\text{O}$  maximum to the preceding minimum of each event; the stadal duration is defined by the interval between the midpoint of the stepwise temperature change at the start and end of a stadial on the extended GICC05 age scale<sup>9,21</sup>. Error bars reflect the estimated uncertainty in the definition of the maxima and minima in  $\delta^{18}\text{O}$  at EDML and in the duration of the concurrent stadial period. Numbers indicate the corresponding AIMs and D–O events.

which reflects the connection of southern warming to reduced oceanic heat transport into the North Atlantic during stadials. The timing and duration of the AIMs relative to D–O events is also indirectly supported by the comparison of changes in deep-water masses linked to Antarctic Bottom Water formation and Atlantic surface water changes, as archived in sediment records offshore of Portugal<sup>24</sup>.

Most striking is the varying amplitude of the AIMs, which is linearly dependent on the duration of stadials in the north, as shown in Fig. 3. The only significant deviation from this linear relationship during MIS3 is AIM4, in which the error in the stadal duration estimate is quite large. We conclude that the duration of a reduced MOC—and, hence, the duration of the warming period in the Southern Ocean—determines the amount of heat accumulated in the Southern Ocean heat reservoir, strongly supporting the general applicability of the thermal bipolar seesaw<sup>6</sup> concept within the range of stadial events encountered during MIS3. We note that for longer cessations of the MOC a new equilibrium temperature in the Southern Ocean would be reached and the warming would eventually have to cease. This linear relationship also implies that the Antarctic warming rate—and thus the heat flux from the Southern Ocean to the Atlantic—is similar for all warming events during MIS3. If we assume the same spatial configuration of the overturning cell for cold intervals in MIS3, this would suggest that the strength of the MOC is approximately constant for all stadials, challenging the notion of different overturning rates<sup>25</sup> for stadials in which massive iceberg discharges into the North Atlantic (the so-called Heinrich events in Fig. 2: H1–H5) occurred compared to stadials without Heinrich events. Note however, that the stadials before D–O 8 and D–O 12 in which Heinrich events occurred were the longest and the related Antarctic warmings the largest. This may be due to the longer time needed to mix away the large freshwater anomalies during Heinrich events. There is, however, a less clear relationship for other Heinrich events. Comparison of the millennial climate variability during MIS3 at EDML and EDC shows no significant difference in the amplitude of the isotopic change in the Atlantic and Indian Ocean sectors of the Southern Ocean. This implies a uniform ocean heat reservoir controlling temperature changes at both sites and reflects the rapid mixing of the Southern Ocean by the Antarctic Circumpolar Current.

In the EDML  $\delta^{18}\text{O}$  record a major warm event (AIM2, connected to D–O 2) is seen during the Last Glacial Maximum, which cannot be clearly identified in the EDC core but is present in the Dome F record (Fig. 1). AIM2 also shows a decrease in high-resolution mineral dust concentrations at EDC, as do all the other AIMs<sup>26</sup>. We therefore

conclude that AIM2 is a warm event comparable to the other AIMs in MIS3 but is not sufficiently resolved in the EDC record owing to its lower accumulation. The corresponding D–O 2 event in the North Atlantic is preceded by the longest cold period in the NGRIP record (Fig. 2) and accordingly, a higher temperature amplitude of AIM2 is to be expected if the same bipolar seesaw concept holds as for D–O events during MIS3. However, sea level and temperature conditions were significantly different during the Last Glacial Maximum, potentially affecting the spatial configuration and strength of the overturning cell in the North Atlantic. The fact that AIM2 is only 2,000 yr long suggests that the strength of the MOC was not significantly reduced for the entire cold period in the North, but collapsed only about 1,000 yr before D–O 2, which would be in line with significant iceberg discharge depositing ice-rafted debris in the North Atlantic during H2 (ref. 27).

In summary, a strong interhemispheric coupling of all bipolar climate variations during MIS3 via the MOC is supported by the new high-resolution  $\delta^{18}\text{O}$  record from EDML indicating that Antarctic warming rates and potentially also overturning rates have been similar for all events in MIS3. The question of what triggers the switch from stadial to interstadial conditions remains. Transitions in the strength of the MOC and its effect on the Atlantic Southern Ocean heat exchange are simulated in response to changes in the North Atlantic freshwater balance<sup>7,8</sup>; however, the origin of such variations in freshwater input are still not ascertained for all individual D–O events. In addition, large iceberg discharge from the Laurentide ice sheet does not systematically coincide with either the onset or the end of stadials<sup>27,28</sup>. Recently, the potential role of a change in Southern Ocean sea-ice cover for reinstalling a stronger MOC has been identified for the onset of the Bølling/Allerød warming<sup>29,30</sup>. The intrinsic feedback of a reduced sea-ice cover in the Southern Ocean during AIMs, followed by a delayed onset of deep-water formation in the North, could potentially explain the interhemispheric climate coupling seen in our records during MIS3.

Received 26 May; accepted 22 September 2006.

- Blunier, T. & Brook, E. J. Timing of millennial-scale climate change in Antarctica and Greenland during the last glacial period. *Science* **291**, 109–112 (2001).
- Blunier, T. *et al.* Asynchrony of Antarctic and Greenland climate change during the last glacial period. *Nature* **394**, 739–743 (1998).
- Johnsen, S. J. *et al.* Irregular glacial interstadials recorded in a new Greenland ice core. *Nature* **359**, 311–313 (1992).
- Bond, G. *et al.* Correlations between records from North Atlantic sediments and Greenland ice. *Nature* **365**, 143–147 (1993).
- McManus, J. F., Oppo, D. W. & Cullen, J. L. A 0.5-million-year record of millennial climate variability in the North Atlantic. *Science* **283**, 971–975 (1999).
- Stocker, T. F. & Johnsen, S. J. A minimum thermodynamic model of the bipolar seesaw. *Paleoceanography* **18**, art. no. 1087 (2003).
- Knutti, R., Flückiger, J., Stocker, T. F. & Timmermann, A. Strong hemispheric coupling of glacial climate through freshwater discharge and ocean circulation. *Nature* **430**, 851–856 (2004).
- Ganopolski, A. & Rahmstorf, S. Rapid changes of glacial climate simulated in a coupled climate model. *Nature* **409**, 153–158 (2001).
- North Greenland Ice Core Project members. High resolution climate record of the northern hemisphere reaching into the last interglacial period. *Nature* **431**, 147–151 (2004).
- Landais, A. *et al.* Quantification of rapid temperature change during DO event 12 and phasing with methane inferred from air isotopic measurements. *Earth Planet. Sci. Lett.* **225**, 221–232 (2004).
- Huber, C. *et al.* Isotope calibrated Greenland temperature record over Marine Isotope Stage 3 and its relation to  $\text{CH}_4$ . *Earth Planet. Sci. Lett.* **245**, 504–519 (2006).
- EPICA community members. Eight glacial cycles from an Antarctic ice core. *Nature* **429**, 623–628 (2004).
- Watanabe, O. *et al.* Homogeneous climate variability across East Antarctica over the past three glacial cycles. *Nature* **422**, 509–512 (2003).
- Roe, G. H. & Steig, E. J. Characterization of millennial-scale climate variability. *J. Clim.* **17**, 1929–1944 (2004).
- Oerter, H. *et al.* Accumulation rates in Dronning Maud Land, Antarctica, as revealed by dielectric-profiling measurements of shallow firn cores. *Ann. Glaciol.* **30**, 27–34 (2000).
- Reijmer, C. H., van den Broeke, M. R. & Scheele, M. P. Air parcel trajectories to five deep drilling locations on Antarctica, based on the ERA-15 data set. *J. Clim.* **15**, 1957–1968 (2002).

17. Petit, J. R. *et al.* Climate and atmospheric history of the past 420,000 years from the Vostok ice core, Antarctica. *Nature* **399**, 429–436 (1999).
18. Basile, I. *et al.* Patagonian origin of glacial dust deposited in East Antarctica (Vostok and Dome C) during glacial stages 2, 4 and 6. *Earth Planet. Sci. Lett.* **146**, 573–589 (1997).
19. Bianchi, C. & Gersonde, R. The Southern Ocean surface between Marine Isotope Stage 6 and 5d: Shape and timing of climate changes. *Palaeogeogr. Palaeoclimatol. Palaeoecol.* **187**, 151–177 (2002).
20. Rasmussen, S. O. *et al.* A new Greenland ice core chronology for the last glacial termination. *J. Geophys. Res.* **111**, D06102 (2006).
21. Andersen, K. K. *et al.* The Greenland ice core chronology 2005, 15–42 kyr. Part 1: Constructing the time scale. *Quat. Sci. Rev.* (in the press).
22. Stenni, B. *et al.* A late-glacial high-resolution site and source temperature record derived from the EPICA Dome C isotope records (East Antarctica). *Earth Planet. Sci. Lett.* **217**, 183–195 (2003).
23. Raisbeck, G., Yiou, F. & Jouzel, J. Cosmogenic <sup>10</sup>Be as a high resolution correlation tool for climate records. *Geochim. Cosmochim. Acta* **66**, abstr. A623 (2002).
24. Shackleton, N. J., Hall, M. A. & Vincent, E. Phase relationships between millennial-scale events 64,000–24,000 years ago. *Paleoceanography* **15**, 565–569 (2000).
25. Rahmstorf, S. Ocean circulation and climate during the past 120,000 years. *Nature* **419**, 207–214 (2002).
26. Röthlisberger, R. *et al.* Dust and sea-salt variability in central East Antarctica (Dome C) over the last 45 kyr and its implications for southern high-latitude climate. *Geophys. Res. Lett.* **29**, article no. 1963 (2002).
27. Bond, G. & Lotti, R. Iceberg discharges into the North Atlantic on millennial time scales during the last glaciation. *Science* **267**, 1005–1010 (1995).
28. de Abreu, L., Shackleton, N. J., Joachim Schönfeld, J., Hall, M. & Chapman, M. Millennial-scale oceanic climate variability off the Western Iberian margin during the last two glacial periods. *Mar. Geol.* **196**, 1–20 (2003).
29. Knorr, G. & Lohmann, G. Southern Ocean origin for the resumption of Atlantic thermohaline circulation during deglaciation. *Nature* **424**, 532–536 (2003).
30. Stocker, T. F. & Wright, D. G. Rapid transitions of the ocean's deep circulation induced by changes in surface water fluxes. *Nature* **351**, 729–732 (1991).

**Supplementary Information** is linked to the online version of the paper at [www.nature.com/nature](http://www.nature.com/nature).

**Acknowledgements** This work is a contribution to the European Project for Ice Coring in Antarctica (EPICA), a joint European Science Foundation/European Commission scientific programme, funded by the EU (EPICA-MIS) and by national contributions from Belgium, Denmark, France, Germany, Italy, the Netherlands, Norway, Sweden, Switzerland and the UK. The main logistic support was provided by IPEV and PNRA (at Dome C) and AWI (at Dronning Maud Land).

**Author Information** Reprints and permissions information is available at [www.nature.com/reprints](http://www.nature.com/reprints). The authors declare no competing financial interests. Correspondence and requests for materials should be addressed to H. F. ([hufischer@awi-bremerhaven.de](mailto:hufischer@awi-bremerhaven.de)).

**EPICA Community Members (listed in alphabetical order):** C. Barbante<sup>1,2</sup>, J.-M. Barnola<sup>3</sup>, S. Becagli<sup>4</sup>, J. Beer<sup>5</sup>, M. Bigler<sup>6,7</sup>, C. Boutron<sup>3</sup>, T. Blunier<sup>6</sup>, E. Castellano<sup>4</sup>, O. Cattani<sup>8</sup>, J. Chappellaz<sup>2</sup>, D. Dahl-Jensen<sup>7</sup>, M. Debret<sup>3</sup>, B. Delmonte<sup>9</sup>, D. Dick<sup>10</sup>, S. Falourd<sup>8</sup>, S. Faria<sup>10,11</sup>, U. Federer<sup>6</sup>, H. Fischer<sup>10</sup>, J. Freitag<sup>10</sup>, A. Frenzel<sup>10</sup>, D. Fritzsche<sup>12</sup>, F. Fundel<sup>10</sup>, P. Gabrielli<sup>2,3</sup>, V. Gaspari<sup>1</sup>, R. Gersonde<sup>10</sup>, W. Graf<sup>13</sup>, D. Grigoriev<sup>14</sup>, I. Hamann<sup>10</sup>, M. Hansson<sup>15</sup>, G. Hoffmann<sup>8</sup>, M. A. Hutterli<sup>6,16</sup>, P. Huybrechts<sup>10,17</sup>, E. Isaksson<sup>18</sup>, S. Johnsen<sup>7</sup>, J. Jouzel<sup>8</sup>, M. Kaczmarek<sup>18</sup>, T. Karlin<sup>15</sup>, P. Kaufmann<sup>6</sup>, S. Kipfstuhl<sup>10</sup>, M. Kohno<sup>10</sup>, F. Lambert<sup>6</sup>, Anja Lambrecht<sup>10</sup>, Astrid Lambrecht<sup>10</sup>, A. Landais<sup>8</sup>, G. Lawer<sup>10</sup>, M. Leuenberger<sup>6</sup>, G. Littot<sup>16</sup>, L. Loulergue<sup>3</sup>, D. Lüthi<sup>6</sup>, V. Maggi<sup>9</sup>, F. Marino<sup>9</sup>, V. Masson-Delmotte<sup>8</sup>, H. Meyer<sup>12</sup>, H. Miller<sup>10</sup>, R. Mulvaney<sup>16</sup>, B. Narcisi<sup>19</sup>, J. Oerlemans<sup>20</sup>, H. Oerter<sup>10</sup>, F. Parrenin<sup>3</sup>, J.-R. Petit<sup>2</sup>, G. Raisbeck<sup>21</sup>, D. Raynaud<sup>2</sup>, R. Röthlisberger<sup>16</sup>, U. Ruth<sup>10</sup>, O. Rybak<sup>10</sup>, M. Severi<sup>4</sup>, J. Schmitt<sup>10</sup>, J. Schwander<sup>6</sup>, U. Siegenthaler<sup>6</sup>, M.-L. Siggaard-Andersen<sup>7</sup>, R. Spahni<sup>6</sup>, J. P. Steffensen<sup>7</sup>, B. Stenni<sup>22</sup>, T. F. Stocker<sup>6</sup>, J.-L. Tison<sup>23</sup>, R. Traversi<sup>4</sup>, R. Udisti<sup>4</sup>, F. Valero-Delgado<sup>10</sup>, M. R. van den Broeke<sup>20</sup>, R. S. W. van de Wal<sup>20</sup>, D. Wagenbach<sup>24</sup>, A. Wegner<sup>10</sup>, K. Weiler<sup>6</sup>, F. Wilhelms<sup>10</sup>, J.-G. Winther<sup>18</sup> & E. Wolff<sup>16</sup>

<sup>1</sup>Department of Environmental Sciences, University Ca' Foscari of Venice, <sup>2</sup>Institute for the Dynamics of Environmental Processes-CNR, Dorsoduro 2137, 30123 Venice, Italy. <sup>3</sup>Laboratoire de Glaciologie et Géophysique de l'Environnement (LGGE), CNRS-UJF, BP96 38402 Saint-Martin-d'Hères cedex, France. <sup>4</sup>Department of Chemistry, University of Florence, Via della Lastruccia 3, 50019 Sesto Fiorentino, Florence, Italy. <sup>5</sup>EAWAG, PO Box 611, 8600 Dübendorf, Switzerland. <sup>6</sup>Climate and Environmental Physics, Physics Institute, University of Bern, Sidlerstrasse 5, 3012 Bern, Switzerland. <sup>7</sup>Niels Bohr Institute, University of Copenhagen, Juliane Maries Vej 30, 2100 Copenhagen OE, Denmark. <sup>8</sup>Laboratoire des Sciences du Climat et de l'Environnement (LSCE/IPSL), CEA-CNRS-UVSQ, CE Saclay 91191, Gif sur Yvette, France. <sup>9</sup>Environmental Sciences Department, University of Milano Bicocca, Piazza della Scienza 1, 20126 Milano, Italy. <sup>10</sup>Alfred-Wegener-Institute for Polar and Marine Research, Columbusstrasse, D-27568 Bremerhaven, Germany. <sup>11</sup>Max Planck Institute for Mathematics in the Sciences, Inselstrasse 22, 04103 Leipzig, Germany. <sup>12</sup>Alfred Wegener Institute for Polar and Marine Research, Research Unit Potsdam, Telegrafenberg A 43, 14473 Potsdam, Germany. <sup>13</sup>GSF National Center for Environment and Health, Ingolstädter Landstrasse 1, 85764 Neuherberg, Germany. <sup>14</sup>University College London, Gower Street, London WC1E 6BT, UK. <sup>15</sup>Department of Physical Geography and Quaternary Geology, Stockholm University, 106 91 Stockholm, Sweden. <sup>16</sup>British Antarctic Survey, High Cross, Madingley Road, Cambridge CB3 0ET, UK. <sup>17</sup>Department Geografie, Vrije Universiteit Brussel, Pleinlaan 2, 1050 Brussel, Belgium. <sup>18</sup>Norwegian Polar Institute, 9296 Tromsø, Norway. <sup>19</sup>ENEA, C. R. Casaccia, Via Anguillarese 301, 00060 Roma, Italy. <sup>20</sup>Utrecht University, Institute for Marine and Atmospheric Research, PO Box 80005, 3508 TA Utrecht, The Netherlands. <sup>21</sup>CNSM/IN2P3/CNRS, Bat. 108, 91405 Orsay, France. <sup>22</sup>Department of Geological, Environmental and Marine Sciences, University of Trieste, Via E. Weiss 2, 34127 Trieste, Italy. <sup>23</sup>Département des Sciences de la Terre, Université Libre de Bruxelles, CP160/03, 1050 Brussels, Belgium. <sup>24</sup>Institute for Environmental Physics, University of Heidelberg, INF229, 69120 Heidelberg, Germany.